A University of Sussex PhD thesis

Available online via Sussex Research Online:

http://sro.sussex.ac.uk/

This thesis is protected by copyright which belongs to the author.

This thesis cannot be reproduced or quoted extensively from without first obtaining permission in writing from the Author

The content must not be changed in any way or sold commercially in any format or medium without the formal permission of the Author

When referring to this work, full bibliographic details including the author, title, awarding institution and date of the thesis must be given

Please visit Sussex Research Online for more information and further details

Evaluating Model Performance and Constraining Uncertainty using a Processed-Based Framework for Southern African Precipitation in Historical and Future Climate Projections

Melissa J. Lazenby

Thesis submitted for the Degree of Doctor of Philosophy

Department of Geography

University of Sussex

United Kingdom

December 2016

"It always seems impossible until it's done." Nelson Mandela

Abstract

This thesis develops an innovative process-based analysis of contemporary model performance of precipitation over southern Africa. This region is typically understudied and not fully understood due to the complexity of various influences and drivers of precipitation. Historical simulations of precipitation are assessed including principal drivers, sources of biases and dominant modes of interannual variability. The South Indian Ocean Convergence Zone (SIOCZ), a large-scale, austral summer rainfall feature extending across southern Africa into the south-west Indian Ocean, is evaluated as the feature of interest in historical simulations.

Most CMIP5 models simulate an SIOCZ feature, but are typically too zonally oriented and discontinued between land and the adjacent Indian Ocean. Excessive precipitation over the continent is likely associated with excessively high low-level moisture flux around the Angola Low, which is almost entirely due to model circulation biases. Drivers of precipitation over southern Africa include three dominant moisture flux transport pathways which originate from flow around the SIOHP and SAOHP and monsoon winds. Interannual variability in the SIOCZ is shown by a clear dipole pattern, indicative of a northeast-southwest movement of the SIOCZ. Drivers of this shift are significantly related to the El Niño Southern Oscillation and the subtropical Indian Ocean dipole in observations. However models do not capture these teleconnections well, limiting confidence in model representation of variability.

A large majority of the population rely heavily on precipitation over southern Africa for agricultural purposes. Therefore spatial and temporal changes in precipitation are crucial to identify and understand with intentions to ultimately provide useful climate information regarding water security over the region. Key climate change signals over southern Africa are established in this thesis (OND and DJF), in which the dominant regional mechanisms of precipitation change over southern Africa are quantified. Robustness and credibility of these changes are additionally quantified. The most notable projected change in precipitation over southern Africa is the distinct drying signal evident in the pre-summer season (OND). This has the implication of delaying the onset of the rainy season affecting planting and harvesting times. Future projections of the SIOCZ are determined, which indicate a northward shift of approximately 200km.

A dipole pattern of precipitation wetting/drying is evident, where wetting occurs to the north of the climatological axis of maximum rainfall, hence implying a northward shift of the ITCZ, consistent with the SIOCZ shift. Using a decomposition method it is established that ΔP*'s dipole pattern emerges largely from the dynamic component, which holds most uncertainty, particularly over the south-west Indian Ocean. Changes in precipitation over land are not solely driven by dynamical changes but additionally driven by thermodynamic contributions, implying projected changes over land and ocean regions require different approaches. SST patterns of warming over the Indian Ocean corroborate the warmest-get-wetter mechanism driving wetting over the south-west Indian Ocean, which is robust in both key seasons. Coherent model behaviour is understood via across model correlation plots of principal components, whereby patterns of coherent warming patterns are identified. Composite analyses of diagnostic variables across models illustrate patterns driving projected precipitation changes.*

Drying is more robust over land than over the south-west Indian Ocean. Clear robust drying signal in OND, however magnitude is uncertain. Drivers of uncertainty include SST pattern changes, which modulate atmospheric circulation patterns. Therefore reductions in uncertainty rely on the accurate representation of these processes within climate models to become more robust.

There is a desire from both climate scientists and policy-makers to reduce uncertainty in future projections. No one particular methodology is unanimously agreed upon, however one approach is analysed in this thesis. Uncertainties of future precipitation projections are addressed using a process-based model ranking framework. Several metrics most applicable to southern African climate are selected and ranked, which include aspects of both mean state and variability.

A sensitivity test via a Monte Carlo approach is performed for various sub-samples of "top" performing models within the CMIP5 model dataset. Uncertainty is significantly reduced when particular sub-sets of "top" performing models are selected, however only for austral summer over the continent. The result has the implication that potential value is established in performing a process-based model ranking over southern Africa. However additional investigation is required before such an approach may become viable and sufficiently credible and robust. Reductions in model spread are additionally established in SIOCZ projections, whereby model processes of change exhibit agreement, despite differing initial SIOCZ conditions. Therefore model process convergence and coherence is established with respect to projected changes in the SIOCZ, irrespective of initial climatology biases.

Supervisors

Prof. Martin C. Todd

Department of Geography, University of Sussex, United Kingdom

Dr. Yi Wang

Department of Geography, University of Sussex, United Kingdom

Funding

I am truly grateful to my sponsor Peter Carpenter who generously fully funded 3 years of my PhD studies through an African Climate Change Scholarship. Without his funding, this research would not have been possible.

Declaration

I declare that this thesis is my own work, both in concept and execution and that apart from the normal guidance and advice from my supervisors and external collaborators, I have received no assistance except from what has been acknowledged. I declare that neither the ideas nor any particular part of my thesis has been submitted in the past, or is currently being, or is to be submitted for a degree at Sussex University or at any other University.

Chapter 3 of this manuscript has been published in Climate Research and Chapter 5 is intended to be submitted to Journal of Climate for publication. I confirm that this above declaration holds true for the publication too, and the co-authorship of my two

supervisors and external collaborator (Robin Chadwick) represents their assistance in improving the paper and advising me through the peer-review process.

……

Signed

Acknowledgements

This thesis has only been possible due to the influence and input from numerous wonderful people in my life both professionally and personally. Attempts are made to thank everyone involved on this PhD journey with me. Firstly my supervisors, Prof. Martin Todd and Dr. Yi Wang are thanked for their support, guidance and patience. Most of all, I thank Martin for the constant supervision and help throughout my 4 years at Sussex. My growth as a researcher and individual are a true reflection of Martin's input into my work and development of ideas. My journey would not have been as successful and enjoyable without the constant support and help I have received from Martin over the past 4 years.

Peter Carpenter is thanked immensely for funding the majority of my PhD studies. Without this funding my PhD studies would not have been possible. I am grateful to Robin Chadwick for numerous discussions which have helped shaped the last few chapters of my thesis and his contributions as a co-author. Willem Landman is mentioned as he has been a mentor from my postgraduate studies and has always believed in me and my ability to be a climate scientist, without your belief in me I would not be where I am today - thank you! Who knew the Japanese Symposium we attended in 2011 would have predicted my future through a typo of Dr Lazenby on my name tag. Here I am on the verge of obtaining that title!

This process has been a challenging one but a significantly rewarding one. Leaving all I knew back in South Africa to venture to chilly England has made me grow in ways I never thought possible. Personal experience gained through this process cannot be measured, but to all the challenges I faced in my 4 years of studies – thank you! I am now a stronger and more resilient woman. Thanks to Parktown Girls High for teaching

me to be a confident and courageous young woman, ready and willing to meet any challenge that comes her way. Professionally I have pushed my intellectual boundaries and broken through programming barriers I feared for many years. Thanks to the NCL support group who always returned my emails no matter how trivial the question.

Teaching has been one of the most enjoyable parts of my PhD and thanks must go to all the students I have taught throughout my 4 years for helping me come to the realisation that teaching is one of my passions. Thanks to my office colleagues, who have come and gone throughout my time here, but each of you have added a little something to my PhD journey. A special mention to my office colleague and close friend Jamie, you have been my surrogate British brother and have always been a shoulder I could cry on and talk to about anything. Thank you for all your support and friendship, I am going to miss our office chats. Thanks to the doctoral school Thesis Boot Camp, which was one of the highlights of my PhD process, which helped kick start the writing process.

To all my friends in the UK who have become my surrogate family and helped me through all the ups and downs, you guys were great, thank you! Special mentions to Corin my former roommate and best friend, Roisin my close friend who I met through playing squash and Sara, my current roommate, friend and squash partner – Team BlondieBrownie! A special mention to the Sussex Gym and squash team for maintaining my sanity, without all those classes and squash matches my stress levels would have been unmanageable.

To Martin - thank you for all our chats about my research and everything else, including top holiday destinations, the weather (obviously), sports and life in general. I always thoroughly enjoyed how our discussions could be swayed from the most intense discussion of dynamical influences on climate projections to topics more appealing such

as watching YouTube videos of aussie rules football. The expansive knowledge I have gained from you, both academically and personally, is invaluable.

My family's support has been unwavering and I am deeply thankful for their encouragement and support via our weekly Skype chats and holidays back to SA whenever possible. The countless letters and postcards and words of encouragement when I felt like giving up have contributed greatly to getting me where I am today!

To my sister plebbie who has always been such a role model to me, thank you for always believing in me and supporting me in my PhD. Your constant example has helped me even when you may not have noticed so thank you plebbie!

To my dad, you have allowed me all these great opportunities and I am only here today due to your sacrifice and hard work. I cannot express my gratitude in words as no words will be enough. Thank you for also teaching me how to budget, I am a proper Lazenby!

To my mom, you have been the solid foundation and constant support system getting me through each and every day, good and bad. Thank you for all the saffa treats you have ready for me when I arrive home or that you send with friends to the UK. Your daily WhatsApp messages always brightened my day. Thank you for always making me a priority in your day, you are simply the best. I love you to the moon and back!

To my late grandfather Oupie, who always showed genuine interested in my studies and was so deeply proud of my achievements, I did it Oups! And finally to the Big Man upstairs, words could not be enough to thank you for all the support, as I know you were walking with me every step of the way.

"The beginning of knowledge is the discovery of something we do not understand." - *Frank Herbert*

Contents

Chapter 4:

Summary of Projected Key Climate Change Signals over SA/SWIO

Chapter 5:

Future Precipitation Projections over Central Southern Africa and the Adjacent Indian Ocean: What Causes Uncertainty?

Chapter 6:

Understanding Future Change and Reduction in Uncertainty

List of acronyms used

SA – Southern Africa

SWIO – South West Indian Ocean

SIOCZ – South Indian Ocean Convergence Zone

SACZ – South Atlantic Convergence Zone

SPCZ – South Pacific Convergence Zone

ITCZ – Inter Tropical Convergence Zone

OND – October November December

DJF – December January February

AL – Angola Low

HL – Heat Low

BH – Botswana High

SIOHP – South Indian Ocean High Pressure

SAOHP – South Atlantic Ocean High Pressure

TTT – Tropical Temperate Trough

SST – Sea Surface Temperature

IPCC – Intergovernmental Panel on Climate Change

WCRP - World Climate Research Programme

AR5 – Fifth Assessment Report

AMIP – Atmosphere-only Model Intercomparsion Project

CMIP – Coupled Model Intercomparison Project

RCP – Representative Concentration Pathway

GCM – General Circulation Model

MMM – Multi-Model Ensemble Mean

MME – Multi-Model Ensemble

ENSO – El Niño Southern Oscillation

SIOD – Subtropical Indian Ocean Dipole

IOD – Indian Ocean Dipole

CIO – Central Indian Ocean Index

EOF – Empirical Orthogonal Function

PC – Principal Component

RMSE – Root Mean Square Error

SD – Standard Deviation

IQR – Inter-quartile Range

"If a man will begin with certainties, he shall end in doubts; but if he will be content to begin with doubts he shall end in certainties." - Sir Francis Bacon

Chapter 1

1. Introduction

1.1. Motivation

Southern Africa is underdeveloped and poverty afflicted where climate change and variability, due to anthropogenic forcing, play a significant role in this underdevelopment resulting in an enhanced state of vulnerability (Basher and Briceno, 2006; Meadows, 2006; IPCC, 2007). However, much economic growth is currently developing in this region; therefore it is imperative that decisions are made with the most accurate climate change information in mind, as well as an awareness of intrinsic uncertainties. This will aid in ensuring economic growth is more sustainable in subsequent decades when the climate exhibits larger signals and hence have amplified impacts on water and food security.

There are various causes of uncertainty in numerical weather predictions and projections of future climate change over Africa (e.g. Palmer, 1999), hence the need to create a better understanding of what climate models are physically doing when constructing a prediction. Evaluation of model performance has shown large amounts of uncertainty but is still the only way to indicate if models are trustworthy when simulating future climate. A more quantitative approach to process-based model evaluation is required, which is explored in this study.

Within the climate change time-scale, these uncertainties' consist of systematic errors within climate models, for example the parameterization of cumulus convection is a particular source of uncertainty in model simulations over Africa (Ratna et al, 2014). Due to the inherent probabilistic nature of both numerical weather prediction and the projection of future climate change, the concern of probabilistic statements has become the norm across a range of time-scales from the next few days, to seasonal, to interannual, to decadal or even multi-decadal. There has been a growing demand from policy-makers and stakeholders for more quantitative simulations of the future climate deemed sufficiently reliable to aid in decision making in terms of adaption and mitigation (Collins et al, 2012; Knutti et al, 2010).

This study proposes to evaluate and potentially reduce uncertainties associated with predicting future climate change and variability over the southern Africa, focusing on the prominent South Indian Ocean Convergence Zone otherwise known and hereafter stated as the SIOCZ. The SIOCZ is a convergence zone responsible for the majority of austral summer rainfall that occurs during December-January-February (DJF) (Cook, 2000), as well as the shift in this feature being the leading pattern of interannual variability. During El Niño events or drier years the SIOCZ shifts north-eastward and during La Niña events or wetter years the SIOCZ shifts south-westward. Hence the SIOCZ has a significant impact on the many people, particularly commercial and subsistence farmers who rely on this consistent summer rainfall as their main form of livelihood. Therefore it is important to assess what possible future changes may occur with regards to this large-scale circulation system, such that appropriate planning measures may be put in place if and where necessary.

This feature and associated diagnostics will be analysed in terms of spatial and temporal variability, as well onset and intensity by evaluating contemporary climate to verify the most sophisticated coupled models available. A framework of process-based analyses will be developed to evaluate the different models credibility and hence constrain uncertainty and potentially increase confidence for future precipitation analyses. Projections of future characteristics of the SIOCZ system will be performed. Projected regional precipitation changes are identified over southern Africa and the south-west Indian Ocean. Using a decomposition methodology the main components (i.e. mechanisms of change) driving precipitation change are identified and attempts are made to understand change further through physically sensible diagnostics with the objective of reducing uncertainty of future precipitation projections over southern Africa.

Decisions will be made in terms of model ranking according to the results found in the model evaluation stage. Uncertainties associated with future precipitation projections over the region will be quantified and potentially constrained through this model ranking framework. Particular attention will be paid to the dynamics of the SIOCZ feature and how models currently capture this feature and associated processes, as well as assessing the main modes of variability, so that future projections of this feature and southern African climate change can potentially be understood and articulated with more confidence, certainty, credibility and understanding.

1.2. Key Thesis Questions

1. How well do current CMIP5 models perform at simulating present day precipitation over southern Africa with respect to mean state and variability?

2. What are the key climate change signals over southern Africa?

3. What are the dominant regional mechanisms of precipitation change over southern Africa?

4. How robust and credible are changes in projected precipitation over southern Africa?

5. Can uncertainty be significantly reduced for projected precipitation changes over southern Africa?

2. Literature Review

2.1. Southern African Precipitation Climatology

Southern Africa exhibits a distinct seasonal cycle throughout the year with more than 80% of annual rainfall occurring between October and March (Tyson, 1986). Austral summer in December-January-February (DJF) accounts for the largest proportion of annual rainfall, which is experienced for most of the region except for south-western extreme of the continent, which experiences winter rainfall in June-July-August (JJA) (Tyson, 1986). A large majority of southern Africa relies heavily on water for

agricultural purposes, both in commercial and subsistence sectors (Mason and Joubert, 1995, Hansen et al., 2011). Therefore changes in precipitation over southern Africa have large societal impacts that are far reaching and therefore need to be understood and constrained with as much confidence as possible. Not only do these uncertainties in future precipitation projections need to be quantified, but additionally communicated effectively to the relevant end-users (Webster, 2003).

The majority of austral summer rainfall over southern Africa can be attributed to convective activity, provided local conditions are optimum, such as sufficient moisture being available (Tyson, 1986; Tyson and Preston-Whyte, 2000). Convective activity is largely modulated by the influence of diurnal heating but additionally by various dynamic contributions from large-scale forcings and mesoscale and local effects (Tyson, 1986). These large-scale forcings include pressure systems such as localised heat lows, mid-latitude systems and ridging high pressures that provide a moisture transport pathways towards potential convective regions, causing low-level and mid-level convergence and hence uplift resulting in convection (Taljaard, 1996).

These influences from both tropical and subtropical conditions are conducive to the formation of enhanced precipitation that extends out into the south-west Indian Ocean (Cook, 2000). This enhanced band of diagonal precipitation over southern Africa and the adjacent Indian Ocean has been identified as a distinct feature of southern African mean climatology for many years (Taljaard, 1953; Streten, 1973; Tyson, 1986; Cook, 2000). This mean climatological feature is responsible for the majority of southern African summer rainfall, known as the South Indian Ocean Convergence Zone (SIOCZ), which is described in more detail in section 2.1.1. Convergence zones form as

part of a fundamental response of the atmosphere of the southern hemisphere in relation to the influence of land in the tropical and subtropical regions (Cook, 2000).

2.1.1. The South Indian Ocean Convergence Zone (SIOCZ)

Streten (1973) identified three dominant cloud bands that appeared semi-stationary in nature in the southern hemisphere. These are known today as the three major convergence zones namely, the South Pacific Convergence Zone (SPCZ), the South Atlantic Convergence Zone (SACZ) and finally the South Indian Ocean Convergence Zone (SIOCZ). These three convergence zones are responsible for producing significant precipitation amounts during the Southern Hemisphere summer by creating links between the tropics and mid-latitudes (Streten, 1973). Initial studies regarding these convergence zones established two requirements being essential to the formation of these systems, firstly flow into the subtropical regions via the subtropical jet and secondly lower-level flow towards the poles along the western edges of the subtropical high pressure systems i.e. south Indian Ocean high pressure (Kodama, 1992; 1993; Barreiro et al., 2002).

Differences exist between the three known southern hemispheric convergence zones, the most obvious being the SPCZ differing from the SIOCZ and SACZ due to the SPCZ being located over ocean only, whereas the SIOCZ and SACZ are located over land and extend into adjacent ocean regions (Cook, 2000; Figueroa et al., 1995; Lenters et al., 1995; Carvalho, 2004; Van Der Weil et al., 2015). Therefore the SPCZ is almost solely modulated via sea surface temperatures and associated circulation (Widlansky, 2013; Van der Weil, 2015). The SIOCZ and SACZ are modulated by a combination of effects

from both land and ocean namely, diabatic heating, land-sea contrasts, topographical influences and differences in relative humidity (Figueroa et al., 1995; Lenters et al., 1995; Chadwick, 2016; Puaud, 2016). There is, however, a commonality identified between these three aforementioned convergence zones, which is their relationship with mid-latitude wave trains (i.e. Rossby waves). The vorticity maxima of these wave trains tend to extend equator-wards, which in turn interact enhancing atmospheric instability and therefore resulting in deeper convective activity over these three regions (Widlansky et al., 2011; Macron et al., 2014; Puaud et al., 2016).

The SIOCZ, which is a land-based convergence zone (LBCZ) similar to the SACZ, was identified via the dynamic link between the large scale circulation and precipitation pattern found over southern Africa (Tyson, 1986; Cook, 1998; 2000; Niñomiya, 2008). This band is diagonal with a north-west south-east orientation that extends off into the south-east coastal regions (Cook, 1998; Niñomiya, 2008). Due to this feature spanning over both land and ocean regions, the position and intensity of this feature is influenced by surface conditions over southern Africa and additionally by the adjacent Indian Ocean (Cook, 2000; Lazenby et al., 2016). The SIOCZ can also be identified using other variables such as OLR, convergence fields, vertical uplift, high clouds and mean sea level pressure (SLP) (Liebmann et al., 1999; Brown et al., 2010) seen in Figure 1.

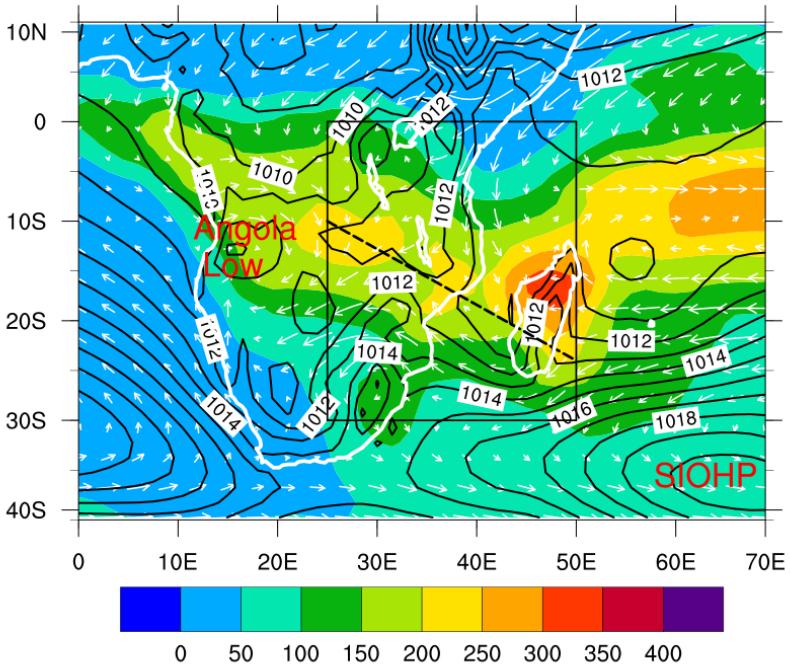

Figure 1: Overlay image of ERA-Interim mean sea level pressure (solid black lines) in hPa, mean CMAP precipitation (shaded colour contours) in mm month^{-1} and ERA-Interim moisture flux at 850hPa (white arrows - length indicative of magnitude) in g kg^{-1} * m s^{-1} for DJF over southern Africa for the historical period 1979/80-98/99. Dashed black line represents the SIOCZ and solid black box is chosen as the SIOCZ region.

In Cook's (2000) study the SIOCZ is defined as an area of enhanced precipitation during austral summer, located over the southern African continent that extends off the south-east coast between 10˚S and 40˚S that extends to approximately 60˚E. The analysis indicated that LBCZ's and hence the SIOCZ's rainfall is influenced by zonal wind convergence, moisture convergence by transient eddy activity and lastly moisture convergence associated with moisture advection, whereas within the ITCZ moisture convergence in that region is a result of meridonal wind convergence in a moist environment (Cook, 2000). The zonal wind convergence that occurs between the

thermal low (Angola Low) and subtropical high pressure (South Indian Ocean high pressure (SIOHP)) is responsible for the dominant boundary for the SIOCZ over the southern African continent (Cook, 2000). These pressure systems draw in moisture from the Atlantic Ocean via circulation around the Angola Low and additionally from the Indian Ocean via the SIOHP circulation (Macron et al., 2014). There is an additional moisture source that originates from the north-western monsoon region, totalling three moisture pathways into the SIOCZ (Lazenby et al., 2016). The extension of the SIOCZ out into the Indian Ocean is mainly a result of the partially compensating influences of moisture advection and moist transient eddy activity as well as meridonal wind convergence (Cook, 2000).

The SIOCZ has additionally been assumed to be a poleward excursion of the inter tropical convergence zone (ITCZ) (Taljaard, 1953; Tyson, 1986) and some coupled models, particularly from the older model generations, are unable to distinguish between the two features and simulate what is called a “double ITCZ” as both features appear very zonal in structure (Cook, 2000; Brown et al., 2010). A similar manifestation occurs for particular coupled models when assessing the SPCZ (Brown et al., 2010) therefore a common problem when attempting to identify these convergence zones. It is valuable to consider these LBCZ such as the SIOCZ as their own distinct feature from the ITCZ rather than just a poleward extension of the ITCZ and assess the rainfall observations according to this framework such that a physical understanding of rainfall variability over southern Africa can be established (Cook, 2000).

2.2. Southern African Precipitation Variability

Southern African precipitation varies significantly in both spatial and temporal aspects (Tyson, 1986; Mason and Jury, 1997), whereby the continental region experiences wetter and drier seasons/years over varying regions over the continent (Fauchereau et al., 2003). This makes understanding the variability of southern Africa complex in nature. Southern African precipitation variability ranges from daily all the way through to multi-decadal time-scales. However in this thesis emphasis is placed on interannual time-scales of precipitation variability over southern Africa. Links have been derived between southern African precipitation variability and climatic drivers such as sea surface temperatures (SSTs) both locally and through remote interactions (Reason and Mulenga, 1999; Richard et al., 2000; Camberlin, 2001; Nicholson et al., 2001; Fauchereau et al., 2003).

Variability over southern Africa has been captured over the austral summer season by several studies which show a dipole pattern in OLR, convection and rainfall (Cook, 2000). This dipole pattern is evident on daily time scales (Lyons, 1991; Todd and Washington, 1998) all the way to interannual time scales (Lindesay, 1988; Jury, 1992; Pohl et al., 2009; Puaud et al., 2016). This dipole signifies an opposing correlation between the north-eastern regions including Madagascar and the eastern African regions below 20˚S (Cook, 2000). A General Circulation Model (GCM) ensemble forecast showed a north-eastward movement of the SIOCZ when evaluating an El Niño Southern Oscillation (ENSO)-like warming in the eastern Pacific region due to a convergence anomaly forming off the southeast coast of Africa (Cook, 2000). This was due to a weakening of the South Indian high pressure in the western parts, which in turn produces the dipole pattern in rainfall, where there is higher rainfall experienced in the

northeast and lower rainfall experienced in the southwest, which corresponds to typical warm events over southern Africa (Cook, 2000).

In a recent study done by Dieppois et al (2016) more thorough analysis was performed regarding variability over southern Africa at various dominant time-scales. Three significant time-scales of variability were identified i.) interannual (2-8 years) ii.) quasi decadal (8-13 years) and iii.) interdecadal (15-28 years) (Dieppois et al., 2016). At these three different time-scales of variability, each showed differing relationships with SSTs and circulation patterns and hence implying the need to be dealt with independently regarding understanding of these drivers of variability. The main driver of austral summer precipitation variability stems from tropical or subtropical teleconnections (Dieppois et al., 2016).

Interannual variability is the most well understood time-scale of variability in studies over southern Africa with the primary driver of variability at this time-scale being driven by ENSO (Lindesay, 1988; Mason and Jury; 1997; Rouault and Richard, 2005; Ratnam et al., 2014; Dieppois et al., 2015; Lazenby et al., 2016). However, ENSO influences over southern Africa can exhibit non-linear and interactions between synoptic-scale and interannual variability may occur e.g. Links between El Niño producing Rossby waves, resulting in a north-eastward shift of the SIOCZ (Cook, 2001; Ratnam et al., 2014), as well as El Niño causing northward shifts of the subtropical high pressure systems such as the SIOHP, reducing moisture flux into the southern African continent (Mulenga et al., 2003; Cook, 2004; Vigaud et al., 2009; Dieppois et al., 2015).

LBCZ's are interfaces between thermal lows over the continent and subtropical high pressures over the ocean and therefore are affected by any changes within either of these features (Cook, 2000). For instance, if the thermal low over southern Africa (namely the Angola Low) shifts in position and/or becomes more intense due to enhanced thermal heating, this is likely to affect and alter the position and intensity of the SIOCZ. Additionally influences from global-scale processes, such as the proposed widening of the tropical circulation through the expansion of the Hadley circulation (Scheff and Frierson, 2012b; Lucas et al., 2014) can affect the SIOCZ by altering the subtropical highs magnitude, location and/or shape. Hence all these aforementioned interactions are physical factors that can potentially modulate variability of precipitation over this region (Cook, 2000).

Another more general source of seasonal precipitation variability over tropical and southern African are changes in sea surface temperatures (SSTs), which are partially responsible for large interannual anomalies in precipitation patterns (Rowell, 2013). These types of teleconnections can prove useful in providing probabilistic information in advance about potential anomalously wet or dry seasons over vulnerable areas such as Africa. Rowell (2013) shows that specific regions over south-west and south-east Africa have particularly strong teleconnections between the Central Indian Ocean (CIO) index as well as having links to ENSO in which drier seasons over the region are associated with El Niño years and a warming of the central Indian Ocean (Makarau and Jury, 1997; Nicholson et al., 2001; Hoerling et al., 2006; Rowell, 2013). According to previous studies (Reason, 2002; Washington and Preston, 2006; Morioka et al., 2015), the influence of the Subtropical Indian Ocean SST dipole (SIOD) could also induce an

anomalous anti-cyclonic circulation pattern which in turn drives anomalously low-level easterly moisture flux toward southern Africa at interannual and decadal timescales.

An analysis over southern Africa was explored by Engelbrecht et al (2009), whereby climate change signals were projected by the Conformal-Cubic Atmospheric Model (CCAM) according to the A2 Special Report on Emissions Scenario (SRES), which is closely comparable to the new Representative Concentration Pathway (RCP) 8.5. Results from this study included changes in the precipitation climate-change signal in terms of location and intensity of the subtropical high pressure belt, specifically the South Indian Ocean High Pressure (SIOHP) (Engelbrecht et al., 2009). In spring over the southern hemisphere future climate suggests a deepening of the low level continental trough over the western parts of the interior as well as a strengthening of the SIOHP in both mid and upper levels over the Indian Ocean and central and eastern interior of southern Africa (Engelbrecht et al., 2009).

This type of circumstance leads to the development of cloud bands over the central parts of South Africa, which translates into an increase in the frequency of occurrence of the SIOCZ (Washington and Todd, 1999; Cook, 2000; Engelbrecht et al., 2009). In another study done by Shongwe et al (2009), which is based on precipitation extremes over southern Africa using an ensemble of global climate models prepared for the Intergovernmental Panel on Climate Change (IPCC) Fourth Assessment Report (AR4), it was found that in spring a significant decrease in moisture influx from the south-western Indian Ocean was projected and therefore possibly responsible for the late onset of precipitation (Shongwe et al., 2009).

Engelbrecht (2009) states that future summer conditions show a broad deepening of the continental trough, which may be interpreted as an expansion of the tropical belt (Seidel et al., 2008; Engelbrecht et al., 2009; Lucas et al., 2014). Therefore some form of intensification of the Angola Low is implied, which is of interest in this study due to the Angola low being associated with the tropical component of SIOCZ development and maintenance. The SIOHP is found to intensify but now in the lower and mid-levels over the south western parts of the Indian Ocean and Madagascar, which leads to a favourable circulation pattern for more rainfall over the eastern parts of southern Africa due to the more frequent occurrence of the SIOCZ over the south-eastern interior (Washington and Todd, 1999; Cook, 2000; Engelbrecht et al., 2009).

It has been implied that cloud band formation may gradually shift westwards in future climate over southern Africa due to mid-level high pressure systems becoming continually prominent over the eastern region of southern Africa (Engelbrecht, 2004; Engelbrecht et al., 2009). Shongwe et al's (2009) study opposes this westward shift of the SIOCZ system as his study projects a possible offshore (north-easterly) shift of the cloud band, which is consistent with more severe droughts in the south-western parts of southern Africa and enhanced precipitation farther north in Zambia, Malawi, and northern Mozambique (Shongwe et al., 2009).

The reason for the contrasting projections of future climate of southern Africa may be due to the difference in resolution of the two studies, as the study by Engelbrecht (2009) was performed at a much higher resolution than Shongwe et al's (2009) study and may be more accurate in resolving smaller scale features and additionally more effective at

resolving the influence of topography, which plays a significant role in convection and precipitation over the southern African region.

The SIOCZ is associated with the occurrence of tropical temperate troughs (TTTs) (e.g. Todd and Washington, 1998; 1999; Hart et al., 2010), as they are developed due to large amounts of moisture convergence. TTT events amalgamate on daily time-scales throughout the austral summer season to produce the climatological SIOCZ rain band feature (Hart et al., 2010). Therefore changes established in the SIOCZ, will imply consistent changes with respect to TTT's in terms of frequency, intensity and position and precipitation.

There is the working assumption stating the vast majority of local and regional climate change will come about via changes experienced by synoptic scale-circulation features in terms of intensity, persistence and frequency (Hewitson and Crane, 1996; Hart et al, 2010). There will be a degree of uncertainty associated with this assumption due to potential large-scale changes in variables such as water vapour, which could in turn modify the relationship between circulation and precipitation as well as effect on the radiative properties on the modified airmass (Hewitson and Crane, 1996).

2.3. Model Performance Evaluation

Global climate model resolution is increasing as well as becoming more physically complex with the ultimate goal of improving accuracy, however future projections of these models still contain a vast amount of uncertainty, especially for precipitation (IPCC, 2007; Schaller et al., 2011). In order to make future climate simulations or

predictions with confidence using a particular model, it is essential that the model is able to adequately simulate the present climate (Sushama et al., 2006; Engelbrecht et al., 2009). This is vital as the ability of a particular model's future climate predictions depends somewhat on its ability to predict the current climate (Sushama et al., 2006; Engelbrecht et al., 2009).

There are several different ways to evaluate model performance with no one particular metric being proven best, as numerous studies have shown that different metrics result in different model rankings and little agreement has been found in separating 'good' versus 'bad' models (Gleckler et al., 2008; Knutti et al., 2009; Rowell et al., 2016). Model performance is generally evaluated on a grid point basis, disregarding the fact that models frequently produce results that are unreliable at such small spatial scales (Masson and Knutti, 2011).

A common evaluator of model performance is error analysis of global maps against observations (Schaller et al., 2011) as well as correlations (spatial and temporal) between historical model simulations and observations. Masson and Knutti (2011) use a spatial smoothing technique that has a variable scale parameter, which shows a decrease in model errors as well as inter-model spread as the smoothing scale increases. This technique does however reduce the ability of small scale features to be replicated and simulated patterns become fuzzy (Masson and Knutti, 2011). A similar methodology with kernel smoothing was used by Jun et al (2008a) to investigate if model biases are correlated therefore implying model dependence, which was shown to be true and a second approach using local eigenvalue analysis in Jun et al (2008b) proved similar results using the CMIP3 models. (Jun et al., 2008a; Jun et al., 2008b).

2.3.1. Process-based model diagnosis of change

An alternative approach to evaluating model performance is by assessing the representation of vital climate feedback processes on a number of different spatial and temporal scales. Feature-based metrics that are defined on a regional domain for only one variable may be a more practical and possibly better way in choosing which model is the most reliable (Schaller et al., 2011). In a study done by Christensen et al (2010) that explored performance based weighting of different RCM's, the method of evaluating the performance of the various RCM's included replication of large scale circulation patterns, detection of meso-scale signals, distributions of daily temperature and precipitation as well as capturing extremes, trends and the annual cycle (Christensen et al., 2010). Another more recent study by Thibeault and Seth (2013) used a similar technique, whereby a set of process-based analyses were developed forming a framework for evaluating model credibility in north-eastern North America. This study measured the model's ability to simulate observed spatial patterns, intensity of precipitation, dynamical atmospheric circulation features (i.e. the SIOCZ), moisture transport and divergence, long-term trends and SST patterns (Thibeault and Seth, 2013).

It has been stated by Knutti et al (2009) that more quantitative methods are required to assess global model performance and are of key importance in optimizing the value of future climate change projections (Knutti et al., 2009). A potential way to address this and add quantitative value could be established by separating the models lack of agreement from the models lack of signal due to the natural internal variability found within models i.e. signal to noise ratio (Tebaldi et al., 2011).

It is important that models are able to simulate long term mean circulation patterns and surface fields with a fair amount of skill compared to observations, as well as the variability on all time-scales (Battisti, 1995; Renwick et al., 1999; Engelbrecht et al., 2009). Combining multiple models is a practical way to identify the degree of model uncertainty and to hopefully lead to more reliable future climate projections (Knutti et al., 2012; Weigel et al., 2010); however determining the reliability of the projections still remains a challenge (Collins et al., 2012). A study done by Schaller et al (2011) showed that multi-model ensemble means, with regard to global fields, outperform all single individual models, however, when assessing the ensemble mean based on feature rankings the result is not as impressive and only average (Schaller et al., 2011).

Interpretation of multi-model outputs has the following main challenges, i) the inability to verify future climate change projections (Tebaldi and Knutti, 2007), ii) the issue of models not being justifiably independent from one another (Jun et al., 2008b; Knutti, 2010; Masson and Knutti, 2011; Knutti et al., 2013), iii) the lack of agreement between models possibly partly due to a low signal-to-noise ratio which can result in misleading information on the magnitude and sign of change (Schaller et al., 2011; Tebaldi et al., 2011), iv) the number of models within the ensembles is typically small, (Knutti et al., 2009), and iv) model bias and tuning effects (Tebaldi and Knutti, 2007). There is a large concern that development and evaluation of these models, as well as post weighting or ranking are all utilizing the same dataset (Knutti et al., 2009).

2.3.2. Model ranking schemes

Model weighting or ranking is a new avenue that is still rather contentious as it has been shown to potentially add another degree of uncertainty as there is no compelling and consistent evidence indicating improved performance by weighting models than when using equal weighting from each individual model (Christensen et al., 2010; Rowell et al., 2016). According to Rowell et al (2016), only "moderate" discrimination is established in his study of a model ranking framework. This is due to the fact that much more knowledge and understanding is required before accurate weighted modelling can be performed, because if done incorrectly can result in a more unreliable projection (Weigel et al., 2010). Another more feasible possibility would be to remove 'bad' models if they have been proven to lack essential mechanisms that are necessary for valuable future climate predictions (Weigel et al., 2010; Lazenby et al., 2016).

In this study an evaluation of the South Indian Convergence Zone (SIOCZ) and its seasonal climatology and interannual variability will aid in determining model performance of the current CMIP5 models by investigating if these AR5 models are able to capture the mean SIOCZ position and its associated variability. Therefore by using feature based metrics and developing a process-based framework in which to evaluate models, such as determining the large-scale processes imperative to southern African precipitation, conclusions may be drawn about "top" performing models and exclusion of "poor" models, which do not simulate this large-scale convergence zone over southern Africa with sufficient accuracy.

In attempting to reduce the uncertainty in projections of future climate change with regard to the SIOCZ, it would essentially result in more reliable statements about the future climate and water security of southern Africa, including statements that are

physically defendable and actionable to such an extent that they can advise adaptation procedures. This study will attempt to quantify and improve the reliability level of probabilistic statements of the multi-decadal (Fauchereau et al., 2003; Malherbe et al., 2012) climate futures over southern Africa. Moreover, research of the predictability and variability of the SIOCZ on verifiable time scales will provide insight into the limitations of predictability of the ocean-land-atmosphere system, and therefore insight into both models ability to realistically simulate weather and climate phenomena on extended time scales (e.g. Engelbrecht et al., 2011). The future simulations of southern African rainfall in terms of the SIOCZ can be used to highlight the processes that lead to model disagreement, therefore emphasising the processes that may be predominantly applicable in evaluating model credibility (Thibeault and Seth, 2013).

2.4. Mechanisms of Change

Based on analysis of precipitation projections various mechanisms have been proposed which link increased global temperatures and precipitation changes which approximate 1-3% precipitation increases per degree global warming (Collins et al., 2013), notably the thermodynamic wet-get-wetter process of rainfall change also termed the rich-get-richer mechanism (Held and Soden 2000; 2006; Allen et al., 2010; Christensen et al., 2013; Chou and Neelin, 2004; Meehl et al., 2007, Chou et al., 2009; Seager et al., 2010). This process is defined through increases in global specific humidity in a warmer atmosphere leads to an increase (decrease) in precipitation in the regions of mean moisture convergence (divergence). This is likely to be offset by the weakening of the mean tropical overturning Hadley circulation caused by a reduction in convective mass flux in regions of known high ascent due to a divergent feedback loop (Chadwick et al.,

2013; Christensen et al., 2013; Ma and Xie, 2013; DiNezio et al., 2013; Vecchi et al., 2016).

Chadwick et al (2013) proposes the wet-get-wetter mechanism alone does not explain the global pattern of multi-model mean (MMM) projected rainfall change (the spatial correlation of projected change in precipitation (ΔP) and mean precipitation (P) globally is low, such that at regional and seasonal scales in the tropics other processes dominate. These processes are substantially related to processes driving changes in spatial location of moisture convergence and hence convection. These include dynamic effects of regional gradients in near surface temperature change over oceans i.e. warmest-get-wetter mechanism (Xie et al., 2010), whereby patterns of SST warming determine tropical precipitation change, land-sea temperature contrasts (Dong et al., 2009), land surface processes, aerosol direct, indirect and semi-direct effects and changes in circulation (moisture flux convergence) (Shepherd, 2014).

Huang et al (2013) identifies an additional or rather modified mechanism of change known as the ‘modified warm-get-wetter’ mechanism. This ‘modified warmer-get-wetter’ mechanism is described as the combination of SST changes (warmer-get-wetter effect) that is modified by background climatological moisture and SSTs due to the non-linear relationship between tropical convection and SSTs.

Another school of thought is the ‘upped-ante’ mechanism of change, which is explained by tropical tropospheric warming requiring a particular amount of moist static energy to become convectively unstable (Neelin et al., 2003). This additional energy required is comparable to an increased ante just like in a poker game. This leads to the convective

edges experiencing a lack of precipitation and even potential drought conditions to be experienced over these convective margins (Neelin et al., 2003).

Generally, processes operating over the ocean are better understood than those over land due to continental regions having additional factors to consider. Land-sea contrasts cause knock-on effects towards changes in atmospheric general circulation patterns and hence potential changes in precipitation (Bayr and Dommenget, 2013; Byrne and O'Gorman, 2013). Land-sea contrasts are more applicable and influential when assessing regional changes in climate (Joshi et al., 2008; 2013).

There has been additional studies regarding widening of the tropical circulation, which is summarised in a recent study done by Lucas et al (2014). This effect of widening tropical circulation is attributed to forcings such as increased greenhouse gas concentrations, anthropogenic aerosols and stratospheric ozone depletion (Lucas et al., 2014). GCMs tend to underestimate this widening, which may due to lack of accuracy within model representation of these physical and dynamical responses. Models exhibit clear drying patterns over the majority of subtropical regions, whereby these subtropical regions are associated with the downward flank of the Hadley circulation, or rather lie on the edge of the tropics. One proposed response to anthropogenic climate change is a shift of this circulation pattern towards the poles, hence enlarging the area experiencing more frequent drought conditions (Scheff and Frierson, 2012b).

However, in all cases differing representation of these processes across models is likely driving projection uncertainty. Rowell et al (2015) highlights the importance of understanding the mechanisms of change within individual models as he identifies six

diverse hypotheses which could potentially explain the differences in East African rainfall change. He concludes stating further investigation should be aimed at developing expert judgement of process-based mechanisms and their reliability of projections, the role of natural variability and finally more exploration on the effect of anthropogenic aerosol emissions (Rowell et al., 2015).

2.4.1. Decomposition Methodology

Decomposition methodologies are a common way of understanding various components of a particular variable. Precipitation is often broken down into thermodynamic and dynamic components to potentially understand the mechanisms of change. There are various ways in which to break precipitation down, where slightly varying assumptions are used. For example Seager et al (2010) bases a precipitation decomposition on the projected changes in the term precipitation minus evaporation (P – E). Another example by Emori and Brown (2005) whereby the dynamic and thermodynamic breakdown is based on the probability density function using vertical velocity as the key variable. Chadwick et al (2013a; 2014) uses the assumption that P = M*q, where P is precipitation, M is convective mass flux and q is near surface specific humidity. The latter approach is utilised in this thesis and will be explained in further detail in Chapter 5.

2.5. Uncertainty and Robustness of Precipitation Projections

Uncertainty in precipitation projections presents challenges to climate adaptation policy (Webster, 2003; Swart et al., 2009), and therefore there is considerable interest in

improving our understanding of mechanisms of model projected changes so that we may quantify and potentially improve the robustness and credibility of projections. The science of climate change attempts to identify changes and gauge physical understanding of the changes but it is equally important to quantify these projected changes at regional scales as well as provide levels of uncertainties (Webster, 2003; Shepherd, 2014). The awareness of these unknown uncertainties are enhanced by extreme events, such as the recent drought conditions experienced over southern Africa during and after 2015-2016's El Niño event and the resultant effects on water supply and security resulting in restrictions in many provinces including Kwa-Zulu Natal and Limpopo. The question is then raised about the frequency of occurrence of these types of extreme events and can such events be predicted with greater certainty.

There is a clear need to understand why climate models generate particular patterns of projected change to precipitation in future climate simulations for all the aforementioned reasons. General circulation model (GCM) output is used to inform decision-making at regional levels and therefore these outputs require understanding and a significant level of credibility and robustness (Tebaldi and Knutti, 2007). Due to the large ensemble of various models and their various different outputs regarding future projections uncertainty remains a problem that requires further understanding. The physical processes potentially driving projected change are numerous and may vary amongst models and lead to considerable uncertainty in the sign and magnitude of projected change (Rowell, 2012; Collins et al., 2013; Kent et al., 2015). Improvement of the understanding of these physical processes that govern projected precipitation changes in coupled and atmospheric models will contribute positively to reductions in uncertainty.

Precipitation is particularly more difficult to constrain as it is influenced by both temperature driven (thermodynamic) and circulation (dynamic) influences, therefore implying the majority of uncertainty arises from the circulation or more typically the dynamic component, as temperature changes are typically more robust and more easily constrained (Shepherd, 2014). The spatial scale at which precipitation projections are produced is imperative due to global projections being controlled by different mechanisms to that of projections at a regional or sub-regional scale (Chadwick, 2016).

Global changes in precipitation are driven largely by atmospheric energy balances (Allen and Ingram, 2002); whereas regional changes in precipitation, particularly in tropical regions are controlled mainly through shifts in convection associated with atmospheric circulation changes (Chadwick et al., 2013a, Kent et al., 2015). When predicting precipitation on a regional-scale, there is a large influence from circulation dynamics, which requires clear understanding of the particular regions circulation patterns. Unfortunately there is generally weak theoretical understanding of circulation aspects of regional climate change as the dynamic responses are more indirect. There is often a lack of agreement on the model processes that drive circulation changes and hence projected precipitation changes (IPCC, 2014).

There are several hypotheses that potentially explain the lack of convergence and associated reduction of uncertainty in CMIP5 models (Knutti and Sedlacek, 2013).

(1) inherent limitations in the way models are built given limited computational resources and spatial resolution

(2) lack of process understanding,

(3) lack of accurate long term observations to constrain models,

(4) lack of consensus on metrics of present-day model performance that clearly separate better from worse models in terms of projection quality,

(5) inherent limitation of climate change not being predictable owing to internal variability,

(6) addition of dissimilar models from institutions new in CMIP5 and

(7) addition of new processes, components, or forcings in CMIP5 that are not well understood, not well represented in the model, or not well constrained by observations.

In this thesis a key focus is to make an attempt to reduce uncertainty in projected precipitation over southern Africa, which is addressed by paying particular attention to point 2 and 4 listed above.

3. Thesis Research Aims and Objectives

This thesis has the overall aim of evaluating models in contemporary climate using a process-based approach that can be used to understand regional projected changes over southern Africa, as well as potentially significantly reducing uncertainty for future climate change projections over southern Africa.

Specific aims and objectives of this thesis are listed below:

- **<u>Aim 1:</u> Evaluate current CMIP5 model performance in simulating historical mean state climatology and variability over southern Africa.**

Objectives:

1.1. Identify the austral summer climatological precipitation pattern (i.e. the SIOCZ) in observations and CMIP5 models and derive biases.

1.2. Determine the key dynamic processes that drive precipitation over southern Africa.

1.3. Determine coherent behaviour between model processes that can potentially explain model biases.

1.4. Investigate dominant modes and drivers of interannual variability over southern Africa in both observations and model simulations.

- **<u>Aim 2:</u> Identify the key precipitation climate change signals over southern Africa**

Objectives:

2.1. Determine and summarize the key projected precipitation changes over southern Africa (SA) and the adjacent south-west Indian Ocean (SWIO) in latest CMIP5 models.

2.2. Identify in which months/seasons the largest and most significant precipitation climate change signals are evident over southern Africa.

2.3. Quantify uncertainty in projected future precipitation change with respect to robustness (model agreement) and credibility (physically feasible mechanisms driving change).

2.4. Determine future changes of the SIOCZ over southern Africa including intensity, orientation and movement.

2.5. Highlight coherent model behaviour between projected future precipitation and various diagnostic variables.

2.6. Assess future AMIP experiments to determine if idealised experiments provide insight in understanding future precipitation projections over southern Africa.

- **<u>Aim 3:</u> Explore the regional mechanisms of change over southern African**

Objectives:

3.1. Unpack the key atmospheric processes vital to southern Africa pre-summer and austral summer precipitation through a precipitation decomposition analysis.

3.2. Quantify contributions from the various components (dynamic and thermodynamic) of the mechanisms of change.

3.3. Determine the proportion of uncertainty associated with the various mechanisms of change.

3.4. Investigate potential drivers of multi-model ensemble uncertainty in precipitation projections through identifying the dominant patterns of inter-model precipitation change.

- **<u>Aim 4:</u> Constrain uncertainty of future changes in precipitation over southern Africa.**

Objectives:

4.1. Create a ranking framework using the process-based model evaluation approach in Chapter 3 to broadly identify, good, average and poor models.

4.2. Using the ‘top’ performing models from the ranking framework developed, determine future precipitation projections for key seasons of interest OND and DJF.

4.3. Assess if model exclusion i.e. selecting “top” performing models over southern Africa increases confidence and significantly reduces uncertainty in future precipitation projections.

4.4. Discuss implications and findings with respect to future climate and water security over southern Africa.

4.5. Discuss how future work can be used to provide additional insights and potentially reduce uncertainty further.

Chapter 2

1. Research Data and Methodology

1.1. Overview

This thesis evaluates regional precipitation in both historical and future projections over southern African and the adjacent Indian Ocean. A brief overview of the data and methodology will be discussed in this Chapter, however in the substantive results chapters (Chapter 3, 4, 5 and 6) more extensive detail regarding the data and methodology will be provided.

2. Datasets utilised in this thesis

2.1. Observational datasets

The observational precipitation dataset used primarily in this thesis is the monthly Climate Prediction Center Merged Analysis of Precipitation (CMAP, Xie and Arkin, 1997). Other precipitation gridded gauge datasets were tested with essentially equivalent results (i.e. the Global Precipitation Climatology Project (GPCP) (Adler et al., 2003; Yin et al., 2004). The period of historical observed precipitation analysis includes a 20 year climatology from 1979-1999 due to the availability of CMAP data. Additional observed datasets used in this thesis include NOAA sea surface temperatures

(SSTs) (Reynolds et al., 2007) and various ERA-Interim reanalysis fields (Dee et al., 2011).

2.2. Model datasets

Twentieth century simulations from the World Climate Research Programme (WCRP) Coupled Model Intercomparison Project Phase 5 (CMIP5) multi-model dataset, in the most recent Assessment Report (Fifth Assessment report (AR5)) of the Intergovernmental Panel on Climate Change (IPCC) are used in Chapter 3 (Meehl et al., 2007, Taylor et al., 2012) (Table 1). Additionally Atmospheric Model Intercomparison Project (AMIP) (Gates, 1992; Gates et al., 1999) are analysed in historical simulations.

Monthly data was extracted and analysed over southern Africa. Focus is placed on particular seasonal averages, which are derived for the transitional pre-summer season October-November-December (OND) and austral summer season December-January-February (DJF) for key diagnostic variables to understand essential processes related to southern African climatology. The period of historical model analysis includes a 20 year climatology in Chapter 3 (due to the CMAP data constraint) and a 30 year climatology for the remainder of the analysis for the period 1971-2000. The first ensemble member was utilized in creating the MMM. All model data was interpolated to a common grid of 1.5˚ X 1.5˚ to ensure uniformity.

For the evaluation of projected precipitation changes over southern Africa (Chapter 4, 5 and 6), output from simulations of the 20th century and the 21st century (under the

RCP8.5 emissions scenario) from varying CMIP5 models (Table 1) are used (Meehl et al., 2007, Taylor et al., 2012). From the set of emission scenarios referred to as Representative Concentration Pathways (RCPs) (Moss et al, 2010; van Vuuren et al, 2011), the RCP8.5 emissions scenario was selected in the thesis for analysis. This emissions scenario corresponds to a high greenhouse gas emissions pathway (IPCC, 2008), which is used in numerous studies of CMIP5 model evaluation (Chadwick, 2016; Rowell, 2016; Dieppois et al, 2015; Kent et al, 2015; Cai et al, 2014; Maloney et al, 2014; Thibeault and Seth, 2014; Weller et al, 2014; Brown et al, 2013; Chadwick et al, 2013; Zheng et al, 2013). RCP8.5 was chosen for this study due to (i) it has good data availability (large domain of variables available), (ii) it has the largest signal-to-noise ratios (i.e. it maximises the climate change signal compared to other scenarios (Fisher et al, 2007), and (iii) it exhibits the greatest consistency with present-day emission trends which "track the high end of the latest generation of emission scenarios" (Friedlingstein et al, 2014; Clarke et al, 2014). Additionally, AMIP future experiments (Gates, 1992; Gates et al., 1999) are analysed to understand the role of SST warming and pattern effects (see glossary of future AMIP experiments defined in Chapter 4).

Monthly CMIP5 model data were extracted for key diagnostic variables to understand essential processes linked to projected precipitation changes over the SA/SWIO sector. The period of analysis includes a 30 year climatology, which is derived from the future RCP8.5 scenario 2071-2100 minus the historical period 1971-2000, similarly to historical simulations. The first ensemble member was utilized and all model data was interpolated to a common grid of 1.5˚ X 1.5˚ to ensure uniformity.

Table 1: List of CMIP5 models used in this thesis including modelling center, institute ID and atmospheric resolution. (Models with an * indicate an equivalent atmosphere-only model experiment, whereas models marked in italics are the atmosphere-only version of the CMIP5 model utilised in this study.)

Model Name	Modeling Center (or Group)	Institute ID	Atmospheric Resolution
ACCESS1.0* **ACCESS1.3***	Commonwealth Scientific and Industrial Research Organization (CSIRO) and Bureau of Meteorology (BOM), Australia	CSIRO-BOM	1.25˚ x 1.9˚
BCC-CSM1.1* **BCC-CSM1.1(m)***	Beijing Climate Center, China Meteorological Administration	BCC	2.8˚ x 2.8˚ 1.12˚ x 1.12˚
BNU-ESM*	College of Global Change and Earth System Science, Beijing Normal University	GCESS	2.8˚ x 2.8˚
CanESM2 ***CanAM4****	Canadian Centre for Climate Modeling and Analysis	CCCMA	2.8˚ x 2.8˚
CCSM4*	National Center for Atmospheric Research	NCAR	0.94˚ x 1.25˚
CESM1(BGC) **CESM1(CAM5)** **CESM1(FASTCHEM)** **CESM1(WACCM)**	Community Earth System Model Contributors	NSF-DOE-NCAR	0.94˚ x 1.25˚
CMCC-CESM **CMCC-CM*** **CMCC-CMS**	Centro Euro-Mediterraneo per I Cambiamenti Climatici	CMCC	3.71˚ x 3.75˚ 0.75˚ x 0.75˚ 1.9˚ x 1.9˚
CNRM-CM5*	Centre National de Recherches Météorologiques / Centre Européen de Recherche et Formation Avancée en Calcul Scientifique	CNRM-CERFACS	1.4˚ x 1.4˚
CSIRO-Mk3.6.0*	Commonwealth Scientific and Industrial Research Organization in collaboration with Queensland Climate Change Centre of Excellence	CSIRO-QCCCE	1.9˚ x 1.9˚
EC-EARTH*	EC-EARTH consortium	EC-EARTH	1.1˚ x 1.1˚
FGOALS-g2*	LASG, Institute of Atmospheric Physics, Chinese Academy of Sciences	LASG-CESS	2.8˚ x 2.8˚

	and CESS,Tsinghua University		
FGOALS-s2*	LASG, Institute of Atmospheric Physics, Chinese Academy of Sciences	LASG-IAP	1.7˚ x 2.8˚
FIO-ESM	The First Institute of Oceanography, SOA, China	FIO	2.8˚ x 2.8˚
GFDL-CM3* **GFDL-ESM2G** **GFDL-ESM2M** ***GFDL-HIRAM-C180**** ***GFDL-HIRAM-C360****	NOAA Geophysical Fluid Dynamics Laboratory	NOAA GFDL	2.0˚ x 2.5˚
GISS-E2-H **GISS-E2-H-CC** **GISS-E2-R*** **GISS-E2-R-CC**	NASA Goddard Institute for Space Studies	NASA GISS	2.0˚ x 2.5˚
HadGEM2-AO	National Institute of Meteorological Research/Korea Meteorological Administration	NIMR/KMA	1.25˚ x 1.9˚
HadGEM2-CC **HadGEM2-ES** ***HadGEM2-A****	Met Office Hadley Centre (additional HadGEM2-ES realizations contributed by Instituto Nacional de Pesquisas Espaciais)	MOHC (additional realizations by INPE)	1.25˚ x 1.9˚
INM-CM4*	Institute for Numerical Mathematics	INM	1.5˚ x 2˚
IPSL-CM5A-LR* **IPSL-CM5A-MR *** **IPSL-CM5B-LR***	Institut Pierre-Simon Laplace	IPSL	1.9˚ x 3.75˚ 1.25˚ x 2.5˚ 1.9˚ x 3.75˚
MIROC-ESM **MIROC-ESM-CHEM**	Japan Agency for Marine-Earth Science and Technology, Atmosphere and Ocean Research Institute (The University of Tokyo), and National Institute for Environmental Studies	MIROC	2.8˚ x 2.8˚
MIROC4h **MIROC5***	Atmosphere and Ocean Research Institute (The University of Tokyo), National Institute for Environmental Studies, and Japan Agency for Marine-Earth Science and Technology	MIROC	0.56˚ x 0.56˚ 1.4˚ x 1.4˚
MPI-ESM-LR* **MPI-ESM-MR***	Max-Planck-Institutfür Meteorologie (Max Planck Institute for Meteorology)	MPI-M	1.9˚ x 1.9˚

MPI-ESM-P			
MRI-CGCM3*	Meteorological Research Institute	MRI	1.1˚ x 1.1˚
NorESM1-M* **NorESM1-ME**	Norwegian Climate Centre	NCC	1.9˚ x 2.5˚

Varying numbers of CMIP5 and AMIP models are utilised in alternate chapters of this thesis but are noted within those chapters as to the amount and choice of models utilised in each of the analyses. The majority of models are utilised whenever possible. In Chapter 5 a subset of 20 CMIP5 models are utilised from the above table of CMIP5 models and will be shown as Table 1 in Chapter 5. A subset of only 20 CMIP5 models are evaluated in Chapter 5 due to the derivation of the alpha coefficient for the decomposition methodology, which was only derived for those specific 20 CMIP5 models. In Chapter 4 and 6 larger subsets of 39 CMIP5 models from the above table are utilised due to the availability of future RCP85 scenario model runs.

3. Research Methodology

3.1. Framework for process-based model evaluation

3.1.1. Model performance metrics: mean state and variability

The ability of CMIP5 models to capture the SIOCZ feature is evaluated through spatial correlations of mean observed and model precipitation in Chapter 3 over the SIOCZ

region (domain: 0˚- 30˚S, 25˚E - 50˚E illustrated by black rectangle in Figure 1: Chapter 1). Model error is quantified through mean bias and root mean square errors (RMSEs).

To diagnose model errors, atmosphere-only experiments are evaluated to identify potential coupling errors with respect to SST biases and inconsistencies. SST climatology is assessed in multi-model ensembles (MMEs) to investigate potential relationships between SST biases and precipitation. Errors in circulation are additionally determined through analysis of model low-level moisture flux into the SIOCZ region compared to observed circulation patterns. This is performed to establish whether the key controls and drivers in the formation and maintenance the SIOCZ are simulated in models. Moisture flux is decomposed into observed and modelled wind fields and combinations of the two fields are derived and analysed to determine which component of moisture flux is contributing most significantly to the moisture flux bias.

To determine SIOCZ variability, empirical orthogonal functions (EOFs) of DJF precipitation, for a 30 year period over southern Africa are derived for both models and observations. The first three primary EOFs are calculated for observations, as well as for all CMIP5 and AMIP models, from which the EOF exhibiting the highest association with the observed primary EOF is chosen for further model analysis. Composite analyses of moisture flux anomalies are evaluated to link the large-scale circulation to interannual variability of the SIOCZ. Global maps correlating the primary EOF (time coefficients) to global SSTs are generated to determine major SST teleconnections in observations and models ability to replicate and capture these remote and local teleconnections similarly.

3.2. Future Projected Changes

3.2.1. Future precipitation projections and associated diagnostic variables

To determine and summarize key changes in future southern African precipitation, the multi-model mean (MMM) of a total of 39 CMIP5 models is used. Individual models are additionally assessed in determining particular model processes in common driving changes in precipitation over southern Africa. Various diagnostic variables both thermodynamic and dynamic are analysed regarding future change in precipitation which include, temperature, SSTs, pressure, moisture, circulation and vertical velocity.

Future precipitation projections in Chapter 4 are analysed in absolute terms and percentage change (see Appendix for individual CMIP5 model absolute and percentage change – Figures 2 to 5). This addresses the issue of signals that are over inflated in particular regions, solely due to the fact that historical precipitation totals are significantly smaller over those regions. Signal to noise ratios are derived for each calendar month to determine in which months the signal of precipitation change exceeds that of internal model variability or disagreement (Tebaldi et al., 2011).

Atmosphere-only experiments are assessed to further understand future precipitation changes. Five AMIP future experiments are assessed in Chapter 4 to typically gauge additional understanding of SST influences in future change. AMIP future experiments may exhibit limited value in some instances and in Chapter 4 it is established whether or

not future AMIP experiments add additional understanding to projected precipitation change and their potential drivers over southern Africa.

3.2.2. Projections in the SIOCZ

Future simulations of the SIOCZ are determined over southern Africa in Chapter 4, with respect to intensity and movement. The SIOCZ is identified quantitatively by applying an algorithm adapted from Brown et al (2011) to the SIOCZ region. The SIOCZ region here is defined as the domain covering 0˚ to 30˚S and 25˚E to 50˚E. Cook (2000) defines the SIOCZ as being an area of enhanced precipitation during austral summer, which corresponds well and consistent with Brown et al's (2011) definition of the SPCZ.

The SIOCZ is characterised and classified using a simple metric to identify the SIOCZ's mean latitude and orientation (slope) by insertion of an SIOCZ axis. This process involves extracting for each longitude point, the maximum precipitation value and corresponding latitude, and deriving the best fit/regression line through these maximum precipitation values over the chosen domain. This provides an objective way to compare the slope and mean latitudes of the SIOCZ, between the models and their corresponding observations (Brown et al., 2011). This process is performed over the defined SIOCZ region using the austral summer mean season DJF in both historical and future projections. Differences are analysed using individual model and MMM plots, such that projected changes in the SIOCZ can be established.

3.3. Mechanisms of Change

3.3.1. Decomposition methodology

Projected changes in precipitation are often decomposed into thermodynamic and dynamic components using a number of variations e.g. Seager et al (2010) and Emori and Brown (2005). In this thesis the decomposition methodology developed by Chadwick et al (2013a; 2014) is utilised. This methodology is based on the assumption that $P = Mq$, where P is precipitation, M is convective mass flux and q is near surface specific humidity. This approach is based on the assumption that in convective climate regimes mean precipitation *(P)* is equivalent to the vertical mass flux from boundary layer to free troposphere *(M)* multiplied by specific humidity in the boundary layer *(q)*) (Held and Soden, 2006). Extensive detail regarding this methodology is explained in Chapter 5. Additional clarity regarding this methodology can be found in the paper Chadwick et al (2013a).

3.3.2. Analysis of uncertainty: climate sensitivity

Normalising changes in precipitation removes the uncertainty associated with rates/magnitude of warming between models. This allows sole focus on patterns of change, not particularly magnitudes of change. This approach is used in Chapter 5 to potentially understand and unpack the mechanisms of change within models that cause changes.

MMM of change is used as the main parameter of change in Chapter 5, whereby 20 CMIP5 models are used. All components of projected MMM change are normalised by the mean global surface temperature change of each individual model *(ΔT_{global})*, therefore are expressed as per degree global warming. This removes the uncertainty due to inter-model spread in climate sensitivity and makes the results scalable to the magnitude of warming, which is tractable when informing policy-makers under different warming threshold scenarios. Removing the effect on ΔP of uncertainty in model ΔT_{global} related to model climate sensitivity has only a minor input on results (see section 2.3 in Chapter 5). Kent et al (2015) using the same decomposition method found no significant influence of global mean temperature change on ΔP in terms of understanding i) the spatial pattern of ΔP and relative contributions to ΔP of the various mechanisms of change in the decomposition, ii) the inter-model spread in ΔP, such that Kent et al (2015) states that dynamical uncertainty is unrelated to climate sensitivity which dominates precipitation change uncertainty across the globe.

To quantify uncertainty of these projected changes, box-whisker plots and standard deviations (i.e. model spread) are derived. Land and ocean regions over southern Africa are assessed individually in Chapter 5 due to varying influences over the two domains. Dominant patterns of variation are established through EOF analysis of ΔP and additionally ΔP_{Shift}. Correlations of model coefficients versus global SST pattern changes are derived to determine coherent model behaviour and understand potential drivers of precipitation change. Composite analysis is performed on circulation patterns to determine patterns associated with projected precipitation changes.

3.4. Model Ranking Framework

3.4.1. Model ranking in contemporary climate

A model ranking framework is developed in Chapter 6 whereby ranks are awarded to models based on 7 metrics in total, whereby 4 are mean state metrics and 3 variability metrics. The framework is based on the 44 CMIP5 models evaluated in contemporary climate in Chapter 3. Mean state metrics include models ability to simulate observed spatial patterns and intensity of mean precipitation over southern Africa for austral summer (DJF) using spatial correlations and zonal averages of precipitation against observations. Biases and RMSE values for the region are also included. Variability metrics include models ability to simulate interannual variability of austral summer precipitation and associated drivers i.e. teleconnections vital to southern African precipitation. Model convergence between mean state and variability processes amongst models are evaluated.

3.4.2. Reducing uncertainty in precipitation projections

In the final substantive chapter of this thesis (Chapter 6), results from previous chapters are synthesised to make an attempt to significantly reduce uncertainty in future precipitation projections over southern Africa. This is determined by using analysis output from Chapter 3 to create a model framing work explained above in section 3.4.1 and in more detail in Chapter 6. From this model ranking framework the "top" 10, 20 and 30 performing models are selected to determine the standard deviation, inter-quartile range and range of these three subsets of CMIP5 models.

A sensitivity analysis is performed by randomly sub-sampling 10, 20 and 30 models by 10,000 iterations each i.e. using a Monte Carlo approach. Frequency distributions of the above spread statistics are derived for the 10^{th} and 90^{th} percentiles and compared to the critical values when models were "intelligently" selected. Results lying beyond the frequency distribution when randomly sub-sampled are deemed significant i.e. there is value in intelligently sub-sampling models over randomly sub-sampling. Therefore this analysis uses the understanding of process-based metrics to investigate whether uncertainty in projected precipitation over southern Africa can be significantly reduced. Results, if deemed significant in reducing uncertainty require additional scrutiny to establish whether results are physically credible or potentially falsely constrained.

3.4.3. Addressing uncertainty in SIOCZ projections

Uncertainty of future projections of the SIOCZ is analysed using box-whisker plot analysis to determine inter-model spread. An experiment is conducted to determine if models indicate enhanced agreement or convergence in future changes in the SIOCZ, irrespective of the individual models initial SIOCZ location in contemporary climate. To test this hypothesis a threshold value of greater than 5.5 mm day^{-1} (~165 mm/month) is chosen as the mask to identify the SIOCZ in historical simulations (derived from analysis completed in Chapter 3). The mask is determined for the MMM of the 39 CMIP5 models and additionally for each individual CMIP5 model. Future projected precipitation changes over the SIOCZ are then derived for both the MMM and individual models. Results of future SIOCZ precipitation projections are plotted using box-whisker plots of area averaged percentage change in precipitation. Spread between the two different experiments is established.

3.4.4. Creating useable information for policymakers

Significant results from this study regarding changes in the SIOCZ and precipitation changes will be beneficial in providing insight and understanding of the value of this type of ranking approach over southern Africa. Additional work is required to determine the credibility of projected changes in precipitation and to confidently inform end-users of these possible changes and their associated impacts (Webster, 2003; Swart et al., 2009).

Chapter 3

Climate Model Simulation of the South Indian Ocean Convergence Zone: Mean State and Variability

Overview

The dominant climatological feature over southern Africa responsible for the majority of austral summer rainfall (the SIOCZ) is evaluated in CMIP5 models in this chapter. Both the mean state and variability of this feature is evaluated. The main drivers of this system are additionally identified. Interannual variability of the SIOCZ is investigated in both observations and models as well as subsequent drivers of variability.

Key Questions:

1. How well do current CMIP5 models perform in identifying the key austral summer feature over southern Africa i.e. the SIOCZ?
2. Can sources of precipitation biases be identified in models?
3. Investigate dominant modes and drivers of interannual variability over southern Africa i.e. teleconnections.
4. Are current CMIP5 models able to identify modes of variability and subsequent drivers?

Climate model simulation of the South Indian Ocean Convergence Zone: mean state and variability

Melissa J. Lazenby*, Martin C. Todd, Yi Wang

Department of Geography, University of Sussex, Brighton, East Sussex BN1 9RH, UK

ABSTRACT

Evaluation of climate model performance at regional scales is essential in determining confidence in simulations of present and future climate. Here we developed a process-based approach focussing on the South Indian Ocean Convergence Zone (SIOCZ), a large-scale, austral summer rainfall feature extending across southern Africa into the southwest Indian Ocean. Simulation of the SIOCZ was evaluated for the Coupled Model Intercomparison Project (CMIP5). Comparison was made between CMIP5 and Atmospheric Model Intercomparison Project (AMIP) models to diagnose sources of biases associated with coupled ocean-atmosphere processes. Models were assessed in terms of mean SIOCZ characteristics and processes of interannual variability. Most models simulated a SIOCZ feature, but were typically too zonally oriented. A systematic bias of excessive precipitation was found over southern Africa and the Indian Ocean,

but not particularly along the SIOCZ. Excessive precipitation over the continent may be associated with excessively high low-level moisture flux around the Angola Low found in most models, which is almost entirely due to circulation biases in models. AMIP models represented precipitation more realistically over the Indian Ocean, implying a potential coupling error. Interannual variability in the SIOCZ was evaluated through empirical orthogonal function analysis, where results showed a clear dipole pattern, indicative of a northeast−southwest movement of the SIOCZ. The drivers of this shift were significantly related to the El Niño Southern Oscillation and the sub-tropical Indian Ocean dipole in observations. However, the models did not capture these teleconnections well, limiting our confidence in model representation of variability.

*Corresponding author: M.Lazenby@sussex.ac.uk

KEY WORDS: CMIP5 · ENSO · Ensemble · Teleconnection · Model evaluation · South Indian Ocean Convergence Zone · SIOCZ · Southern Africa · December-January-February · DJF

1. Introduction

1.1.Model evaluation

Future projections of climate still contain a large amount of uncertainty, especially for precipitation (Schaller et al., 2011; Collins et al., 2013). In order to make future climate simulations with confidence, it is essential that models are able to adequately simulate

the present climate (Sushama et al., 2006; Engelbrecht et al., 2009), as well as long term mean circulation patterns and surface fields, and also particularly variability on all time scales (Battisti, 1995; Renwick et al., 1999; Engelbrecht et al., 2009).

Common evaluators of model performance include error (bias) against observations (Schaller et al., 2011) and correlations (spatial and temporal) between historical model simulations and observations (Taylor, 2001). Complementary and more recent approaches to evaluate model performance suggest process-based analyses to form a framework for evaluating model credibility (e.g. Glecker et al., 2008; Thibeault and Seth, 2014). This includes evaluating models ability to capture the large-scale processes, such as the general circulation and variability of a particular feature or variable (Thibeault and Seth, 2014). The objective aims to identify the mechanisms or processes causing future change in models, therefore not solely relying on representation of present climatology as an indicator of credibility in future projections (Shongwe et al., 2011; Thibeault and Seth 2014; James et al., 2015).

1.2. The South Indian Ocean Convergence Zone (SIOCZ)

Southern African climate is relatively understudied and due to its generally high vulnerability to climate variability and change and low adaptive capacity, there is a growing demand from policymakers for more robust estimates of the future climate deemed sufficiently reliable to aid in decision making for adaption (Callaway, 2004; Knutti et al., 2010). Southern African climate is dominated by the SIOCZ, a diagonal north-west to south-east band of enhanced low-level convergence and precipitation during austral summer extending from the southern African continent into the southwest Indian Ocean over the south-east coast between 10˚S and 40˚S and 0˚E to 60˚E (Cook,

1998; 2000). It is a land-based convergence zone (LBCZ) that forms the dynamic link between the large scale circulation and the precipitation over southern Africa and south-west Indian Ocean (Tyson, 1986; Cook, 1998; 2000; Niñomiya, 2008). It can be identified using variables such as OLR, convergence fields, vertical uplift, high clouds and mean sea level pressure (SLP), which has been done previously to identify the SACZ (Liebmann et al., 1999), and the SPCZ (Brown et al., 2011).

The zonal wind convergence occurring between the thermal low (Angola Low) and South Indian Ocean High Pressure (SIOHP, a.k.a the Mascarene high pressure) are responsible for the dominant boundary of the SIOCZ over the southern African continent (Cook, 2000; Niñomiya, 2008) (Figure 1). The extension of the SIOCZ into the Indian Ocean is mainly a result of the partially compensating influences of moisture advection and moist transient eddy activity and meridonal wind convergence (Cook 2000). Three clear sources of moisture flux to be noted in Figure 1 are: 1.) moisture flux from the circulation around the Angola Low, 2.) moisture flux from the NE monsoon region and lastly 3.) moisture flux from the circulation around the SIOHP that ridge over the continent.

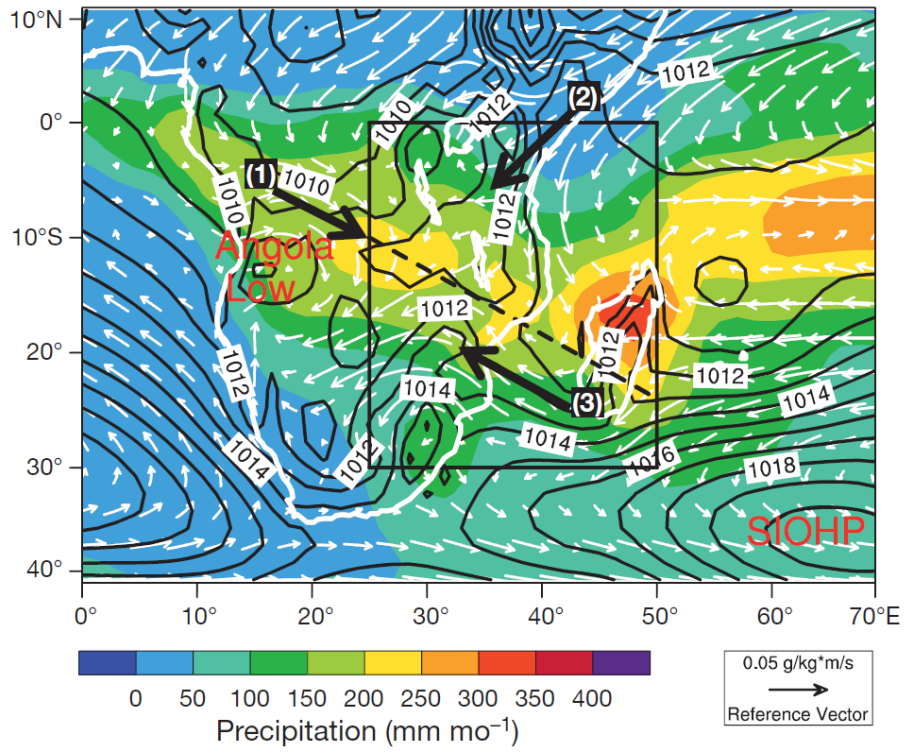

FIG 1: Mean DJF climate over study region 1979/80-98/99. Sea level pressure (hPa, solid black lines from ERA-Interim data), precipitation (mm month^{-1}), shaded colour contours from CMAP) and moisture flux at 850hPa (g kg^{-1} *m s^{-1}, white arrows - length indicative of magnitude from ERA-Interim). Black box indicates the chosen SIOCZ region (0˚S - 30˚S, 25˚E - 50˚E) and the dashed black line represents the SIOCZ. Black arrows labelled 1, 2 and 3 represent the three major moisture flux pathways into the SIOCZ (see text for details).

Climate variability over southern Africa and the south-western Indian Ocean is dominated by a dipole pattern in OLR, convection and rainfall, which can be interpreted as the interannual shift in the position of the SIOCZ (Cook, 2000) (see section 5). This dipole between the north-eastern regions and the eastern African regions (Cook, 1998) has a strong association with El Niño Southern Oscillation (ENSO) and the Indian Ocean (Makarau and Jury, 1997; Goddard and Graham, 1999; Nicolson et al., 2001;

Hoerling et al., 2006; Rowell, 2013). The subtropical Indian Ocean dipole (SIOD) is important in understanding southern African rainfall variability over interannual time-scales (Goddard and Graham, 1999; Cook, 2000; Behera and Yamagata, 2001; Reason, 2001).

In this paper models are evaluated in terms of their ability to simulate the mean state of the SIOCZ and variability on an interannual time scale. The drivers of the interannual variability will also be identified in observations and models. It is important to note that the simulation of the SIOCZ has not previously been evaluated using the suite of CMIP5 climate models, and information about the SIOCZ in models will provide input for evaluating uncertainty in regional climate projections for southern Africa.

2. Data & Methods

2.1 Data

The gridded precipitation observational dataset used here was the monthly Climate Prediction Center Merged Analysis of Precipitation (CMAP, Xie and Arkin, 1997). The period of historical observed precipitation from CMAP includes a 20 year climatology from 1979/80 to 1998/99 due to the availability of CMAP data. Other precipitation gridded gauge datasets were tested with essentially equivalent results (i.e. the Global Precipitation Climatology Project (GPCP) (Adler et al., 2003; Yin et al., 2004). Other observed datasets used include NOAA sea surface temperatures (SSTs) (Reynolds et al., 2007) and ERA-Interim reanalysis fields (Dee et al., 2011).

Twentieth century simulations from a total of 44 models from the World Climate Research Programme (WCRP) Coupled Model Intercomparison Project Phase 5 (CMIP5) multi-model dataset, in the most recent Assessment Report (Fifth Assessment report (AR5)) of the Intergovernmental Panel on Climate Change (IPCC) are used (Meehl et al., 2007; Taylor et al., 2012) (Table 1). The historical model analysis includes a 20 year climatology, allowing for a common period of comparison between observed and modelled rainfall climatology, as the CMIP5 model data available was only from 1975-2005 and preference of analysis was in periods of decades. The potential implication of only using a 20 year period could result in an enhanced modification from strong wet and dry rainfall seasons within the chosen time period, however a comparison of a 20 and 30 year observed climatological period (not shown here) did not exhibit significant differences and therefore a 20 year historical period is deemed sufficient for the analysis in section 3.

A 30 year period is used for the remainder of the analysis i.e. from section 4 onwards as EOF analyses prove more robust with larger sample size i.e. larger number of time steps. Additionally 27 Atmospheric Model Intercomparison Project (AMIP) (Gates, 1992; Gates et al., 1999) are analysed to attribute the source of biases. Monthly data was extracted for the December-January-February (DJF) austral summer season of key diagnostic variables to understand essential processes of southern African climate.

Table 1: CMIP5 model list of the 44 models used including modelling center, institute ID and atmospheric. (Models marked with a * indicates the models where the atmosphere-only version of the model was also used in the analysis)

Model Name	Modeling Center (or Group)	Institute ID	Atmospheric Resolution
ACCESS1.0* **ACCESS1.3***	Commonwealth Scientific and Industrial Research Organization (CSIRO) and Bureau of Meteorology (BOM), Australia	CSIRO-BOM	1.25˚ x 1.9˚
BCC-CSM1.1* **BCC-CSM1.1(m)***	Beijing Climate Center, China Meteorological Administration	BCC	2.8˚ x 2.8˚ 1.12˚ x 1.12˚
BNU-ESM*	College of Global Change and Earth System Science, Beijing Normal University	GCESS	2.8˚ x 2.8˚
CanESM2 ***CanAM4****	Canadian Centre for Climate Modeling and Analysis	CCCMA	2.8˚ x 2.8˚
CCSM4*	National Center for Atmospheric Research	NCAR	0.94˚ x 1.25˚
CESM1(BGC) **CESM1(CAM5)** **CESM1(FASTCHEM)** **CESM1(WACCM)**	Community Earth System Model Contributors	NSF-DOE-NCAR	0.94˚ x 1.25˚
CMCC-CESM **CMCC-CM*** **CMCC-CMS**	Centro Euro-Mediterraneo per I Cambiamenti Climatici	CMCC	3.71˚ x 3.75˚ 0.75˚ x 0.75˚ 1.9˚ x 1.9˚
CNRM-CM5*	Centre National de Recherches Météorologiques / Centre Européen de Recherche et Formation Avancée en Calcul Scientifique	CNRM-CERFACS	1.4˚ x 1.4˚
CSIRO-Mk3.6.0*	Commonwealth Scientific and Industrial Research Organization in collaboration with Queensland Climate Change Centre of Excellence	CSIRO-QCCCE	1.9˚ x 1.9˚
EC-EARTH*	EC-EARTH consortium	EC-EARTH	1.1˚ x 1.1˚
FGOALS-g2*	LASG, Institute of Atmospheric Physics, Chinese Academy of Sciences and CESS,Tsinghua University	LASG-CESS	2.8˚ x 2.8˚
FGOALS-s2*	LASG, Institute of Atmospheric Physics, Chinese Academy of Sciences	LASG-IAP	1.7˚ x 2.8˚
FIO-ESM	The First Institute of Oceanography, SOA, China	FIO	2.8˚ x 2.8˚
GFDL-CM3*	NOAA Geophysical Fluid Dynamics	NOAA GFDL	

GFDL-ESM2G **GFDL-ESM2M** ***GFDL-HIRAM-C180**** ***GFDL-HIRAM-C360****	Laboratory		2.0˚ x 2.5˚
GISS-E2-H **GISS-E2-H-CC** **GISS-E2-R*** **GISS-E2-R-CC**	NASA Goddard Institute for Space Studies	NASA GISS	2.0˚ x 2.5˚
HadGEM2-AO	National Institute of Meteorological Research/Korea Meteorological Administration	NIMR/KMA	1.25˚ x 1.9˚
HadGEM2-CC **HadGEM2-ES** ***HadGEM2-A****	Met Office Hadley Centre (additional HadGEM2-ES realizations contributed by Instituto Nacional de Pesquisas Espaciais)	MOHC (additional realizations by INPE)	1.25˚ x 1.9˚
INM-CM4*	Institute for Numerical Mathematics	INM	1.5˚ x 2˚
IPSL-CM5A-LR* **IPSL-CM5A-MR *** **IPSL-CM5B-LR***	Institut Pierre-Simon Laplace	IPSL	1.9˚ x 3.75˚ 1.25˚ x 2.5˚ 1.9˚ x 3.75˚
MIROC-ESM **MIROC-ESM-CHEM**	Japan Agency for Marine-Earth Science and Technology, Atmosphere and Ocean Research Institute (The University of Tokyo), and National Institute for Environmental Studies	MIROC	2.8˚ x 2.8˚
MIROC4h **MIROC5***	Atmosphere and Ocean Research Institute (The University of Tokyo), National Institute for Environmental Studies, and Japan Agency for Marine-Earth Science and Technology	MIROC	0.56˚ x 0.56˚ 1.4˚ x 1.4˚
MPI-ESM-LR* **MPI-ESM-MR*** **MPI-ESM-P**	Max-Planck-Institutfür Meteorologie (Max Planck Institute for Meteorology)	MPI-M	1.9˚ x 1.9˚
MRI-CGCM3*	Meteorological Research Institute	MRI	1.1˚ x 1.1˚
NorESM1-M* **NorESM1-ME**	Norwegian Climate Centre	NCC	1.9˚ x 2.5˚

2.2 Model performance metrics

The ability of models to capture the SIOCZ structure is derived through spatial correlations of the mean observed and model precipitation over the SIOCZ region (domain: 0˚- 30˚S, 25˚E - 50˚E illustrated by black rectangle in Figure 1). Model error is quantified through mean bias and root mean square errors (RMSEs) (metrics listed in Table 2). Both model and observational data were assessed for a 20 year climatological DJF period from 1979/80 to 1998/99, except for section 4's analysis where a 30 year time period was utilised (1979/80 – 2008/09) due to EOF analyses becoming more robust with a larger sample size.

Table 2: Spatial Correlations of precipitation between observations (CMAP) and CMIP5 models over the SIOCZ region. Area averages, model biases and RMSE calculated over the SIOCZ region. All calculations based on the period 1979/80-1998/99.

Model/Observation	**SIOCZ Region Spatial Correlation**	**Area Average (mm/month)**	**Model Bias (mm/month)**	**Model RMSE (mm/month)**
CMAP	/	135	/	/
ACCESS1-0	0.85	159	24	63
ACCESS1-3	0.77	183	48	94
bcc-csm1-1	0.85	144	9	42
bcc-csm1-1-m	0.84	138	3	47
BNU-ESM	0.75	180	45	86
CanESM2	0.82	150	15	59
CCSM4	0.85	180	45	72
CESM1-BGC	0.85	177	42	71
CESM1-CAM5	0.87	156	21	53

CESM1-FASTCHEM	0.84	174	39	70
CESM1-WACCM	0.74	174	39	80
CMCC-CESM	0.74	147	12	57
CMCC-CM	0.77	126	-9	49
CMCC-CMS	0.75	147	12	56
CNRM-CM5	0.70	153	18	58
CSIRO-Mk3-6-0	0.75	135	0	78
EC-EARTH	0.81	147	12	46
FGOALS-g2	0.83	114	-21	44
FGOALS-s2	0.80	129	-6	51
FIO-ESM	0.57	165	30	91
GFDL-CM3	0.81	174	39	68
GFDL-ESM2G	0.78	192	57	89
GFDL-ESM2M	0.81	192	57	84
GISS-E2-H	0.73	138	3	65
GISS-E2-H-CC	0.66	138	3	76
GISS-E2-R	0.73	129	-6	70
GISS-E2-R-CC	0.74	129	-6	68
HadGEM2-AO	0.84	156	21	67
HadGEM2-CC	0.84	150	15	58
HadGEM2-ES	0.83	150	15	64
inmcm4	0.82	150	15	57
IPSL-CM5A-LR	0.72	174	39	81
IPSL-CM5A-MR	0.73	177	42	88
IPSL-CM5B-LR	0.84	159	24	58
MIROC4h	0.67	171	36	86
MIROC5	0.70	189	54	103
MIROC-ESM	0.48	174	39	105
MIROC-ESM-CHEM	0.55	177	42	100
MPI-ESM-LR	0.68	162	27	67
MPI-ESM-MR	0.69	165	30	71
MPI-ESM-P	0.68	156	21	64
MRI-CGCM3	0.76	132	-3	60

NorESM1-M	0.54	189	54	107
NorESM1-ME	0.58	189	54	103
Model Mean (44)	**0.79**	**159**	**24**	**71**

To diagnose model errors, we determine the errors in the structure of low level moisture flux into the SIOCZ region in models to understand the key controls in the formation and maintenance the SIOCZ. SST climatology is also assessed in multi-model ensembles to investigate the links and potential relationships between SSTs and precipitation.

To determine SIOCZ variability, empirical orthogonal functions (EOFs) of DJF precipitation, for a 30 year period over southern Africa are derived for both models and observations. The first 3 EOFs are calculated for observations, as well as for all CMIP5 and AMIP models, from which the EOF with the highest association with the observed EOF 1 is chosen for further model analysis. Composite analysis of specific humidity, zonal and meridonal winds are evaluated to link the large-scale circulation to interannual variability of the SIOCZ. Global maps correlating the EOF (time coefficients) to global SSTs are created to determine major SST teleconnection regions.

3. Model representation of the SIOCZ

3.1. SIOCZ climatology bias

As discussed in Section 1 southern African austral summer climate is dominated the SIOCZ, which is driven by the circulation around the Angola Low and SIOHP, and an additional influx from the north-west region. These three moisture flux pathways converge at low-levels (850hPa) to form the SIOCZ (Figure 1).

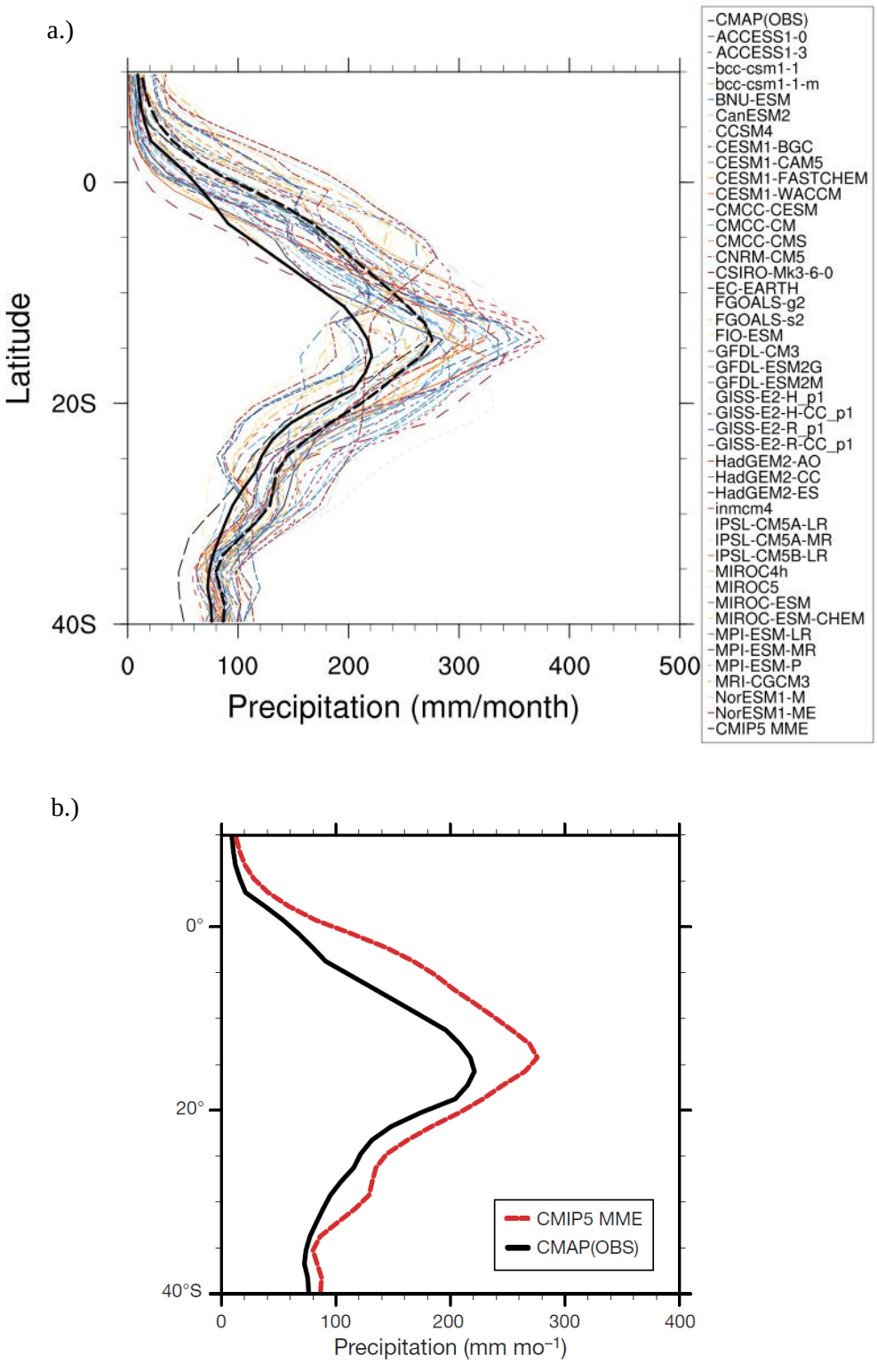

FIG 2: (a) Zonal mean (averaged over longitudes 25˚E to 50˚E) DJF precipitation from observations (CMAP – solid bold black line), 44 individual CMIP5 models and CMIP5 MME (dashed bold black line) for the period 1979/80-1998/99. (b) same as (a) but only

including observations (CMAP — solid bold black line), and the CMIP5 multi-model ensemble (MME, dashed red line).

The zonal mean precipitation distribution indicates that most CMIP5 models overestimate the intensity of precipitation over the SIOCZ region in some models by up to 100 mm/month (Figure 2). The overall model bias over the SIOCZ region is 24 mm/month, which is 18% of the observed mean of 135 mm/month (Table 2), with a standard deviation (not shown) of 17 mm/month. This indicates the multi-model mean (MMM) is relatively close to observations; however individual models show relatively high positive biases as well as excessively large RMSEs. Model RMSE average 71 mm/month, which is approximately 53% or over a factor of 2 in excess of the climatological mean.

3.2. Spatial structure of the SIOCZ

The majority of CMIP5 models capture the spatial distribution of precipitation reasonably well in terms of identifying the SIOCZ (Figure 3). Main points to note are i) models exhibit a lack of continuity in the SIOCZ, i.e., a clear break in precipitation is seen between land and ocean, ii) majority of models simulate excessive precipitation over the southern African continent and adjacent Indian Ocean.

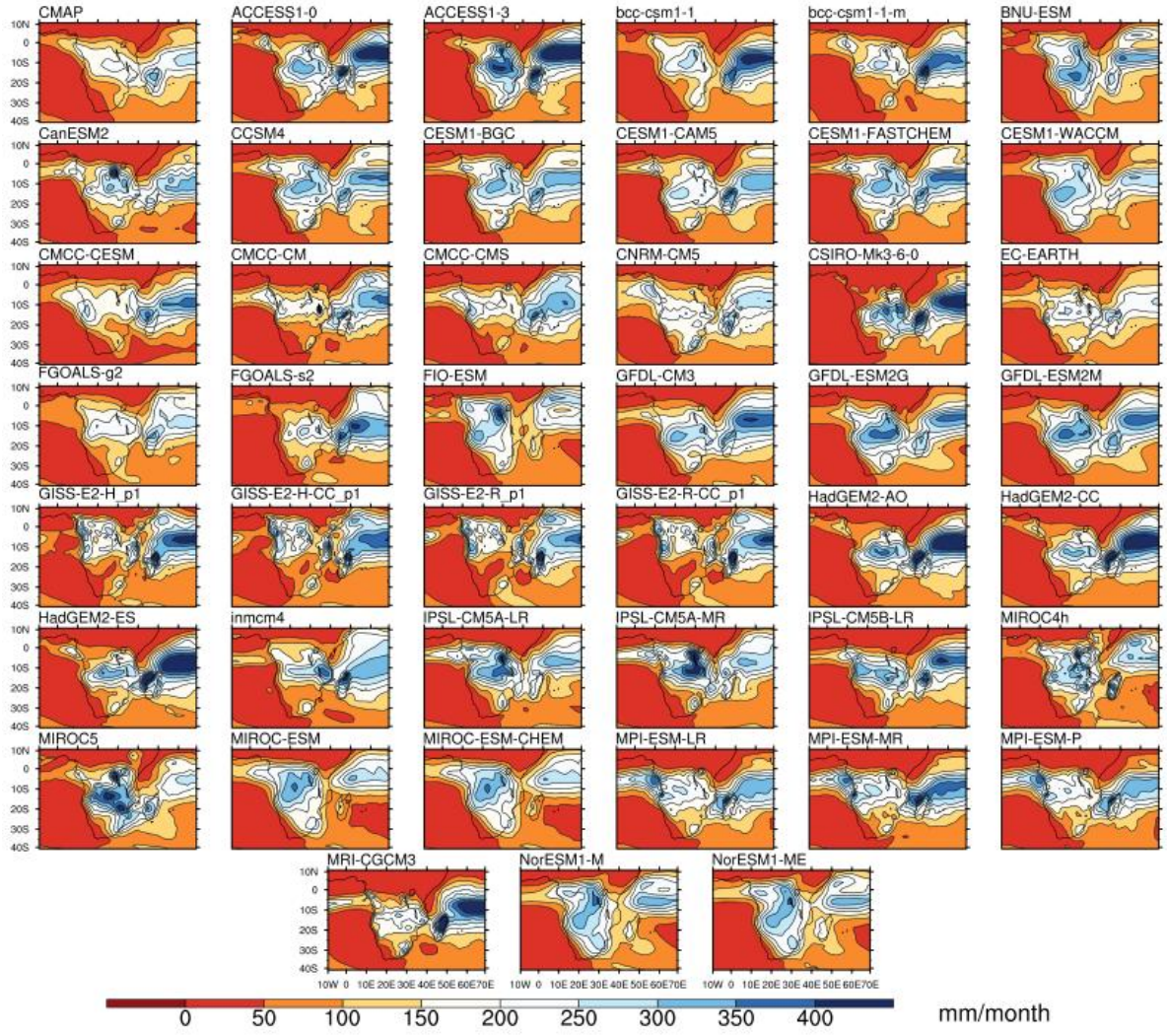

FIG 3: Mean DJF precipitation (mm month^{-1}) over wider study region (1979/80-1998/99) for the 44 CMIP5 models.

The MMEs for both CMIP5 and AMIP have a SIOCZ that is relatively underestimated when compared to the positive precipitation bias over the continent and Indian Ocean (Figure 4). The SIOCZ does not have a negative bias, however when compared to the excessive bias over land and the Indian Ocean, the SIOCZ is potentially being relatively underestimated in models. AMIP has however reduced these biases in both regions demonstrating a coupled model error. Both MME plots show the SIOCZ to be too zonal in structure, particularly the CMIP5 MME.

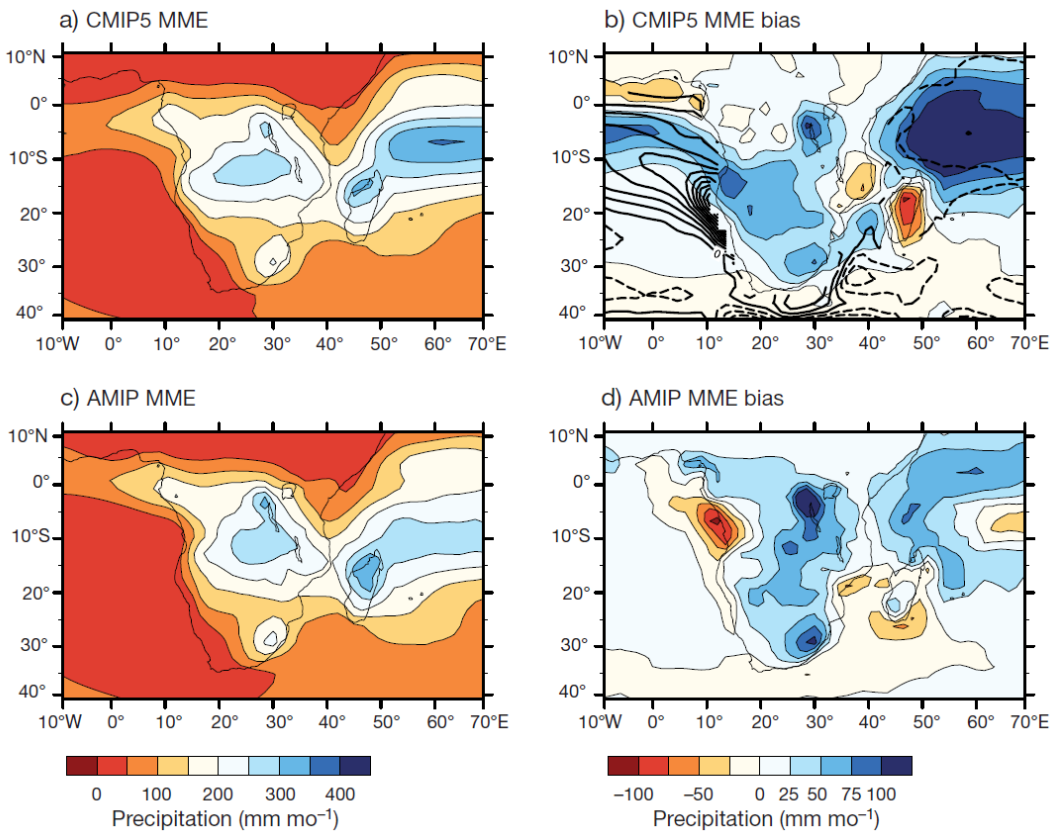

FIG 4: Model simulations of study region precipitation. Multi-model ensemble (MME) mean DJF precipitation (mm month^{-1}, 1979/80-1998/99) from CMIP5 (a) and AMIP (c) model runs (using the 27 models in common) and their respective biases against CMAP (see Figure 1). In (b) SST MME mean bias from CMIP overlaid (black contours with 0.5 K intervals where solid lines are positive and dashed negative values.

SSTs are overlaid on the CMIP5 MME bias plot (b) to potentially understand the large ocean precipitation bias. A negative SST bias (~-0.5˚C) is found over the Indian Ocean, therefore not explicitly explaining the overestimation of precipitation in this area by means of an overly warm ocean. Whereas, over the Atlantic Ocean, there is a large positive SST bias (~2˚C), which may be linked to the precipitation bias over this region. However both thermodynamic (local SST) and dynamic (circulation) components can contribute to precipitation biases. In recent studies by Bollasina and Ming (2013) the

dynamic contribution tends to explain the excessive precipitation bias through anomalous circulation over the Indian Ocean.

Spatial correlations between observed and modelled DJF precipitation over the SIOCZ region are shown in Table 2. Majority of models have a correlation coefficient above 0.7 and only 1 model (MIROC-ESM) below 0.5, therefore confirming that the vast majority of the models are able to capture the spatial structure of the summer rainfall pattern well over the SIOCZ region. Models with the highest spatial correlations e.g. bcc-csm1-1 (0.85) and CESM1-CAM5 (0.87), also tend to have the lowest or lower biases (0.3 & 0.7) and RMSEs (1.41 & 1.77).

3.3. Moisture flux and large scale regional circulation

The MME moisture flux bias shows that models on average over-simulate the three sources of moisture flux into the SIOCZ, particularly moisture flux pathway (2) from the NE Monsoon flow (from Figure 1), as well as the low-level moisture flux around the Angola Low, moisture flux pathway (1), where more moisture flux convergence (orange and red shading) is evident in Figure 5a. This may explain the excessive precipitation found over the continent in models. To deduce if moisture (specific humidity) or circulation (zonal and meridonal winds) contributes less/more/equally to the moisture flux bias, plots of observed specific humidity and MME wind bias and observed winds and MME specific humidity biases at 850hPa are shown in Figure 5(b) and (c) respectively. By plotting one observed component and one MME component of moisture flux at a time, this can determine which variable contributes most to the moisture flux bias. In this case the circulation component is almost solely responsible for the bias of moisture flux in CMIP5 models.

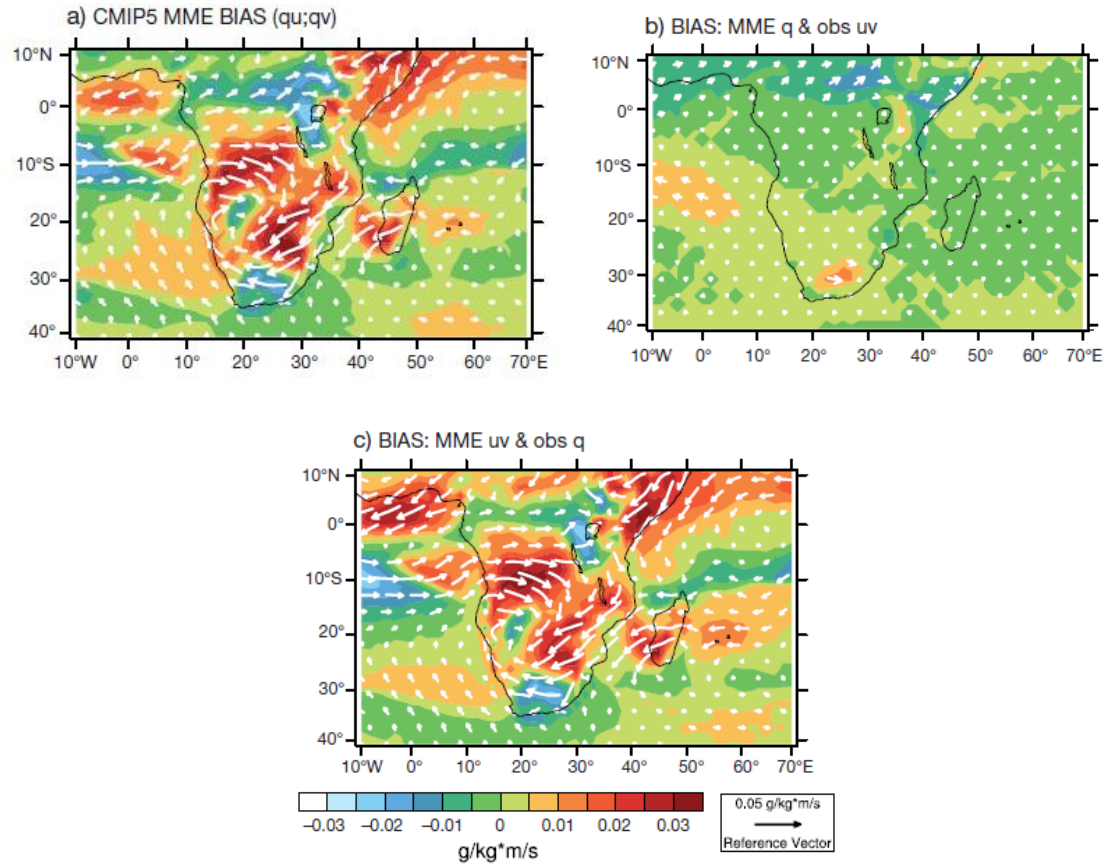

FIG 5: (a) CMIP DJF 850hPa moisture flux bias (g kg^{-1} * m s^{-1}, magnitude shaded) for the period 1979/80-1998/99. (b) as (a) but derived using observed ERA-Interim winds and CMIP MME mean specific humidity bias and (c) same as (a) but derived using observed ERA-Interim specific humidity and CMIP MME mean u and v wind biases.

Figure 6 shows three individual model biases for 850hPa moisture flux and moisture flux magnitude. ACCESS1-0 shows a moisture flux bias pattern most representative of most CMIP5 models. FGOALS-g2 bias is lower than most models and notably does not exhibit excessive precipitation in the DJF climatology (Figure 3). MIROC-ESM-CHEM exhibits large biases from all three moisture flux pathways identified in Figure 1. It is interesting to note that very wet models (seen in Figure 3) tend to show excessive moisture flux in excessively wet regions. For example ACCESS1-3 and MIROC-ESM-CHEM exhibit excessive precipitation over central southern Africa and both models

show a large positive bias of low-level moisture flux over the same region. Therefore low-level moisture flux in models that is erroneously high may be a reason for the precipitation bias, particularly over the continent (e.g. Washington et al. 2013).

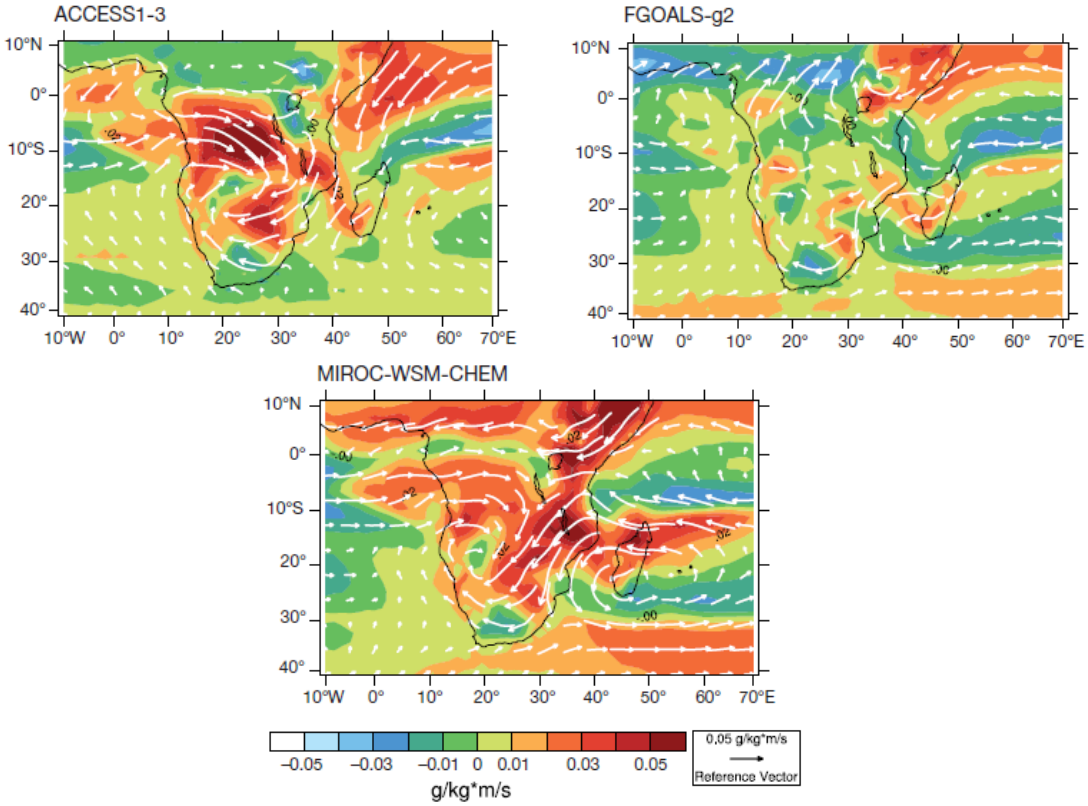

FIG 6: As Figure 5(a) but for 3 individual selected, contrasting models from the CMIP archive.

4. Interannual Variability of the SIOCZ

4.1. Observed variability

Interannual modes of SIOCZ variability in both observations and models are determined using EOF analysis. In observations variability is characterised by a clear dipole pattern, which can be interpreted as a NE-SW shift in the position of the SIOCZ axis (Figure 7) (Cook, 2001). Composite analysis was applied to other diagnostic fields, specifically low-level specific humidity and wind reanalysis fields. The top minus the bottom 5

years from observed EOF 1 time series were derived. The variability of the wind circulation appears to be driven by anomalously strong anti-cyclonic circulation in the south-west Indian Ocean (Figure 8), which brings in moisture from the Indian Ocean into the convergence zone (moisture flux pathway 3, see Figure 1).

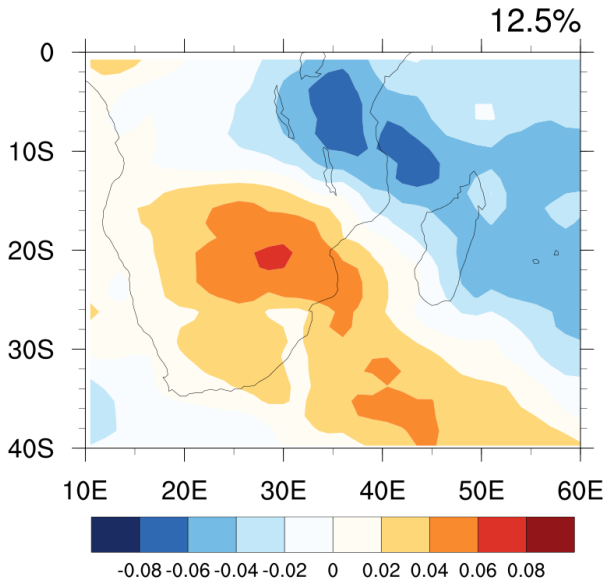

FIG 7: Primary DJF precipitation EOF calculated for CMAP for the 30 year period from 1979/80-2008/09. The percentage of the total variance explained is shown in the top right-hand corner of the plot.

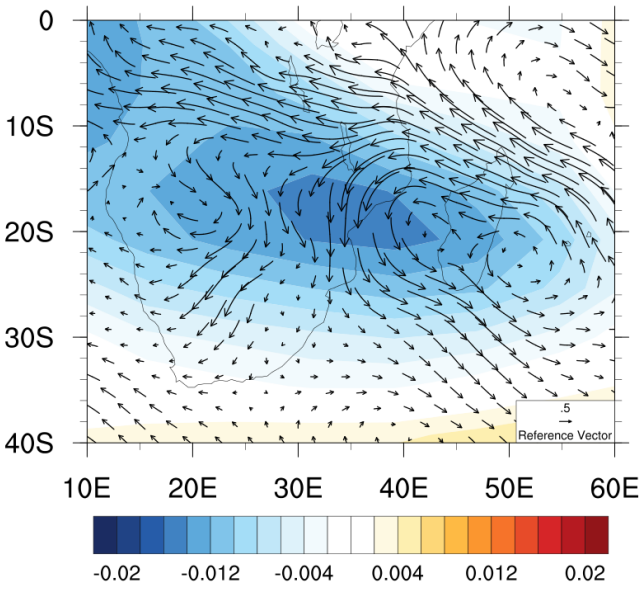

FIG 8: Moisture transport patterns associated with shifts in SIOCZ. 850hPa DJF moisture flux composite anomalies (g kg^{-1} * m s^{-1}) for top 5 DJF seasons minus the bottom 5 DJF seasons of the CMAP precipitation EOF time series (see text for details).

SIOCZ is clearly associated with dominant global and regional modes of interannual variability, apparent through correlations of EOF 1 time coefficients with global tropical SSTs (Figure 9 and Table 3). Specifically there is a significant correlation with ENSO and the SIOD at the 95% confidence interval (Table 3). The mean position of the SIOCZ lies approximately between the dipole pattern as shown in EOF 1 in Figure 7, consistent with previous analysis e.g. Cook (2001). Therefore the dipole pattern is indicating the variability of this feature, which is dominated by ENSO and the Indian Ocean (see Figure 9).

Table 3: Spatial correlations of CMAP EOF 1 against model EOF 1, 2, or 3 (whichever highest) and temporal correlations of CMIP5 models EOF 1 against the Niño3.4 index and SIOD index. (Significant correlations at 95% confidence interval given in italics in column 3 and 4)

Model/Observation	EOF Spatial Correlation	Temporal correlation of EOF 1 vs. Niño3.4	Temporal correlation of EOF 1 vs. SIOD
CMAP	/	*-0.39*	*-0.37*
ACCESS1-0	-0.69	-0.25	-0.06
ACCESS1-3	0.41	-0.01	-0.09
bcc-csm1-1	-0.51	0.07	-0.21
bcc-csm1-1-m	-0.61	0.24	-0.11

BNU-ESM	-0.35	*-0.42*	0.15
CanESM2	-0.83	-0.04	0.04
CCSM4	0.53	-0.27	0.19
CESM1-BGC	0.61	0.30	-0.03
CESM1-CAM5	-0.40	0.12	0.01
CESM1-FASTCHEM	-0.50	0.25	0.02
CESM1-WACCM	0.62	-0.15	0.01
CMCC-CESM	-0.33	0.21	0.03
CMCC-CM	-0.69	-0.01	0.05
CMCC-CMS	-0.83	0.09	0.10
CNRM-CM5	-0.41	-0.30	-0.10
CSIRO-Mk3-6-0	0.53	-0.29	-0.11
EC-EARTH	-0.72	-0.03	-0.02
FGOALS-g2	-0.54	0.16	0.07
FGOALS-s2	-0.68	0.01	0.02
FIO-ESM	-0.55	-0.05	0.05
GFDL-CM3	-0.71	-0.11	0.04
GFDL-ESM2G	0.54	-0.06	0.05
GFDL-ESM2M	0.68	*-0.43*	0.16
GISS-E2-H	0.54	-0.10	0.21
GISS-E2-H-CC	-0.69	0.07	0.24
GISS-E2-R	-0.38	0.02	0.03
GISS-E2-R-CC	0.43	0.10	-0.06
HadGEM2-AO	0.58	0.05	-0.15
HadGEM2-CC	0.68	0.09	0.02
HadGEM2-ES	-0.28	0.00	0.17
INMCM4	-0.51	0.24	-0.09
IPSL-CM5A-LR	-0.63	-0.10	0.15
IPSL-CM5A-MR	0.61	0.01	-0.09
IPSL-CM5B-LR	-0.47	-0.11	-0.21
MIROC4h	-0.46	0.05	0.04
MIROC5	0.44	-0.19	0.11
MIROC-ESM-CHEM	0.81	-0.10	*-0.34*

MIROC-ESM	-0.79	0.02	-0.02
MPI-ESM-LR	-0.4	-0.21	0.11
MPI-ESM-MR	0.58	0.11	-0.10
MPI-ESM-P	0.55	-0.11	0.24
MRI_CGCM3	0.49	-0.20	0.14
NorESM1-M	0.25	0.10	-0.20
NorESM1-ME	0.39	-0.07	-0.25

4.2. Model variability

In the majority of models a NW/SE dipole pattern indicative of the SIOCZ interannual variability emerges in the leading EOF. There was not any notable difference in skill between the CMIP5 and AMIP EOF plots. For 7 CMIP5 models there is no discernible SIOCZ dipole pattern similar to observations.

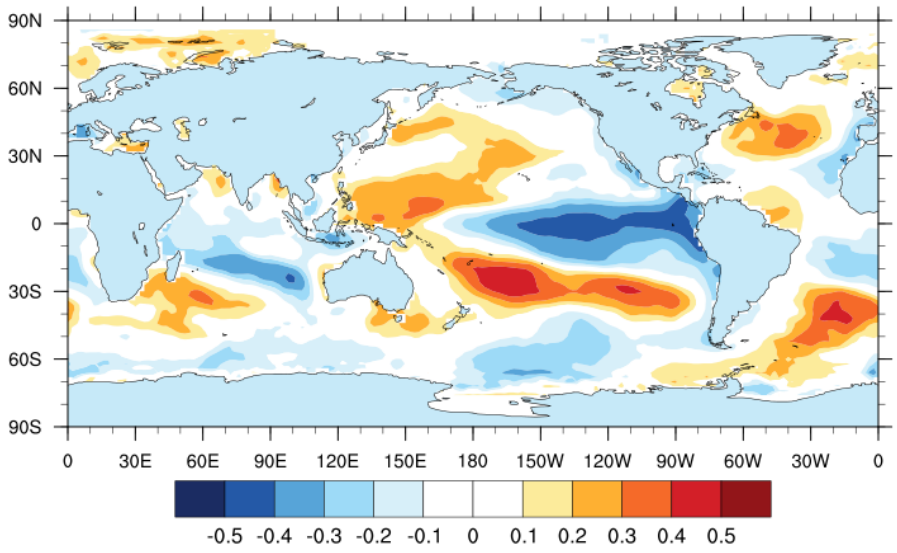

FIG 9: Teleconnections associated with SIOCZ variability. Correlation of CMAP EOF 1 time coefficients and observed global SSTs for DJF 1979/80-2008/09.

Observed drivers of variability are clearly distinguishable from Figure 9, with regions of highest correlations (~0.4) over the central Pacific and Indian Ocean. These global plots were replicated for CMIP5 and AMIP, however not shown due to space constraints. 17 out of 44 CMIP5 models have EOF spatial correlations greater than 0.6 compared to the observed EOF 1, in which 6 of these models correlations of greater than 0.6 are found in EOF 2. Of the 17 models that exhibit this dipole, only 9 depict global SST correlation patterns similar to observations, i.e. with highest correlations found over the Pacific and Indian Ocean.

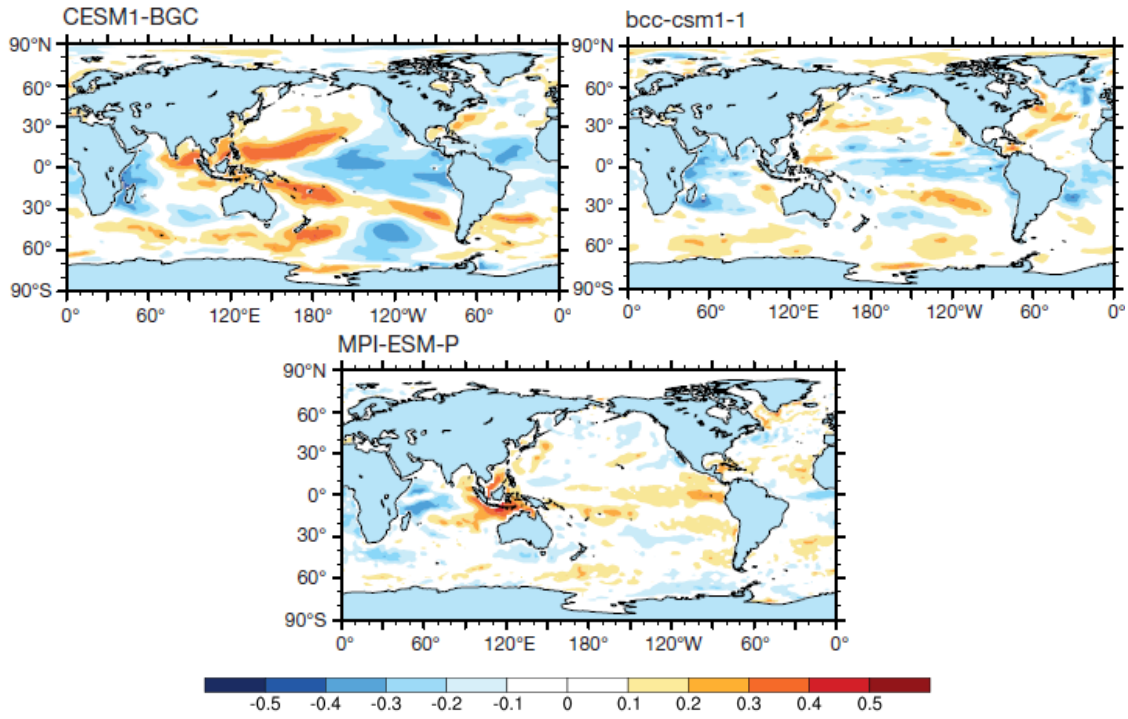

FIG 10: As in Fig. 9, but for 3 selected and contrasting CMIP models (CESM1-BGC: good, bcc-csm1-1: average, and MPI-ESM_P: poor)

Therefore the majority of CMIP5 models are not able to capture the relationship between the Pacific and Indian Ocean as in observations i.e. teleconnections. Three examples of these global correlation maps (CESM1-BGC: good, bcc-csm1-1: average

and MPI-ESM_P: poor) are shown (Figure 10). The vast majority of models are not able to capture the observed teleconnections, however are evidently better at capturing the ENSO teleconnection than the Indian Ocean influence (SIOD) (Table 3).

5. Discussion and Conclusions

The first key conclusion from this study is the majority of CMIP5 models perform well at simulating the spatial pattern of seasonal rainfall for DJF over southern Africa. An overall systematic bias toward an excessively wet southern African region is found, which is confirmed by the predominate amount of positive model biases and high RMSEs. However the SIOCZ itself is not particularly wet, but more the surrounding regions that exhibit excessive precipitation. Reasons for the SIOCZ itself not being particularly wet may be due to the dominant bias in the Indian Ocean as well as circulation biases that enhance moisture flux into the surrounding regions. There is a noticeable break in the SIOCZ in the vast majority of models between land and ocean. A potential reason for this break could be due to the different dynamics within models over land and ocean.

These systematic biases implied the need to identify the cause (potentially excessive moisture flux convergence in models (Washington et al., 2013) and SST biases in models (e.g. Brown et al., 2011) so these can be corrected for in models. Therefore biases in model moisture flux were investigated and were found to be anomalously high around the Angola Low. The bias is mainly due to large-scale circulation biases and not specific humidity biases (Figure 5).

SST biases showed a small negative bias over the Indian Ocean region in the MME, therefore not linked to the excessive precipitation through overly warm ocean temperatures resulting in more convection and hence rainfall. Further studies are required to understand this Indian Ocean precipitation bias, SST gradients in models may also be a potential contributor.

The EOF analysis provided the pattern of variabilty of the SIOCZ with the typical mean position of the SIOCZ located between the dipole pattern found in the primary EOF. This primary EOF also correlated significantly to Niño3.4 and the SIOD in observations. The dipole pattern found in EOF 1 could be interpreted as the movement or shift of the SIOCZ in wet and dry years i.e. La Niña and El Niño years respectively similar to the north-south displacement of the SPCZ during El Niño and La Nina years (e.g. Vincent et al., 2011), which is well captured by most CMIP3 (Brown et al., 2011) and CMIP5 (Brown et al., 2013) models. Most CMIP5 and AMIP (not shown) models captured the primary EOF dipole pattern consistent with observations, which imples the models do exhibit characteristics of variability to some extent, which is a step further in our understanding of model processes and dynamics. SIOCZ rainfall is complex in terms of variability as it is not just influenced by one major source but potentially several e.g. wave activity such as Rossby waves and the Matsuno-Gill response (Ratnam et al., 2014).

The large-scale circulation of the SIOCZ was linked through to variability via composite analysis of the primary observed EOF time series and moisture flux fields. Variability is dominated by moisture flux pathway 3 (anti-cyclonic circulation around

the SIOHP), feeding into the eastern parts of southern Africa. This anomalous circulation of moisture flux highlights the change of importance in the 3 moisture flux pathways.

There is a significant influence of ENSO and the SIOD on the meridonal position of the SIOCZ found in observations, however the CMIP5 and AMIP models were not able to significantly capture this relationship. Models make the SIOCZ shift north and southwards but not for the correct reasons i.e. weak correlations with Indian Ocean and Pacific SSTs. Implications are future climate change signals will be partly due to changes in SST gradients in the Pacific and Indian Ocean (e.g. changes to ENSO) (Power et al., 2006; Adler, 2011; Stevenson, 2012). Therefore models need to correctly simulate teleconnections presently, so future analyses can be valuable.

The findings of this paper are the first of its kind in which CMIP5 models are evaluated regarding their ability to capture the climatology and variability of the SIOCZ. These results have implications for regional climate projections using the set of CMIP5 models, such as which models are more accurate in capturing both mean state and variability (bcc-csm1-1 and bcc-csm1-1-m). Other implications include where biases are likely to be important within CMIP5 models such as in regions where there is excessive moisture convergence in those regions. Further work is needed to explore what processes are responsible for the model precipitation biases and what other potential drivers are driving variability within CMIP5 models besides the observed influence of ENSO and the SIOD.

6. Acknowledgments

This work was supported by the Peter Carpenter Scholarship for African Climate Change through the University of Sussex and the Natural Environment Research Council (NERC) Future Climate for Africa (FCFA) regional consortium project 'UMFULA', reference: NE/M020258. We also acknowledge the World Climate Research Programme's Working Group on Coupled Modelling responsible for the CMIP5 model data, which was provided by the Program for Climate Model Diagnosis and Intercomparison (PCMDI). More information on this model data can be found at the PCMDI website (http://www.pcmdi.llnl.gov).

7. Caveats and Implications

Biases exhibited over the Indian Ocean are not well understood and cannot be explained in this chapter and hence require further analysis. CMIP5 model parameterisation schemes are most likely responsible for creating the Indian Ocean bias.

Austral summer over southern Africa is not only influenced by interannual variability but additionally decadal variability (Dieppois et al., 2016). The signal of decadal variability is not as large as that of interannual variability over the region and hence the reason for exclusion in this chapter. However, climate change signals occur at decadal time-scales and therefore should be assessed in historical variability to determine and understand drivers of this decadal variability. This is a noted caveat in this thesis and

therefore future work including analysis of variability at this time-scale should prove valuable and provide additional insight to southern African variability.

Another note to highlight regarding the lack of significant teleconnections exhibited in CMIP5 models compared to observations may be due the fact that the dominant mode of variability does not emerge within the first 3 principal components of the EOF analysis. Additional principal components could be derived and correlated to global SST's to address this, however is not likely as principal components reduce in the amount of variability explained as more principal components are derived.

Chapter 4

Summary of Projected Key Climate Change Signals over SA/SWIO

Overview

This chapter summarises future changes of projected precipitation and various diagnostic variables over southern Africa (SA) and the south-west Indian Ocean (SWIO). The most prominent climate change signals are identified and investigated in more detail. Future changes in the dominant austral summer feature, the SIOCZ, are additionally evaluated using an algorithm to quantitatively identify this feature in both historical and future simulations. Model processes of change are understood through determining potential links between projected precipitation changes and various diagnostic variables such sea surface temperatures and circulation patterns. Idealised future atmosphere-only experiments are assessed to potentially enhance understanding in projections.

Key Questions:

1. What are the key projected changes in precipitation over southern Africa?

2. When do the key projected precipitation climate change signals occur?

3. What are the changes to the SIOCZ feature in future projections?

4. Are links established between precipitation changes and diagnostic variables?

5. Do atmosphere-only (AMIP) future experiments aid understanding of projected precipitation changes?

6. What is the importance and implications of these projected changes and potential impacts on the region?

1. Introduction

1.1. Water security over southern Africa

It is important to identify and understand future changes of precipitation over southern Africa, as it is a region of low adaptive capacity and particularly vulnerable to climate change (Basher and Briceno, 2006; Meadows, 2006; Kusangaya et al., 2014). Economic growth over the region is on the rise and therefore vitally important for future decisions to be addressed with the most advanced climate change information available; however additional understanding and awareness regarding the level of associated uncertainty with these projected changes (Swart et al., 2009). More informed adaptation decisions can therefore be made regarding water security in terms of agriculture and subsistence farming (Collins et al., 2012; Knutti et al., 2010). The ultimate goal aims to ensure

economic growth becoming sustainable in future decades when climate change signals are most prominent and therefore have enhanced impacts on water security.

1.2. Seasons of future importance

Projected monthly changes in precipitation are assessed to determine in which months/seasons the most prominent climate change signals emerge. Focus is placed on projected precipitation changes for the seasons OND and DJF, which will be analysed more thoroughly throughout this chapter and subsequent chapters. This is due to the importance of these two seasons i) DJF - austral summer and dominant rainfall season over the region providing largest contributions to annual rainfall over SA/SWIO and ii) OND - determines the onset of summer rainfall over southern Africa, impacting planting and harvesting timing for agriculture.

The dominant austral summer rainfall feature (the SIOCZ), previously evaluated in contemporary climatology in Chapter 3, is analysed here regarding future projected changes in the SIOCZ. Projected changes in orientation, position and intensity of the SIOCZ are assessed, due to the significant reliance on this feature in providing the majority of rainfall totals over the region (Cook, 2000; Manhique et al., 2011).

Considering global tropical changes in moisture and circulation, it is noted over the Pacific Ocean how flow has altered and re-directed out of the SPCZ region and into the equatorial ITCZ region. Various studies confirm drying of the SPCZ (Widlansky et al., 2011; Widlansky et al., 2013; Chung et al., 2014) and the ITCZ is shown to get

increasingly wet. Studies state that the warmest-get-wetter hypothesis holds true for the ITCZ in the Pacific Ocean region (Brown et al., 2012; Brown et al., 2013; Widlansky et al., 2013). Therefore a potential and consistent hypothesis over tropical southern Africa could be the SIOCZ becomes less prominent i.e. less wet, while the Indian Ocean ITCZ becomes enhanced with increased wetting, through enhanced convergence and moisture flux into the region.

1.3. Understanding model change

Decreased precipitation over the subtropics is a commonly accepted notion of future climate projections (Allen and Ingram, 2002; Neelin et al., 2006; IPCC, 2007; Cai et al., 2012; He and Soden, 2016). Difficultly arises in determining drivers of this projected change and how credible these changes are (He and Soden, 2016; Long et al., 2016). Two mechanisms of change over the subtropics are typically used to inform understanding i) increased moisture flux away from the subtropics and into the warmest-get-wetter regions (Held and Soden, 2006; Huang et al., 2013)) and ii) a shift of subsidence over the subtropics towards the polar regions due to the poleward expansion of the Hadley cell (Cai et al., 2012; Scheff and Frierson, 2012a; 2012b). Individual models are used to highlight common processes within models creating future change.

Atmosphere-only (AMIP) simulations for various future experiments can be used to aid understanding of future precipitation projections. AMIP models provide insight through idealising specific scenarios such as focusing on the effect of one or more particular forcings at a time (Gates, 1999). For example future precipitation change can be

assessed using CO_2 as the dominant forcing, other examples include prescribing models with future SST patterns to determine how change is affected and shown to change. This chapter aims to understand and provide insight into model behaviour i.e. whether models act in a coherent manner regarding their future projected precipitation changes. Links are investigated between model processes and projected changes in precipitation (i.e. do CMIP5 models that produce large wetting climate change signals exhibit excessive moisture flux transport as identified as a previous bias in Chapter 3? Or higher SSTs?)

2. Data and Methods

2.1. Data

To identify and summarise future precipitation projections and diagnostic variables over SA and the SWIO, output from a total of 39 CMIP5 model simulations for the 20th century and the 21st century (under the RCP8.5 emissions scenario) are used (see Table 1). Models used are from the WCRP CMIP5 multi-model dataset, which provide results for the most recent assessment report (AR5) of the IPCC (Meehl et al., 2007; Taylor et al., 2012).

Additionally five AMIP future experiments (Gates, 1992; Gates et al., 1999) are analysed to understand the role of SST warming, CO_2 and pattern effects (see glossary of future AMIP experiments defined in section 3.5).

Both the multi-model mean (MMM) of the 39 chosen CMIP5 models are analysed as well as inter-model spread of model projections across the 39 model ensemble. Monthly data was extracted for precipitation and other key diagnostic variables to understand processes that may be linked to precipitation changes over the SA/SWIO sector. Area of future analysis includes 10˚N - 40˚S and 0˚ - 80˚E. The period of analysis was derived from the RCP8.5 scenario 2071-2100 minus the historical period 1971-2000, where only the first ensemble member was utilized in creating the MMM. For the future AMIP experiments precipitation anomalies are taken as the 30 year mean of each experiment minus the 30 year mean of the AMIP control run using the period 1979-2008. All model data was interpolated to a common grid of 1.5˚ X 1.5˚ to ensure uniformity.

Table 1: CMIP5 model list of the 39 CMIP5 models used including modelling center, institute ID and atmospheric. (Models marked with an asterisk (*) indicates models where the atmosphere-only version of the model was also used in the analysis). Models in italics are where only the atmosphere-only version is used.

Model Name	**Modeling Center (or Group)**	**Institute ID**	**Atmospheric Resolution**
ACCESS1.0 **ACCESS1.3**	Commonwealth Scientific and Industrial Research Organization (CSIRO) and Bureau of Meteorology (BOM), Australia	CSIRO-BOM	1.25˚ x 1.9˚
BCC-CSM1.1*	Beijing Climate Center, China Meteorological Administration	BCC	2.8˚ x 2.8˚
BNU-ESM	College of Global Change and Earth System Science, Beijing Normal University	GCESS	2.8˚ x 2.8˚
CanESM2 ***CanAM4****	Canadian Centre for Climate Modeling and Analysis	CCCMA	2.8˚ x 2.8˚
CCSM4*	National Center for Atmospheric Research	NCAR	0.94˚ x 1.25˚

CESM1(BGC) **CESM1(CAM5)**	Community Earth System Model Contributors	NSF-DOE-NCAR	0.94˚ x 1.25˚
CMCC-CM **CMCC-CMS**	Centro Euro-Mediterraneo per I Cambiamenti Climatici	CMCC	0.75˚ x 0.75˚ 1.9˚ x 1.9˚
CNRM-CM5*	Centre National de Recherches Météorologiques / Centre Européen de Recherche et Formation Avancée en Calcul Scientifique	CNRM-CERFACS	1.4˚ x 1.4˚
CSIRO-Mk3.6.0	Commonwealth Scientific and Industrial Research Organization in collaboration with Queensland Climate Change Centre of Excellence	CSIRO-QCCCE	1.9˚ x 1.9˚
EC-EARTH*	EC-EARTH consortium	EC-EARTH	1.1˚ x 1.1˚
FGOALS-g2	LASG, Institute of Atmospheric Physics, Chinese Academy of Sciences and CESS,Tsinghua University	LASG-CESS	2.8˚ x 2.8˚
FIO-ESM	The First Institute of Oceanography, SOA, China	FIO	2.8˚ x 2.8˚
GFDL-CM3 **GFDL-ESM2G** **GFDL-ESM2M**	NOAA Geophysical Fluid Dynamics Laboratory	NOAA GFDL	2.0˚ x 2.5˚
GISS-E2-H_p1 **GISS-E2-H_p2** **GISS-E2-H_p3** **GISS-E2-R_p1** **GISS-E2-R_p2** **GISS-E2-R_p3**	NASA Goddard Institute for Space Studies	NASA GISS	2.0˚ x 2.5˚
HadGEM2-AO ***HadGEM2-A******	National Institute of Meteorological Research/Korea Meteorological Administration	NIMR/KMA	1.25˚ x 1.9˚
HadGEM2-CC **HadGEM2-ES**	Met Office Hadley Centre (additional HadGEM2-ES realizations contributed by Instituto Nacional de Pesquisas Espaciais)	MOHC (additional realizations by INPE)	1.25˚ x 1.9˚
INM-CM4	Institute for Numerical Mathematics	INM	1.5˚ x 2˚
IPSL-CM5A-LR* **IPSL-CM5A-MR** **IPSL-CM5B-LR***	Institut Pierre-Simon Laplace	IPSL	1.9˚ x 3.75˚ 1.25˚ x 2.5˚ 1.9˚ x 3.75˚

MIROC-ESM **MIROC-ESM-CHEM**	Japan Agency for Marine-Earth Science and Technology, Atmosphere and Ocean Research Institute (The University of Tokyo), and National Institute for Environmental Studies	MIROC	2.8˚ x 2.8˚
MIROC5*	Atmosphere and Ocean Research Institute (The University of Tokyo), National Institute for Environmental Studies, and Japan Agency for Marine-Earth Science and Technology	MIROC	1.4˚ x 1.4˚
MPI-ESM-LR* **MPI-ESM-MR***	Max-Planck-Institutfür Meteorologie (Max Planck Institute for Meteorology)	MPI-M	1.9˚ x 1.9˚
MRI-CGCM3*	Meteorological Research Institute	MRI	1.1˚ x 1.1˚
NorESM1-M **NorESM1-ME**	Norwegian Climate Centre	NCC	1.9˚ x 2.5˚

2.2. Multi-model analysis of change and spread

There is no definitive consensus regarding which models to choose when understanding future projections (IPCC, 2001; Tebaldi and Knutti, 2007) and hence when evaluating future change the consensus is to use the multi-model mean (MMM) change (e.g. IPCC, 2013a). Therefore to identify and summarize changes in precipitation projections and various diagnostic variables, the MMM is used predominantly throughout this chapter. To gauge the level of model agreement within these changes, the standard deviation is derived for the MMM of projected precipitation change. Individual models are additionally assessed to highlight processes most likely creating future change in precipitation using diagnostic variable analysis.

Changes in precipitation in this chapter are expressed in both absolute terms and percentage change. Percentage change is calculated by dividing the future 30 year mean change (2071-2100) by the historical 30 year mean climatology (1971-2000) and multiplying by 100. This is to ensure larger signals in absolute terms in projected

precipitation changes are not misinterpreted due to the effect of historical precipitation totals over a specific region. Percentage change ensures that model change is scaled accordingly with respect to historical totals of individual models, therefore removing individual model sensitivity to projected change. Signal to noise ratios are additionally derived to determine which regions over southern Africa exhibit signals of precipitation change exceeding model disagreement. The signal to noise ratio in this study is calculated as follows:

$Signal / Noise = |\Delta P| / \sigma\Delta P$,

Where $|\Delta P|$ is the absolute value of the MMM precipitation change and

$\sigma\Delta P$ is the standard deviation of the MMM precipitation change.

2.3. SIOCZ algorithm to quantify future change

The SIOCZ is a diagonally oriented precipitation band which is the dominant austral summer climatological feature over southern Africa. In order to quantify projected changes in this feature a quantitative metric is applied to identify the SIOCZ in observations and historical simulations. The algorithm involves deriving a best-fit line along maximum precipitation values within the SIOCZ domain (chosen to cover 0˚ - 30˚S and 25˚E - 50˚E). This metric is adapted from Brown et al's (2011) methodology, where the algorithm is applied to identify the SPCZ. The mean latitude and slope values of the SIOCZ axis are derived for observations, historical simulations and future projected changes, which are compared regarding position and orientation. This algorithm has inherent limitations attributable to the best-fit line being influenced by outliers of maximum precipitation loci within the chosen domain in individual models. To address this problem as best as possible the region is constrained to a rather small

domain such that the ITCZ is not included in the SIOCZ signal. Additionally MMM projected changes in the SIOCZ are assessed, therefore reducing the influence of individual model errors of misplaced ITCZ loci.

2.4. Diagnostic variables of future projections

In this Chapter the following variables and diagnostic variables will be assessed, projected changes in precipitation, annual cycle of precipitation, temperature, sea surface temperatures, mean sea level pressure, specific humidity at 850hPa, zonal and meridonal winds at 850hPa (circulation), low-level moisture flux at 850hPa and vertical velocity (uplift) at 500hPa i.e. to assess weakening of the tropical circulation.

2.5. Future atmosphere-only experiments

Atmosphere-only simulations for five various AMIP future experiments are assessed to determine if idealised future experiments aid in understanding projected precipitation changes over southern Africa. There are a limited number of AMIP model runs and all available AMIP future experiment model runs (11 individual AMIP models) are utilised for this analysis. To ensure consistency in comparison, the same 11 models from the coupled runs (CMIP5) were used to create the MMM of future precipitation changes for the RCP8.5 scenario (see Figure 11 below).

3. Key changes over southern Africa and the SWIO

3.1. Projected changes in precipitation

3.1.1. Spatial patterns of annual precipitation change

Projected changes in annual precipitation and temperature are initially evaluated to obtain a broad overview of future change over southern African (Figure 1a and b). Precipitation over much of the continent is indicated to decrease and more significantly in the subtropical regions from approximately 10˚S to 30˚S, where warming is also enhanced (Figure 1b). Whereas tropical regions, i.e. Congo (~0˚S) are getting wetter and warming at a slightly lower rate than the subtropics. Northern and Eastern southern Africa show increasing precipitation, as well as the adjacent Indian Ocean in the more northern regions. The pattern of projected precipitation change exhibits a distinct zonal structure typical of a dipole pattern, where defined bands of wetting from approximately 10˚N to 10˚S and drying from 10˚ to 40˚S. There is a localised wetting signal (stronger in magnitude in austral summer – see Figure 4 and 6) at approximately 30˚S and 30˚E. This is a coastal region with increased orography as one moves inland over the escapement towards Lesotho.

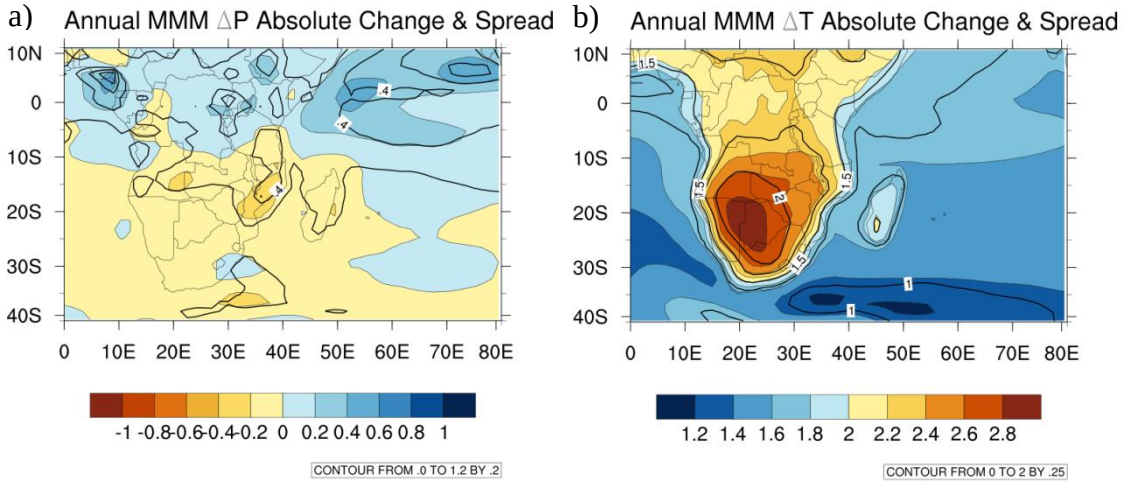

Figure 1: Absolute projected annual MMM (a) precipitation and (b) temperature change (mm day^{-1} and K respectively) for the period 2071-2100 minus 1971-2000 for RCP8.5 emissions scenario. Overlaid contours (black) indicate standard deviation in mm day^{-1} ranging from 0 to 1.2 in intervals of 0.2 and 0 to 2 by 0.25 respectively.

Additionally each calendar month of absolute precipitation change is analysed to determine in which months the largest precipitation climate change signals emerge. From Figure 2, drying is projected over much of the subtropical southern African continent for each calendar month (evident in Figure 1); however the largest and most dominant signals of wetting and drying are evident in October, November and December. This dipole of projected precipitation change is most noteworthy during those months, which indicate a zonal climate change signal that is clear over both the continent and Indian Ocean (less zonal in October, with a drying locus evident over the western continent at ~10˚S). The drying signal evident in the early summer transition season can have significant impacts including later onset of summer rainfall and/or reduced rainfall totals received, adversely affecting agriculture over the region. Therefore this assessment of projected precipitation change highlights OND as an important season of future change requiring further investigation.

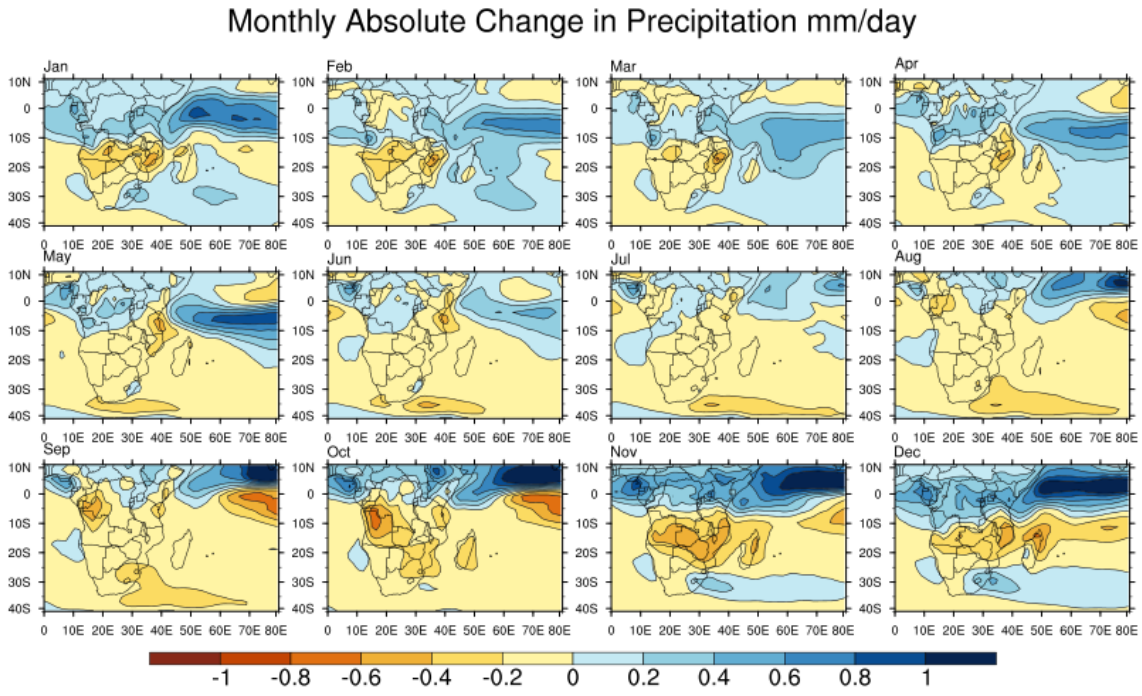

Figure 2: Absolute projected monthly MMM precipitation change in mm day^{-1} for the period 2071-2100 minus 1971-2000 for RCP8.5 emissions scenario.

3.1.2. Projected changes in the annual cycle of precipitation

Time versus latitude plots (Figure 3) of absolute changes in projected precipitation *(*ΔP*)* confirms a dipole (tripole in some regions) pattern that emerges in the spatial plots of ΔP over southern Africa (Figure 2). The climate change signal is most prominent and largest in magnitude from approximately September/October through to December, when the dipole pattern of wetting and drying is most evident over both SA and the SWIO.

The most notable differences between land and ocean regions projected precipitation changes are i) the timing of the dipole and ii) the intensity of wetting and drying signals.

Over the SA continent the dipole pattern is most prominent during October-November-December and over the SWIO is most prominent later on during November-December-January. Interesting result to note the drying signal commences earlier over the continent than over the adjacent Indian Ocean region. This lag between ocean and continent may be explained by ocean influences driving continental changes through circulation patterns and moisture flux transport (Shepherd, 2014) from the Indian Ocean or land-sea contrasts (Dong et al., 2009; Byrne and O'Gorman, 2013; 2015). This is explored further in Chapter 5.

Regarding intensity of projected precipitation changes, the Indian Ocean exhibits the strongest wetting signal over the equatorial regions commencing from July-August and tapering off towards January-February. The wetting signal over the SWIO migrates southward of the equator into the southern hemisphere only towards December-January. The drying signal is similar in magnitude over both land and ocean; however over land drying covers a slightly larger domain. Wetting is additionally much weaker over the continent than the ocean, which is expected due to the unlimited availability of moisture over the ocean.

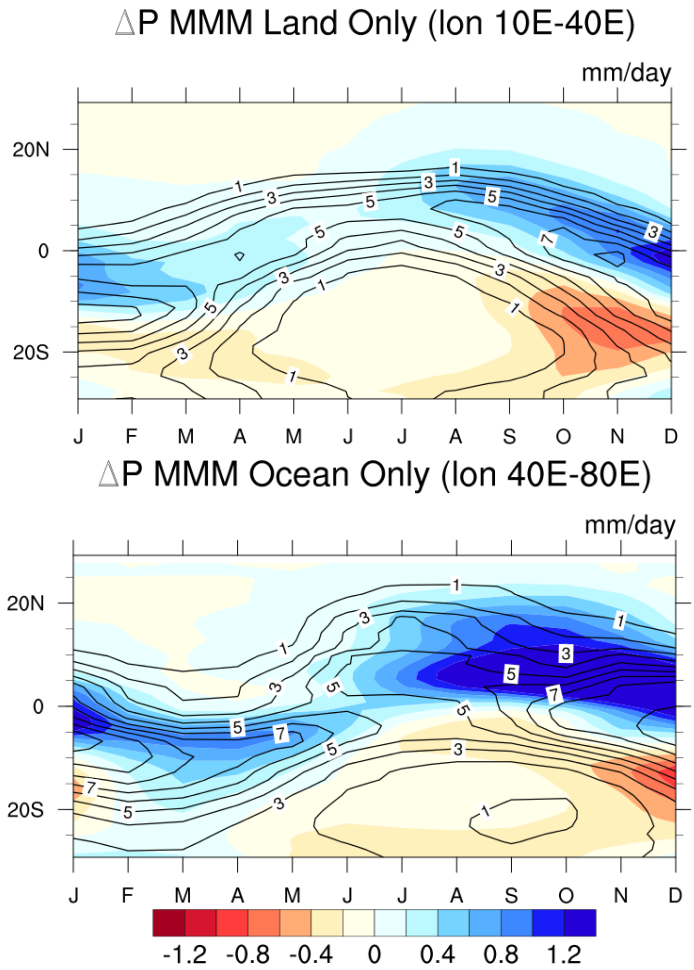

Figure 3: Time versus latitude plots of absolute precipitation changes *(ΔP)* in mm day^{-1} for both land (top) and ocean (bottom) (regions 0˚ - 30˚S and 10˚E - 40˚E and 40˚E - 80˚E respectively) for RCP8.5 for the period 2071-2100 minus 1971-2000. Overlaid black contours represent present day precipitation climatology in mm day^{-1} contoured from 1 to 10.

Continental and ocean regions historical precipitation contours are overlaid in Figure 3, which do not coincide with projected changes in precipitation, but rather more evidently the wetting/drying signal straddles the climatological maximum of historical precipitation, particularly over land in DJF. Therefore confirming that the wet-get-wetter mechanism of change does not hold true for the southern African region under

analysis. Due to the wetting signal being located over the equatorial regions; implications of a warmer-get-wetter mechanism of change is more plausible, which is explored in the Chapter 5. Over the continent historical precipitation maxima occurs during November, however future precipitation projections indicate precipitation a maximum shift eastwards (i.e. towards December). This implies a lag or delay in the precipitation maximum compared to contemporary climate, essentially delaying the onset of rainfall by approximately a month in the MMM. This is an important finding as this will impact agricultural practises and harvesting times over the region.

3.1.3. Seasonal changes in precipitation

Southern African experiences four distinct seasons throughout the year (Tyson and Preston-Whyte, 2000). Absolute precipitation change is assessed for these four seasons to identify when the largest absolute changes in precipitation occur, as well as inter-model spread. Spatial patterns of precipitation change in three out of the four season's exhibit a common trend of wetting over the northern parts and drying over the central continent, which is evident in the annual mean (Figure 1) and monthly analysis (Figure 2). Only JJA, the winter season exhibits a distinctly different pattern of precipitation change.

It is evident that spring (SON) and austral summer (DJF) exhibit the most notable absolute drying over most of the subtropical continent, with wetting evident over the northern Indian Ocean and equatorial continental region (Figure 4). Drying in SON spans a larger domain spanning further north than DJF wetting, which is located from 10˚S and northwards. This was established in Figure 2 where October exhibits a drying

loci evident over ~10˚S essentially shifting the drying signal into the nearby equatorial regions.

JJA is currently dry over most parts of southern Africa and especially the south-western region, however is projected to get even drier in future, particularly over the adjacent SWIO. Autumn (MAM) exhibits fairly similar spatial patterns of projected precipitation change to DJF, however slightly reduced magnitudes of change, especially drying over the subcontinent. In MAM drying over much of the continent is evident and wetting to the north (from ~10˚S) and over the adjacent Indian Ocean; however wetting is located more centrally over the Indian Ocean during the MAM season.

Inter-model spread is more prevalent over the wetting regions with larger model disagreement in those regions of change. Drying is somewhat more robust in terms of model agreement in most seasons; however DJF exhibits the highest model disagreement over the drying regions with largest standard deviations in the eastern subtropical continental region. Therefore drying over the south-western SA continent throughout the year can be deemed rather robust and hence more plausible.

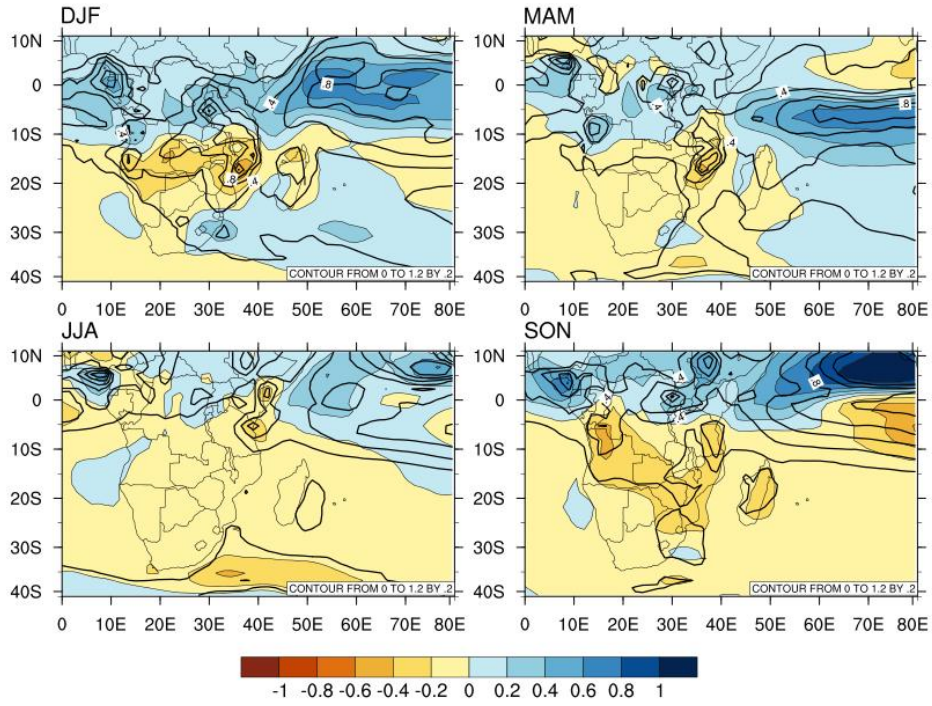

Figure 4: Plots of projected precipitation changes for the MMM using 39 CMIP5 models for the period 2071-2100 minus 1971-2000 for RCP8.5. All four seasonal means are displayed (DJF, MAM, JJA, SON). Overlaid contours (black) indicate standard deviation in mm day^{-1} ranging from 0 to 1.2 in intervals of 0.2.

Signal to noise ratios are useful in addressing impact assessments of climate change, as they provide a measure of signal strength compared to inter-model disagreement i.e. noise. Signal to noise ratios for all 12 calendar months over southern Africa are derived and displayed in Figure 5. The higher the ratio value, the larger the precipitation signal strength opposed to noise from model uncertainty.

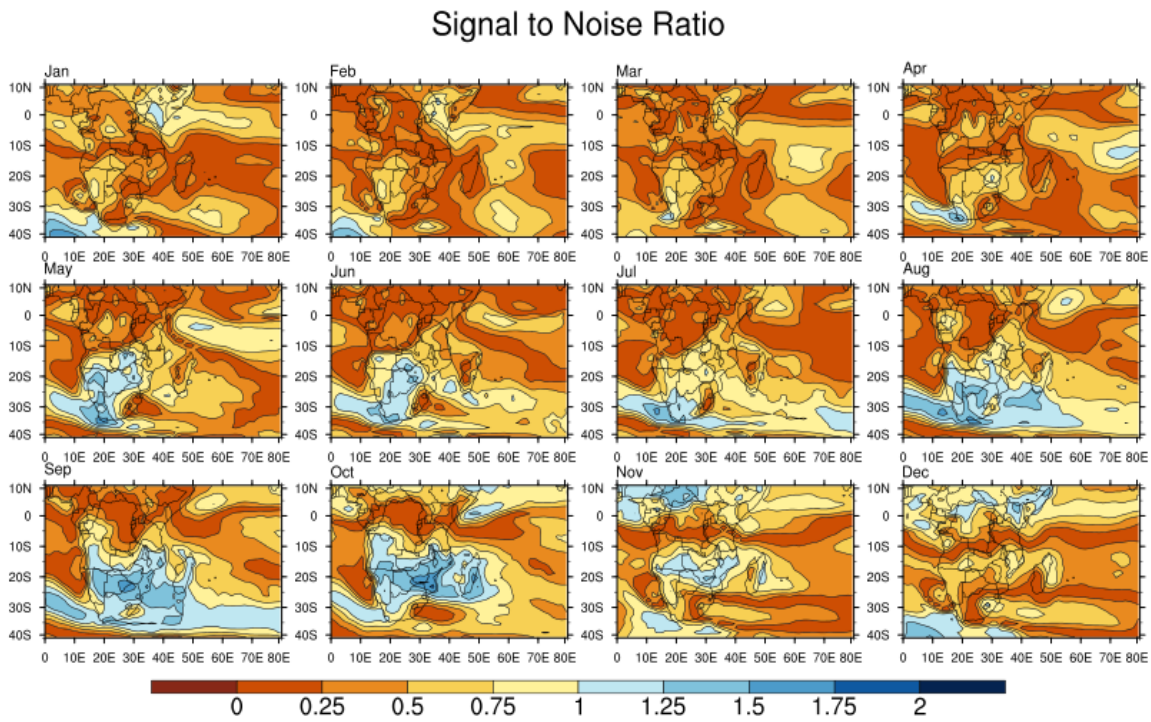

Figure 5: Signal to noise ratio of projected precipitation changes for the MMM using 39 CMIP5 models for the period 2071-2100 minus 1971-2000 for RCP8.5. All 12 calendar months are displayed from January to December. Light blue shading and darker indicate ratios equal to a value of one and above.

The climate change precipitation signal dominates over local variability between models in regions where change is most dominant (see Figure 2) i.e. over wetting and drying regions of largest magnitude particularly in September and October; however noise (i.e. model disagreement) dominates over the transition zones or boundaries between wetting and drying (e.g. between 0˚ and 10˚S). This implies models are not able to agree on the precise location of where wetting ceases and drying commences. However larger agreement is evident over the projected drying regions during September and October, again the implication being drying over the SA continent is more plausible.

From individual month analysis and seasonal cycle analysis, months of significant change include October, November and December, particularly over land in Figure 3. The large drying signal over the SA continent in OND is concerning as this will affect the onset of austral summer rainfall and have large and potentially adverse impacts on agriculture. DJF is the main rainfall season over southern Africa, whereby the majority of rainfall is experienced and projected changes show relatively large amounts of drying over the continent. Therefore analysis from this point forwards will focus on the early summer transition season OND and austral summer season DJF, due to the projected signal strength and impact on water security. Constraining uncertainty in these two key seasons would be largely beneficial, which is investigated in Chapter 6.

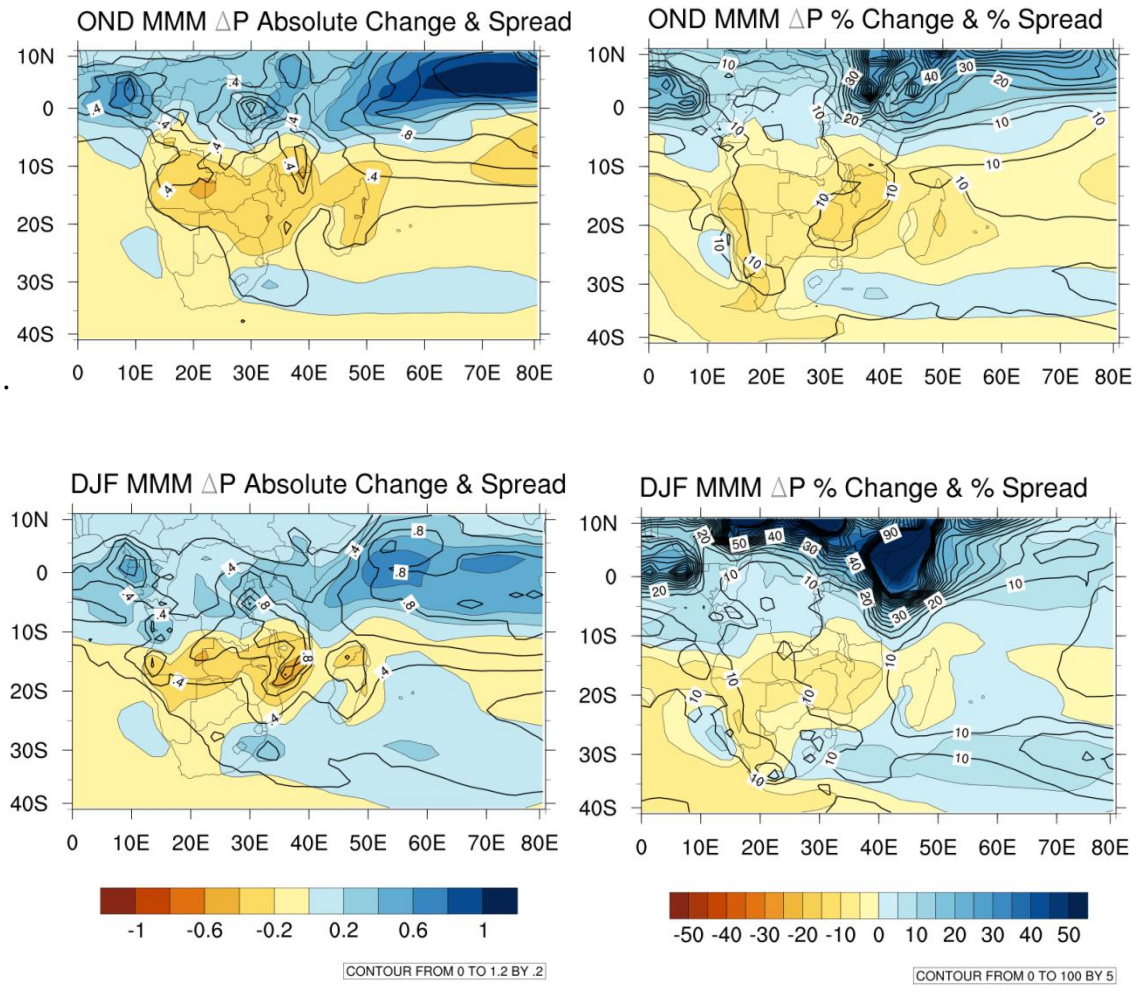

Figure 6: ΔP in absolute and percentage change for OND (top) and DJF (bottom) over SA/SWIO for 39 CMIP5 models for the period 2071-2100 minus 1971-2000 for the RCP8.5 emissions scenario. Units are in mm day^{-1} and % respectively. Plots are overlaid with black contours representing standard deviation from 0 to 1.2 in intervals of 0.2 for absolute change and from 0 to 100 in intervals of 5 for percentage change.

Figure 6 illustrates both absolute and percentage projected change in precipitation for both OND and DJF overlaid with model spread. Differences between the two categories of change are relatively small, with spatial patterns of change matching closely to one another between absolute and percentage change. This holds true for the vast majority of individual models (see Figures 2, 3, 4 and 5 in appendix illustrating this). This implies absolute projected signals are not largely skewed by historical climatology. Notable differences in precipitation projections include slightly higher rates of wetting over the Indian Ocean in absolute terms compared to percentage change. This indicates individual models historically simulate larger precipitation totals over the SWIO.

Projected percentage wetting peaks at approximately 50% higher than historical precipitation climatology over the equatorial continent and northwards, whereas drying lies in the vicinity of ~20% drier than historical precipitation climatology. Interesting to note that over regions with largest projected drying, particularly in OND; inter-model spread over those regions are fairly low in comparison to wetting regions, which exhibit the highest inter-model spread.

3.2. Projected changes in diagnostic variables

An analysis of 7 various diagnostic variables are assessed using the CMIP5 MMM. These diagnostics include, temperature, SSTs, mean seal level pressure, low-level moisture, low-level circulation patterns, low-level moisture flux and vertical velocity. All variables assessed are associated with driving or influencing precipitation over SA and the SWIO.

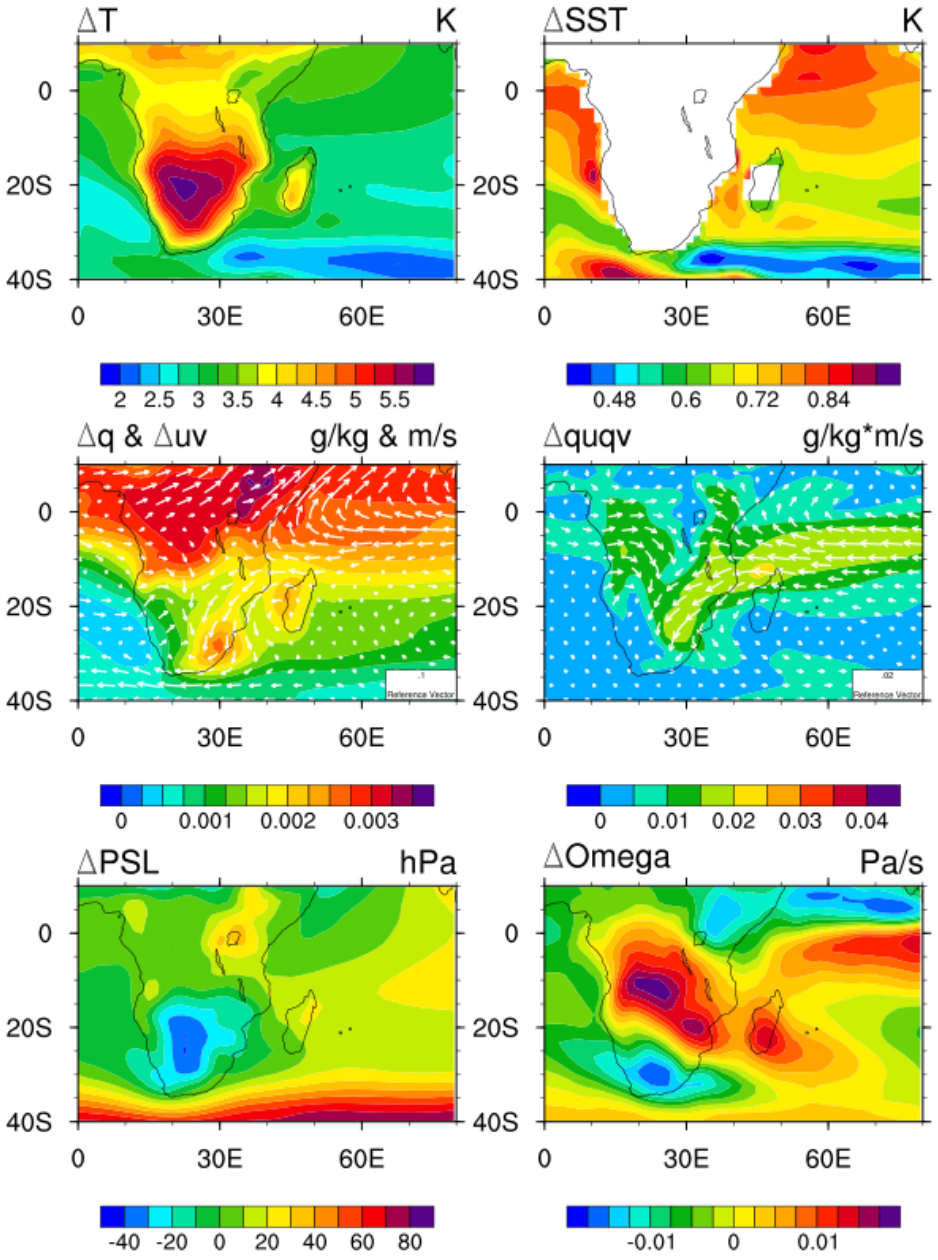

Figure 7: Projected future OND changes of 6 diagnostic variables for the period 2071-2100 minus 1971-2000 for RCP8.5 MMM of 39 CMIP5 models. 1.) Temperature 2.) SSTs 3.) Specific humidity and zonal and meridonal winds at 850hPa 4.) Moisture flux at 850hPa 5.) Mean sea level pressure and 6.) Vertical velocity at 500hPa. Units are shown on the top right-hand side of each plot.

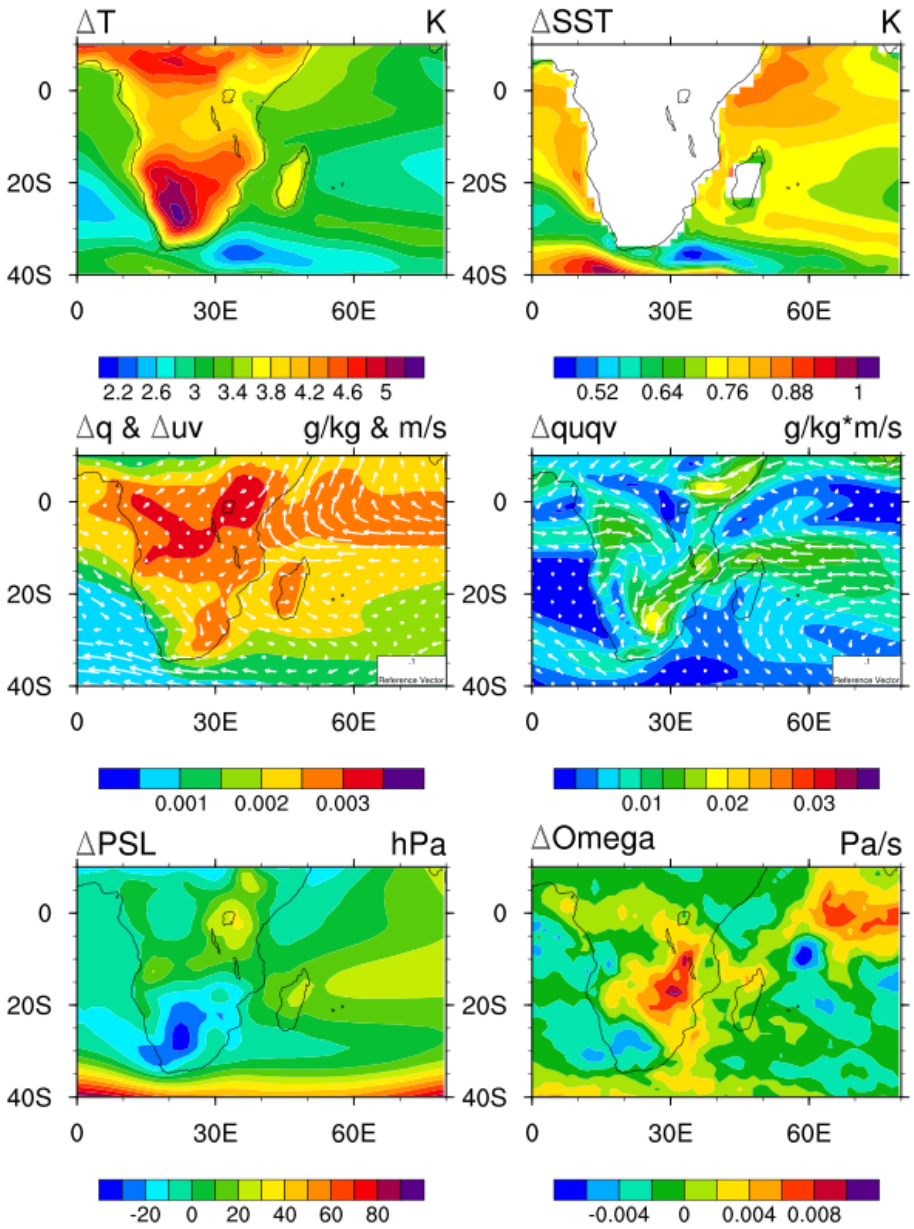

Figure 8: Same as Fig 7 but for DJF.

3.2.1. Changes in temperature

It is well established that temperatures are on the rise and to a large extent more rapidly over Africa and sub-Saharan Africa (IPCC, 2007). Changes in temperatures have significant knock-on effects and influences regarding changes in other variables, such as precipitation and circulation and therefore should be understood in model analysis. Land heats up faster than ocean regions and does not exhibit a moderating effect, whereby heat is retained. Numerous studies show that changes in warming patterns, particularly over the ocean, affect the circulation (Xie et al., 2010; Long et al., 2016). Therefore it is imperative to establish these projected temperature patterns and their effect on projected precipitation changes in future.

Changes in temperatures show large increases over the central southern African continent ranging from increases of 4K to 6K in OND and 3.5K to 5.2K in DJF (see Figure 7 and 8), with the adjacent SWIO warming at a slightly slower rate of approximately 2K to 4K in both OND and DJF. There is a clear large scale warming over the continent, which is significantly larger in magnitude than the global average increase in temperature (Figure 1b). A direct inverse relationship is established over the southern African continent, whereby largest MMM projected warming is associated with regions of largest drying projections.

A differential pattern of warming is notable over the Indian Ocean in both OND and DJF, whereby the northern Indian Ocean warms substantially more rapidly than the south, creating an enhanced SST gradient warming pattern. This notable differential warming pattern can be related to the difference in projected precipitation over the

region where wetting is clear in the north and drying in the southern parts of the Indian Ocean. This leads to the implication of the warmest-get-wetter hypothesis (Huang, 2013; Weller et al., 2014). This hypothesis is assessed in more detail in Chapter 5.

3.2.2. Changes in pressure

The dominant pressure systems common to southern African climate are the South Indian Ocean High Pressure (SIOHP), South Atlantic Ocean High Pressure (SAOHP), Angola Low (AL), Heat Low (HL), just south of the Angola Low, and Botswana High (BH) (at 500 hPa) (Hart et al., 2010). These pressure systems are typically evident in austral summer. In the MMM the mean sea level pressure over land displays a rather zonal structure consisting of decreases in the north, increases in the central regions and decreases over South Africa. Projected changes in pressure in the MMM in both OND and DJF indicate a decrease of approximately 30-35 hPa over the south-western southern African continent, essentially indicating an intensification of the Heat Low. This is most likely due to a direct effect from the intense warming projected over that region in mode projections.

Over the central Indian Ocean there is an increase in pressure in both OND and DJF, which could allude to the SIOHP strengthening. An intensification of the SIOHP will inevitably result in amplified flow and moisture influx from the Indian Ocean via enhanced easterly flow. This enhanced easterly flow could translate into increased cloud band formation imperative to the formation and maintenance of the SIOCZ, therefore potentially resulting in larger precipitation totals (e.g. Engelbrecht et al., 2008). An increase in pressure is evident over the adjacent Atlantic Ocean; implying divergence of

flow away from the western continent and therefore enhanced drying in the south-west region, which is projected over the south-west continent in both OND and DJF.

Over the more northern continent, pressure is projected to decrease, which coincides with the wetting signal. This signal is physically sensible and easier to interpret, as low pressure systems are typically associated with enhanced low-level convergence and uplift resulting in precipitation. The main difference between this region and southern Africa is the equatorial region is access to moisture and moisture transport. All conditions need to be met for precipitation to result and any missing component will inhibit precipitation. Despite increased uplift in mid-levels being projected over South Africa (see Figure 7 and 8), insufficient moisture will inhibit precipitation.

Large increases of pressure are projected around 40˚S, with extremely large relative magnitudes of change. Two implications emerge i) the dominant high pressure systems migrate southwards, ii) pressure over that region has vastly increased relative to historical climatology. The reason is most likely linked to what other studies have called the widening of the subtropical belt (Siedel et al., 2008) and additionally the poleward migration of the subtropical belt (Scheff and Frierson, 2012b).

3.2.3. Changes in moisture, circulation and moisture flux convergence

Moisture is clearly increasing everywhere; however there is a differential pattern evident, with the highest increases in moisture evident from approximately 10˚S extending northwards in OND and 20˚S extending northwards in DJF over both land

and ocean. Projected circulation patterns in OND and DJF indicate flow extending from the Indian Ocean and diverging into the continent with one divergent circulation pathway extending up into the north-eastern continent and adjacent Indian Ocean and the other diverging into southern Africa. Flow into the northern regions is towards regions of enhanced projected moisture, whereas southern Africa displays reduced moisture availability in future. This potentially explains and is seemingly linked to the dipole pattern of wetting/drying to the north/south over the continent. Projected flow into the northern Indian Ocean region is particularly strong, which is consistent with the projected wetting region over the SWIO. Therefore projected changes in circulation patterns corroborate the result of increased projected wetting in the northern regions, drying over the central continent and a small-scale wetting evident over the extreme south-eastern continent, most likely due to enhanced onshore flow over a region of increased topography.

Important processes that drive precipitation over southern Africa and the adjacent SWIO in models are circulation patterns and moisture availability (Tyson and Preston-Whyte, 2000; Held and Soden, 2006; Ma and Xie 2013; He et al., 2014). These changes in low-level moisture and circulation consistently agree with how models create future changes in precipitation. Circulation patterns are dynamic drivers which require better understanding as they are linked to direct and indirect thermodynamic effects i.e. through SST warming and pattern change respectively (Ma and Xie, 2013).

Southern African austral summer precipitation is driven by 3 moisture flux pathways identified in Chapter 3 (Lazenby et al., 2016). These include cyclonic flow around the

Angola Low, moisture flux into the south-eastern continent via circulation around the SIOHP and finally moisture flow from the equatorial region into the central continent, normally referred to as easterlies or easterly flow. These 3 moisture transport pathways feed into the SIOCZ system creating low-level convergence over SA and the SWIO. However future projections in the easterly flow is shown to dampened into the continent and transform into a divergent flow away from the continent towards the northern Indian Ocean Region. Projected enhanced flow around the Angola Low is not dominant and lacking in moisture access and availability, which likely explains the reduction in precipitation over the central parts of SA. Flow around the SIOHP remains evident in future projections, however tends to diverge before reaching land and only provides convergence and uplift over a small region, which coincides with the region over Lesotho, which indicates enhanced rainfall.

Future projections in low-level moisture increase largely over the equatorial and northern continent, but additionally over Madagascar and the south-eastern parts of the continent. Over the SIOCZ region there is no clear convergence with respect to low-level circulation over the SIOCZ but contrastingly divergence to the north and south.

Projected moisture flux fields exhibit the largest increases over the eastern periphery of the continent and over Angola and slightly northwards. Over the Indian Ocean larger differences between OND and DJF are exhibited, whereby enhanced moisture flux increases are located over the central Indian Ocean in OND and slightly southwards in DJF. This coincides with the drying signal in OND in comparison to DJF over the continent and ocean, as there is a larger difference in moisture availability and flux

being transported into those regions. Particularly interesting to note over the Indian Ocean in both DJF and OND, but more so in OND; moisture flux converges towards the equatorial regions, where the wetting signal is evident in projections. Moisture flux around the Angola Low indicates an increasing trend of enhanced flow.

3.2.3. Changes in tropical circulation

Omega also known as vertical velocity is used to diagnose changes in uplift and subsidence in the mid-levels of the atmosphere. In DJF the signal is particularly noisy with some subsidence evident over south-eastern Africa. Projected changes in MMM vertical velocity (ΔOmega) shown in Figure 7 and 8 show notable patterns similar and closely consistent to those of Δ*P,* especially for OND, where a spatial correlation of -0.66 is found and a correlation of -0.59 for DJF (both significant at the 0.05 significance level). Possible reasons for this spatial correlation not being higher include i) the influence of extra-tropical storm tracks are present, e.g. the southern tip of Africa, ii) omega includes the weakening circulation as well as circulation shifts and lastly iii) circulation changes in regions where no precipitation is present will show up in omega, but not in Δ*P*.

This result implies weakening of the tropical circulation is more abrupt in OND than DJF. Many studies show a weakening of the tropical circulation (Vecchi et al., 2006; Vecchi and Soden, 2007; Chou et al, 2009; Bony et al., 2013; Ma and Xie 2013). There is a clear decrease in uplift over most of the central southern African continent, which inhibits rainfall to a large extent. Weakening in tropical circulation is most prominent in OND and tends to taper off slightly into DJF where subsidence slightly reduces in

magnitude but is still evident. Over the northern SWIO in OND there is evidence of a dipole pattern in vertical velocity, which maps closely onto the dipole of wetting and drying found over the SWIO. This finding physically reaffirms model projected drying over most of the subcontinent, which appears to be attributed to model increased subsidence over the region, as well as the ascent/descent dipole evident in precipitation projections in the SWIO in OND.

3.3. Projected changes in the SIOCZ

The key difference between observations and the historical MMM of the SIOCZ using the algorithm described in section 2.3 is the SIOCZ is simulated as too zonal in the CMIP5 MMM (already established from Chapter 3). However, positioning in terms of mean latitude is reasonably similar to observations with the MMM SIOCZ axis located slightly northwards by comparison. Projected future simulations of the SIOCZ in the MMM indicate a notably steeper slope in the SIOCZ and a northward shift of approximately ~200km (northward shift of 1.76˚ in mean latitude). The steeper slope simulated in future MMM projections can be attributed to the fact that maximum precipitation over the continent shifts northward in future projections (see Figure 9 – Difference MMM).

The SIOCZ does not project consistent changes along the axis of the SIOCZ, but significant increases over the most north-western tip of the SIOCZ axis and decreases towards the south-eastern tip of the SIOCZ axis. Wetting over the northern regions of

the continent tend to shift the SIOCZ axis northwards and cause a steepening in orientation. The most notable changes are the wetting/drying dipole over the continent that extends out into the SWIO (already established in Figure 6 for DJF), not particularly along the axis of the SIOCZ. An alternate interpretation of the movement of the SIOCZ could be a reduction of southwards migration of the SIOCZ in future projections than in present day climatology.

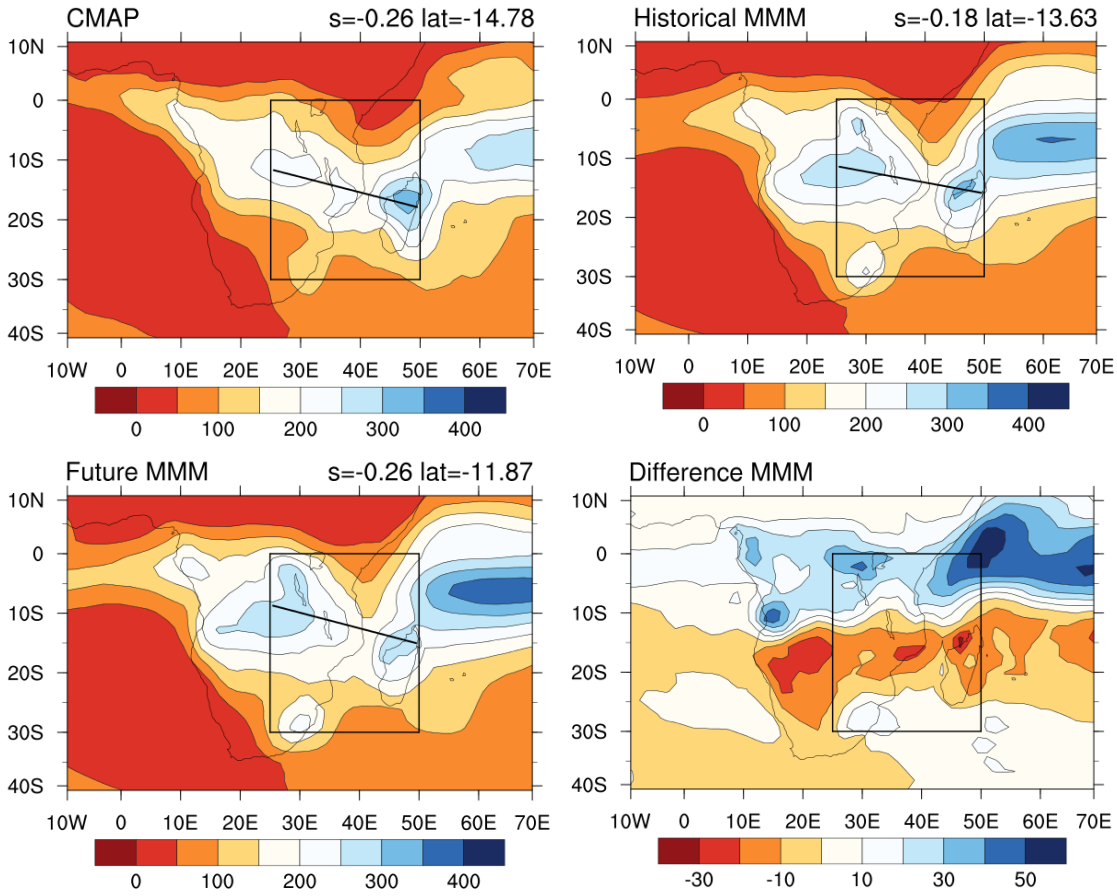

Figure 9: Mean CMAP, historical MMM, future MMM and difference MMM plots of DJF precipitation over southern Africa for the historical 30 year period 1971-2000 and future period 2071-2100 under RCP8.5 emissions scenario. The black block indicates the SIOCZ region (0˚S - 30˚S, 25˚E - 50˚E) where a best-fit line of maximum precipitation was derived over the longitude range 25˚E to 50˚E. Top right hand corner of each plot indicates the slope and mean latitude of the SIOCZ line.

Projected changes in the SIOCZ's position is informative as it affects agriculture and subsistence farming that will no longer lie within the SIOCZ region in future. There is additionally a projected delay in the onset of the rainy season due to OND exhibiting a very large drying signal over much of the subcontinent (Figure 6 – OND). All results are important directly affecting decision-makers and particularly farmers at a local-scale over the region.

Models are equivalently assessed individually regarding projected changes in the SIOCZ using the aforementioned algorithm. Figure 10 illustrates individual CMIP5 models projected future SIOCZ axes as dashed black lines. Historical and observed individual SIOCZ plots are not shown here but are shown in the appendix - Figure 1 as a comparative reference. Individual CMIP5 models historical and future SIOCZ axes mean latitude and slope values as well as differences between the two are tabulated in Table 2. 20 CMIP5 models out of the total 39 individual models exhibit future SIOCZ axes almost horizontal in structure (depicted clearly in all 3 HadGEM2 models), providing consistency towards projected future change, which exhibits a zonal wetting/drying pattern towards the north/south of the historical climatological mean precipitation.

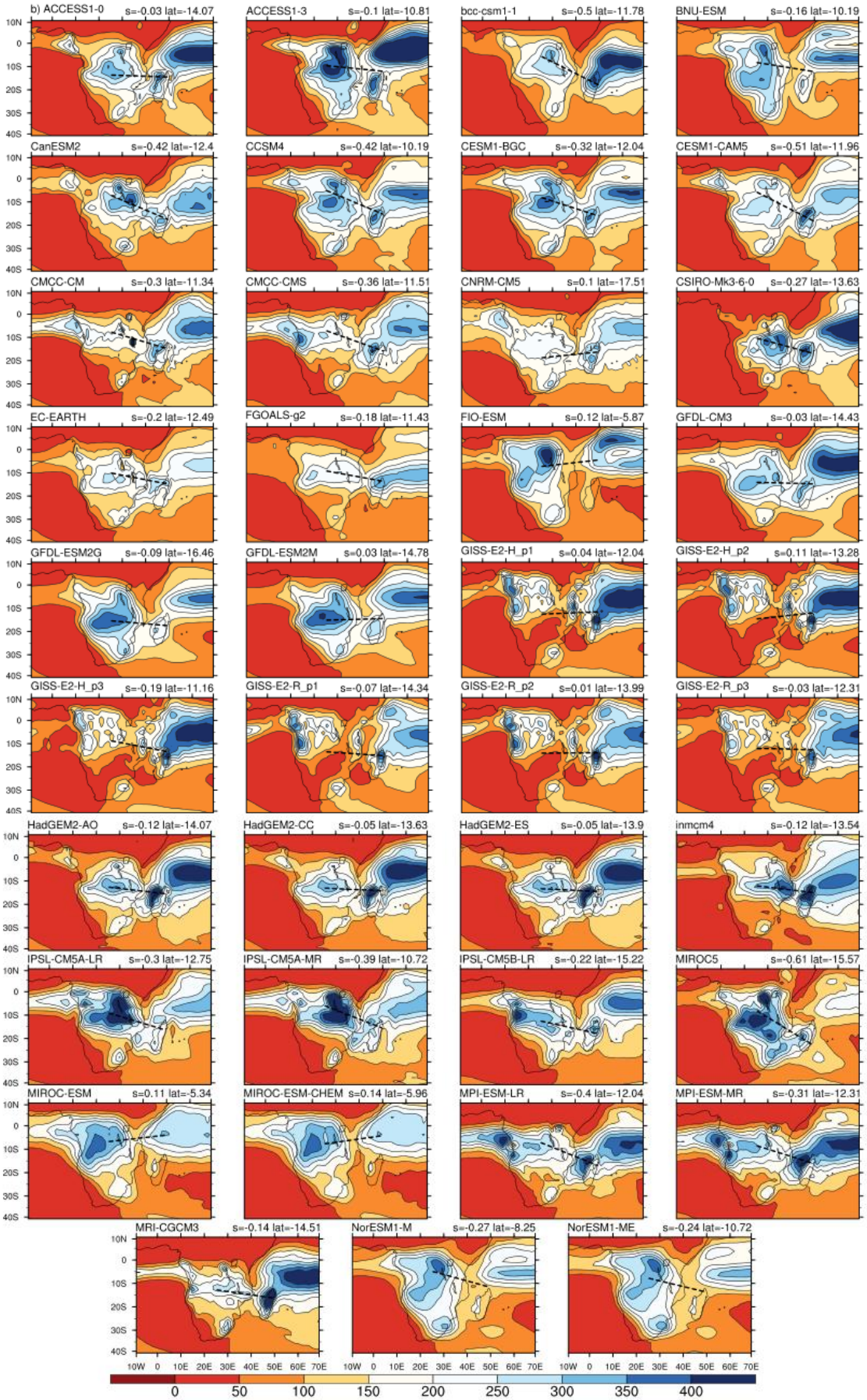
b) ACCESS1-0 s=-0.03 lat=-14.07
ACCESS1-3 s=-0.1 lat=-10.81
bcc-csm1-1 s=-0.5 lat=-11.78
BNU-ESM s=-0.16 lat=-10.19
CanESM2 s=-0.42 lat=-12.4
CCSM4 s=-0.42 lat=-10.19
CESM1-BGC s=-0.32 lat=-12.04
CESM1-CAM5 s=-0.51 lat=-11.96
CMCC-CM s=-0.3 lat=-11.34
CMCC-CMS s=-0.36 lat=-11.51
CNRM-CM5 s=0.1 lat=-17.51
CSIRO-Mk3-6-0 s=-0.27 lat=-13.63
EC-EARTH s=-0.2 lat=-12.49
FGOALS-g2 s=-0.18 lat=-11.43
FIO-ESM s=0.12 lat=-5.87
GFDL-CM3 s=-0.03 lat=-14.43
GFDL-ESM2G s=-0.09 lat=-16.46
GFDL-ESM2M s=0.03 lat=-14.78
GISS-E2-H_p1 s=0.04 lat=-12.04
GISS-E2-H_p2 s=0.11 lat=-13.28
GISS-E2-H_p3 s=-0.19 lat=-11.16
GISS-E2-R_p1 s=-0.07 lat=-14.34
GISS-E2-R_p2 s=0.01 lat=-13.99
GISS-E2-R_p3 s=-0.03 lat=-12.31
HadGEM2-AO s=-0.12 lat=-14.07
HadGEM2-CC s=-0.05 lat=-13.63
HadGEM2-ES s=-0.05 lat=-13.9
inmcm4 s=-0.12 lat=-13.54
IPSL-CM5A-LR s=-0.3 lat=-12.75
IPSL-CM5A-MR s=-0.39 lat=-10.72
IPSL-CM5B-LR s=-0.22 lat=-15.22
MIROC5 s=-0.61 lat=-15.57
MIROC-ESM s=0.11 lat=-5.34
MIROC-ESM-CHEM s=0.14 lat=-5.96
MPI-ESM-LR s=-0.4 lat=-12.04
MPI-ESM-MR s=-0.31 lat=-12.31
MRI-CGCM3 s=-0.14 lat=-14.51
NorESM1-M s=-0.27 lat=-8.25
NorESM1-ME s=-0.24 lat=-10.72
10N
0
10S
20S
30S
40S
10W 0 10E 20E 30E 40E 50E 60E 70E
0 50 100 150 200 250 300 350 400

Figure 10: Projected future DJF precipitation plots over southern Africa for the period 2071-2100 under the RCP8.5 scenario for 39 individual CMIP5 models. Spatial plots are overlaid with model SIOCZ axis (dashed) fitted to the maximum precipitation values along the longitudes 25˚E - 50˚E. Slope (s) and mean latitude (lat) are shown on the top right of each image. Units are in mm month^{-1}.

Table 2: Table of individual CMIP5 models historical and future mean latitude and slope of the SIOCZ. Differences between future and historical parameters are additionally derived and tabulated

Name of Model	Historical (slope)	Future (slope)	Difference (slope)	Historical (latitude)	Future (latitude)	Difference (latitude)
ACCESS1-0	-0.04	-0.03	0.01	-13.99	-14.07	-0.08
ACCESS1-3	-0.07	-0.1	-0.03	-14.34	-10.81	3.53
bcc-csm1-1	-0.43	-0.5	-0.07	-12.4	-11.78	0.62
BNU-ESM	0.06	-0.16	-0.22	-14.87	-10.19	4.68
CanESM2	-0.47	-0.42	0.05	-12.75	-12.4	0.35
CCSM4	-0.16	-0.42	-0.26	-11.78	-10.19	1.59
CESM1-BGC	-0.25	-0.32	-0.07	-11.96	-12.04	-0.08
CESM1-CAM5	-0.13	-0.51	-0.38	-14.51	-11.96	2.55
CMCC-CM	-0.34	-0.3	0.04	-13.54	-11.34	2.2
CMCC-CMS	-0.2	-0.36	-0.16	-13.19	-11.51	1.68
CNRM-CM5	0.13	0.1	-0.03	-19.1	-17.51	1.59
CSIRO-Mk3-6-0	-0.28	-0.27	0.01	-15.13	-13.63	1.5
EC-EARTH	-0.09	-0.2	-0.11	-14.69	-12.49	2.2
FGOALS-g2	-0.18	-0.18	0	-12.22	-11.43	0.79
FIO-ESM	-0.26	0.12	0.38	-8.43	-5.87	2.56
GFDL-CM3	-0.02	-0.03	-0.01	-14.87	-14.43	0.44
GFDL-ESM2G	-0.06	-0.09	-0.03	-15.49	-16.46	-0.97
GFDL-ESM2M	-0.06	0.03	0.09	-14.87	-14.78	0.09
GISS-E2-H	-0.28	0.04	0.32	-10.81	-12.04	-1.23

GISS-E2-R	-0.3	-0.07	0.23	-12.66	-14.34	-1.68
HadGEM2-AO	-0.11	-0.12	-0.01	-13.54	-14.07	-0.53
HadGEM2-CC	-0.09	-0.05	0.04	-14.25	-13.63	0.62
HadGEM2-ES	-0.12	-0.05	0.07	-14.16	-13.9	0.26
inmcm4	-0.18	-0.12	0.06	-12.75	-13.54	-0.79
IPSL-CM5A-LR	-0.17	-0.3	-0.13	-12.57	-12.75	-0.18
IPSL-CM5A-MR	-0.11	-0.39	-0.28	-11.96	-10.72	1.24
IPSL-CM5B-LR	-0.09	-0.22	-0.13	-15.93	-15.22	0.71
MIROC5	-0.3	-0.61	-0.31	-18.93	-15.57	3.36
MIROC-ESM	0.09	0.11	0.02	-6.93	-5.34	1.59
MIROC-ESM-CHEM	0.08	0.14	0.06	-6.93	5.96	12.89
MPI-ESM-LR	-0.17	-0.4	-0.23	-13.99	-12.04	1.95
MPI-ESM-MR	-0.21	-0.31	-0.1	-13.28	-12.31	0.97
MRI-CGCM3	-0.08	-0.14	-0.06	-15.93	-14.51	1.42
NorESM1-M	-0.13	-0.27	-0.14	-8.78	-8.25	0.53
NorESM1-ME	-0.32	-0.24	0.08	-9.04	-10.72	-1.68
Model Mean	**-0.15**	**-0.19**	**-0.04**	**-13.16**	**-11.88**	**1.28**

Projected changes amongst individual CMIP5 models SIOCZ location and orientation are largely varied. Individual models with excessive precipitation over the continent and adjacent Indian Ocean typically exhibit more zonal SIOCZ structures, almost horizontal, which mirror the dipole change found in the MMM in Figure 9. A vast majority of 30 out of the 39 CMIP5 models indicate a northward shift in the SIOCZ axis i.e. a positive difference between historical and future mean latitude (column 7 in Table 2). Therefore can conclude there is no distinct and consistent change along the SIOCZ feature in projected future climate, however there is consensus regarding an overall northward shift in the SIOCZ in austral summer precipitation.

The SIOCZ's interannual variability is dominated by local and remote SST drivers, i.e. the subtropical Indian Ocean dipole (SIOD) and ENSO (i.e. Niño3.4 region), which was established in Chapter 3 (Cook, 2000; Lazenby et al., 2016). In Chapter 3 it is established a dipole pattern describes the shift in the SIOCZ i.e. when there are warmer temperatures in the Pacific Niño3.4 region and the SIOD is positive, the SIOCZ shifts northwards and when there are cooler temperatures over the Pacific and the SIOD is negative/weaker the SIOCZ shifts southwards.

Hypothetically if future climate leaned towards a permanent El Niño type phase, the SIOCZ would permanently be shifted northwards. However studies are not conclusive whether this hypothesis holds true (Collins et al., 2010). The pattern of projected precipitation change additionally does not mirror the pattern of interannual variability. Further investigation is required to determine drivers of SIOCZ change including local and remote SST influences, as well as understanding potential links between variability and projected change over southern Africa.

Regional changes to the SIOCZ are complex to fully understand and are likely to exhibit various drivers of change, as it spans from land and extends into the Indian Ocean, unlike the more well-defined SPCZ, which is entirely an ocean-based convergence zone. Therefore changes in the SPCZ are more easily determined and understood (Brown et al, 2011; 2013). Changes in SSTs will have a direct impact on the SIOCZ which extend into the Indian Ocean, as well as affecting the SIOCZ over land through circulation changes, however, the land component of the SIOCZ will potentially have additional factors affecting changes in this feature such as land-sea

contrasts (He and Soden, 2016) and therefore be more complex to fully understand, which is investigated in more detail in Chapter 5.

3.4. Relationships between diagnostic variables and individual models

Some notable relationships emerge when evaluating individual models future precipitation projections and various diagnostic variables. This type of analysis aids in identifying which processes in models tend to dominant and drive precipitation changes and additionally uncertainty. Knowledge of model biases in diagnostic parameters can inform model correction to reduce uncertainty through improvements of model parameterization schemes and specific physical processes. Here 3 individual models are highlighted with respect to precipitation changes and associated diagnostic variables potentially driving change in DJF and OND. Individual models analysed include CSIRO-Mk3-6-0, HadGEM2-ES and IPSL-CM5B-LR.

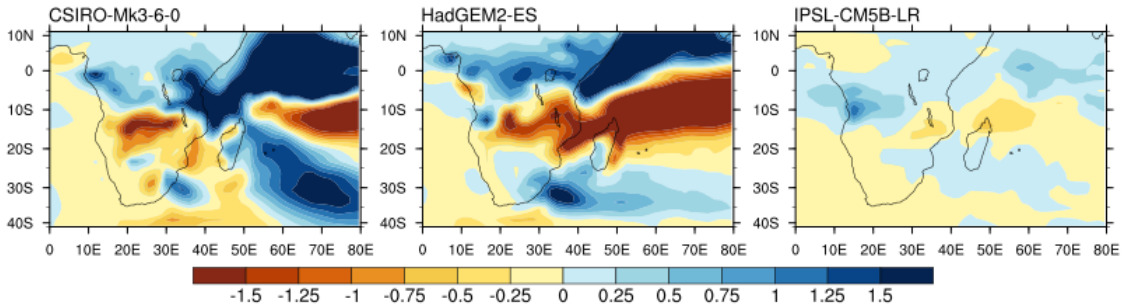

Figure 11: Selected individual CMIP5 plots of absolute ΔP over SA and the SWIO for RCP8.5 for the period 2071-2100 minus 1971-2000 for DJF. Units are in mm day^{-1}.

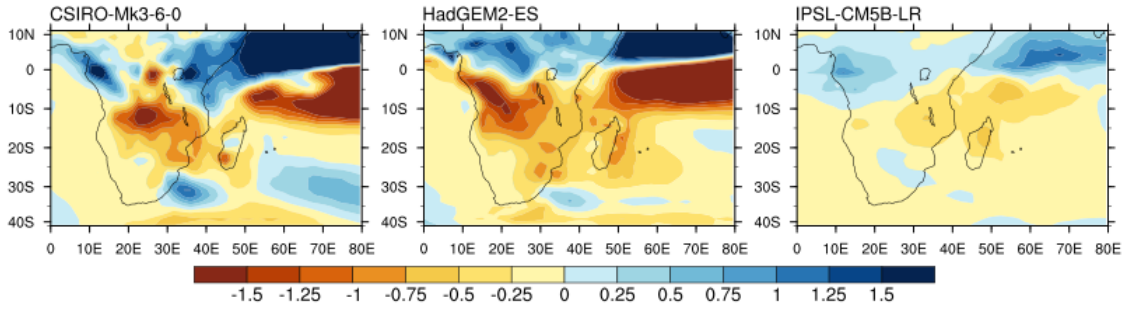

Figure 12: Same as Figure 11 but for OND.

These 3 individual CMIP5 models exhibit differing patterns of precipitation change with respect to spatial patterns and intensity, however in both seasons a dipole and almost tripole pattern of change is distinct over the domain. CSIRO-Mk3-6-0 and HadGEM2-ES exhibit notably stronger wetting/drying signals, whereas IPSL-CM5B-LR indicates more moderate precipitation changes. IPSL-CM5B particularly simulates less sub continental drying in OND and DJF in comparison to the other 2 individual CMIP5 models analysed here.

The majority of CMIP5 models typically exhibit differential SST warming patterns over the Indian Ocean (not shown here due to space constraints), whereby higher rates of SST warming are evident over the northern Indian Ocean region. The differential warming pattern is clear in the 3 selected models (Figure 11 and 12), with strongest differential warming shown for CSIRO-Mk3-6-0 and subsequently HadGEM2-ES. The warmest regions coincide with the wetting region over the northern Indian Ocean (see Figure 11 and 12 vs. 13 and 14). This implies a warmest-get-wetter mechanism of change (Held and Soden, 2006; Xie et al., 2010; Huang et al., 2013), which is explored

in more detail in Chapter 5. Differential rates of warming show distinct associations with wetter regions projected over the Indian Ocean.

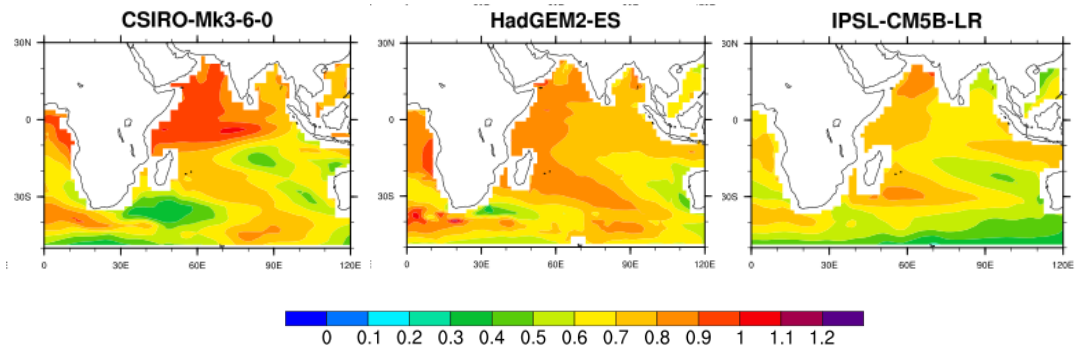

Figure 13: Selected individual CMIP5 plots of projected ΔSST over SA and the SWIO for RCP8.5 for the period 2071-2100 minus 1971-2000 for DJF. Units are in Kelvin.

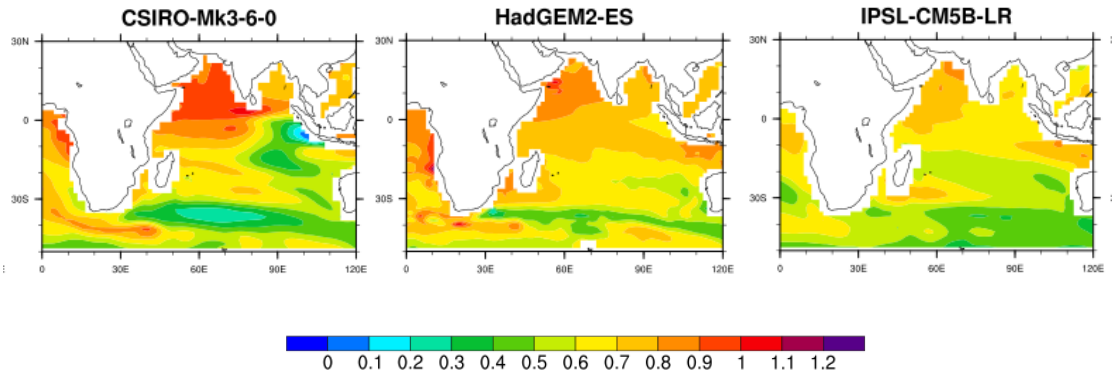

Figure 14: Same as Figure 13 but for OND.

Over the southern African continent individual models exhibiting larger climate change signals of wetting tend to indicate enhanced low-level moisture and circulation flow towards projected wetting regions from the 3 predefined moisture flux pathways in Chapter 3 (Lazenby et al., 2016). Models exhibiting higher lower-level moisture over the continent and SWIO typically exhibit higher rates of associated wetting. Additionally relationships are established between models exhibiting low-level convergence over the continent and projected wetting (e.g. HadGEM2-ES over East Africa). Individual models show large agreement in projected circulation changes,

which indicates flow from the central Indian Ocean diverging northwards towards equatorial regions to enhance the Indian Ocean ITCZ. The ITCZ over the Indian Ocean is projected to shift northwards and the circulation patterns within individual models show physically sensible and agreeable processes which corroborate the projected northward shift.

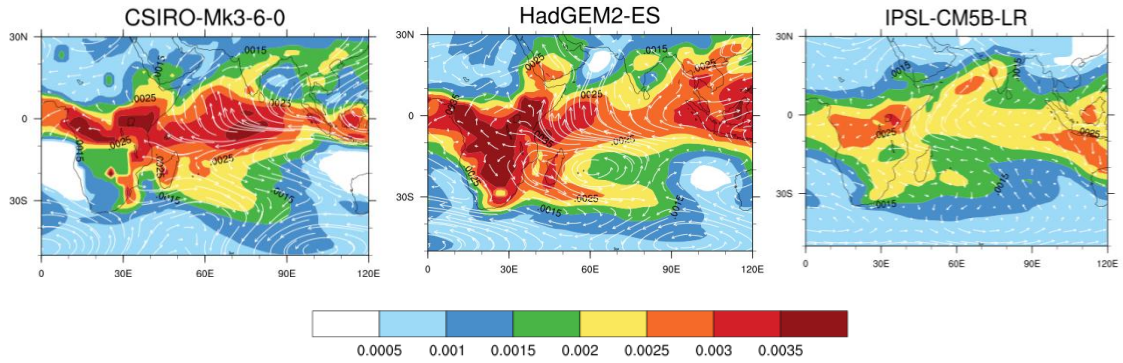

Figure 15: Selected individual CMIP5 plots of low-level moisture (colour shading) and circulation (white vectors) projections over SA and the SWIO for RCP8.5 for the period 2071-2100 minus 1971-2000 for DJF. Units are in g/kg and m/s respectively.

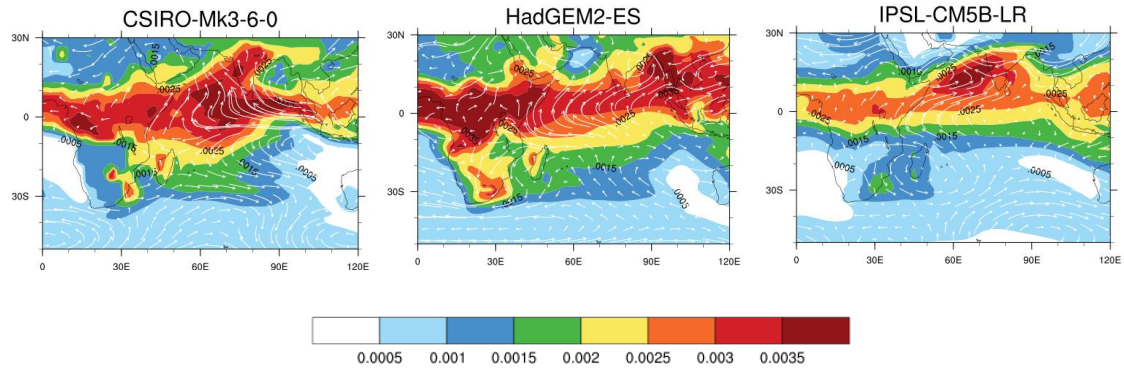

Figure 16: Same as Fig 15 but for OND.

3.5. Future precipitation projections in atmosphere-only models

To evaluate the role of SST patterns, SST warming and direct CO_2 influences in determining projected changes in future precipitation, several AMIP future experiments are analysed (5 in total). AMIP future models are useful in attempting to understand model processes potentially causing projected precipitation changes, such as the projected drying over the subtropical regions (He and Soden, 2016).

Glossary of AMIP experiments:

- AMIP: Atmospheric-only simulation with no coupling, provided with observed SSTs and sea ice from 1979 to near present.

AMIP Future Experiments

- AMIP4K: As AMIP but with a uniform 4K anomaly applied to the SSTs.
- AMIP4xCO2: As AMIP but with 4xCO2 (without plant response), and fixed SSTs.
- AMIPFuture: As AMIP but with an SST pattern anomaly applied from the ensemble mean of CMIP3 models in the 1% per year except, at time of CO_2 doubling.
- AMIPPattern = AMIPFuture – AMIP4K
- AMIPTotal = AMIPFuture + AMIP4xCO2

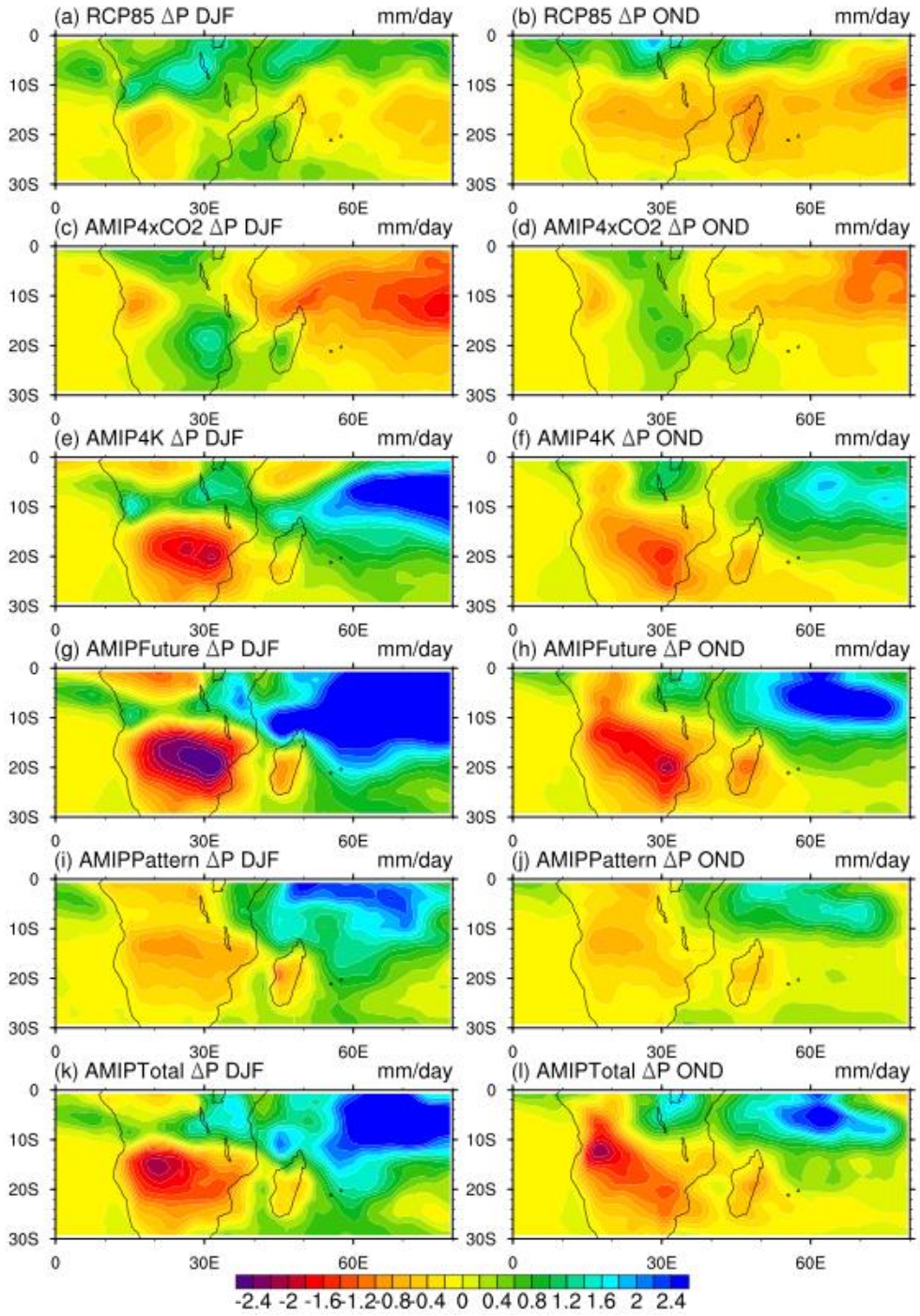

Figure 17: Panel of absolute MMM future precipitation changes (ΔP) for RCP8.5 and various AMIP future experiments for the period 2071-2100 minus 1971-2000 for DJF (left column) and OND (right column). 11 CMIP5 and AMIP models are used to create the MMM. Future experiments included are (a) & (b) RCP8.5, (c) & (d) AMIP4xCO2, (e) & (f) AMIP4K, (g) & (h) AMIPFuture, (i) & (j) AMIPPattern and (k) & (l) AMIPTotal.

Table 3: Table of ΔP correlations of the MMM RCP8.5 scenario versus the MMM future AMIP experiments for 11 CMIP5 models in common to both experiments. Correlations are derived for the study region 0˚- 30˚S and 0˚-80˚E for OND and DJF for the period 2071-2100 minus 1971-2000.

Future AMIP experiments	**RCP8.5 DJF ΔP**	**RCP8.5 OND ΔP**
AMIP4xCO2	0.12	0.22
AMIP4K	0.22	0.27
AMIPFuture	0.1	0.2
AMIPPattern	0.13	0.27
AMIPTotal	0.25	0.38

Table 3 provides spatial correlations of MMM ΔP for coupled RCP8.5 CMIP5 models and 5 various future AMIP experiments. In order to determine whether AMIP experiments are useful over a particular region when determining the role of SST patterns, one needs to indicate whether AMIPTotal (AMIPFuture + AMIP4xCO2) appears significantly similar to the spatial pattern found in RCP8.5's ΔP coupled MMM.

From Table 3 correlations against the various AMIP future experiments indicate no significant relationship established between Δ*P* MMM RCP8.5 scenario and AMIPTotal (even though highest correlations were established for this experiment), for either DJF or OND. The implication being AMIP future scenarios over SA/SWIO appear to be of limited value in understanding future changes in precipitation in OND and DJF. However, interesting to note correlations were highest in OND in all 5 AMIP future experiments versus the coupled future change. Potential implications of this finding allude to OND precipitation change being seemingly less influenced by SST pattern

change than DJF i.e. more uncertainty arises in DJF from SST pattern change. Other influences such as the CO_2 direct effect (Chadwick et al., 2014) and thermodynamic effects may be more influential. He and Soden (2016) establish that AMIP experiments aid in diagnosing subtropical drying drivers over the global tropical oceans in annual means, however over land results appear inconclusive, with suggestions of hydrological processes being more important over land. Here the focus is regional analysis over subtropical land regions and for particular seasons OND and DJF and not annual means. Additional insight regarding dynamic and thermodynamic influences is determined in Chapter 5.

As a side note AMIP experiments are not ideal when examining the influence of SST pattern change, as the current AMIPFuture scenario only uses a single SST pattern of change for all individual models. New experiments in CMIP6 should be able to provide more insight into this issue (Eyring et al., 2016). It is equally important to note these future AMIP experiments are idealised and are most useful when analysing MMMs, not uncertainty across models. Therefore AMIP projections are not utilised further in this thesis to aid understanding of future precipitation projections over southern Africa.

4. Summary and Conclusions

Key changes in precipitation over southern Africa and the Indian Ocean include a distinct wetting/drying/wetting pattern indicative of a northward shift of the ITCZ. This pattern has strong seasonal cycle that peaks during the transition season (OND) and extends into austral summer (DJF) in the southern hemisphere. The general pattern of

precipitation change has a strong zonal north/south dipole structure over southern Africa that extends out into the Indian Ocean. When assessed in more detail, changes in precipitation over land and ocean have delayed and varied signals regarding the distinct dipole pattern of change i.e. wetting to the north of the climatological precipitation axis and drying to the south of this axis. Over the southern African continent drying peaks during November, whereas over the Indian Ocean the drying signal peaks later on in December. Alternatively, the wetting signal tends to peak earlier over ocean (August) and later over land (December). The dipole pattern of change weakens towards mid-late to summer.

Potential reasons for these variations in timing may be due to the unlimited supply of moisture over the oceans in comparison to land regions and although conditions may be similar over both land and ocean with regards to increased wetting, the difference is moisture availability. The drying signal over land may occur before ocean drying due to land-atmosphere feedbacks. Circulation patterns are likely driving the differing timings on the wetting/drying dipole signal over southern Africa (He and Soden, 2016).

Local variability between models is exceeded most evidently in the spring season peaking in October, whereby the signal of drying over the continent is dominant. This is essentially when model agreement is largest and the drying signal exceeds the “noise” from model disagreement.

Diagnostic variables including SST warming patterns, moisture flux and (uplift) vertical velocity show indications of driving projected precipitation changes, such that processes within models create precipitation changes. It is important to make sense of the physical processes that models use to project changes, as this enlightens our understanding of model processes of change. Regions of largest warming map closely onto wetting regions over the northern Indian Ocean in both MMM and individual CMIP5 models. Differential rates of SST warming show distinct associations with projected wetting regions the Indian Ocean. Implying a warmest-get-wetter mechanism of change over the northern Indian Ocean (Held and Soden, 2006; Xie et al., 2010; Huang et al., 2013), which is explored in more detail in Chapter 5. Projected changes over land are not as well understood and require additional insight and analysis. This thesis aims to understand why models are producing certain changes and additionally identifying whether models are behaving in a coherent manner, which is explored in subsequent chapters.

Future changes in the SIOCZ feature are determined using a best-fit line along the maximum precipitation axis in the SIOCZ region. The SIOCZ feature does not show radical changes in precipitation along its projected axis; however a northward shift in the SIOCZ is evident of approximately 200km. This change impacts regions reliant on agricultural practises which lie within the proposed 200km region and would potentially require altered methods of farming such as drought resistant crop use or change in crop type requiring less water. The SIOCZ shift is likely linked to the northward shift of the ITCZ over the adjacent Indian Ocean and is likely driven by SST patterns and circulation changes (Power et al., 2006; Adler, 2011; Stevenson, 2012; He and Soden, 2016), particularly variability in terms of the South Indian Ocean High (Dieppois et al.,

2016). However, changes in precipitation do not project onto the climatological SIOCZ or the pattern of the interannual variability of the SIOCZ. Therefore additional analysis is required to understand the mechanisms of projected change in austral summer over southern Africa which is explored in Chapter 5.

Individual model analysis established the following notable links regarding diagnostic variables and projected model precipitation change i) enhanced differential SST pattern projected warming over the Indian Ocean is associated with higher projected precipitation totals over the northern Indian Ocean region i.e. SST warming pattern associated with dipole pattern in the Indian Ocean, ii) continental projected wetting exhibits links with increased low-level moisture availability and enhanced low-level easterly flow, particularly over East Africa and iii) enhanced flow directed towards the northern Indian Ocean region in both OND and DJF i.e. larger magnitudes of flow are associated with enhanced projected wetting signals.

Atmosphere only experiments are generally useful when attempting to gauge more understanding of the impacts of model SST patterns and coupling influences. Future atmosphere only experiments prove to have limited use in understanding future precipitation change over southern Africa, as they are not able to replicate the coupled RCP8.5 emissions scenario with sufficient skill in AMIPTotal. CMIP6 experiments will be able to deal with this issue more accurately (Eyring et al., 2016), as not only one MMM SST pattern will be utilised in these experiments. An aside comment when considering the AMIP future experiments was that during OND correlations were higher than DJF in all experiments, which seemingly infers OND precipitation changes

are potentially less influenced by SST influences and dynamics. This finding is physically sensible due to increased dynamic contributions in austral summer from increased convective activity than during pre-summer months (OND), when less convection is experienced, however this is more of an intriguing observation than a valid finding and should be noted with caution.

These identified changes in precipitation over southern Africa will have significant impacts in terms of water security which affects livelihoods as well as commercial and subsistence farming over the region. Relatively small changes of 200km northward shifts in the SIOCZ will have magnified on the ground impacts. Therefore the robustness and credibility of these changes will be determined in the next 2 chapters (5 and 6) whereby precipitation is decomposed into its dynamic and thermodynamic components as a means to identify which component is driving uncertainty and if we can potentially reduce that uncertainty, with the understanding of model processes and performance over the southern African region.

5. Caveats and Implications

This chapter summarises key changes in precipitation over the region and potential understanding of model processes resulting in projected precipitation changes. Some caveats need to be highlighted with regards to the SIOCZ algorithm to identify this feature in contemporary and future climate in CMIP5 models. The SIOCZ is a land-based convergence zone that extends out into the SWIO, where the Indian Ocean ITCZ

feature is also apparent. The algorithm used to identify this feature is using a best-fit line along values of maximum precipitation along specified longitudes. Within this domain several models include the Indian Ocean ITCZ, which exhibits much larger magnitudes in precipitation than the SIOCZ. This results in the best-fit line deviating towards the Indian Ocean ITCZ, typically creating a more zonally orientated SIOCZ axis. The algorithm is constrained such that the majority of models exclude this Indian Ocean ITCZ loci influence, however this is not possible to account for all CMIP5 models, therefore being a noted caveat in this methodology. An approach to counteract this caveat would be to create a SIOCZ mask using a threshold value specific to the SIOCZ, which is performed in Chapter 6.

Atmosphere-only future experiments are analysed in the hope of yielding additional information regarding SST patterns. Current AMIP experiments are not ideal when examining the influence of SST pattern change, due to the AMIPFuture experiment only consisting of a single CMIP3 SST pattern change for all individual models. New experiments in CMIP6 should be able to provide more insight into this issue (Eyring et al., 2016) and therefore results presented here are provisional. Due to AMIP future experiments being idealised and most useful when analysing MMM's, not particularly when assessing uncertainty across models, which is dealt with in the next chapter, therefore the AMIP analysis is taken no further due to the aforementioned limitations.

Chapter 5

Future Precipitation Projections over Central Southern Africa and the Adjacent Indian Ocean: What Causes Uncertainty?

Overview

Decomposition analyses are common methods used to understand precipitation change, however has not been performed using this particular methodology over southern Africa. This chapter provides new insight of projected precipitation mechanisms of change over southern Africa. Dominant contributors and potential drivers of projected precipitation change and associated uncertainty is additionally established. This analysis will determine gaps within model process understanding and potentially aid in reducing uncertainty of future precipitation changes.

Key Questions:

1. What are the key climate change signals over southern Africa for future precipitation projections?
2. What are the mechanisms of change over southern Africa for the key identified seasons OND and DJF?

3. Which component dominates projected precipitation change over southern Africa?
4. How certain and robust are these components?
5. What drives the dominant dynamical component and associated uncertainty?
6. What are the dominant patterns of variation in projected precipitation change over southern Africa?
7. What patterns of circulation are associated with future dynamic precipitation projections in OND and DJF?

ABSTRACT

Future projections of precipitation at the regional scale are vital to inform climate change adaptation activities and decision-making. However, for most of the tropics such projections remain highly uncertain, presenting a major barrier to the uptake of climate projections in adaptation decisions. Therefore, is it important to quantify projected changes and associated uncertainty (robustness), and to understand the model processes responsible. This paper addresses these challenges for Southern Africa and the adjacent Indian Ocean with a focus on the local summer wet season, critical to agriculture and associated livelihoods in this region which is especially vulnerable to climate change. Projections for the end of the 21st century indicate a pronounced dipole pattern in the CMIP5 multi-model mean of changes to precipitation over the region. The dipole indicates future wetting (drying) to the north (south) of the climatological axis of maximum rainfall, implying a northward shift of the ITCZ and South Indian Ocean Convergence Zone, and therefore not consistent with a simple 'wet-get-wetter'

pattern. This pattern is most pronounced in the early Austral summer wet season suggesting a later and shorter wet season over much of southern Africa centred on ~15˚S. Using a decomposition method the physical mechanisms underlying this dipole pattern of projected change are investigated. Uncertainty in future projections represented by the inter-model spread is additionally analysed. The projected precipitation change dipole is found to be largely associated with shifts in the location of convection associated with dynamical processes. This may reflect the response to patterns of SST changes in that future north-south SST gradients over the Indian Ocean are consistent with a 'warmest-get-wetter' mechanism driving the apparent northward shift in the ITCZ, further corroborated by the moderate association across the model ensemble between the projected precipitation and SST changes. Over land the subtropical drying signal is relatively robust, especially in the early season. This is associated with both dynamical shifts in location of convection, which may be related to SST structures in the Southern Indian Ocean but also thermodynamic contributions through a decline in relative humidity. Given that the dynamical shifts in convection hold most of the inter-model uncertainty the results suggests further analysis of the physical mechanism responsible for projected SST changes may inform interpretation of the credibility of model projections.

1. Introduction

Africa is highly vulnerable to climate change, evident from the reliance on seasonal precipitation for agriculture, water supply and energy generation over the majority of sub-Saharan Africa (Basher and Briceno 2006; Meadows 2006). The region exhibits relatively low adaptive capacity (Kusangaya et al. 2014), as the El Niño drought event

of 2015-2016 amply demonstrates. Therefore future changes in rainfall over this region need to be identified and understood, such that stakeholders, from civil society to policymakers, can make informed decisions about future adaptation planning in key sectors (Collins et al. 2012; Knutti et al. 2010).

For most of the tropics, at least at regional scales relevant to decision-making, considerable uncertainty is evident across the ensemble of global and regional models currently available in both sign and magnitude of future precipitation projections (Rowell 2012; Knutti, and Sedláček 2013; McSweeney and Jones 2013). Central and southern Africa are no exception (see Section 3) and there is a clear need for improved understanding due in part to a complex climatological setting in which regional climate drivers as well as remote influences affecting the region (Christensen et al. 2013; Solomon et al. 2007 (IPCC); Kusangaya et al. 2014). This presents challenges to climate adaption policy and the persistence of uncertainty in climate projections has led to the development of 'Decision-making Under Climate Uncertainty' approaches in adaptation e.g. Hallegatte et al. (2012). There is, therefore considerable interest in improving our understanding of physical mechanisms driving the particular patterns of projected model changes, so that we may determine and potentially improve the robustness and credibility of projections. The physical processes driving projected change are numerous and may vary between models. Projection uncertainty is a result of varying processes found within models including, amongst other, parameterizations schemes, climate sensitivity, and regional patterns of SST changes.

Based on analysis of projections, various mechanisms have been proposed which link increased global temperatures and precipitation changes, notably the thermodynamic

wet-get-wetter process of rainfall change (Held and Soden 2000, 2006, Allen et al. 2010; Christensen et al. 2013; Chou and Neelin 2004; Meehl et al. 2007; Chou et al. 2009; Seager et al. 2010). This operates at the largest scales e.g. zonal means and involves the increase in global specific humidity in a warmer atmosphere leading to an increase (decrease) in precipitation in the regions of mean moisture convergence (divergence). In the tropics this is likely to be offset by the weakening of the mean tropical overturning circulation associated with a reduction in convective mass flux in regions of present-day high ascent (Chadwick et al. 2013; Christensen et al. 2013; Ma and Xie 2013; DiNezio et al. 2013; Vecchi et al. 2016).

Chadwick et al. (2013), hereafter C13, however, proposed that the wet-get-wetter mechanism alone does not explain well the global pattern of multi-model mean (MMM) projected rainfall change. The spatial correlation of future precipitation change (ΔP) and mean precipitation (P) globally is low, such that at regional and seasonal scales in the tropics other processes dominate. These processes are substantially related to changes in the spatial location of moisture convergence and hence convection. These include dynamic effects of regional gradients in near surface temperature change over oceans i.e. warmer-get-wetter (Xie et al. 2010), land-sea temperature contrasts (Dong et al. 2009; O'Gorman et al., 2015), land surface processes (Pitman 2003), aerosol direct, indirect and semi-direct effects (Huang et al. 2007; Lohmann and Feichter 2005; Ackerman et al. 2000; Hansen et al. 1997) and changes in circulation (Sherperd 2014). The thermodynamic balance of the 'upped-ante' (Neelin et al. 2003) mechanisms additionally contributes leading to results such as the 'modified warm-get-wetter' mechanism (Huang et al. 2013). The 'modified warmer-get-wetter' mechanism is described as the combination of SST changes (warmer-get-wetter effect) modified by

background climatological moisture and SSTs due to the non-linear relationship between tropical convection and SSTs.

Generally, the processes operating over the ocean are better understood than those over land but in all cases differing representation of these processes across models is likely to drive projection uncertainty. Most previous analyses have focused on the multi-model mean projected change quantities but Rowell et al. (2015) highlighted the importance of understanding the mechanisms of change within individual models and concluded further investigation be aimed at developing expert judgement of process-based mechanisms and their reliability of projections (Rowell et al. 2015).

In this context, the aims of this paper are to 1) Determine the mechanisms of projected regional precipitation changes by decomposition into thermodynamic and dynamic components 2) Quantify the contribution to total ensemble projection uncertainty, as represented by inter-model spread, associated with these mechanisms 3) Identify possible causes of uncertainty, and to draw inferences regarding the robustness and credibility of projected changes. The mechanism of change decomposition method of C13 is used to identify causes of precipitation change (aim 1) and associated uncertainty (aim 2) (reported in Section 3.1) and causes of uncertainty are inferred (aim 3) through analysis of the inter-model spread (reported in Section 3.2). This paper focuses on projected regional precipitation changes over Southern Africa (SA) and the adjacent southwest Indian Ocean (SWIO) sector (0˚- 30˚S and 10˚E - 80˚E), where wet season rainfall is dominated by the South Indian Ocean convergence zone (SIOCZ) (Cook 2000; Lazenby et al. 2016).

2. Data and Methods

2.1. Data

Output from simulations of the 20th century and the 21st century (under the RCP8.5 emissions scenario) from 20 models (those used in C13, Table 1) from the World Climate Research Program (WCRP) Coupled Model Intercomparison Project Phase 5 (CMIP5) multi-model dataset are used, which provide results for the most recent 5th Assessment Report (AR5) of the Intergovernmental Panel on Climate Change (IPCC) (Meehl et al. 2007; Taylor et al. 2012) (Table 1). Both the multi-model mean (MMM) of the 20 chosen CMIP5 models and the spread of model projections across the 20 model ensemble are considered, to address aims 1/2 and 3, respectively. Monthly data was extracted for key diagnostic variables to understand potential physical processes linked to precipitation changes over the SA/SWIO sector. The period of analysis for projected climate changes is 2071-2100 (in RCP8.5 experiment) minus the historical period 1971-2000. Only the first ensemble member was utilized in creating the MMM. All model data was interpolated to a common grid of 1.5˚ X 1.5˚ to ensure uniformity.

Table 1: CMIP5 model list of the 20 models used including modeling center, institute ID and atmospheric. (Models marked with a * indicates the models where the atmosphere-only version of the model was used in the analysis)

	Modeling Center (or Group)	**Institute ID**	**Atmospheric Resolution**
BCC-CSM1.1(m) ***BCC-CSM1.1****	Beijing Climate Center, China Meteorological Administration	BCC	2.8˚ x 2.8˚ 1.12˚ x 1.12˚
BNU-ESM	College of Global Change and Earth System Science, Beijing Normal	GCESS	2.8˚ x 2.8˚

	University		
CanESM2 ***CanAM4******	Canadian Centre for Climate Modeling and Analysis	CCCMA	2.8˚ x 2.8˚
CCSM4*	National Center for Atmospheric Research	NCAR	0.94˚ x 1.25˚
CESM1(BGC) **CESM1(CAM5)**	Community Earth System Model Contributors	NSF-DOE-NCAR	0.94˚ x 1.25˚
CNRM-CM5*	Centre National de Recherches Météorologiques / Centre Européen de Recherche et Formation Avancée en Calcul Scientifique	CNRM-CERFACS	1.4˚ x 1.4˚
CSIRO-Mk3.6.0	Commonwealth Scientific and Industrial Research Organization in collaboration with Queensland Climate Change Centre of Excellence	CSIRO-QCCCE	1.9˚ x 1.9˚
FIO-ESM	The First Institute of Oceanography, SOA, China	FIO	2.8˚ x 2.8˚
GFDL-CM3 **GFDL-ESM2G** **GFDL-ESM2M**	NOAA Geophysical Fluid Dynamics Laboratory	NOAA GFDL	2.0˚ x 2.5˚
GISS-E2-H	NASA Goddard Institute for Space Studies	NASA GISS	2.0˚ x 2.5˚
HadGEM2-CC **HadGEM2-ES** ***HadGEM2-A****	Met Office Hadley Centre (additional HadGEM2-ES realizations contributed by Instituto Nacional de Pesquisas Espaciais)	MOHC (additional realizations by INPE)	1.25˚ x 1.9˚
IPSL-CM5A-LR* **IPSL-CM5A-MR** ***IPSL-CM5B-LR****	Institut Pierre-Simon Laplace	IPSL	1.9˚ x 3.75˚ 1.25˚ x 2.5˚ 1.9˚ x 3.75˚
MIROC5*	Atmosphere and Ocean Research Institute (The University of Tokyo), National Institute for Environmental Studies, and Japan Agency for Marine-Earth Science and Technology	MIROC	0.56˚ x 0.56˚ 1.4˚ x 1.4˚
MPI-ESM-LR ***MPI-ESM-MR****	Max-Planck-Institutfür Meteorologie (Max Planck Institute for Meteorology)	MPI-M	1.9˚ x 1.9˚
MRI-CGCM3*	Meteorological Research Institute	MRI	1.1˚ x 1.1˚

NorESM1-M **NorESM1-ME**	Norwegian Climate Centre	NCC	1.9˚ x 2.5˚

2.2 The 'mechanism of change' decomposition methodology

To determine the main contributors to both the MMM precipitation change (see Section 3.1) and associated uncertainty (i.e. inter-model spread, Section 3.2) over the study domain, the C13 decomposition of change methodology was applied to data from each model for each calendar month. Focus is then specifically placed on the early and main SA/SWIO wet seasons OND and DJF, respectively.

Projected changes in precipitation can be decomposed into the dominant mechanisms of change; the thermodynamic and dynamic components. A number of methods have been proposed for the purpose e.g. Seager et al. (2010); Emori and Brown (2005). The method of C13 is utilised, which is based on the assumption that in convective climate regimes mean precipitation *(P)* is equivalent to the vertical mass flux from boundary layer to free troposphere *(M)* multiplied by specific humidity in the boundary layer *(q)*) (Held and Soden 2006);

$$P = Mq \qquad (1)$$

Because *M* (as defined here) is not directly available from most CMIP5 model outputs, in the decomposition a suitable surrogate *M** is derived directly from model mean *P* and q:

$$M^* = \frac{P}{q} \qquad (2)$$

C13 demonstrated M^* to be a suitable replacement for actual column-integrated convective mass flux M_{int} at the grid point level in global climate models. Therefore, the projected precipitation change, ΔP, can be expressed as,

$$\Delta P = \Delta(M^* q), \quad (3)$$

$$\Delta P = M^* \Delta q + q \Delta M^* + \Delta q \Delta M^*, \quad (4)$$

where M^* and q are the present day mean climatological values (1971–2000) of proxy mass flux and 2m specific humidity respectively and ΔM^* and Δq are the projected changes in those quantities over the period 2071-2100 compared to 1971-2000.

In this formulation Δq and ΔM^* represent the thermodynamic and dynamic components of change, respectively. The C13 method has the advantage that the dynamical term ΔM^* can be further separated into, ΔM^*_{weak} and ΔM^*_{shift}. ΔM^*_{weak} represents the tropics-wide weakening of the large-scale overturning circulation. It is derived from the climatological mean M^* ($\Delta M^*_{weak} = -\alpha M^*$), where α is a constant derived for each model, separately from the strong negative relationship observed between climatological M^* and ΔM^* across all grid cells in the tropics i.e. areas with higher M^* experience greater declines in ΔM^*, common to all models (see Figures 3 and 6 from C13).

The weakening in tropical circulation (zonally asymmetric i.e. Walker circulation) is typically representative of a weakening in convective mass flux (Held and Soden, 2006; C13) as a consequence of global warming. This occurs due to tropospheric warming following the moist adiabat in tropical regions, and therefore increasing static stability

globally in response to SST warming (Ma et al., 2012). Studies indicate the circulation is weakened by a decrease in the occurrence of strong updrafts and an increase of weak updrafts (Vecchi and Soden, 2007). This response is robust amongst models; however, the mechanism causing this weakening is not as distinctly understood.

Proposed reasons for this weakening are due to (i) the more rapid increase in dry static stability than in subtropical radiative cooling under enhanced greenhouse gas forcing (Knutson and Manabe, 1995), (ii) the less rapid increase of global-mean precipitation than atmospheric specific humidity (Held and Soden, 2006), (iii) higher extent of convection under global warming resulting in an uplift of the tropopause and therefore a more stable atmosphere (Chou and Chen, 2010). The aforementioned proposed mechanisms are linked to greater column warming that interacts with the mean circulation, thereby decelerating the tropical circulation (Ma et al., 2012). There is additionally a contribution to circulation weakening from the direct radiative effect of increased CO_2 concentrations (e.g. Bony et al. 2013).

$\Delta M^*_{shift} = \Delta M^* - \Delta M^*_{weak}$ i.e. the deviation in ΔM^* from that estimated directly from the regression of M^* and ΔM^*, and represents the effective 'shift' at a given grid cell towards a greater/weaker convective mass flux.

Δq can also be further separated into two components:

- Δq_{cc} the Clausius–Clapeyron change in surface q for the change in mean 2m temperature at each location (expected under fixed relative humidity).
- Δq_{rh} is the residual of Δq - Δq_{cc}, associated with changes in near surface relative humidity.

On this basis ΔP for each model can be decomposed into its individual components as,

$$\Delta P = M^{*}\Delta q_{cc} + M^{*}\Delta q_{rh} + q\Delta M^{*}{}_{weak} + q\Delta M^{*}{}_{shift} + \Delta q\Delta M^{*}, \quad (5)$$

which for convenience in terminology can then be expressed as:

$$\Delta P = \Delta P_{T} + \Delta P_{RH} + \Delta P_{Weak} + \Delta P_{Shift} + \Delta P_{Cross}, \text{ where,} \quad (6)$$

- ΔP is the change in precipitation expressed per degree global warming
- $\Delta P_{T} = M^{*}\Delta q_{cc}$ is the thermodynamic change due to Clausius–Clapeyron-driven increases in specific humidity
- $\Delta P_{RH} = M^{*}\Delta q_{rh}$ is the change due to near surface relative humidity changes
- $\Delta P_{Weak} = q\Delta M^{*}{}_{weak}$ is the change due to the weakening tropical circulation
- $\Delta P_{Shift} = q\Delta M^{*}{}_{shift}$ is the change due to spatial shifts in the pattern of convective mass flux
- $\Delta P_{Cross} = \Delta q\Delta M^{*}$ is the cross component of precipitation change, associated with interactions between the other components.

The total thermodynamic component consists of $\Delta P_{T} + \Delta P_{RH}$. For simplicity, the total thermodynamic component ($\Delta P_{T} + \Delta P_{RH}$) is combined with the dynamic component associated with the weakening of the tropical circulation (ΔP_{Weak}) to create a new component named ΔP_{twrh} (hereafter named the 'thermodynamic residual' term, from Kent et al. 2015). ΔP_{Weak} is included with the thermodynamic terms due to the strong anti-correlation between these components. This analysis of the mechanisms of change as applied to the ensemble MMM is presented in Section 3.1.

2.3 Analysis of uncertainty

In order to quantify model uncertainty in projected change the spread in the precipitation change components over the 20-model member ensemble (Section 3.2) are assessed. The dominant spatial pattern of variation in ΔP_{Shift} between models is identified with EOF analysis, applied to the cross model ΔP_{Shift} fields (standardised) for two separate domains with our study region: the Southern African continental land region (10˚S - 30˚S, 10˚E - 40˚E) and Indian Ocean (0˚S - 30˚S, 40˚E - 80˚E) region, (see section 3.3). Potential drivers of this uncertainty are then assessed through correlations of the ΔP_{Shift} EOF component scores with diagnostic fields (SST and circulation indices) across the model ensemble and through composite analysis of diagnostic fields from models sampling the upper and lower 25% of models from the EOF scores (see section 3.3).

Note: all components of projected change in this analysis are normalised by the mean global surface temperature change (ΔT_{global}) of each individual model, and therefore all quantities are expressed as per degree global warming. This removes the uncertainty due to inter-model spread in climate sensitivity and makes results scalable to the magnitude of warming (assuming quasi-linearity of regional precipitation change with warming), and therefore tractable when applied to pre-defined warming levels for policymakers. Removing the effect on ΔP of uncertainty in model ΔT_{global} related to model climate sensitivity has minor influence on our results (see Figure 1). The implication of normalising each component by ΔT_{global} does not result in an effective removal of the Clausius–Clapeyron effect in the ΔP_T term, but rather expresses the term as the local change measured per degree global warming.

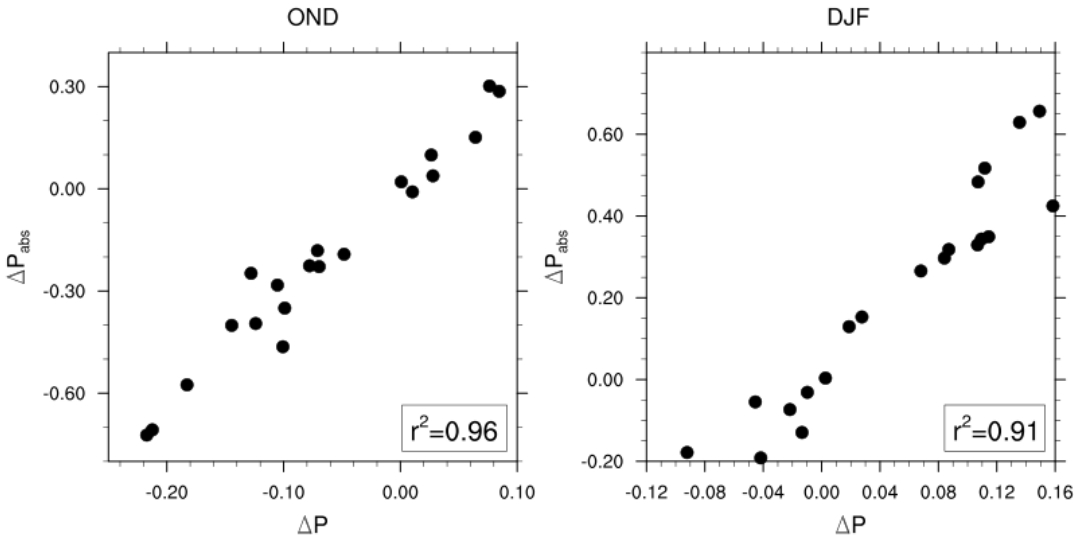

Figure 1: Relation of absolute projected precipitation ΔP_{abs} change versus normalised precipitation change ΔP for the 20 CMIP5 models for the period 2071-2100 minus 1971-2000 under the RCP8.5 scenario for the seasons DJF and OND respectively. Quantities are area averaged over the study domain (0˚- 30˚S – 10˚- 80˚E).

3. Results and discussion

3.1. Changes in multi-model mean precipitation over southern Africa and adjacent Indian Ocean

First, the annual cycle of zonally averaged MMM precipitation changes are considered over the study domain for land and ocean regions (Figure 2a and 2b, respectively). The most pronounced feature of projected changes in rainfall over both land and ocean is an opposing dipole of future wetter/drier conditions, which is oriented to the north/south, respectively of the climatological axis of maximum rainfall. As such, this ΔP wetter/drier dipole structure effectively straddles the ITCZ with wetting (Feature A in

Figure 2a, e) and drying (Feature B in Figure 2a, e) located to the north and south, respectively, of the ITCZ axis. This indicates an effective northward shift in the ITCZ. This dipole pattern however, has a strong seasonal cycle peaking in the austral spring (SOND) over both land and ocean. The OND season is often overlooked in studies of SA/SWIO climate in favour of the main rainy season, DJF, but here, a remarkably strong rainfall change signal in OND demands explanation.

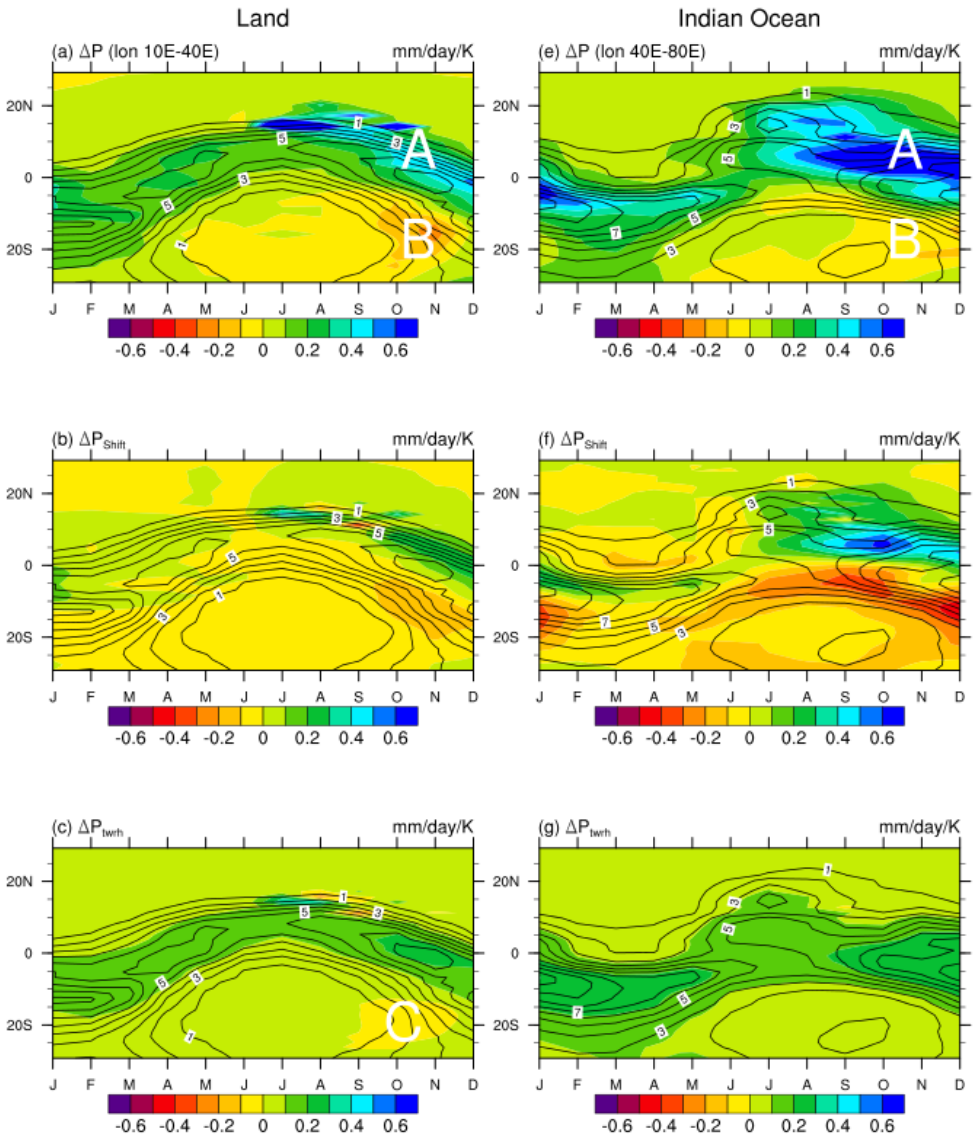

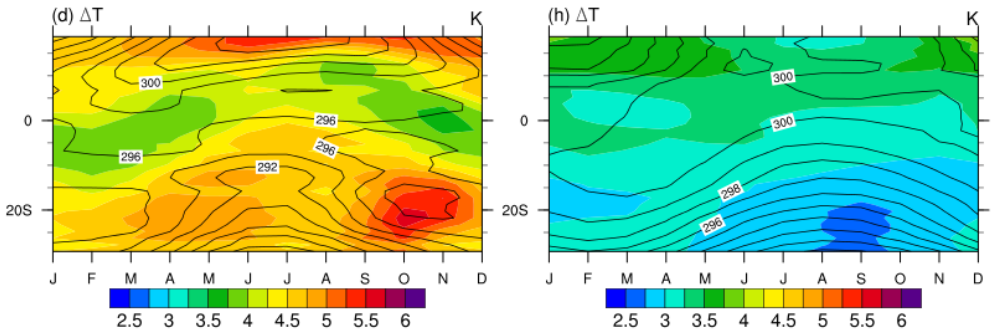

Figure 2: Time-latitude plots of projected MMM changes in precipitation, and related mechanisms of change components, derived from the 20 CMIP5 models for the future period 2071-2100 minus 1971-2000 under the RCP8.5 scenario. Values are averaged over longitude bands indicative of the SA continent 10˚ - 40˚E for (land-only, left column) and the Indian Ocean 40˚ - 80˚E (ocean-only, right column). (a) and (e) show ΔP (shaded) overlaid with historical climatological P (1971-2000). (b) and (f) as (a) and (e) but for ΔP_{Shift} (shaded). (c) and (g) as (a) and (e) but for ΔP_{twrh} (shaded). (d) and (h) show ΔT overlaid with historical climatological T. Units of ΔP and associated components are in mm day^{-1} per degree global warming and P in mm day^{-1}. Units of ΔT and T are in degrees Kelvin. See text for explanation of features marked A and B.

The spatial patterns of MMM precipitation change over the study region for the key seasons OND and DJF (Figures 3 and 4) illustrate clearly this dominant zonally-oriented pattern of wetter/drier conditions located to the north/south of the mean ITCZ, apparently connecting precipitation changes over the southern African continent with those in the equatorial and southwest Indian Ocean. The continental drying is most pronounced in OND (Figure 2, Feature B) centred ~15˚S over the SA continent. This may and may indicate a later start and reduced length of the growing season rainfall with serious implications on the agricultural sector. In addition to the wetting-drying

dipole there is evidence of additional wetting over 25˚ - 30˚S over eastern South Africa and across into the southwest Indian Ocean, especially in DJF.

Table 2: Spatial correlations of MMM Δ*P* versus the different mechanisms of change components for both DJF and OND for the SA/SWIO region (0˚-30˚S and between 10˚-80˚E) (Using a student's t test correlation values above 0.44 are deemed significant at the 0.05 confidence interval, shown in bold)

DJF	**Δ*P* (0˚-30˚S 10˚-80˚E)**	**Δ*P* Land (0˚-30˚S 10˚-40˚E)**	**Δ*P* Ocean (0˚-30˚S 40˚-80˚E)**	**OND**	**Δ*P* (0˚-30˚S 10˚-80˚E)**	**Δ*P* Land (0˚-30˚S 10˚-40˚E)**	**Δ*P* Ocean (0˚-30˚S 40˚-80˚E)**
ΔP_{Shift}	**0.96**	**0.97**	**0.97**	ΔP_{Shift}	**0.94**	**0.95**	**0.95**
ΔP_{T}	0.18	0.04	0.24	ΔP_{T}	0.29	0.26	0.29
ΔP_{Weak}	-0.23	-0.16	-0.29	ΔP_{Weak}	-0.35	-0.39	-0.33
ΔP_{RH}	0.12	0.40	0.30	ΔP_{RH}	0.21	**0.46**	**0.54**
ΔP_{twrh}	0.30	**0.53**	0.27	ΔP_{twrh}	**0.46**	**0.70**	0.33
ΔP_{Cross}	**0.57**	**0.51**	**0.58**	ΔP_{Cross}	0.35	0.19	0.43
P	0.18	0.12	0.22	P	0.30	0.34	0.27

The decomposition can aid in understanding the processes driving these changes. The thermodynamic component $\Delta P_{T,}$ (Figure 3d, 4d) results in a wetting signal everywhere but whose magnitude is proportional to a rise in temperature through the Clausius-Clapeyron relation i.e. it represents the 'wet-get-wetter' process and maps substantially onto mean rainfall. It is substantially offset by an equivalent pattern of drying from the weakening of the tropical overturning circulation ΔP_{Weak} (Figure 3e, 4e), which is inversely proportional to M^* and as such maps onto mean P. In addition, over land wetting from ΔP_T is offset by drying from ΔP_{RH} (Figure 3f, 4f), due to reduced relative

humidity, presumably resulting from moisture supply not keeping pace with increasing temperature. Together, these terms constitute the 'thermodynamic residual' term ΔP_{twrh} (Figures 2c, 2g, 3g and 4g) which drives a net wetting signal, peaking over the oceanic climatological ITCZ and humid land regions. ΔP is therefore partly composed of a thermodynamic wet-get-wetter process magnifying the mean ITCZ rainband. However, the thermodynamic ΔP_{RH} response also drives up to ~50% of the drying over subtropical land regions during OND (Feature C in Figure 2c) centred on ~20˚S. This is broadly coincident with the maxima in ΔT (Figure 2d, Feature D), suggestive of a land-atmosphere positive feedback response in early wet season, which is overcome during the peak DJF wet season. As such over land in OND ΔP_{twrh} is an important driver of the spatial pattern of ΔP (r = 0.70), substantially associated with $\Delta P_{RH.}$

However, overall the study region as a whole, it is clear from Figures 2-4 and Table 2 that the spatial pattern of ΔP in OND or DJF is not closely related to that of mean precipitation (P) (spatial correlations are not significant) nor to the thermodynamic residual term ΔP_{twrh} (r = 0.46 and 0.3 for OND and DJF, respectively) such that the notable dipole features of ΔP are not driven by the 'wet-get-wetter' process. Rather ΔP most closely matches the dynamical component ΔP_{Shift} (r = 0.94 for OND and 0.94 for DJF) such that it is changes in the location of convection that explain the dipole. ΔP_{Shift} contributes most of the wetting/drying dipole over land and almost all of it over ocean, especially the drying signal south of the ITCZ. It is postulated here that this projected northward shift of the ITCZ over the Indian Ocean may be related to projected changes in the SST structure through a 'warmest-get-wetter' mechanism. The north-south gradient in SST over the Indian Ocean broadly representative of the ΔP dipole (~5˚N - 20˚S) in the present day of ~2 - 4K over the austral summer-winter seasons (Figure 2h)

is enhanced in the MMM projections by ~0.5K (Figure 2h, 3h and 4h). This may lead to a northward displacement of convection towards the warmest oceanic waters, similar to that noted for the tropical Pacific (Widlansky et al. 2013).

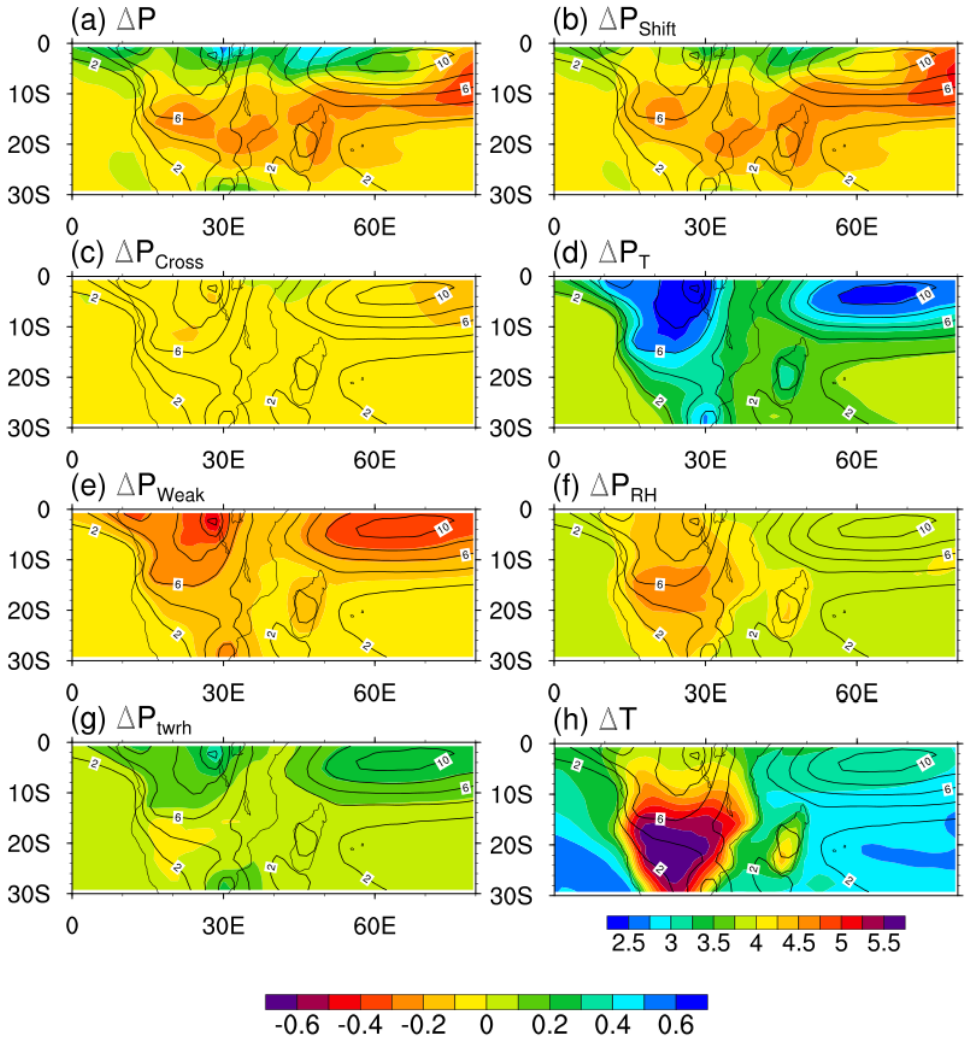

Figure 3: Projected MMM changes in precipitation (a), and related mechanisms of change components (b)-(g), derived from the 20 CMIP5 models for the future period 2071-2100 minus 1971-2000 under the RCP8.5 scenario, for the OND season over SA and the SWIO region. ΔP_{twrh} is the sum of ΔP_T + ΔP_{Weak} + ΔP_{RH}. Black contours overlaid represent climatological precipitation for the specific season contoured from 0 to 10 mm/day in intervals of 2 mm/day. Units are in absolute change per degree global

warming. (h) Projected 20 CMIP5 MMM temperature changes for the same time period and region with units in degrees Kelvin.

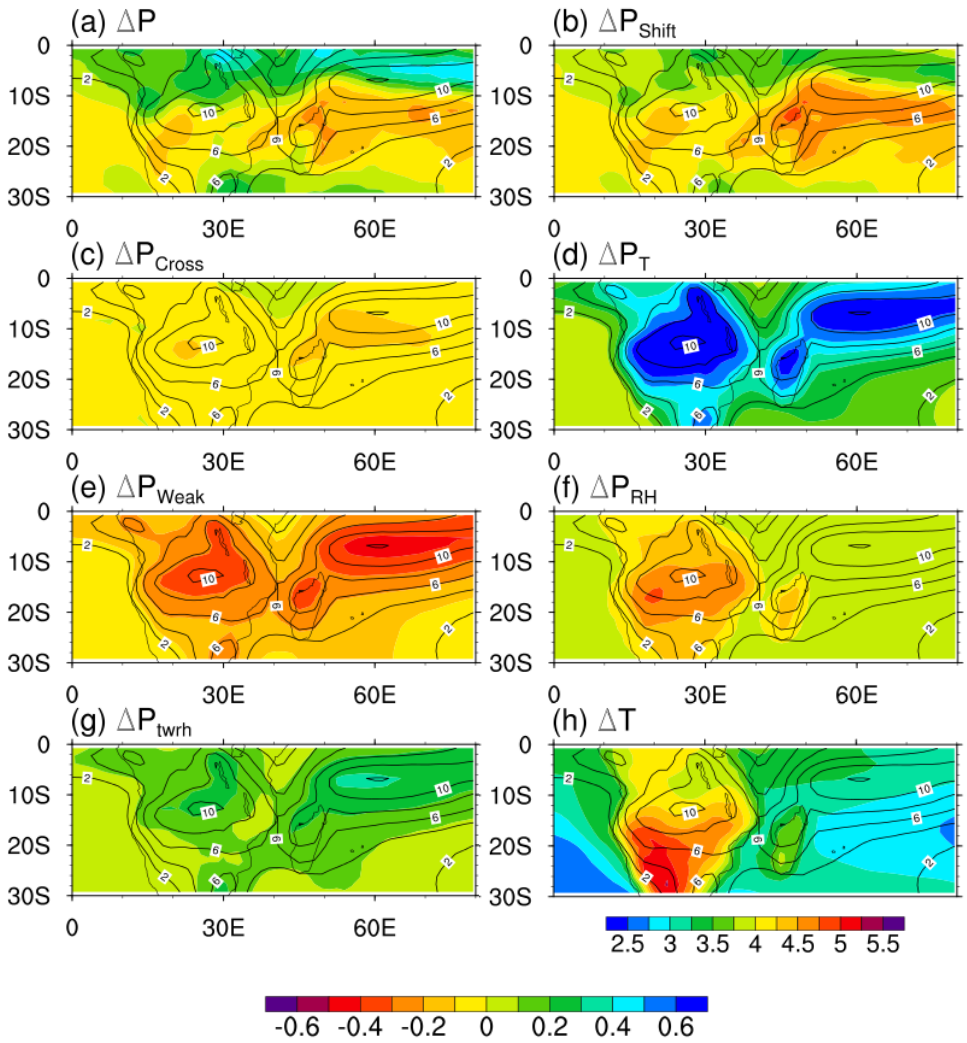

Figure 4: Same as Fig 3 but for the DJF season

3.2. Quantifying uncertainty in projected change in precipitation: ensemble spread

Uncertainty across the multi-model ensemble remains a feature in projections of future precipitation across the tropics and is a major barrier to effective use of climate information in adaptation activities, notwithstanding approaches to 'decision making under climate uncertainty' e.g. Lempert and Collins (2007). Here, the contributions to total ensemble uncertainty from the various mechanisms of change are assessed in the

decomposition. The robustness of projected changes is evaluated from the magnitude of inter-model spread for each component as represented in two forms: First, as maps of the standard deviation of the ensemble at each grid cell (Figure 5 and 6). Second, as box-whisker plots of inter-model spread for each component averaged over specific regions of interest (Figure 7). Area averages over where the MMM change signal shows mean future wetting or drying to help inform interpretation of the robustness of key signals emerging from MMM commonly used e.g. IPCC WG1 Chapter 9 (Stocker et al. 2013). Further, land and ocean are analysed separately given the differing level of importance for adaptation actions and mechanism driving changes. A number of broad signals emerge.

(i) Changes in precipitation are more robust over land than ocean for both the future drying and the wetting signals i.e. total uncertainty in ΔP is lower for land compared to ocean (Figure, 7). This difference in the spread of ΔP is largely related to that in ΔP_{Shift}, such that uncertainty in the dynamical drives of projected change is dominant. The contribution of inter-model differences is explored in SST structures to uncertainty in ΔP_{Shift} Section 3.3.

(ii) The MMM projected drying is more robust than the wetting over both land and ocean and in OND, but differences are small in DJF. The future signal with the greatest robustness is the continental drying over (especially western) SA during the OND season (Figure 5 and 7), reinforcing the importance of this early wet season component of the larger scale rainfall change dipole. During DJF (Figures 6 and 7) the MMM drying signal is less robust, and there are ‘hotpots’ of non-robust change include parts of Malawi, Tanzania, Madagascar and northern Mozambique with potentially important

implications for approaches to climate change adaptation. Areas of robust wetting include East Africa and the western Indian Ocean at ~0˚N.

(iii) The local 'hotspots' in inter-model ΔP standard deviation show that uncertainty in ΔP does not simply scale with the absolute magnitude of ΔP. These are located for example proximate to the African great lakes, regions of complex topography (e.g. Madagascar), and at the transition boundaries of wetting-drying over the Indian Ocean (Figure 5a, 6a), raises the possibility that inter-model differences in background climatology may project onto the uncertainty in ΔP. However, only some of these hotpots of uncertainty correspond to locations of high inter-model spread in mean P (Figures 5h and 6h) such that most of the spatial pattern in uncertainty in ΔP is unrelated to background climatology. The high uncertainty in ΔP often apparent in wetting to drying transition zones suggest that caution needs to be attached to interpretation of near zero MMM ΔP change.

(iv) Most of the total uncertainty in ΔP is contained in the ΔP_{Shift} component, whose uncertainty is typically greater by a factor of 2-4 times than that of the thermodynamic residual. Inter-model standard deviation within the ΔP_{Shift} term is markedly higher over ocean than land, notably over the ΔP dipole region. Whilst the MMM wetting/drying dipole over the Indian Ocean may result from a 'warmest-get-wetter' response to changes in the SST structure, high uncertainty in ΔP_{Shift} suggests strong inter-model divergence in the form of the ΔSST patterns responsible (Chadwick 2016), which is explored in Section 3.3. Indeed, in many regions, notably the region of projected drying over the Indian Ocean at 10˚-15˚S, the model uncertainty in ΔP_{Shift} is higher

than that in ΔP. ΔP_{twrh} is especially robust over the ocean ITCZ where the thermodynamic response is closest to that of ΔP_T.

(v) Since the total uncertainty can be less than the sum of the individual components (e.g. Figure 7) it is inferred that the inter-model components are anti-correlated across models and offset each other, which acts to constrain total uncertainty in ΔP. For the drying over continental SA (during OND) and to a lesser extent over the Indian Ocean, uncertainty in the dynamical ΔP_{Shift} and thermodynamic residual term ΔP_{twrh} terms appear to offset each other, resulting in a total inter-model standard deviation of ΔP which is much less than the sum of the component terms.

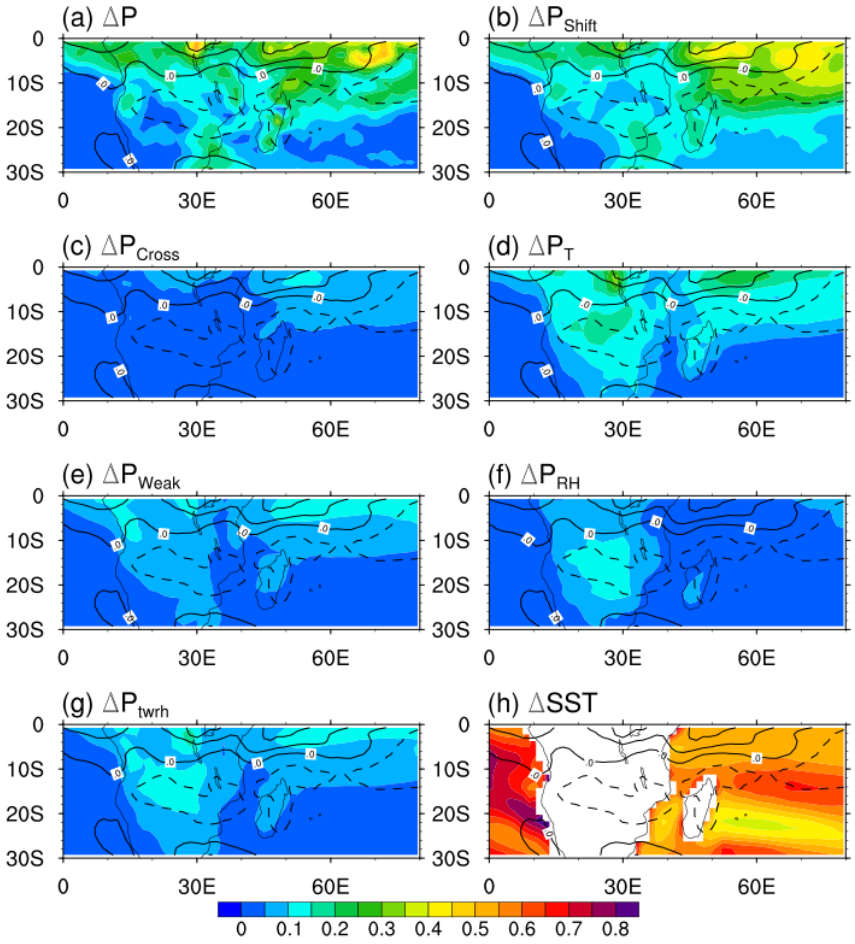

Figure 5: Inter-model standard deviation (shaded) in (a) ΔP (units mm/day/K), (b) - (g) and mechanism of change components therein (unit mm/day/K) and (h) ΔSST (units K),

for the OND season. Contours show MMM ΔP (values from -0.6 to 0.6 mm/day/K in intervals of 0.2, where dashed contours show negative values). Change quantities are for the period 2071-2100 minus 1971-2000 under the RCP8.5 scenario.

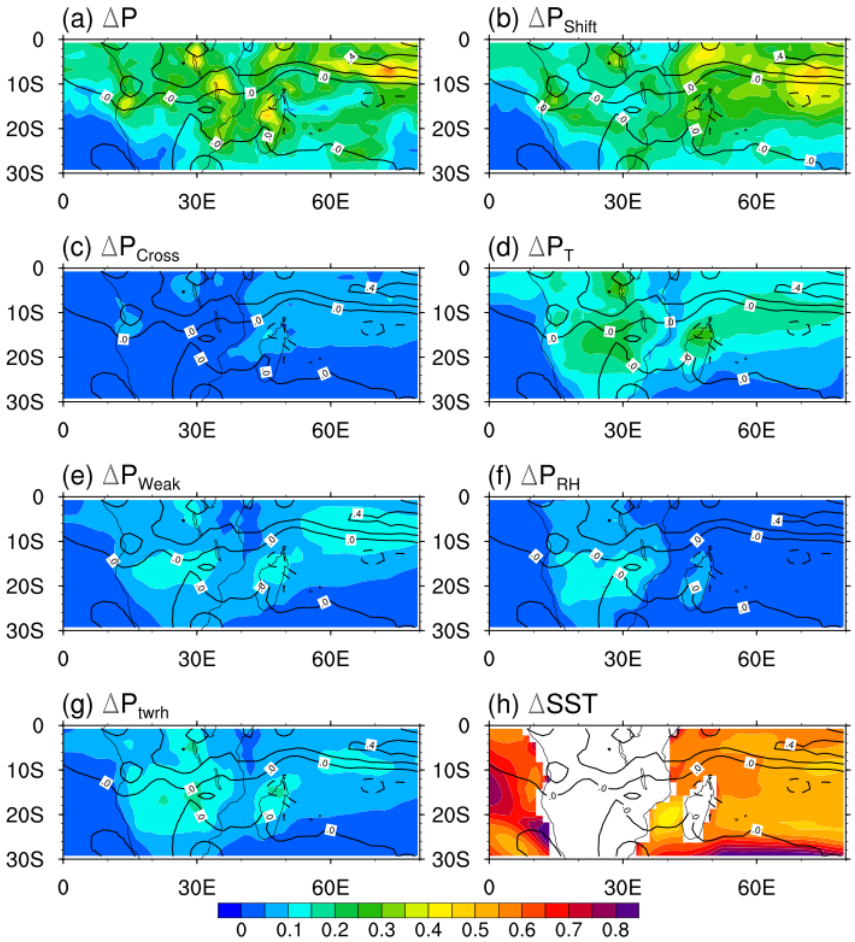

Figure 6: Same as Fig 5 but for DJF

DJF Box Plot over SA Drying (Land -Only) (10-40E 0S-30S)

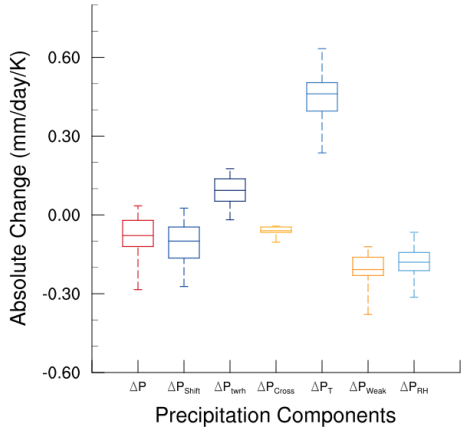

OND Box Plot over SA Drying (Land -Only) (10-40E 0S-30S)

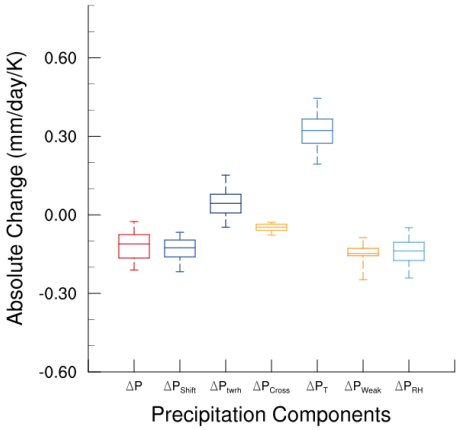

DJF Box Plot over SA Wetting (Land -Only) (10-40E 0S-30S)

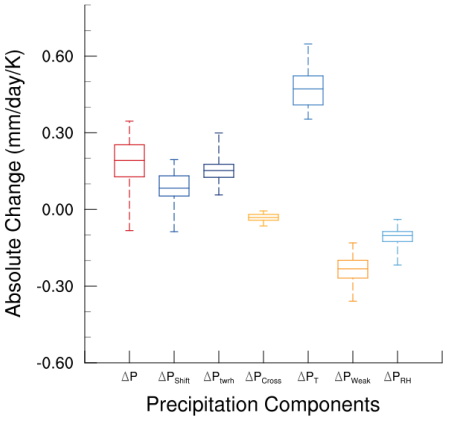

OND Box Plot over SA Wetting (Land -Only) (10-40E 0S-30S)

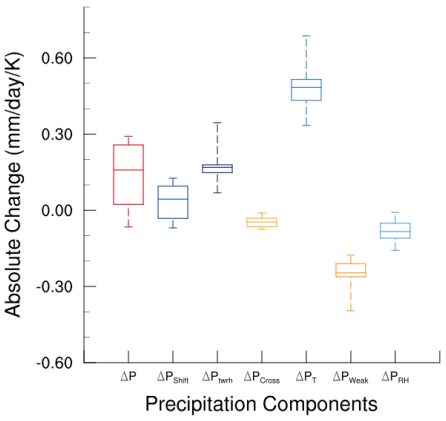

DJF Box Plot over SA Drying (Ocean -Only) (40-80E 0S-30S)

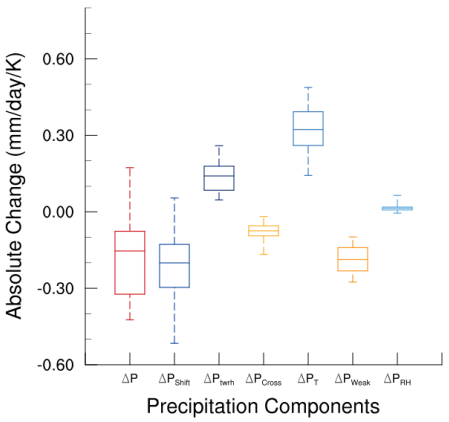

OND Box Plot over SA Drying (Ocean -Only) (40-80E 0S-30S)

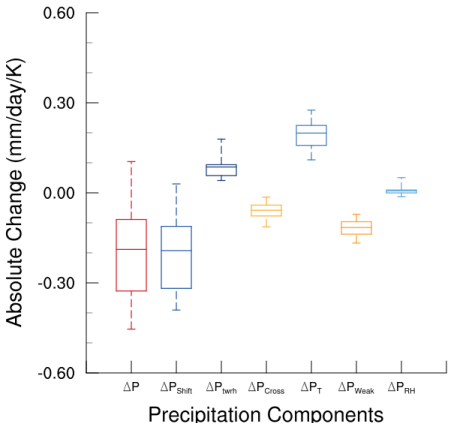

DJF Box Plot over SA Wetting (Ocean -Only) (40-80E 0S-30S)

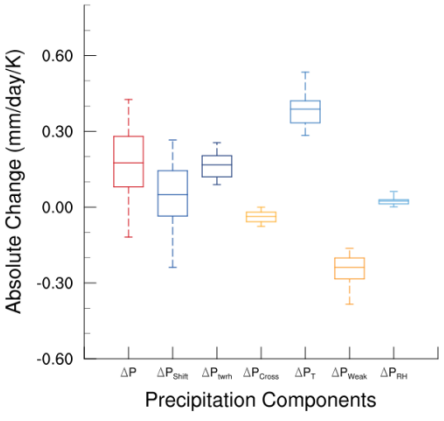

OND Box Plot over SA Wetting (Ocean -Only) (40-80E 0S-30S)

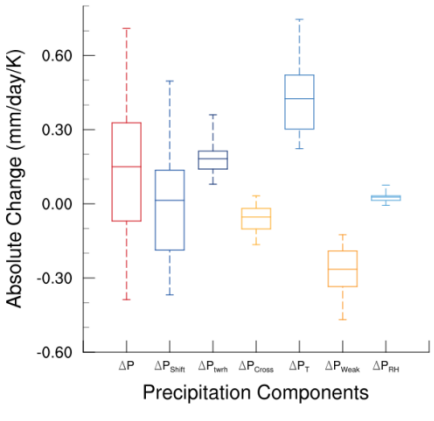

Figure 7: Box-whisker plots of the future change in ΔP and various components therein from the 20 CMIP5 models, for the period 2071-2100 minus 1971-2000 for RCP8.5 of CMIP5 models for both land and ocean drying and wetting regions for OND and DJF respectively. Units are absolute change per degree global warming

3.3. Understanding potential causes of uncertainty in the dynamic component of projected change

The dynamical ΔP_{Shift} term provides the primary contribution to inter-model uncertainty in future projections of precipitation. Amongst the potential causes of this uncertainty in the location of tropical convection, a primary candidate is the varying patterns of model projected SST changes. This is explored here using EOF analysis of the inter-model ΔP_{Shift} patterns. Over the Indian Ocean domain during both OND and DJF the leading mode of inter-model ΔP_{Shift} variability shows a loading pattern (Figure 8a and 8b) which projects strongly onto the pattern of the future wetting/drying dipole in ΔP_{Shift} (Figure 3b and 4b), and indeed in ΔP explaining 37% and 31.5% of variability, respectively. These EOFs therefore represent well the strength of the MMM ΔP wetting/drying dipole, oriented broadly north-south, in individual models.

The component scores of this leading EOF correlate moderately with inter-model ΔSST over the Indian Ocean in both OND and DJF (Figures 8c and 8d). In both cases the correlation is such that a stronger north/south wetting/drying dipole in individual models is associated with lower rates of SST warming in the Indian Ocean south of the Equator, and hence an increased north-south SST gradient across the Indian Ocean. This

response across models is consistent with the 'warmest-get-wetter' mechanism inferred from the MMM changes in precipitation and SST (Section 3.1). Moderate correlations also exist with Δ*SST* in the tropical Pacific broadly around the Nino3.4 region. During OND there is an additional indication that the ΔP_{Shift} EOF dipole is related to changes in mean the east-west SST gradient reminiscent of the Indian Ocean Dipole (IOD) mode of inter-annual variability active in this season (Saji et al., 1999). Previous analysis has related changes in long-term mean precipitation to a shift towards a preference for the positive mode of the IOD in some coupled models (Shongwe et al. 2011) which remains consistent with the 'warmest-get-wetter' mechanism.

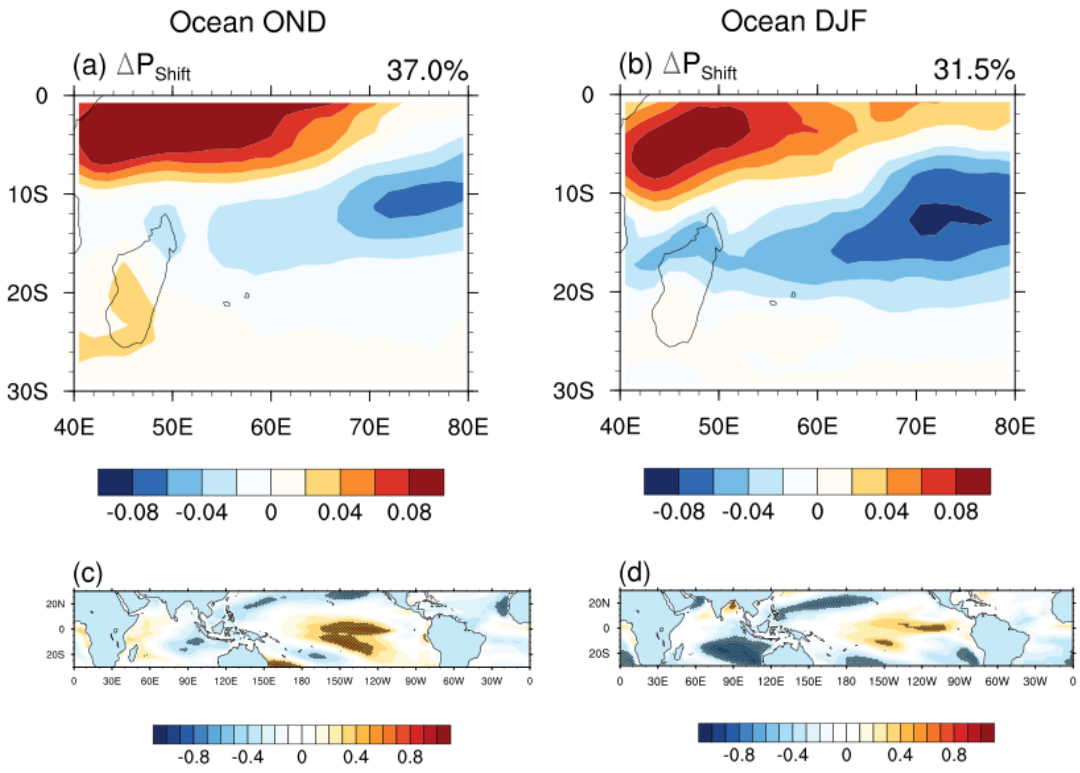

Figure 8: Leading EOF loading patterns of inter-model ΔP_{Shift} for 20 CMIP5 models over the Indian Ocean domain for (a) OND and (b) DJF. (c) and (d) respectively show the correlation coefficients of the EOF component scores versus inter-model Δ*SST*. Significant correlations at the 90% percentile are stippled.

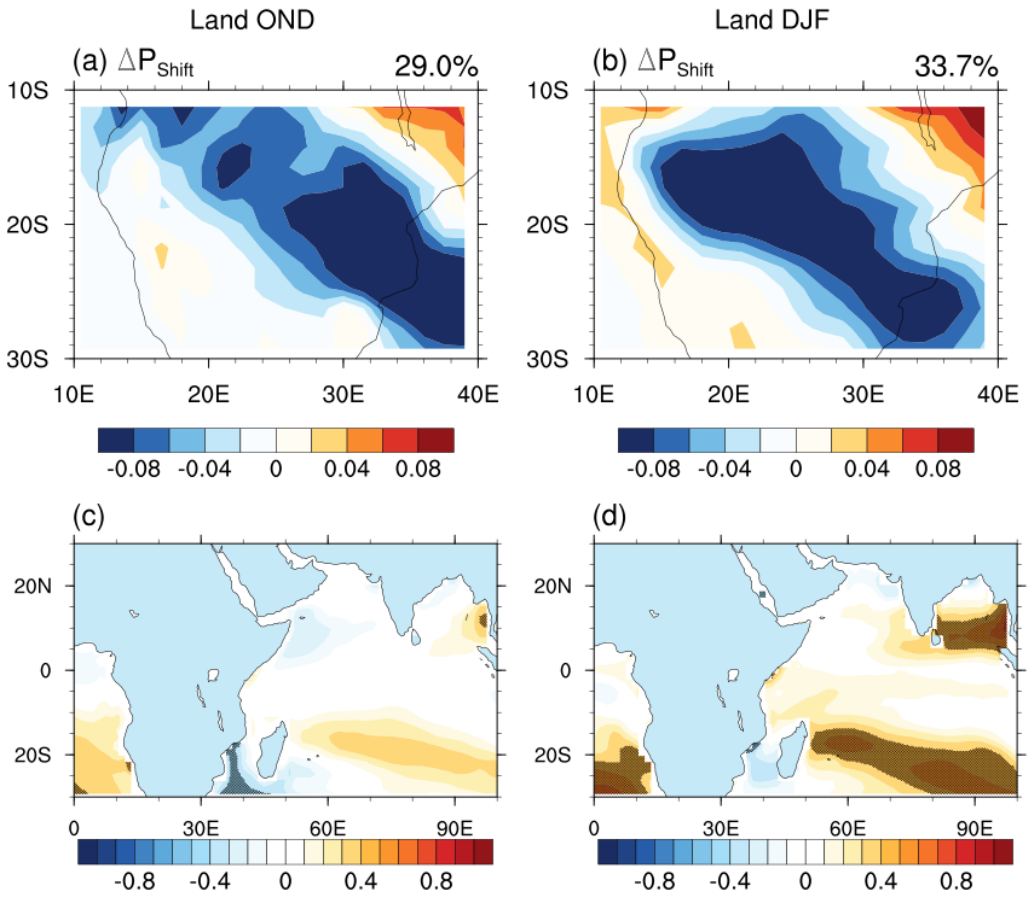

Figure 9: Same as Figure 8 but for the Southern Africa land domain whereby Δ*SST* correlations are restricted only to the SWIO domain.

Over the domain centred on the SA landmass the inter-model ΔP_{Shift} EOF analysis for both the OND and DJF seasons reveals a dominant EOF loading pattern oriented diagonally northwest to southeast across SA towards the southwest Indian Ocean (Figures 9a and 9b). The peak loadings lie to the southwest of the position of the mean SIOCZ feature such that the EOF represents the magnitude of the MMM drying signal to the south of the mean rainfall maximum. The MMM projected pattern of ΔP_{Shift} change across the region is more zonally oriented than the EOF SIOCZ-like orientation

(Figure 3b,4b see Section 3.1) such that the MMM change clearly masks considerable spread within the ensemble.

The EOF pattern of inter-model ΔP_{Shift} appears associated with inter-model variability in SST, land heating and circulation and resulting moisture fluxes based on both correlations (Figure 9c, 9d) and composites of diagnostic fields based on samples of the upper and lower 25% of models from the EOF component scores (Figure 10). The EOF is rather weakly correlated to the inter-model structures of projected changes to SST across the southern Indian Ocean with an east-west dipole structure of correlation with the EOF component scores along ~20˚ - 25˚S (Figure 9c and 9d) and corroborated in the composites (Figure 10). For both the OND and DJF EOF, stronger future drying over SA in models is associated with weaker future warming in the Mozambique channel/southwest Indian Ocean and stronger warming in the Eastern subtropical Indian Ocean.

Further, more intense drying over SA in models is associated with cyclonic low level circulation over the southwest Indian Ocean (Figure 10) around a weaker subtropical high, which will cause moisture divergence over SA and convergence over the adjacent Indian Ocean, driving the effective northeastward shift in the axis of the SIOCZ (Lazenby et al, 2016). In DJF (Figure 10b) intense drying is also favoured in models in which strong land heating at ~20˚S drives an intensification of the continental low pressure centre (the ‘Angolan low’ feature) and cyclonic low level circulation further pushing the shift in convergence northeastward.

These structures of inter-model differences in ΔSST, land temperature and low-level circulation that may drive the leading pattern of inter-model spread in ΔP_{Shift} over SA have some resonances with modes and structures of inter-annual variability in the region. Notably, (i) the regional response to ENSO characterised by the displacement in the SIOCZ associated with cyclonic low level anomalies over the southwest Indian Ocean during El Niño events (Cook 2001), similar to that in Figure 10. However, it is cautionary to note that the physical mechanisms and influence of local Indian Ocean SST (e.g. Goddard and Graham, 1999) versus remote Pacific SSTs (e.g. Cook, 2001, Ratnam et al, 2014) in driving this in the observed climate remain to be fully resolved. (ii) The South Indian Ocean dipole mode of east-west SST gradient in the subtropical Indian Ocean (Behera and Yamagata, 2001). In this case, although the form of the association of ΔP_{Shift} over SA and ΔSST matches that of inter-annual variability in SA rainfall and the phase of the SIOD (Reason, 2001), the circulation responses diverge. (iii) The intensity of the Angolan Low and associated circulation changes, known to be an important control on present day precipitation in observations (e.g. Manhique et al., 2011) and in models (Munday and Washington, 2017). Differential rates of future warming over land versus ocean may be expected to intensify and displace the Angolan low and a clear differential response across models is seen, which are strongly related to inter-model uncertainty in the structure of future dynamical precipitation responses.

Of course, it is not expected that the dynamical processes of inter-model spread in projected rainfall change to be consistent with all aspects of current inter-annual variability, given (i) the complex suite of inter-annual modes affecting the SA region (ii) the highly variable and mixed ability of coupled models to represent the mean state

and variability both through local processes (Lazenby et al. 2016) and remote teleconnections (e.g. Rowell 2015). Nevertheless the link between processes of climate variability and projected change has proved to be a fruitful focus in recent years in explaining why models make the future changes they do, providing some basis for assessing potential credibility of projected change.

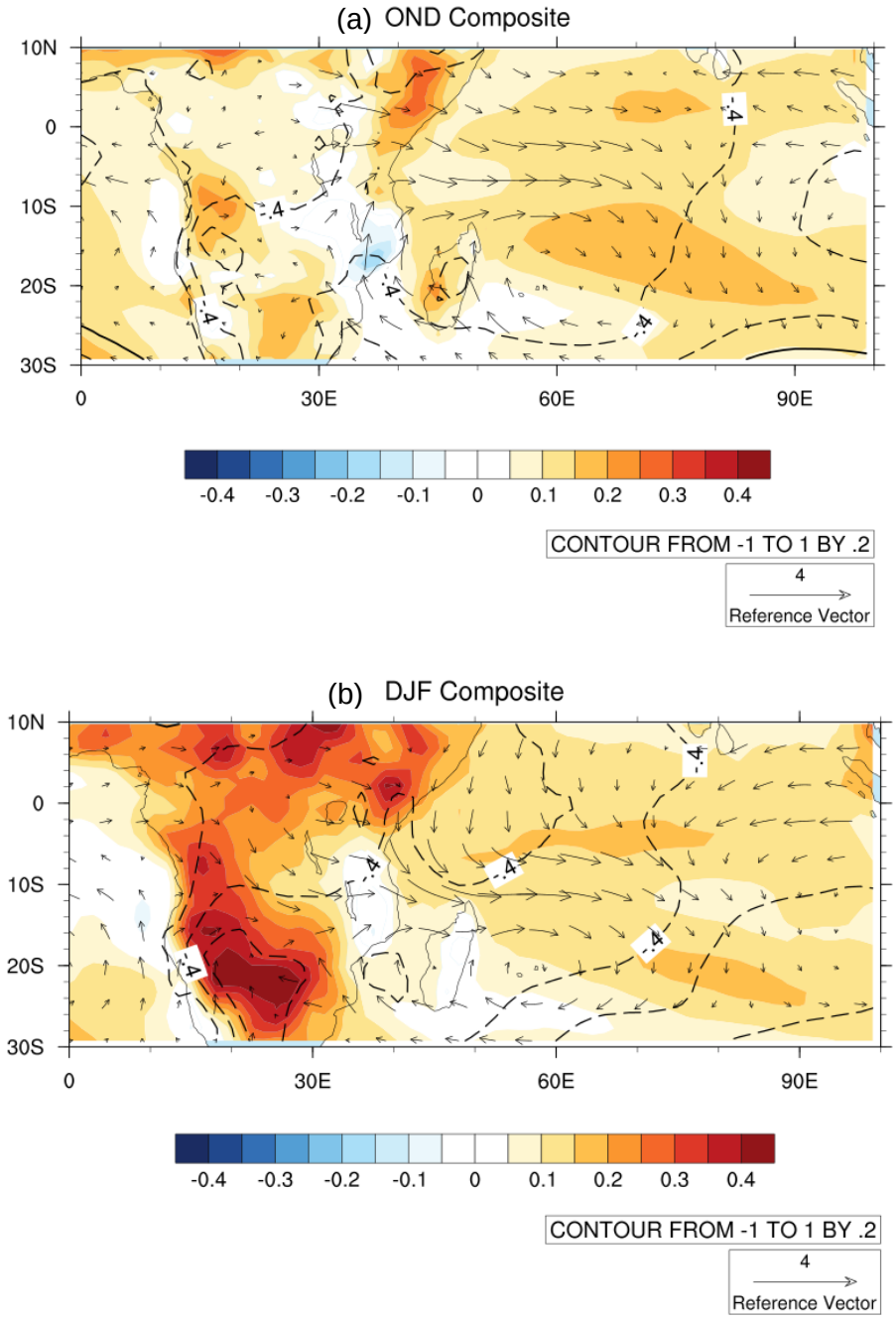

Figure 10: Composite mean fields of diagnostic variables based on samples of the uppermost 25% minus the lowermost 25% of models selected from the component scores of the leading EOF of the inter-model ΔP_{Shift} (Figure 9a and 9b) for (a) OND and (b) DJF. Fields shown are changes in surface temperature (K, shaded), surface pressure (hPa, contours, interval 0.2) and 850hPa OND winds (ms^{-1}, vectors).

4. Discussions and Conclusions

Human influence is expected to drive considerable changes to the hydrological cycle, of particular concern in regions, such as SA, which are currently vulnerable to climate. There is a need to quantify and understand the projections of future precipitation change and associated uncertainty to inform the possible use of climate information in adaptation planning. Our analysis of end of 21st century projections from a sample of 20 models from the CMIP ensemble reveals a dominant dipole pattern of precipitation change over SA/SWIO with a wetting/drying response to the north/south of the ITCZ, therefore an effective northward shift in the ITCZ. Pronounced drying is exhibited over land in OND, implying a delay in the onset of the wet season, an important and relatively robust signal.

A decomposition framework is applied to separate the mechanisms of change in both the MMM and in individual models to shed light on the relative importance of the multiple, coincident and often competing mechanisms which may drive future precipitation changes in a warmer world. It is shown that the dynamical component ΔP_{Shift} representing spatial shifts in convection explains most of the dipole structure of

ΔP, as evidenced by high spatial correlations no less than 0.94 over the study domain. The thermodynamic component of increased moisture is offset by the weakening of the tropical circulation leading to a relatively weak 'wet-get-wetter' contribution. Considering the robustness of projected change, represented by the inter-model dispersal in response, it is found that ΔP_{Shift} holds the most uncertainty, whereas the thermodynamic component is typically more robust. Drying is more robust than wetting over the continent, notably in the early summer OND season.

Over the Indian Ocean sector the dominant dynamically driven ΔP_{Shift} component is related to changes in SST structures. The wetting/drying dipole is associated with patterns of SST change, both in the MMM and across the model ensemble, that is consistent with a 'warmest-get-wetter' mechanism driving the northward shift in the location of convection and convergence. Much of the model uncertainty therefore is associated with inter-model differences in future SST patterns in the tropical Indian and Pacific Ocean and the atmospheric teleconnection response, such that better understanding of these projected changes and in the teleconnections linking these to rainfall may provide some basis for constraining uncertainty in projections.

Changes in rainfall over land are likely more complex. First because over the continental interior of SA the contribution to mean drying of the thermodynamic reduction in relative humidity is roughly equal to that of the dynamical component. Reduced relatively humidity is likely itself to be related to the effects of enhanced land-sea temperature contrasts and physical mechanism for suppression of convection through raised lifting condensation levels have been proposed e.g. Fasullo (2010).

Regarding the dynamical component of change, over the SA landmass it is found that inter-model uncertainty may be associated with low level circulation patterns associated with zonal gradients in SST changes in the subtropical Indian Ocean and the intensity of continental heating and the thermal low pressure centre. The land-sea heating contrast has been hypothesised by Bayr and Dommenget (2013) to be a driver of enhanced convergence over land with implications for convection at the continental scale, however results indicate that the response can be complex in the case leading to a northward shift of the ITCZ/SIOCZ and wetting/drying at the regional scale. Over both the ocean and land examination of inter-model dispersal yields structures with less zonal uniformity of change than represented by the MMM response. The sensitivity of ΔP_{Shift} across models to the pattern of SST structures and their resemblance to contemporary modes of variability suggests that further analysis of future SST patterns and assessment of model representation of present rainfall-SST teleconnections and mean state biases may be useful to inform our interpretation of the credibility of projected changes.

5. Acknowledgements

This work was supported financially by the Peter Carpenter Scholarship for African Climate Change at the University of Sussex and the Future Climate for Africa (FCFA) regional consortium project UMFULA (project grant number NE/M020258/1). The World Climate Research Program's Working Group on Coupled Modelling responsible for CMIP5 model data is also acknowledged, which was provided by the Program for

Climate Model Diagnosis and Intercomparison (PCMDI). More information on this model data can be found at the PCMDI website (http://www.pcmdi.llnl.gov).

6. Caveats and Implications

With consideration of the decomposition methodology, a caveat regarding the derivation of M^* is noted. Although M^* is a reasonably sufficient approximation of the actual moisture flux (M_{int}), it is established CMIP5 models typically tend to underestimate M^* (see appendix and Fig. 13 in Chadwick et al. 2013). Therefore, caution should be taken to scientifically interpret results here. A potential manner to address this issue could be the application of a vertical velocity filter to constrain for convective moisture flux only, by using vertically integrated atmospheric moisture *(q)* between the surface and 700 hPa, instead of using the 2 m specific humidity *(q)* value.

In addition, as noted by Chadwick et al (2013), shallow convection can contribute to the transportation of moisture horizontally into the deep convection cells, which is not excluded in the estimation of M^*. Therefore the underestimation of M^* from M_{int} is likely due to the method including both shallow and deep convection and no discrimination being established between the two types. Future studies could include a precipitation rate filter, which could be applied to vertical velocity that would be representative of deep convection only and exclude shallow convection.

Land and ocean regions exhibit differing drivers of uncertainty of change and the implication is that model analysis over both continental regions and ocean should be

made aware of differing model processes driving change over these regions. Within this chapter the seasons OND and DJF additionally exhibit differing drivers and influences from thermodynamic and dynamic influences and therefore highlighting the importance of treating seasons and even months of change separately to unpick the model processes dominant in each month/season. No one single component explains change and differing nuances should not be ignored as they may prove important.

As a side note when differing ensemble sizes are evaluated for ΔP versus ΔSST, it is established that large differences emerge between the regions of model agreement that influence changes in ΔP over southern Africa. Therefore when investigating potential causes of future changes, one needs to be aware of the effect of ensemble size, which may sway results. Ideally a variety of different sample sizes should be chosen and evaluated to avoid this problem or alternately a sensitivity analysis should be performed on the dataset to determine if results are deemed significant. Therefore caution should be taken when selecting the number of models for future projections analysis. Seemingly when evaluating larger model ensemble sizes i.e. 20 models and above, results indicate more stability opposed to much smaller ensemble sizes.

Chapter 6

Understanding Future Change and Reduction in Uncertainty

Overview

The final chapter of this thesis culminates by drawing upon results from previous chapters to determine the degree of certainty and confidence associated with future precipitation projections over southern Africa for the key identified seasons. Robustness, credibility and convergence of model change are established. A model ranking framework is developed using results from Chapter 3's analysis of contemporary climate over southern Africa to assess whether uncertainty in future precipitation projections over the region can be significantly reduced in OND and DJF. Significant reductions in uncertainty allude to the fact that potential value is established in using this type of approach in model ranking, however this is only one approach and implications are discussed.

Key Questions:

1. Can a model ranking framework developed for southern Africa significantly reduce uncertainty in future precipitation projections?
2. Can future projection uncertainty in the SIOCZ feature over southern Africa be reduced?
3. What are the spatial patterns of future precipitation projections over the southern African continent using "top" performing models?
4. What are the key findings and implications regarding future precipitation projections over southern Africa?

1. Introduction

1.1. Robustness, credibility and convergence

General circulation model (GCM) output is currently our best tool available in determining future projections. It is agreed that multi-model ensemble means (MMM's) are the most consistent and fairest approach to address long term future projections (IPCC, 2001; Tebaldi and Knutti, 2007; Schaller et al., 2011). However, projections from GCMs and their MMM's still exhibit large amounts of uncertainty, making confident statements about future climate challenging, particularly for precipitation (Knutti et al., 2010; Schaller et al., 2011; Rowell, 2012). More confidence is typically associated with models that are able to accurately simulate present day climatology as a

prerequisite to make projections into the future (Krishnamurti et al., 2000; Sushama et al., 2006; Engelbrecht et al., 2009), which was evaluated in Chapter 3.

Robustness, credibility and convergence with respect to model understanding are defined here to ensure clarity regarding the use of these terms.

- **Robustness:** The level of agreement between models i.e. a signal is considered robust if there is a high level of model agreement.
- **Credibility:** The degree to which model change can be considered realistic and believable based on physically sensible principles. E.g. for a climate signal to be credible it needs to be robust as well as physically sensible or justifiable. Similar to Bocking's (2004) pg. 164 definition, which states that scientific credibility is: "the extent to which science is recognised as a source of reliable knowledge about the world, and not simply as, say, random observations, or an expression of the preferences of a particular interest group"
- **Convergence:** Convergence is used in this context to describe agreement in model processes. For instance if models perform well at simulating both mean state and variability of contemporary climate then model convergence is established between those two process-based parameters.

In this final chapter robustness i.e. model agreement of future precipitation projections will be assessed. In OND over southern Africa there is large agreement in the sign of projected precipitation change being negative (a drying signal), however the magnitude of the spread is rather poorly constrained i.e. not robust. To potentially constrain this

spread and determine if model change is more credible i.e. we can believe future projections with increased confidence through physical understanding, a model ranking framework is developed. Additionally performance of a sensitivity analysis can establish whether subsets of ranked models significantly produce more robust projections i.e. significantly reduce uncertainty; therefore potentially producing more credible model precipitation projections. From the model ranking framework developed, it is determined if model convergence is established between mean state and variability process-based metrics.

1.2. Model ranking

Rowell et al (2016) provides an analysis of model ranking using various metrics and concludes no particular amount of metrics are definitively accurate for reducing uncertainty and only makes a difference in some regions. Rowell's study uses the term "moderate" discrimination as his main finding in the study between different rankings of models between different metrics. Therefore it remains unclear how many metrics are the "correct" or optimal amounts of metrics to use when ranking models and is recognised that there is no one clearly defined approach, which is unanimously agreed upon when tackling the task of model ranking.

However, if it can be proved using "top" performing models that significant reductions in uncertainty are established, as well as being physically defensible, then there may be value in such a model ranking approach. In this chapter a model ranking framework is

developed and various sub-samples of the "top" performing models are used to determine if uncertainty can be significantly reduced over southern Africa.

1.3. Implications of regional precipitation projections

A definition from Nicholls (1999) states the ultimate goal of improved climate prediction is the reduction of adverse socioeconomic consequences of climate variability. The provision of climate information is a challenging task and fraught with difficulties, however if robust and credible signals that are physically defendable in future projections are established, it is ultimately beneficial for all parties affected to be informed. A major challenge includes the interpretation and understanding of climate information (Swart et al., 2009). The majority of end-users utilising climate information struggle with understanding probabilities, levels of uncertainty and the plausibility and possibility of risks (Nicholls, 1999; Archer, 2003; Webster, 2003). The common desire for both climate scientists and end-users e.g. decision-makers is to reduce uncertainty in climate change projections.

There is an increasing need for climate research to be aimed towards the needs of end-users and policymakers regarding climate information. This involves the relevant questions being asked by end-users to essentially drive the appropriate climate change research to be undertaken by climate scientists and provision of scientific output relevant to the initial questions proposed. The question this research aims to answer in this final chapter is – What are future precipitation conditions likely to be over southern

Africa? And what level of confidence, certainty and plausibility is associated with the projected changes?

2. Data and Methods

2.1. Data

To evaluate future precipitation projection uncertainty, output from a total of 39 CMIP5 model simulations for the 20th century and the 21st century (under the RCP8.5 emissions scenario) are used (see Table 1 in Chapter 4). CMIP5 models are used from the WCRP multi-model dataset, which provide results for the most recent Assessment Report (AR5) of the IPCC (Meehl et al., 2007; Taylor et al., 2012). Note a total of 44 CMIP5 models (Table 1 in Chapter 3) are used to develop the model ranking framework (using contemporary climate performance), however a slightly smaller and varied subset (39) of CMIP5 models are used in future precipitation projections and sub-sampling analysis, due to limited data availability for future scenarios. The 39 CMIP5 models analysed here are equivalent to those used in IPCC future projections (Collins et al., 2013 in IPCC WG1 AR5 Chapter 12).

Monthly data was extracted for the period of analysis from the RCP8.5 scenario 2071-2100 minus the historical period 1971-2000 and then seasonally averaged for the key seasons OND and DJF. Only the first ensemble member was utilized in creating the MMM. All model data was interpolated to a common grid of 1.5˚ X 1.5˚ to ensure

uniformity. Inter-model spread of CMIP5 model precipitation projections across the 39 model ensemble is evaluated in this chapter.

2.2. Model ranking framework methodology

A model ranking framework is developed here to highlight the "top" performing models in terms of regional southern African seasonal climate (i.e based on the SIOCZ analysis in Chapter 3) and attempts to understand the degree of consistency and convergence between various metrics of model performance. The ranking framework uses a total of 7 metrics evaluated in Chapter 3, which include: 1) spatial correlations of SIOCZ precipitation climatology, 2) spatial correlations of the annual cycle (latitude versus time diagrams), 3) model bias and 4) RMSE, 5) primary EOF spatial correlations of observations versus models, 6) Temporal correlations of primary EOF coefficients versus Niño3.4 and 7) the SIOD.

The first 4 metrics are associated with mean southern African climatology and the latter 3 metrics with interannual variability of southern African climate. Ranks are then awarded to individual CMIP5s model for each metric ranging from 1 to 44 (sample size of 44 models from Chapter 3). Mean ranks and standard deviations are derived for each CMIP5 model. Additionally to determine convergence of model performance between the climatology and variability metrics, mean ranks are calculated for each of the two parameters seperately and compared.

2.3. Reducing uncertainty: sub-sampling via a Monte Carlo approach

To produce confident statements regarding future precipitation projections uncertainty needs to be significantly reduced to ensure projections are sufficiently robust and credible. One approach to make attempts in addressing this issue is to use a sub-sample of "top" performing models from a model ranking framework. A sensitivity analysis provides a platform to discriminate if there are significant differences between "random" sub-sampling and "intellegent" sub-sampling i.e. when choosing varying numbers of "top" performing models over the region.

A sensitivity analysis is performed for DJF and OND over both land and ocean regions whereby 10, 20 and 30 models from the avaliable 39 CMIP5 models are sub-sampled 10,000 times using a Monte Carlo approach (e.g. New and Hulme, 2000; Knutti et al., 2002). The Monte Carlo approach is a statistical technique used here to transform uncertainties in precipitation projections of model output into a probability distribution function (New and Hulme, 2000). By combinations of the distributions and selecting models at random, it recalculates the simulated model a large number of times (in this case 10,000 times) and provides the probability of the output occuring.

Distributions of 3 statistical parameters measuring spread are dervied at the 10^{th} and 90^{th} percentile levels. These parameters include standard deviation, range and inter-quartile range. For results to be deemed significant and hence uncertainty to be significantly reduced, the "intellegently" sampled crtitcal value needs to lie beyond the distribution of spread (i.e. below the 10^{th}%tile value or above the 90^{th}%tile value). Results from the

sub-sampling experiment will indicate if a significant difference is established when choosing models randomly opposed to choosing models “intellegently” based on the model ranking framework developed.

To determine whether CMIP5 models indicate convergence in future precipitation change processes over the SIOCZ, an experiment was conducted to test this hypothesis. A threshold of greater than 5.5 mm day-1 (~165 mm/month) is chosen as the mask to identify the SIOCZ in historical simulations; derived from analysis completed in Chapter 3. This threshold is applied to the 39 CMIP5 MMM and additionally to the 39 individual CMIP5 models. Future projections over the SIOCZ are then derived for both the MMM and individual models. Results are plotted using box-whisker plots of area averaged percentage change in precipitation over the SIOCZ domain (defined here from 0˚ - 30˚S and 10˚E - 50˚E). Therefore spread between the two projected analyses can be established.

3. Results and Discussion

3.1. Model ranking framework

Results from the ranking framework (Table 1) show that the 10 highest overall ranked models are bcc-csm1-1-m, bcc-csm1-1, FGOALS-s2, CanESM2, CMCC-CMS, ACCESS1-0, MPI-ESM-MR, CMCC-CM, HadGEM2-CC, MPI-ESM-LR. The 10 lowest ranked models are ACCESS1-3, GISS-E2-R, MIROC5, GISS-E2-R-CC, FIO-

ESM, MIROC-ESM, NorESM1-M, GFDL-ESM2G, MIROC-ESM-CHEM, NorESM1-ME. To determine convergence of model perfomance with respect to all metrics, models from the 10 highest (lowest) ranking models are highlighted (shaded in grey for top 10 models and in italics for bottom 10 models) that lie within the top (bottom) ten models for both SIOCZ climatology and variability metrics. Models in common with respect to the "top" performing models in terms of all metrics are bcc-csm1-1-m and bcc-csm1-1 and the worst ranking models in terms of all metrics are GFDL-ESM2G and NorESM1-ME. Models exhibited standard deviations of ranks ranging from approximately 8 to 17 ranks (not shown here), while better performing models exhibited relatively small standard deviations.

Table 1: Model ranking framework including mean model ranking, mean climatology metric ranks and variability metric ranks. Shaded models indicate the top 10 performing models and models in italics are indicative of bottom 10 performing models. Models in bold are models found within the top 10 best/worst performing models

	Model	**Mean model ranking**	**Model**	**Mean ranking of climatology metrics**	**Model**	**Mean ranking of variability metrics**
1	**bcc-csm1-1-m**	11.5	**bcc-csm1-1**	8.7	GFDL-ESM2M	11.8
2	**bcc-csm1-1**	12.4	**bcc-csm1-1-m**	9.2	CCSM4	12.0
3	FGOALS-s2	14.5	FGOALS-s2	11.2	BNU-ESM	13.4
4	CanESM2	16.1	CanESM2	11.8	**bcc-csm1-1-m**	14.4
5	CMCC-CMS	16.3	CMCC-CM	14.8	CMCC-CMS	14.8
6	ACCESS1-0	16.8	HadGEM2-CC	14.8	GFDL-CM3	15.8
7	CMCC-CM	17.4	CESM1-CAM5	15.2	MPI-ESM-MR	16.2
8	MPI-ESM-MR	17.7	CMCC-CESM	15.7	**bcc-csm1-1**	16.8

9	HadGEM2-CC	17.8	ACCESS1-0	16.0	MIROC-ESM	16.8
10	MPI-ESM-LR	17.8	FGOALS-g2	16.8	FIO-ESM	17.4
11	IPSL-CM5B-LR	18.2	HadGEM2-AO	16.8	ACCESS1-0	17.8
12	CCSM4	18.3	IPSL-CM5B-LR	17.0	MPI-ESM-LR	18.0
13	BNU-ESM	19.2	MPI-ESM-P	17.2	IPSL-CM5A-MR	18.4
14	FGOALS-g2	19.9	CMCC-CMS	17.5	FGOALS-s2	18.6
15	CSIRO-Mk3-6-0	20.1	MPI-ESM-LR	17.7	MIROC5	18.6
16	CMCC-CESM	20.2	HadGEM2-ES	18.2	NorESM1-M	18.6
17	GFDL-CM3	20.3	inmcm4	18.2	IPSL-CM5B-LR	19.6
18	CESM1-FASTCHEM	20.5	CSIRO-Mk3-6-0	18.3	IPSL-CM5A-LR	20.2
19	CESM1-BGC	20.8	EC-EARTH	18.8	CESM1-FASTCHEM	20.4
20	GFDL-ESM2M	21.1	MRI-CGCM3	18.8	CMCC-CM	20.4
21	HadGEM2-ES	21.5	MPI-ESM-MR	19.0	MIROC4h	20.8
22	MRI-CGCM3	21.8	CESM1-BGC	20.2	CanESM2	21.2
23	MPI-ESM-P	22.5	ACCESS1-3	20.5	MIROC-ESM-CHEM	21.2
24	HadGEM2-AO	22.6	CESM1-FASTCHEM	20.7	GISS-E2-H-CC	21.4
25	IPSL-CM5A-LR	22.6	GISS-E2-R	22.5	HadGEM2-CC	21.4
26	inmcm4	23.2	GISS-E2-H	23.0	CESM1-BGC	21.6
27	GISS-E2-H-CC	23.7	CCSM4	23.5	CSIRO-Mk3-6-0	22.2
28	CESM1-WACCM	23.8	GISS-E2-R-CC	23.5	CESM1-WACCM	22.6
29	CESM1-CAM5	23.9	BNU-ESM	24.0	FGOALS-g2	23.6
30	MIROC4h	23.9	GFDL-CM3	24.0	CNRM-CM5	24.8
31	EC-EARTH	24.1	CNRM-CM5	24.7	MRI-CGCM3	25.4
32	IPSL-CM5A-MR	24.1	IPSL-CM5A-LR	24.7	CMCC-CESM	25.6

33	GISS-E2-H	24.2	CESM1-WACCM	24.8	GISS-E2-H	25.6
34	CNRM-CM5	24.7	GISS-E2-H-CC	25.7	HadGEM2-ES	25.6
35	*ACCESS1-3*	*25.7*	*MIROC4h*	*26.5*	***NorESM1-ME***	*26.2*
36	*GISS-E2-R*	*25.7*	***GFDL-ESM2G***	*28.8*	*GISS-E2-R-CC*	*28.6*
37	*MIROC5*	*25.7*	*GFDL-ESM2M*	*28.8*	*MPI-ESM-P*	*29.0*
38	*GISS-E2-R-CC*	*25.8*	*IPSL-CM5A-MR*	*28.8*	*inmcm4*	*29.2*
39	*FIO-ESM*	*27.5*	*MIROC5*	*31.7*	*GISS-E2-R*	*29.6*
40	*MIROC-ESM*	*29.5*	*FIO-ESM*	*35.8*	*HadGEM2-AO*	*29.6*
41	*NorESM1-M*	*30.1*	***NorESM1-ME***	*38.0*	*EC-EARTH*	*30.4*
42	***GFDL-ESM2G***	*30.4*	*MIROC-ESM-CHEM*	*39.7*	*ACCESS1-3*	*32.0*
43	*MIROC-ESM-CHEM*	*31.3*	*NorESM1-M*	*39.7*	***GFDL-ESM2G***	*32.2*
44	***NorESM1-ME***	*32.6*	*MIROC-ESM*	*40.0*	*CESM1-CAM5*	*34.4*

Figure 1 is generated to determine whether model convergence between mean state and variability is illustrated. Correlation and coefficient of determination ($r = 0.081$ and $r^2 = 0.007$ respectively) across CMIP5 models is weak and almost negligible; therefore illustrating models which simulate contemporary precipitation climatology well, do not necessarily simulate variability well over southern Africa. Therefore a lack in convergence in model process performance is evident over the study domain. From the Table 1 it is deduced that only 2 CMIP5 models, namely bcc-csm1-1-m and bcc-csm1-1 (bolded) show clear evidence of performing well in both aspects i.e. climatology and variability (ranking in the top 10 in each category), therefore exhibiting convergence in processes. NorESM1-ME and GFDL-ESM2G (bolded and italicised) are the CMIP5 models that perform equally poorly in both mean state climatology and variability metrics i.e. these models are found in the bottom 10 models in each category.

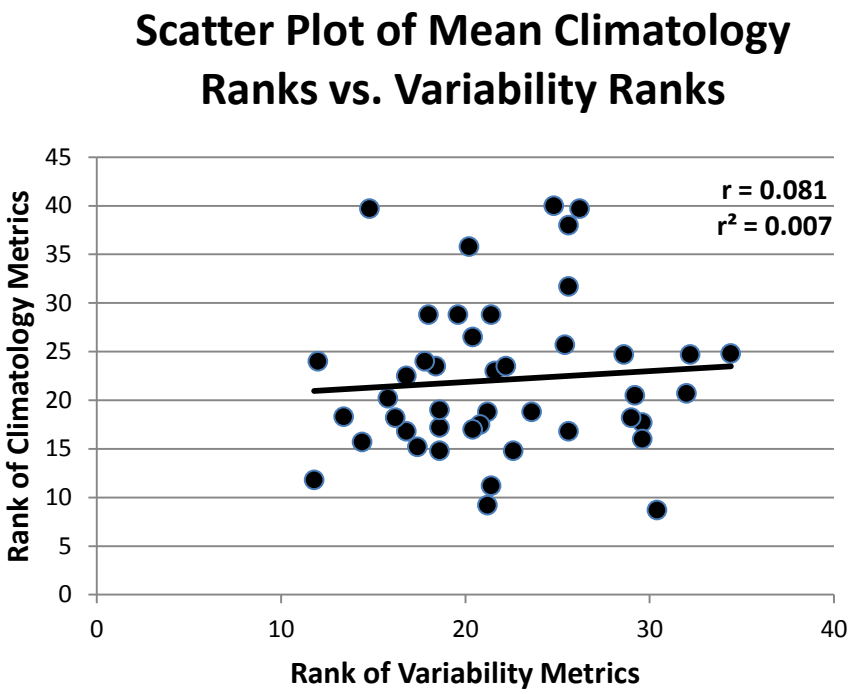

Figure 1: Scatter plot of individual CMIP5 model ranks of mean state climatology metrics versus variability metrics. Units are in rank from 1 to 44.

3.2. Significant reductions in uncertainty

In an attempt to reduce uncertainty of future climate projections of projected precipitation over southern Africa, the "top" 10, 20 and 30 models with the overall highest skill in terms of simulating both mean state and variability over southern Africa were selected. It remains unknown as to what extent to trust models that only capture mean state with high accuracy or alternatively variability well, or if models are able to capture both. The most sensible and fairest option includes models ability to capture both aspects of contemporary climate and use those selected models to understand future projections, which is the approach applied here. Top performing models i.e.

("top" 10, 20 and 30) CMIP5 models are illustrated in box-whisker plots (Figure 2, 3 and 4) as red and blue dots for DJF and OND respectively.

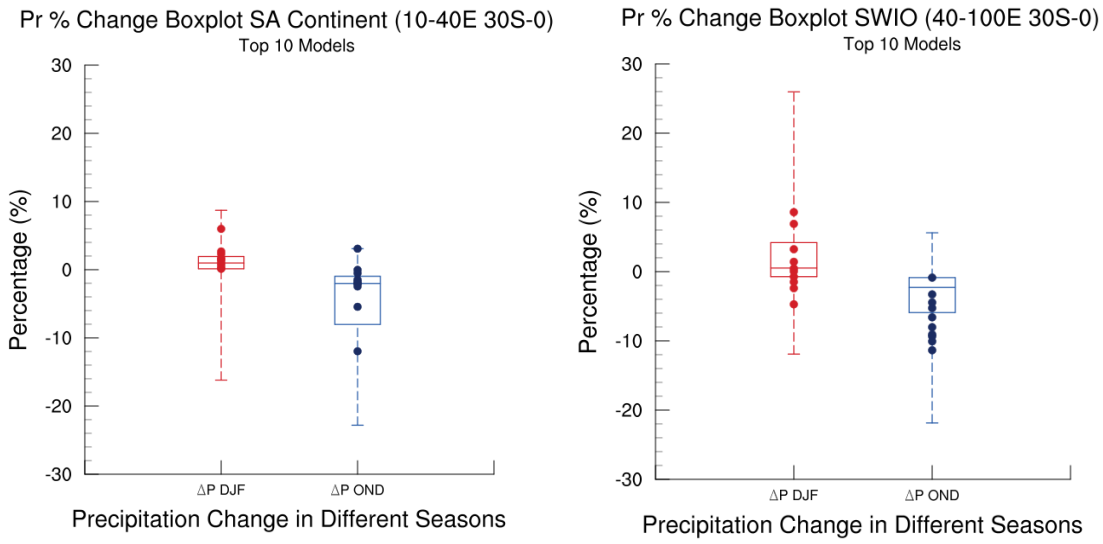

Figure 2: Box-whisker plots illustrating percentage change of precipitation for 39 IPCC models for DJF and OND. Box represents the inclusion of the 25th and 75th percentile values, with the solid line representing the median and whiskers indicating the minimum and maximum values. Solid dots (red DJF and blue OND) represent the "top" 10 models chosen from the ranking framework derived in Chapter 3.

The 10 "top" performing models tend to cluster in Figure 2 more closely over land than ocean. Over the continent in DJF, changes in precipitation percentage range from -16% to 9%. The "top" 10 performing CMIP5 models indicate projected changes in precipitation between 0% and 6%, which hence reduces spread of precipitation changes for DJF over the continent, implying a total wetting signal over the chosen land domain.

This does not imply no drying will occur, as the box-whisker plots are determined for an area average over a chosen spatial domain.

Box-whisker plots additionally do not account for spatial changes in projected patterns of precipitation, which from previous chapters indicates a projected dipole pattern of wetting/drying found to the north/south of the continent. Therefore wetting and drying signals may cancel out to some extent in the box-whisker plot analyses. The wetting magnitude appears to be most dominant in DJF over the continent. Box-whisker plot analysis, however, is useful in determining reductions in model spread over particular domains.

Spatial plots of future precipitation projections over the continent are illustrated in Figure 5 and 6 to avoid this issue and to specifically identify spatial patterns in precipitation projections over southern Africa using “top” performing models. Spatial plots of precipitation projections are only assessed over the southern African continent and not the SWIO, due to the imminent impacts to livelihoods and the need to inform adaption.

For continental OND the total 39 MMM projected precipitation change ranges from -24% to 4%, this is not surprising as the MMM in Chapter 4 and 5 demonstrates a distinct projected drying signal over the majority of southern Africa. Models, however, do not tend to cluster to the same degree as for DJF but still exhibit reduced spread which is constrained to changes of -11% to 4% in OND. The implication being that

“top” performing models indicate a projected drying signal but not of the magnitude initially proposed.

Over the SWIO domain, changes in total MMM projected precipitation exhibit larger inter-model spread than land regions. Projected DJF precipitation changes over the SWIO range from -13% to 27% and for OND from -24% to 6%. In DJF over the SWIO choosing the “top” 10 performing models reduces the spread of possible precipitation change rather notably to -2% and 9%. During OND the spread is constrained to -8% and 6%. The reduction in uncertainty evident in OND and DJF over the SWIO does not explicitly lead to a more robust and credible conclusion, but simply reduces the possible spread of the projected change. This reduction in uncertainty is most likely due to the spatial pattern of change cancelling out (e.g. potentially “top” performing models have similar or equivalent wetting to drying signal ratios over the selected domain due to the projected dipole pattern). Therefore results may be misleading and require additional physical investigation to determine if the reduction in uncertainty is potentially useful and credible.

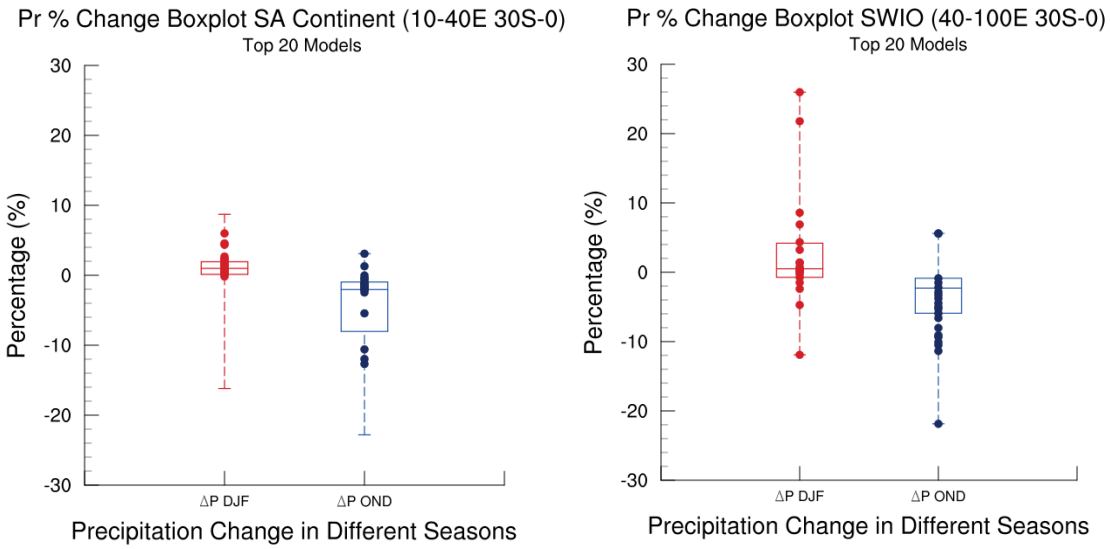

Figure 3: Same as Figure 2 but for the "top" 20 model subset.

When assessing reductions in spread using the "top" 20 performing models over the southern African continent, spread remains rather well constrained, whereby top performing models cluster in both DJF and OND, but specifically DJF. Over the SWIO the range increases to span the entire 39 MMM spread as maximum and minimum outliers are included in the "top" 20 model choice over the SWIO.

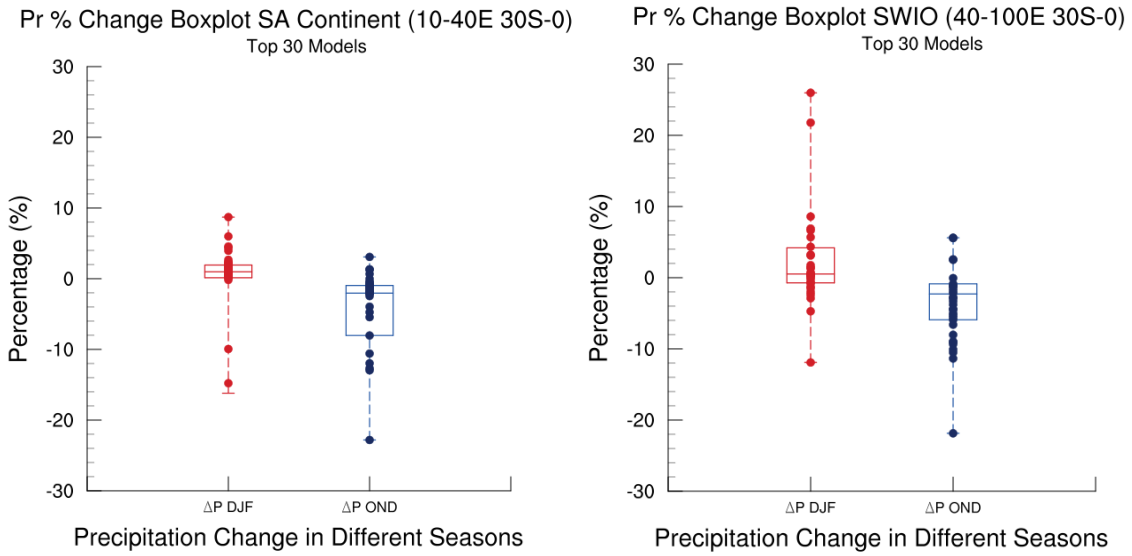

Figure 4: Same as Figure 2 and 3 but for the "top" 30 model subset.

When approximately three quarters of the full MMM is illustrated in box-whisker plots i.e. "top" 30 performing models out of 39 CMIP5 MMM, spread almost entirely covers initial range of projected changes, the exception being for DJF over the continent. It is however interesting to note how the majority of the "top" 30 models tend to cluster together with much fewer outliers spanning the larger domain of spread.

Therefore to summarise in both seasons when choosing the "top" 10 performing CMIP5 models over the continent uncertainty is notably reduced by 13% in OND and 19% in DJF. When choosing increased numbers of "top" performing models i.e. 20 and 30 models, spread tends to increase and include the vast majority of possible outcomes. The notable exception is over land in DJF, the "top" 20 and 30 models tend to cluster rather closely. This type of analysis is useful whereby magnitudes of projected change can be constrained slightly further through omission of bad and average models by

using only the "top" 10, 20 or 30 best model performers. However to determine the significance of these reductions in uncertainty, if any, a sensitivity analysis is performed to determine whether "intelligently" sub-sampling "top" performing models proves significant compared to models being "randomly" sub-sampled.

Table 2: Sensitivity test results from Monte Carlo sub-sampling approach for 10, 20 and 30 models. Distributions for the 10^{th} and 90^{th} percentiles are derived for standard deviation (SD), range and inter-quartile range (IQR). Bolded values are deemed significant at the 90^{th} percentile confidence interval.

10th%tile	90th%tile	Measures of Spread	No. of Models	Domain	Season	"Intelligent" Sub-sampling Critical Value
1.68	7.65	SD	10	Land	DJF	1.71
4.84	23.5	Range	10	Land	DJF	5.85
0.41	2.07	IQR	10	Land	DJF	1.48
3.79	7.09	SD	20	Land	DJF	**1.61**
17.06	24.92	Range	20	Land	DJF	**6.16**
0.99	3.13	IQR	20	Land	DJF	1.60
4.18	6.86	SD	30	Land	DJF	**4.16**
19.34	24.92	Range	30	Land	DJF	23.50
1.03	2.09	IQR	30	Land	DJF	1.62
3.19	7.48	SD	10	Land	OND	3.97
10.19	24.1	Range	10	Land	OND	15.04
0.66	8.23	IQR	10	Land	OND	1.60
3.84	6.76	SD	20	Land	OND	6.02
13.35	25.89	Range	20	Land	OND	25.89
2.13	9.5	IQR	20	Land	OND	4.18
4.12	6.55	SD	30	Land	OND	5.53
14.28	25.89	Range	30	Land	OND	25.89

2.51	9.02	IQR	30	Land	OND	3.70
2.54	9.54	SD	10	Ocean	DJF	4.11
7.87	30.69	Range	10	Ocean	DJF	13.31
0.82	5.17	IQR	10	Ocean	DJF	4.08
3.1	8.46	SD	20	Ocean	DJF	8.36
10.98	37.89	Range	20	Ocean	DJF	37.88
2.14	6.41	IQR	20	Ocean	DJF	3.88
3.64	8.1	SD	30	Ocean	DJF	7.04
18.81	37.89	Range	30	Ocean	DJF	37.88
2.47	5.75	IQR	30	Ocean	DJF	3.93
3.27	7.54	SD	10	Ocean	OND	3.33
10.01	25.56	Range	10	Ocean	OND	10.49
1.01	6.3	IQR	10	Ocean	OND	4.62
3.77	6.74	SD	20	Ocean	OND	6.04
13.63	27.47	Range	20	Ocean	OND	27.47
3.11	7.97	IQR	20	Ocean	OND	6.46
4.03	6.51	SD	30	Ocean	OND	5.53
15.05	27.47	Range	30	Ocean	OND	27.47
3.22	7.47	IQR	30	Ocean	OND	6.39

From Table 2 when selecting the “top” 20 and 30 performing models in DJF versus random sub-sampling, a significant difference is evident at the 90^{th} percentile confidence interval, inferring some added skill when “intelligently” selecting models. For OND this hypothesis does not hold true and random sub-sampling proved equally as skilful in reducing uncertainty compared to selecting “top” performing models. It is however, useful to note that most model metrics in the developed model ranking framework are tailored particularly towards the DJF season. Therefore would be interesting to determine whether an additional analysis of metrics specifically tailored

towards OND would potentially produce significant reductions in uncertainty over southern Africa.

From this sub-sampling analysis, it can be inferred that potential value is evident in this type of model ranking approach over southern Africa. However, extensive research would be required before any consensus regarding this type of approach is considered robust. A noteworthy concern regarding lack of model convergence between mean state and variability metrics immediately raises doubt as to whether the reduction established in uncertainty is valid and physically sensible. Output from model ranking results may be misleading and reductions in uncertainty may be established but for unknown and non-sensible reasons. Another implication of this analysis is that such metrics are not typically perceived as process-based metrics and rather just metrics of performance. Future work can focus on identifying model processes causing precipitation change and be ranked according to those identified processes (hence a more representative process-based analysis and ranking scheme) and not straightforward metrics such as biases, RMSE's, seasonal cycles and variability that are used in this analysis.

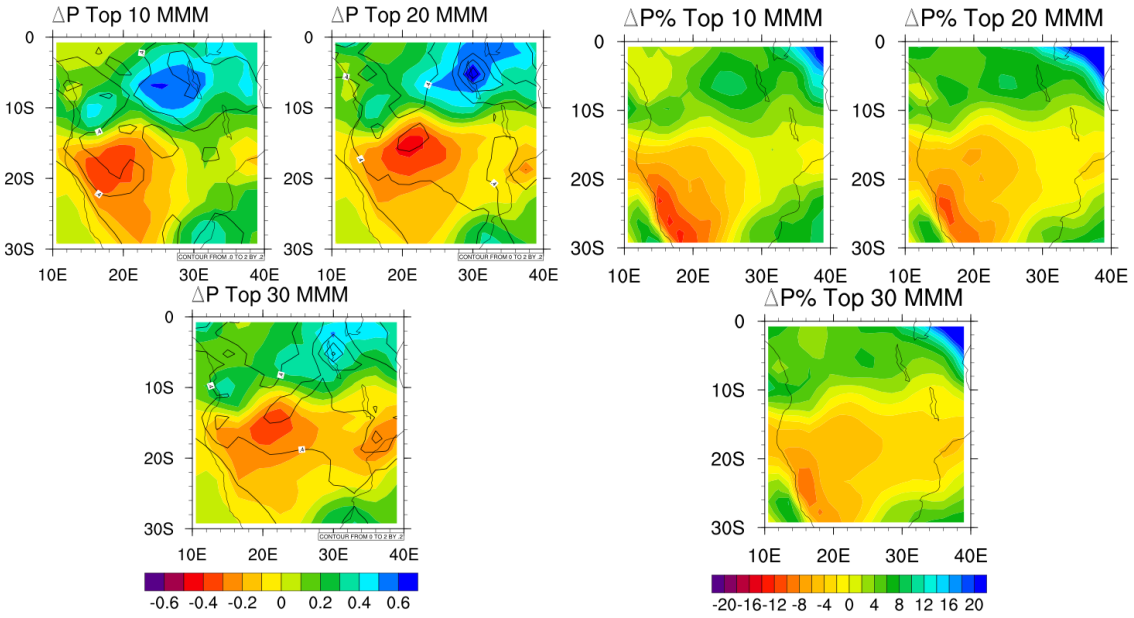

Figure 5: Spatial plots illustrating projected absolute (left) and percentage change (right) in precipitation in mm day^{-1} and % change respectively for DJF using the "top" 10, 20 and 30 MMMs from the suite of 39 available CMIP5 models. Absolute projected change plots are overlaid with back solid lines representing standard deviation values contoured from 0 to 2 in intervals of 0.2.

It is clear from Figure 5 that patterns of projected precipitation change remain relatively similar between the three plots of differing model choice. Notably in the projected changes for the "top" 20 and 30 MMM plots are most similar, with the maximum peak of drying evident around 15˚S with respect to absolute projected changes. Considering projected percentage change in DJF, the notable difference is the drying peak, which is evident over the south-western extreme of the continent at ~25˚S opposed to ~15˚S in the absolute projected change.

Therefore from the sub-sampling sensitivity analysis, which highlights signifcant reductions in uncertainty when using the “top” 20 and 30 performing models, it can be inferred that in DJF drying is projected over much of the southern and south-western parts of the continent with enhanced certainty. Addtionally projected DJF drying signals exhibit lower standard devation values, compared to projected wetting evident over the north-eastern region, corroborating results established previously.

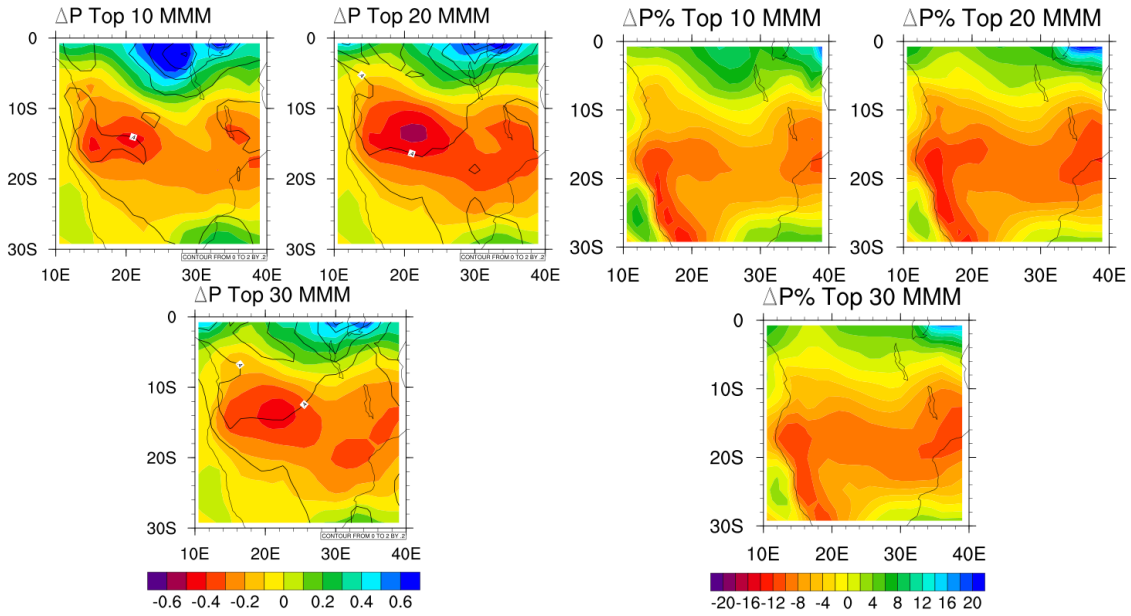

Figure 6: Same as Figure 5 but for OND.

In OND future precipitation projections over the continent, uncertainty was not significantly reduced, however consistency is evident in patterns of projected change between the “top” performing 10, 20 and 30 MMMs. Differences between differing number of “top” models selected include i) a relatively strong absolute wetting signal for the “top” 10 and 20 models over the central equatorial region but to a much lesser

extent for the “top” 30 model MMM and ii) the largest magnitude in absolute and percentage projected drying is evident in the “top” 20 MMM. Projected percentage change in OND shows large consistency between all 3 “top” model subsets with almost equivalent spatial patterns of drying. Projected drying distinctly dominates the majority of the continent, which indicates continuity into DJF (Figure 5), but with increased precipitation projections over the equatorial region and hence a slight southward shift in projected drying. Inter-model spread is also notably lower over the projected drying region in the pre-summer season, which reaffirms confidence through increased model agreement in the continental drying signal.

3.3. Changes in the SIOCZ and associated uncertainty

The SIOCZ feature in contemporary climate is captured by the majority of CMIP5 models which exhibit a diagonal band of enhanced precipitation; however variations are noted between individual CMIP5 models when compared to observations (see appendix: Figure 1). When allowing individual models to provide their own SIOCZ masks (i.e. initial location of the SIOCZ) before projecting future changes in this feature, it tests the hypothesis of whether model processes exhibit agreement, despite differing initial conditions. Typically this type of analysis determines if model convergence is established with respect to processes of future change among models (i.e. coherent model behaviour). To make attempts in constraining SIOCZ projection uncertainty, threshold values greater than 5.5 mm day^{-1} are applied to both CMIP5 MMM and individual CMIP5 models. Future precipitation projections over the SIOCZ

region are then compared for the 2 projected MMMs, whereby one uses only 1 initial SIOCZ mask derived from the MMM and the other which uses 39 initial SIOCZ masks.

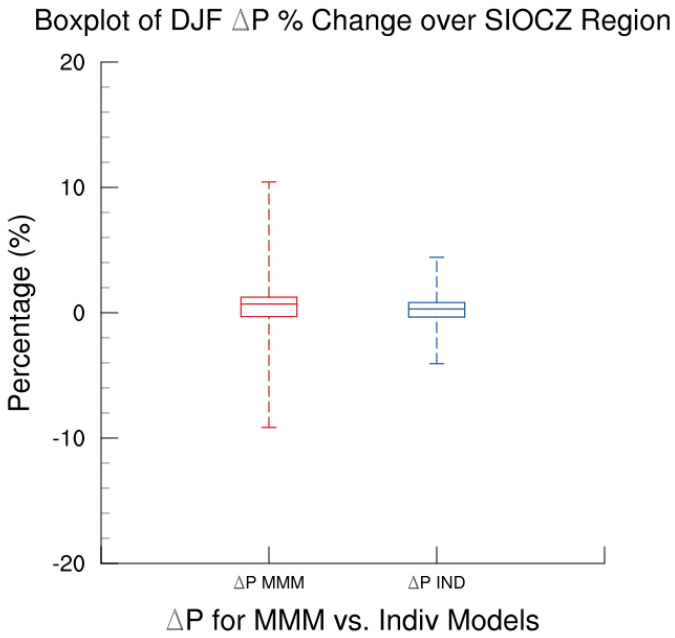

Figure 7: Box-whisker plot of percentage projected change in precipitation over the SIOCZ region (0˚ - 30˚S and 10˚ - 50˚E) of CMIP5 MMM using MMM SIOCZ mask (red) versus CMIP5 MMM using individual CMIP5 model SIOCZ masks (blue) for the period 2071-2100 minus 1971-2000 for RCP8.5 emissions scenario. Box represents the inclusion of the 25th and 75th percentile values, with the solid line representing the median and whiskers indicating the minimum and maximum values.

Figure 7 clearly shows a distinct decrease in spread of possible projected changes in precipitation over the SIOCZ region when using individual models initial conditions versus the MMM single initial condition. Projected change in precipitation ranges from -9% to 11% when using the MMM SIOCZ mask, whereas spread is reduced to -4% and 5% when models are able to use their own individual SIOCZ masks. This again does

not imply there is no change in the SIOCZ; in fact in Chapter 4 it is shown that the SIOCZ shifts northwards by approximately 200km in future projections using a best-fit line algorithm along the axis of maximum precipitation. This spread is projected changes is most likely due to the effect of the dipole pattern of precipitation change evident over the region, which essentially exhibits both wetting and drying signals which may cancel out one another when area averaging.

Therefore there is a notable decrease in spread of 11% from the initial 20% to only 9%, just over half the initial range. This implies models are producing more physically agreeable and potentially sensible processes of change. Models may not locate the initial SIOCZ 100% accurately, however should not be penalized solely for this reason, as convergence in model processes of projected change are established (i.e. evidence of coherent model behaviour creating change). The equivalent analysis was performed for the decomposition analysis (for only 20 CMIP5 models – Table 1 Chapter 5) and similar results were established (see appendix: Figure 8). Spread of projected precipitation change is reduced from -2.3% and 1.8% to -0.5% and 1.8%. Therefore model processes exhibit enhanced agreement despite varying initial positions of the SIOCZ and reduced spread is additionally established despite differing ensemble sizes (20 and 39).

An implication from this analysis is that projected model change may require alternative assessment approaches such as this one. Future analyses could include methods which

separate out model processes from influences of historical skill, which could potentially inform understanding of future change between models.

4. Discussions and Conclusions

A model ranking framework is developed over southern Africa, tailored particularly towards the austral summer season DJF. This framework is developed with the intention of addressing the question of uncertainty and whether significant reductions can be established through using "top" performing models. The framework incorporates both mean state and interannual variability processes, as both aspects are deemed equally important to southern African precipitation (Chapter 3).

Models do not indicate convergence in performance between mean state and variability metrics. From the ranking framework developed a sensitivity analysis is performed where sub-sampling the "top" 10, 20 and 30 CMIP5 models established significant differences between random and "intelligent" sub-sampling of models. Uncertainty is significantly reduced at the 90^{th} percentile confidence interval when models are selected "intelligently" via a process-based analysis approach developed in this thesis for DJF over the continent when using the "top" 20 and 30 models. Therefore implying potential value in this particular approach of model ranking. Unfortunately for the transition season, OND, uncertainty was not significantly reduced. However, the drying signal is relatively credible and plausible with most models in agreement with projected drying over the southern and south-western continent. Precipitation change over the SWIO could not be constrained significantly, however it is most important to be able to

provide significant results over the continent where impacts are imperative and have direct implications for adaption.

The DJF precipitation signal shows an overall area average of positive change in precipitation over the continent, however when assessed spatially using the "top" 10, 20 and 30 selected models; DJF spatial patterns exhibit projected wetting from the equator to 10˚S and projected drying dominates the south-western part of the continent. In OND drying over land is clear in both area averages and spatial plots. Drying patterns over the continent in OND are almost identical for the various choices of "top" model plots.

Projected precipitation changes in DJF are deemed more credible than OND due to significant reductions in uncertainty emerging only in DJF. This thesis simply uses one of many model ranking approaches to provide insight into understanding and potentially reducing uncertainty of future projections. These regional changes have important implications and should be relayed with the appropriate level of probability to policy and decision-makers, which hopefully aids decision-making at regional levels and informs water security measures over the region.

Models are additionally able to constrain uncertainty over the SIOCZ region when allowing individual model masks of historical SIOCZ position, compared to a single MMM mask for the SIOCZ. This provides new insight as to how models produce change when allowed their own initial conditions. Uncertainty is reduced by more than half (spread reduced to 9% from the original 20%) when allowing models to spatially

vary. This alludes to convergence of model processes creating projected change i.e. coherent model behaviour.

5. Caveats and Implications

Model ranking schemes have been an on-going area of investigation with no consensus on which approach is most optimal (Schaller et al., 2011; Rowell et al., 2016). This analysis has demonstrated some value in using mean state and variability metrics to significantly reduce uncertainty over southern Africa in austral summer (DJF). There are a variety of approaches to address uncertainty and this is simply one approach to make attempts in reducing uncertainty. Potential dangers of this methodology should be noted, which include the issue of falsely reducing uncertainty i.e. uncertainty may be significantly reduced, however for the non-sensible reasons and may be misleading. It is established in this chapter that lack of model convergence is evident between mean state and variability metrics between models. Therefore although uncertainty is significantly reduced in some cases, the lack of model agreement in key processes implies this uncertainty might be falsely reduced or rather not physically defendable.

Additionally the choice and number of metrics may not be optimal. To address this issue firstly a larger range of metrics could be derived, and then a sensitivity analysis could be performed, whereby varying numbers and combinations of metrics are chosen to determine if results remain consistent. This type of analysis could add more confidence to this approach in model ranking and reducing uncertainty.

The model ranking framework developed here is heavily tailored towards austral summer processes over southern Africa. It may add supplementary value to create a model ranking framework tailored specifically towards the season of interest i.e. OND in this case would potentially benefit through a ranking framework with metrics specifically tailored towards OND contemporary climatology and variability.

Model ranking frameworks are fraught with difficulties, making the selection of "top" performing models an extremely complex task. Therefore from the aforementioned reasons, further work would be required before this type of model ranking approach becomes robust and potentially useful. However the analysis presented here demonstrates value in this type of approach to model ranking and exclusion.

Future work should focus on identifying more specific model processes causing precipitation change and be ranked according to those identified processes (hence a more representative process-based analysis and ranking scheme) and not solely use straightforward model performance metrics such as spatial correlations, biases, RMSE's, seasonal cycles and variability which are utilised in this model ranking scheme.

Chapter 7

Synthesis and Conclusions

Overview

In this thesis models are evaluated based on their ability to simulate present day climate using a process-based approach of model performance with respect to mean state and variability over southern Africa. Dominant drivers, features and processes essential to precipitation are identified in models in contemporary climate and then used to understand regional projected precipitation changes over southern Africa and the adjacent south-west Indian Ocean. Key future changes in precipitation are identified over southern Africa. Mechanisms of regional precipitation change are investigated using a decomposition methodology of mean precipitation change. Uncertainties of projected change are constrained through a model ranking framework. Results show some evidence that such an approach has potential value regarding significant reductions in uncertainty for seasons of key importance over southern Africa.

1. Final discussion and summary of conclusions

This thesis provides new contributions and insight regarding contemporary and future climate change over southern Africa using a process-based analysis. Initially models are evaluated in terms of contemporary climate in Chapter 3 focusing on mean state and variability in austral summer (i.e. rainy season). The majority of CMIP5 models perform well at simulating the spatial pattern of seasonal rainfall for DJF over southern Africa. Models are additionally able to capture the key austral summer feature (the SIOCZ) that dominates precipitation totals over the southern African continent and SWIO, however variations are noted. An overall systematic bias towards an excessively wet southern African region is established in contemporary climate. Along the SIOCZ axis, precipitation overestimation is relatively low; typically models overestimate precipitation totals in the surrounding regions. Reasons for the SIOCZ itself not being particularly wet may be due to the dominant bias evident over the adjacent Indian Ocean, as well as circulation biases enhancing moisture flux away from the SIOCZ and into surrounding regions.

There is a notable discontinuity in the SIOCZ in the vast majority of CMIP5 models evident between land and ocean. A likely reason for this discontinuity could be the varying dynamics within model processes over land and ocean regions (Chadwick, 2016). Majority of models illustrate a SIOCZ that is generally too zonal in orientation.

Systematic biases are related to various potential causes including SST biases in models (e.g. Brown et al. 2011) and potentially excessive moisture flux convergence in models (Washington et al. 2013; Lazenby et al., 2016). SST biases demonstrate a small negative bias over the Indian Ocean region in the MMM, therefore no direct link to the excessive precipitation through overly warm ocean temperatures resulting in higher moisture flux. Therefore it is likely that model precipitation parameterisation schemes are a potential source of bias or alternatively SST gradient biases within models.

Biases in model moisture flux were additionally investigated. Three moisture flux transport pathways are identified as prominent contributing drivers of southern African precipitation. These moisture pathways originate from flow around the SIOHP, SAHP and monsoon winds, namely easterly flow, which convergence into the SIOCZ region during austral summer. Excessive precipitation over the southern African continent can be explained by excessively high moisture flux circulation patterns around the Angola Low. This bias is revealed to be almost entirely due circulation biases in models.

Interannual variability is known to be the most significant time-scale in which austral summer precipitation varies over the southern African continent and adjacent Indian Ocean. A distinct dipole pattern derived via an EOF analysis depicts the dominant mode of interannual variability, which is interpreted as the northeast-southwest movement of the SIOCZ in wet and dry years i.e. La Niña and El Niño years respectively similar to the northwest-southeast displacement of the SPCZ during El Niño and La Nina years

(e.g. Vincent et al. 2011), which is well captured by the majority of CMIP5 (Brown et al. 2013) models.

Large-scale circulation associated with the dominant mode of interannual variability of the SIOCZ is diagnosed via a composite analysis of the primary pattern of variation and moisture flux fields. Variability is shown to be dominated by anti-cyclonic circulation around the SIOHP, which transports moisture into the eastern regions of southern Africa. This anomalous circulation of moisture flux highlights the dominance of this moisture flux pathway with respect to variability over southern Africa.

The structures and drivers of interannual variability over southern Africa are related to the El Niño Southern Oscillation and subtropical Indian Ocean SST dipole (SIOD) in observations; however this teleconnection is not well captured by CMIP5 individual models, restricting confidence in model understanding of teleconnections. SIOCZ rainfall is complex in terms of variability as it is not just influenced by one major source but potentially several e.g. wave activity such as Rossby waves and the Matsuno-Gill response (Ratnam et al. 2014) and additionally decadal influences (Dieppois et al., 2016).

Key climate change signals that emerge in the CMIP5 MMM over southern Africa are i) the drying signal over the southern African continent peaking in November ii) the dipole pattern of wetting/drying to the north/south of the continent which extends into

the Indian Ocean. This dipole pattern straddles the historical precipitation maximum and is interpreted as a northward shift of the ITCZ particularly over the Indian Ocean. This pattern has strong seasonal cycle that peaks during the transition season (OND) and extends into austral summer (DJF) in the southern hemisphere. Intriguing result of slightly offset timing of the dipole pattern over southern Africa and the south-west Indian Ocean is established in Chapter 4. A delay or lag is evident in projected drying over land peaking in November but subsequently later in December over the SWIO. Moisture availability is likely a factor influencing this result; however other influences may be valid, such as land-atmosphere feedbacks and circulation patterns (He and Soden, 2016).

"Noise" from model disagreement is exceeded by the projected precipitation climate change signal most evidently in October, in which drying over the continent is largely dominant. Therefore the transition season OND is established as an important season regarding future precipitation change.

The SIOCZ feature itself does not show radical changes in projected precipitation along its axis, however using the best-fit line of maximum precipitation, a slight northward shift in the SIOCZ feature is evident of approximately 200km. This shift is potentially linked to the northward shift of the ITCZ over the adjacent Indian Ocean and is likely driven by SST patterns and circulation changes (Power et al., 2006; Adler, 2011; Stevenson, 2012), particularly linked to variability around the South Indian Ocean High driving easterly flow (Dieppois et al., 2016; Lazenby et al., 2016). Changes in

precipitation, however, do not project onto the climatological SIOCZ or the pattern of the interannual variability of the SIOCZ. Therefore additional analysis is required to understand the mechanisms of change in pre- and austral summer over southern Africa explored in Chapter 5.

Diagnostic variables such as SSTs, circulation pattern change (low-level winds and moisture flux) and dynamical uplift (vertical velocity) indicate direct associations with projected precipitation changes. It is important to identify and understand the physical processes governing model changes, as this provides additional insight and can be used to improve accuracy of particular model parameters and potentially reduce uncertainty in future projections. This thesis aims to understand why models produce certain changes by understanding model processes and identifying coherent model behaviour.

Individual model analysis established the following relationships with respect to diagnostic variables and projected model precipitation change i) stronger differential SST pattern warming over the Indian Ocean is associated with higher projected precipitation over the northern Indian Ocean region, ii) enhanced flow towards the northern Indian Ocean region in both OND and DJF i.e. larger magnitudes of flow are associated with larger projected wetting signals and iii) continental projected wetting exhibits associations with increased low-level moisture availability and additionally enhanced low-level easterly flow, particularly into East Africa.

Comparison of coupled and atmosphere-only experiments are particularly useful in attempting to gauge more understanding of the impacts of model SST patterns and coupling influences. However, future atmosphere-only experiments here exhibit limited use in understanding future regional precipitation change over southern Africa, as experiments are not able to replicate the coupled RCP8.5 emissions scenario with sufficient skill in AMIPTotal, which include all forcings essentially equivalent to coupled model experiments. Other studies such as He and Soden (2016) establish value in using future AMIP experiments by diagnosing subtropical drying drivers over the global tropical oceans in annual means. However results appear inconclusive over continental regions, with suggestions of hydrological processes being more important over land. This thesis focuses on regional analysis over both continental and ocean regions and additionally for particular seasons, not annual means. Therefore highlighting the limited value in interpretation of future AMIP experiments. More sophisticated experiments in the newly developed CMIP6 dataset may provide additional insight into regional and seasonal analysis.

Mechanisms of regional projected precipitation change over southern Africa and the south-west Indian Ocean are explored innovatively through a decomposition analysis, providing novel insight into drivers of change and uncertainty over the region. It is established that the ΔP north/south dipole pattern emerges largely from the dynamic component (ΔP_{Shift}), which holds most uncertainty, particularly over the south-west Indian Ocean.

Projected precipitation changes over the continent appear not to be solely driven by ΔP_{Shift} but are additionally driven by thermodynamic contributions (which are typically more robust), particularly from contributions in reductions of relative humidity. Drying over the continent is more robust than wetting. A distinct drying signal is evident across models in OND; however magnitude is uncertain and not particularly well constrained. Other studies performed over the region imply reductions in projected precipitation over the subtropics is related to the expansion of the Hadley Cell (i.e. tropical widening) (Scheff and Frierson, 2012a; 2012b; Lucas et al., 2014), in which OND may be consistent with that notion, however has not been analysed in this study. SST patterns of warming over the Indian Ocean significantly drive wetting, therefore corroborating the warmest-get-wetter mechanism over that SWIO domain.

Drivers of precipitation change appear somewhat varied between land and ocean regions, despite the zonally uniform climate change signal evident extending from the southern African continent into the adjacent Indian Ocean. Over the continent changes are influenced by dynamic and additionally thermodynamic influences, whereas over the SWIO dynamic changes remain dominant.

It appears evident that DJF is more dynamically driven and less so in OND, which was previously alluded to in Chapter 4 from future AMIP experiment correlations. Influences from thermodynamic contributions as well as reductions in relative humidity are additionally driving changes in OND, whereas in DJF spatial shifts in convection (dynamical component) and additional dynamic influences are established to be most prominent. DJF indicates significant associations with ΔP_{Cross} over the continent, which

is a secondary dynamic component. OND does not exhibit significant associations with this term as dynamic influences do not appear as prominent in the pre-summer transition season.

For both OND and DJF pattern variation of projected precipitation change is dominated by a dipole pattern over the Indian Ocean. The dipole pattern appears similarly when applied to ΔP_{Shift}. Significant relationships are established with local Indian Ocean SST patterns of change and to a lesser extent the Pacific Ocean region. Independent analysis of dominant patterns of variation for land and ocean regions establish the following findings, i) land regions in both seasons, but particularly OND exhibit significant associations with the central Pacific Ocean, ii) whereas over the SWIO influences from SSTs tend to remain more local with significant relationships established in the south-west Indian Ocean.

Composite analysis of moisture flux fields across models illustrate circulation patterns driving projected drying in OND and DJF. Due to models exhibiting circulation biases over SA/SWIO in the present day (Lazenby et al., 2016), these biases are most likely responsible for the uncertainty established associated with the dynamic component of future precipitation projections. Drivers of uncertainty include SST pattern changes, which modulate atmospheric circulation patterns (He et al., 2014). Therefore if uncertainty is reduced in terms of replicating model circulation and SST patterns, future precipitation projections over southern Africa and the south-west Indian Ocean are more likely to become more robust and therefore credible.

To address the issue of uncertainty a model ranking framework is developed here, which includes both constituents of mean state and variability processes over southern Africa. Models do not show convergence between mean state and variability metric performance, indicating model inconsistency in performance between the two processes. A sensitivity analysis established significant differences between random and "intelligent" sub-sampling of models. At the 90th percentile uncertainty is significantly reduced when models are selected "intelligently" through the process-based analysis approach developed in this thesis for DJF over the continent when using the "top" 20 and 30 performing models, therefore indicating value in performing such ranking tasks. Unfortunately for the transition season, OND, uncertainty was not significantly reduced however, the drying signal is relatively credible and plausible with most models in agreement exhibiting drying over the southern and south-western continent. Projected precipitation change over the SWIO was not constrained significantly; however priority remains focused on provision of robust and credible projections over continental regions where impacts are most important and have direct implications on adaption.

Models are additionally able to reduce projected precipitation uncertainty over the SIOCZ region when allowing individual model processes to emerge opposed to being penalised based on erroneous initial historical positioning of the SIOCZ. Uncertainty is constrained by more than half when allowing model processes to dominate. This provides new insight as to how models produce change, which appears to be consistent among models and physically agreeable.

Future precipitation projections in DJF are deemed more credible in this thesis, with projected drying apparent over the south-western continent and projected wetting peaking in the north-east. Projected precipitation changes in OND (deemed less credible here, as uncertainty could not be significantly reduced in this season) demonstrate large projected zonal drying over the majority of the southern African continent. Projected changes of 200km shifts in the dominant summer rainfall feature (SIOCZ) will have magnified on the ground impacts. This change will impact regions most reliant on agricultural practises within the 200km region and essentially require altered methods of farming practises, such as inclusion of drought resistant crops or change in crop type.

These identified regional projected changes in precipitation over southern Africa have important implications regarding water security which affect livelihoods, as well as commercial and subsistence farming over the region. Climate information regarding projected future climate possibilities over southern Africa should be communicated to policy and decision-makers with the appropriate level of probability and plausibility.

2. Future work

Model caveats and implications are discussed in more detail within each relevant chapter of the thesis. Discussed here is a summary of the identified caveats of this thesis, providing ideas and approaches to potentially address those issues in future work where possible.

Future work with respect to contemporary climatology over southern Africa could be focused on i) Bias correction in CMIP5 models of the Indian Ocean bias through thorough analysis of model parameterisation schemes and SST pattern influence ii) improved understanding of model teleconnections regarding interannual variability (e.g. deriving additional principal components within models to assess if teleconnections emerge after the 3rd principal component) iii) in depth austral summer variability analysis on all time-scales, particularly decadal time-scales (Dieppois et al., 2016), as this is the time-scale in which climate change occurs, iv) additional analysis of potential suspects driving variability over southern Africa, such as wave activity i.e. Rossby waves and the Matsuno-Gill response (Ratnam et al. 2014). Additonally model processes producing rainfall require further investigation rather than just metrics of performance.

Key changes in precipitation in Chapter 4 include projected changes within the SIOCZ region. Notable caveats regarding the algorithm to quantify the SIOCZ in contemporary and future climate need to be highlighted. The SIOCZ is located within a rather confined domain in which the Indian Ocean ITCZ feature is additionally present in DJF. Therefore deriving the best-fit line along the maximum precipitation axis can prove troublesome in particular models where the Indian Ocean ITCZ is located more westwards towards the SIOCZ domain. Larger magnitudes of rainfall evident in the ITCZ will potentially alter the axis of the SIOCZ, generally modulating the SIOCZ orientation as too zonal. Therefore care was taken to exclude the Indian Ocean ITCZ in this algorithm by constraining the region as tightly as possible, but was not possible to get 100% accurate for all CMIP5 models. An approach to counteract this caveat would

be to apply a SIOCZ mask using a threshold value specific to the SIOCZ, which was performed in Chapter 6 with promising results.

Atmosphere-only future experiments indicate limited value over the chosen regional domain. The AMIPFuture experiment currently only consisting of a single CMIP3 SST pattern of change for all individual models. New results from the newly established CMIP6 dataset (Eyring et al., 2016) will be interesting to analyse and hopefully enhances understanding into SST pattern influences within CMIP models over southern Africa. Studies performed by He and Soden (2016) show value in using AMIP future experiments, however only for annual means over the global domain.

A caveat within the decomposition methodology is identified and approaches to address this issue are discussed. M^* is shown to be a good approximation of actual moisture flux (M_{int}), however models typically tend to underestimate M^*, which Chadwick et al. (2013) states. The method is accepted for analysis even with this known caveat, however an approach to address this underestimation of M^* could include i) a vertical velocity filter to only include convective moisture flux, by using vertically integrated atmospheric moisture (q) between the surface and 700 hPa, instead of the 2 m specific humidity (q) value, ii) future analyses could incorporate a precipitation rate filter for vertical velocity that would be representative of only deep convection and exclude shallow convection.

Understanding drivers of precipitation changes and uncertainty associated with those changes are complex. From this thesis it is established that each key identified season (OND and DJF) and region (land versus ocean) over southern Africa and the SWIO, exhibit varying influences and drivers producing projected change and uncertainty.

Gaps remaining include model understanding with respect to drivers and uncertainty of change i.) SST patterns are likely not the only mechanisms driving changes and do not fully explain changes, particularly over land regions, ii.) SST pattern changes are slightly easier to interpret and understand over ocean precipitation change regions, due to the known effects of temperature increases over regions of unlimited moisture and the warmest-get-wetter mechanism of change proving robust over ocean regions, iii) the concept of the widening of the tropical circulation (e.g. Lucas et al., 2014) is a dynamical response that could be an additional driver of change that requires additional exploration over southern Africa. Drying over the southern African continent is very prominent at 20˚S during OND and this proposed tropical widening effect appears to be consistent along the southern boundary of the subtropics, coinciding with the notable drying signal. Future work could be used to explore this issue further, iv) OND appears to be less dynamically driven in comparison to DJF. Further research is required to unpack this statement and its significance.

No one particular approach to model ranking has been deemed best or most appropriate and therefore several different approaches can be assessed (Schaller et al., 2011; Rowell et al., 2016). This thesis makes attempts to provide further insight using only one

approach, however awareness of other approaches are appreciated. The ranking framework here shows promise with significant reductions in uncertainty being established. However results should be interpreted with caution for the following reasons.

1) There is little to no model convergence between mean state and variability metrics used in the raking framework. This reduces credibility of any significant reductions of uncertainty established as it may be misleading. 2) The model ranking framework established in this thesis is tailored specifically towards austral summer (DJF) and may be a possible reason why no significant reductions in uncertainty were established in OND. To address this and given more time a ranking framework tailored towards OND based metrics could be performed and compared with this analysis. 3) Additionally ranking frameworks could be tailored separately for land and ocean regions, as the two domains exhibit varying influences and drivers of change and uncertainty. 4) The choice and number of metrics used in this analysis may not be optimal. To address this issue firstly a larger range of metrics could be derived, and then a sensitivity analysis could be performed, whereby the number of metrics and combinations of metrics are varied to determine if results remain consistent or change drastically. This could add more confidence to this type of approach in model ranking and reducing uncertainty.

There is ultimately a need to tailor climate change data and projections into useable and credible climate change information. This study uses a process-based approach, whereby climate data is analysed using an understanding of processes that are unique to

the chosen study region. Physically relevant processes and metrics are then derived over the chosen region to rank and used to make attempts in reducing uncertainty in future precipitation projections.

An approach that could prove beneficial and is currently in use is end-user driven research. Climate information should be more tailored towards suiting the adaption needs of policy-makers via initial questions being asked by end-users to drive the scientific climate research. Projecting climate changes under uncertainty through to adaption measures is fraught with difficulties, as this is a highly sophisticated problem and there can be potential trade-offs (Swart et al., 2009). Key points essential in disseminating clear climate projection information as a climate scientist are i) what is the degree of uncertainty associated with future projections? i.e. to quantify the uncertainties and ii) communicate those uncertainties to the appropriate target audience (Webster, 2003). This thesis provides insight and addresses point (i) over southern Africa, which hopefully will ultimately leads to informing point (ii).

References

Ackerman, A. S., Toon, O. B., Stevens, D. E., Heymsfield, A. J., Ramanathan, V., & Welton, E. J. (2000). Reduction of tropical cloudiness by soot. *Science*, *288*(5468), 1042-1047.

Adler, R. F., Huffman, G. J., Chang, A., Ferraro, R., Xie, P. P., Janowiak, J., Rudolf, B., Schneider, U., Curtis, S., Bolvin, D., Gruber, A., Susskind, J., Arkin, P., and Nelkin, E. (2003). The version-2 global precipitation climatology project (GPCP) monthly precipitation analysis (1979–present). *J. Hydrometeor*., 4(6), 1147–1167.

Alder, J. R. (2011). *Simulating past, present, and future changes in ENSO: a model evaluation and data-model comparison*. Oregon State University.

Allen, M. R., & Ingram, W. J. (2002). Constraints on future changes in climate and the hydrologic cycle. *Nature*, *419*(6903), 224-232.

Allen, C.D., Macalady, A.K., Chenchouni, H., Bachelet, D., McDowell, N., Vennetier, M., Kitzberger, T., Rigling, A., Breshears, D.D., Hogg, E.T. and Gonzalez, P. (2010). A global overview of drought and heat-induced tree mortality reveals emerging climate change risks for forests. *Forest ecology and management*, *259*(4), pp.660-684.

Archer, E. R. (2003). Identifying underserved end-user groups in the provision of climate information. *Bulletin of the American Meteorological Society*, *84*(11), 1525.

Basher, R., & Briceno, S. A. L. V. A. N. O. (2006). 25 Climate and disaster risk reduction in Africa. *Climate Change and Africa*, *1564*(3721), 271.

Battisti, D. S., U. S. Bhatt, and M. A. Alexander. (1995). A modeling study of the interannual variability in the wintertime North Atlantic Ocean., *J. Climate.*, 8.12, 3067-3083.

Bayr, T., & Dommenget, D. (2013). The tropospheric land–sea warming contrast as the driver of tropical sea level pressure changes. *Journal of Climate*, *26*(4), 1387-1402.

Behera, S. K., and T. Yamagata. (2001). Subtropical SST dipole events in the southern Indian Ocean. *Geophys. Res. Lett.*, 28, 327–330.

Bollasina, M. A., & Ming, Y. (2013). The general circulation model precipitation bias over the southwestern equatorial Indian Ocean and its implications for simulating the South Asian monsoon. *Climate dynamics*, *40*(3-4), 823-838.

Bocking, S. (2004). *Nature's experts: science, politics, and the environment*. Rutgers University Press.

Bony, S., Bellon, G., Klocke, D., Sherwood, S., Fermepin, S., & Denvil, S. (2013). Robust direct effect of carbon dioxide on tropical circulation and regional precipitation. *Nature Geoscience*, *6*(6), 447-451.

Brown, J. R., Power, S. B., Delage, F. P., Coleman, R. A., Moise, A. F., and Murphy, B. F. (2011). Evaluation of the South Pacific Convergence Zone in IPCC AR4 Climate Model Simulations of the Twentieth Century. *J. Climate*., 24, 1565–1582.

Brown, J. R., Moise, A. F., & Delage, F. P. (2012). Changes in the South Pacific Convergence Zone in IPCC AR4 future climate projections. *Climate dynamics*, *39*(1-2), 1-19.

Brown, J. R., Moise, A. F., & Colman, R. A. (2013). The South Pacific Convergence Zone in CMIP5 simulations of historical and future climate. *Climate dynamics*, *41*(7-8), 2179-2197.

Byrne, M. P., & O'Gorman, P. A. (2013). Link between land-ocean warming contrast and surface relative humidities in simulations with coupled climate models. *Geophysical Research Letters*, *40*(19), 5223-5227.

Byrne, M. P., & O'Gorman, P. A. (2015). The Response of Precipitation Minus Evapotranspiration to Climate Warming: Why the "Wet-Get-Wetter, Dry-Get-Drier" Scaling Does Not Hold over Land. *Journal of Climate*, *28*(20), 8078-8092.

Cai, W., Cowan, T., & Thatcher, M. (2012). Rainfall reductions over Southern Hemisphere semi-arid regions: the role of subtropical dry zone expansion. *Scientific reports*, *2*, 702.

Cai, W., Borlace, S., Lengaigne, M., Van Rensch, P., Collins, M., Vecchi, G., ... & England, M. H. (2014). Increasing frequency of extreme El Niño events due to greenhouse warming. *Nature climate change*, *4*(2), 111-116.

Callaway, J. M. (2004). Adaptation benefits and costs: are they important in the global policy picture and how can we estimate them?. *Global Environmental Change*, *14*(3), 273-282.

Camberlin, P., Janicot, S., & Poccard, I. (2001). Seasonality and atmospheric dynamics of the teleconnection between African rainfall and tropical sea-surface temperature: Atlantic vs. ENSO. *International Journal of Climatology*, *21*(8), 973-1005.

Carvalho, L. M., Jones, C., & Liebmann, B. (2004). The South Atlantic convergence zone: Intensity, form, persistence, and relationships with intraseasonal to interannual activity and extreme rainfall. *Journal of Climate*, *17*(1), 88-108.

Chadwick, R., Boutle, I., & Martin, G. (2013a). Spatial patterns of precipitation change in CMIP5: Why the rich do not get richer in the tropics. *Journal of Climate*, *26*(11), 3803-3822.

Chadwick, R., Wu, P., Good, P., & Andrews, T. (2013b). Asymmetries in tropical rainfall and circulation patterns in idealised CO2 removal experiments. *Climate dynamics*, *40*(1-2), 295-316.

Chadwick, R., Good, P., Andrews, T., & Martin, G. (2014). Surface warming patterns drive tropical rainfall pattern responses to CO2 forcing on all timescales. *Geophysical Research Letters*, *41*(2), 610-615.

Chadwick, R., Good, P., Martin, G., & Rowell, D. P. (2015). Large rainfall changes consistently projected over substantial areas of tropical land. *Nature Climate Change*
Chadwick, R. (2016). Which Aspects of CO2 Forcing and SST Warming Cause Most Uncertainty in Projections of Tropical Rainfall Change over Land and Ocean? *Journal of Climate*, *29*(7), 2493-2509.

Chou, C., & Neelin, J. D. (2004). Mechanisms of global warming impacts on regional tropical precipitation*. *Journal of climate*, *17*(13), 2688-2701.

Chou, C., Neelin, J. D., Chen, C. A., & Tu, J. Y. (2009). Evaluating the "rich-get-richer" mechanism in tropical precipitation change under global warming.*Journal of Climate*, *22*(8), 1982-2005.

Chou, C., & Chen, C. A. (2010). Depth of convection and the weakening of tropical circulation in global warming. *Journal of Climate*, *23*(11), 3019-3030.

Christensen, J. H. Kjellström, E. Giorgi, F. Lenderink, G. Rummukainen, M. (2010): Weight assignment in regional climate models. *Clim Res* 44:179–194

Christensen, J. H., Kanikicharla, K. K., Marshall, G., & Turner, J. (2013). Climate phenomena and their relevance for future regional climate change.

Chung, C. T., Power, S. B., Arblaster, J. M., Rashid, H. A., & Roff, G. L. (2014). Nonlinear precipitation response to El Niño and global warming in the Indo-Pacific. *Climate dynamics*, *42*(7-8), 1837-1856.

Clarke L., K. Jiang, K. Akimoto, M. Babiker, G. Blanford, K. Fisher-Vanden, J.-C. Hourcade, V. Krey, E. Kriegler, A. Löschel, D. McCollum, S. Paltsev, S. Rose, P. R. Shukla, M. Tavoni, B. C. C. van der Zwaan, and D.P. van Vuuren, 2014: Assessing Transformation Pathways. In: Climate Change 2014: Mitigation of Climate Change. Contribution of Working Group III to the Fifth Assessment Report of the Intergovernmental Panel on Climate Change [Edenhofer, O., R. Pichs-Madruga, Y. Sokona, E. Farahani, S. Kadner, K. Seyboth, A. Adler, I. Baum, S. Brunner, P. Eickemeier, B. Kriemann, J. Savolainen, S. Schlömer, C. von Stechow, T. Zwickel and J.C. Minx (eds.)]. Cambridge University Press, Cambridge, United Kingdom and New York, NY, USA.

Collins, M., An, S. I., Cai, W., Ganachaud, A., Guilyardi, E., Jin, F. F., ... & Vecchi, G. (2010). The impact of global warming on the tropical Pacific Ocean and El Niño. *Nature Geoscience*, *3*(6), 391-397.

Collins, M., Chandler, R. E., Cox, P. M., Huthnance, J. M., Rougier, J., & Stephenson, D. B. (2012). Quantifying future climate change. *Nature Climate Change*, *2*(6), 403-409.

Collins, M., R. Knutti, J. Arblaster, J.-L. Dufresne, T. Fichefet, P. Friedlingstein, X. Gao, W.J. Gutowski, T. Johns, G. Krinner, M. Shongwe, C. Tebaldi, A.J. Weaver and M. Wehner. (2013). Long-term Climate Change: Projections, Commitments and Irreversibility. In: *Climate Change 2013: The Physical Science Basis. Contribution of Working Group I to the Fifth Assessment Report of the Intergovernmental Panel on Climate Change* [Stocker, T.F., D. Qin, G.-K. Plattner, M. Tignor, S.K. Allen, J. Boschung, A. Nauels, Y. Xia, V. Bex and P.M. Midgley (eds.)]. Cambridge University Press, Cambridge, United Kingdom and New York, NY, USA.

Cook, K. H. (1998). On the response of the Southern Hemisphere to ENSO. *Proc. 23rd Climate Diagnostics and Prediction Workshop.* Miami, FL, Amer. Meteor. Soc., 323–326.

Cook, K. H. (2000). The South Indian Convergence Zone and Interannual Rainfall Variability over Southern Africa. *J. Climate*., 13, 3789–3804.

Cook, K. H. (2001). A Southern Hemisphere wave response to ENSO with implications for southern Africa precipitation. *Journal of the atmospheric sciences*, *58*(15), 2146-2162.

Dee, D. P., and Coauthors. (2011). The ERA-Interim reanalysis: configuration and performance of the data assimilation system. *Q.J.R. Meteorol. Soc*., 137, 553–597. doi: 10.1002/qj.828

Dieppois, B., Rouault, M., & New, M. (2015). The impact of ENSO on Southern African rainfall in CMIP5 ocean atmosphere coupled climate models. *Climate Dynamics*, *45*(9-10), 2425-2442.

Dieppois, B., Pohl, B., Rouault, M., New, M., Lawler, D., & Keenlyside, N. (2016). Interannual to interdecadal variability of winter and summer southern African rainfall, and their teleconnections. *Journal of Geophysical Research: Atmospheres*.

Dong, B., J. M. Gregory, and R. T. Sutton. (2009). Understanding land–sea warming contrast in response to increasing greenhouse gases. Part I: Transient adjustment. J. Climate, 22, 3079– 3097.

Emori, S., & Brown, S. J. (2005). Dynamic and thermodynamic changes in mean and extreme precipitation under changed climate. *Geophysical Research Letters*, *32*(17).

Engelbrecht, F. A., McGregor, J. L. and Engelbrecht, C. J. (2009). Dynamics of the Conformal-Cubic Atmospheric Model projected climate-change signal over southern Africa. *Int. J. Climatol*., 29, 1013–1033. doi: 10.1002/joc.1742

Engelbrecht, C.J., Engelbrecht, F.A. and Dyson, L.L. (2011). High-resolution model-projected changes in midtropospheric closed-lows and extreme rainfall events over southern Africa. *International Journal of Climatology*., DOI:10.1002/joc.3420.

Eyring, V., Bony, S., Meehl, G. A., Senior, C. A., Stevens, B., Stouffer, R. J., & Taylor, K. E. (2016). Overview of the Coupled Model Intercomparison Project Phase 6 (CMIP6) experimental design and organization. *Geoscientific Model Development*, *9*(5), 1937-1958.

Fasullo, J.T. (2010). Robust land-Ocean contrasts in Energy and water cycle feedbacks. *Journal of Climate*, 23, 4677-4693

Fauchereau N., S. Trzaska, S., Rouault, M., and Richard, Y. (2003). Rainfall variability and changes in southern Africa during the 20th Century in the Global Warming context, *Natural Hazards*, 29, 139-154.

Figueroa, S. N., Satyamurty, P., & Da Silva Dias, P. L. (1995). Simulations of the summer circulation over the South American region with an eta coordinate model. *Journal of the atmospheric sciences*, *52*(10), 1573-1584.

Fisher B, Nakicenovic N, Alfsen K, Corfee Morlot J, De la Chesnaye F, Hourcade J.-C, Jiang K, Kainuma M, La Rovere E, Matysek A, Rana A, Riahi K, Richels R, Rose S, van Vuuren DP, Warren R, (2007) Chapter 3: Issues related to mitigation in the long-term context. In: Climate change 2007: Mitigation. Contribution of Working Group III to the Fourth Assessment Report of the Intergovernmental Panel on Climate Change. Cambridge University Press, Cambridge, United Kingdom and New York, NY, USA

Flato, G., J. Marotzke, B. Abiodun, P. Braconnot, S.C. Chou, W. Collins, P. Cox, F. Driouech, S. Emori, V. Eyring, C. Forest, P. Gleckler, E. Guilyardi, C. Jakob, V. Kattsov, C. Reason and M. Rummukainen, 2013: Evaluation of Climate Models. In: Climate Change 2013: The Physical Science Basis. Contribution of Working Group I to the Fifth Assessment Report of the Intergovernmental Panel on Climate Change [Stocker, T.F., D. Qin, G.-K. Plattner, M. Tignor, S.K. Allen, J. Boschung, A. Nauels, Y. Xia, V. Bex and P.M. Midgley (eds.)]. Cambridge University Press, Cambridge, United Kingdom and New York, NY, USA, pp. 741–866, doi:10.1017/CBO9781107415324.020.

Friedlingstein P, Andrew RM, Rogelj J, Peters GP, Canadell JG, Knutti R, Luderer G, Raupach MR, Schaeffer M, van Vuuren DP, Le Quéré C (2014) Persistent growth of CO2 emissions and implications for reaching climate targets. Nat Geosci 7:709–715

Gates, W. L. (1992) AMIP: The Atmospheric Model Intercomparison Project. Bull. Amer. Meteor. Soc., 73, 1962–1970.

Gates, W. L., and Coauthors. (1999) An overview of the results of the Atmospheric Model Intercomparison Project (AMIP I). *Bull. Amer. Meteor. Soc*., 80, 29–55.

Gleckler, P. J., K. E. Taylor, and C. Doutriaux. (2008). Performance metrics for climate models, *J. Geophys. Res*., 113, D06104, doi:10.1029/2007JD008972.

Goddard, L., & Graham, N. E. (1999). Importance of the Indian Ocean for simulating rainfall anomalies over eastern and southern Africa. *J. Geophys Res: Atm (1984–2012)*, 104(D16), 19099-19116.

Hallegatte, S., Shah, A., Brown, C., Lempert, R., & Gill, S. (2012). Investment decision making under deep uncertainty--application to climate change. *World Bank Policy Research Working Paper*, (6193).

Hansen, J. W., Mason, S. J., Sun, L., & Tall, A. (2011). Review of seasonal climate forecasting for agriculture in sub-Saharan Africa. *Experimental Agriculture*, *47*(02), 205-240.

Hart, N. C. G., Reason, C. J. C., & Fauchereau, N. (2010). Tropical-extratropical interactions over southern Africa: three cases of heavy summer season rainfall. *Monthly weather review*, *138*(7), 2608-2623.

He, J., Soden, B. J., & Kirtman, B. (2014). The robustness of the atmospheric circulation and precipitation response to future anthropogenic surface warming. *Geophysical Research Letters*, *41*(7), 2614-2622.

He, J., & Soden, B. J. (2016). A re-examination of the projected subtropical precipitation decline. *Nature Climate Change*.

Held, I. M., & Soden, B. J. (2000). Water vapor feedback and global warming 1. *Annual review of energy and the environment*, *25*(1), 441-475.

Held, I. M., & Soden, B. J. (2006). Robust responses of the hydrological cycle to global warming. *Journal of Climate*, *19*(21), 5686-5699.

Hoerling, M., J. Hurrell, J. Eischeid, and A. Phillips. (2006). Detection and attribution of twentieth-century northern and southern African rainfall change. *J. Climate*, 19, 3989–4008.

Hsu, P., and T. Li. (2012). Is “rich-get-richer” valid for Indian Ocean and Atlantic ITCZ?, Geophys. Res. Lett., 39, L13705, doi:10.1029/2012GL052399.

Huang, Y., Chameides, W. L., & Dickinson, R. E. (2007). Direct and indirect effects of anthropogenic aerosols on regional precipitation over east Asia. *Journal of Geophysical Research: Atmospheres*, *112*(D3).

Huang, P., Xie, S. P., Hu, K., Huang, G., & Huang, R. (2013). Patterns of the seasonal response of tropical rainfall to global warming. *Nature Geoscience*,*6*(5), 357-361.

IPCC. (2001). 881 Eds. Houghton J.T, Ding Y, Griggs D.J, Noguer M, van der Linden P.J, Xiaosu D, Dai X, Maskell K, Johnson C.A 2001 Cambridge, UK: Cambridge University Press

IPCC. (2007). Climate change 2007: the physical science basis. S. Solomon, D. Qin, M. Manning, Z. Chen, M. Marquis, K.B. Averyt, M. Tignor, H.L. Miller (Eds.), Contribution of Working Group I to the Fourth Assessment Report of the Intergovernmental Panel on Climate Change, Cambridge University Press, Cambridge, United Kingdom and New York, NY, USA.

IPCC (2008) Towards new scenarios for analysis of emissions, climate change, impacts, and response strategies. IPCC Expert Meeting Report on New Scenarios, Noordwijkerhout, Intergovernmental Panel on Climate Change

IPCC, (2013a): Climate Change 2013: The Physical Science Basis. Contribution of Working Group I to the Fifth Assessment Report of the Intergovernmental Panel on Climate Change [Stocker, T.F., D. Qin, G.-K. Plattner, M. Tignor, S.K. Allen, J. Boschung, A. Nauels, Y. Xia, V. Bex and P.M. Midgley (eds.)]. Cambridge University Press, Cambridge, United Kingdom and New York, NY, USA, 1535 pp.

IPCC. (2013b). Summary for policymakers. Climate Change 2013: The Physical Science Basis, T. F. Stocker et al., Eds., Cambridge University Press, 1–29.

IPCC. (2014). Climate Change 2014: Synthesis Report. Contribution of Working Groups I, II and III to the Fifth Assessment Report of the Intergovernmental Panel on Climate Change [Core Writing Team, R.K. Pachauri and L.A. Meyer (eds.)]. IPCC, Geneva, Switzerland, 151 pp.

James, R., Washington, R., & Jones, R. (2015). Process-based assessment of an ensemble of climate projections for West Africa. *Journal of Geophysical Research: Atmospheres*, *120*(4), 1221-1238.

Joshi, M. M., Gregory, J. M., Webb, M. J., Sexton, D. M., & Johns, T. C. (2008). Mechanisms for the land/sea warming contrast exhibited by simulations of climate change. *Climate Dynamics*, *30*(5), 455-465.

Joshi, M. M., F. H. Lambert, and M. J. Webb. (2013). An explanation for the difference between twentieth and twenty-first century land–sea warming ratio in climate models,*Clim. Dyn.*, 41, 1853–1869, doi:10.1007/s00382-013-1664-5.

Jun, M., Knutti, R., & Nychka, D. W. (2008a). Spatial analysis to quantify numerical model bias and dependence: how many climate models are there?. *Journal of the American Statistical Association*, *103*(483), 934-947.

Jun, M., Knutti, R., & Nychka, D. W. (2008b). Local eigenvalue analysis of CMIP3 climate model errors. *Tellus A*, *60*(5), 992-1000.

Jury, M. R. (1992). A climatic dipole governing the interannual variability of convection over the SW Indian Ocean and SE Africa region. *Trends Geophys. Res.*, 1, 165–172.

Kiladis, G. N., H. von Storch, and H. van Loon. (1989). Origin of the South Pacific convergence zone, *Journal of Climate,* 2(10), 1185 – 1195.

Kent, C., Chadwick, R., & Rowell, D. P. (2015). Understanding uncertainties in future projections of seasonal tropical precipitation. *Journal of Climate*, *28* (11), 4390-4413.

Kodama, Y.M. (1992). Large-scale common features of subtropical convergence zones (the Baiu frontal zone, the SPCZ and the SACZ). Part I: Characteristics of subtropical frontal zones. *J.Meteor. Soc. Japan*, 70, 813–836.

Kodama. (1993). Large-scale common features of subtropical convergence zones (the Baiu frontal zone, the SPCZ, and the SACZ). Part II: Conditions of the circulations for generating the STCZs. *J. Meteor.Soc.Japan*, 71, 581–610.

Knutson, T. R., & Manabe, S. (1995). Time-mean response over the tropical Pacific to increased C02 in a coupled ocean-atmosphere model. *Journal of Climate*, *8*(9), 2181-2199.

Knutti, R., Stocker, T. F., Joos, F., & Plattner, G. K. (2002). Constraints on radiative forcing and future climate change from observations and climate model ensembles. *Nature*, *416*(6882), 719-723.

Knutti, Reto. (2010) "The end of model democracy?." *Climatic change* 102.3-4. 395-404.

Knutti. R., Furrer. R., Tebaldi. C., Cermak. J., Meehl. G.A. (2010). Challenges in Combining Projections from Multiple Climate Models. *J. Climate,* 23:10, 2739-2758.

Knutti, R., Masson, D. and Gettelman, A. (2013). "Climate model genealogy: Generation CMIP5 and how we got there." *Geophysical Research Letters*.

Knutti, R., & Sedláček, J. (2013). Robustness and uncertainties in the new CMIP5 climate model projections. *Nature Climate Change*, *3*(4), 369-373.

Krishnamurti, T.N., Kishtawal, C.M., Zhang, Z., LaRow, T., Bachiochi, D., Williford, E., Gadgil, S. and Surendran, S. (2000). Multimodel ensemble forecasts for weather and seasonal climate. *Journal of Climate*, *13*(23), pp.4196-4216.

Kusangaya, S., Warburton, M. L., Van Garderen, E. A., & Jewitt, G. P. (2014). Impacts of climate change on water resources in southern Africa: A review. *Physics and Chemistry of the Earth, Parts A/B/C*, *67*, 47-54.

Lazenby, M. J., Todd, M. C., & Wang, Y. (2016). Climate model simulation of the South Indian Ocean Convergence Zone: mean state and variability. *Climate Research*, *68*(1), 59-71.

Lempert, R.J., and Collins, M.T. (2007). Managing the Risk of Uncertain Threshold Responses: Comparison of Robust, Optimum, and Precautionary Approaches, *Risk Analysis*, 27(4) DOI: 10.1111/j.1539-6924.2007.00940.x

Lenters, J. D., & Cook, K. H. (1995). Simulation and diagnosis of the regional summertime precipitation climatology of South America. *Journal of Climate*, *8*(12), 2988-3005.

Li, G., Xie, S. P., & Du, Y. (2016). A robust but spurious pattern of climate change in model projections over the tropical Indian Ocean. *Journal of Climate*, (2016).

Liebmann, B., Kiladis, G. N., Marengo, J., Ambrizzi, T., and Glick, J. D. (1999) Submonthly convective variability over South America and the South Atlantic convergence zone. *J Climate*, 12(7), 1877-1891.

Lindesay, J. A. (1988). South African rainfall, the Southern Oscillation and a Southern Hemisphere semi-annual cycle. *J. Climatol*., 8, 17–30.

Lohmann, U., & Feichter, J. (2005). Global indirect aerosol effects: a review. *Atmospheric Chemistry and Physics*, *5*(3), 715-737.

Long, S. M., Xie, S. P., & Liu, W. (2016). Uncertainty in tropical rainfall projections: Atmospheric circulation effect and the ocean coupling. *Journal of Climate*, *29*(7), 2671-2687.

Lucas, C., Timbal, B., & Nguyen, H. (2014). The expanding tropics: a critical assessment of the observational and modeling studies. *Wiley Interdisciplinary Reviews: Climate Change*, *5*(1), 89-112.

Lyons, S. W. (1991). Origins of convective variability over equatorial southern Africa during austral summer. *J. Climate*, 4, 23–39.

Ma, J., Xie, S. P., & Kosaka, Y. (2012). Mechanisms for tropical tropospheric circulation change in response to global warming*. *Journal of Climate*, *25*(8), 2979-2994.

Ma, J., & Xie, S. P. (2013). Regional patterns of sea surface temperature change: A source of uncertainty in future projections of precipitation and atmospheric circulation. *Journal of Climate*, *26*(8), 2482-2501.

Macron, C., Pohl, B., Richard, Y., & Bessafi, M. (2014). How do tropical temperate troughs form and develop over southern Africa?. *Journal of Climate*, *27*(4), 1633-1647.

Makarau, A., and M. R. Jury. (1997). Predictability of Zimbabwe summer rainfall. *Int. J. Climatol*., 17, 1421–1432.

Maloney, E. D., Camargo, S. J., Chang, E., Colle, B., Fu, R., Geil, K. L., ... & Kinter, J. (2014). North American climate in CMIP5 experiments: Part III: Assessment of twenty-first-century projections. *Journal of Climate*, *27*(6), 2230-2270.

Manhique, A. J., Reason, C. J. C., Rydberg, L., & Fauchereau, N. (2011). ENSO and Indian Ocean sea surface temperatures and their relationships with tropical temperate troughs over Mozambique and the Southwest Indian Ocean. *International journal of climatology*, *31*(1), 1-13.

Mason, S. J., & Joubert, A. M. (1995). A note on inter-annual rainfall variability and water demand in the Johannesburg region. *Water SA*, *21*(3), 269-270.

Mason, S. J., & Jury, M. R. (1997). Climatic variability and change over southern Africa: a reflection on underlying processes. *Progress in Physical Geography*, *21*(1), 23-50.

Masson, D., & Knutti, R. (2011). Climate model genealogy. *Geophysical Research Letters*, *38*(8).

McSweeney, C. F., & Jones, R. G. (2013). No consensus on consensus: the challenge of finding a universal approach to measuring and mapping ensemble consistency in GCM projections. *Climatic change*, *119*(3-4), 617-629.

Meadows, M. E. (2006). Global change and southern Africa. *Geographical Research*, 44(2), 135-145.

Meehl, G. A., Stocker, T. F., Collins, W. D., Friedlingstein, P., Gaye, A. T., Gregory, J. M., Kitoh, A., Knutti, R., Murphy, J. M., Noda, A., Raper, S. C. B., Watterson, I. G., Weaver, A. J., Zhao, Z. C. (2007). Global Climate Projections. In: Climate Change 2007: The Physical Science Basis. Contribution of Working Group I to the Fourth Assessment Report of the Intergovernmental Panel on Climate. Cambridge University Press, Cambridge, United Kingdom and New York, NY, USA.

Moss, R. H., et al. (2010), The next generation of scenarios for climate change research and assessment, *Nature*, 463, 747–756, doi:10.1038/nature08823.

Mulenga, H. M., Rouault, M., & Reason, C. J. C. (2003). Dry summers over northeastern South Africa and associated circulation anomalies. *Climate Research*, *25*(1), 29-41.

Munday, C. and Washington, R., (2017). Circulation controls on southern African precipitation in coupled models: The role of the Angola Low. *Journal of Geophysical Research Atmosphere*, 122, 861-877

Neelin, J. D., Chou, C., & Su, H. (2003). Tropical drought regions in global warming and El Niño teleconnections. *Geophysical Research Letters*, *30*(24).

Neelin, J. D., Münnich, M., Su, H., Meyerson, J. E., & Holloway, C. E. (2006). Tropical drying trends in global warming models and observations. *Proceedings of the National Academy of Sciences*, *103*(16), 6110-6115.

New, M., & Hulme, M. (2000). Representing uncertainty in climate change scenarios: a Monte-Carlo approach. *Integrated assessment*, *1*(3), 203-213.

Nicholls, N. (1999). Cognitive illusions, heuristics, and climate prediction. *Bulletin of the American Meteorological Society*, *80*(7), 1385.

Nicholson, S. E., D. Leposo, and J. Grist. (2001). The relationship between El Niño and drought over Botswana. J. Climate, 14, 323–335.

Niñomiya, K. (2008). Similarities and differences among the South Indian Ocean convergence zone, North American convergence zone, and other subtropical convergence zones simulated using an AGCM. *気象集誌. 第 2 輯*, 86(1), 141-165.

Palmer, T. (1999). Predicting uncertainty in forecasts of weather and climate. ECMWF Technical Memorandum No 294. pp 63.

Pitman, A. J. (2003). The evolution of, and revolution in, land surface schemes designed for climate models. *International Journal of Climatology*, *23*(5), 479-510.

Pohl, B., Fauchereau, N., Richard, Y., Rouault, M., & Reason, C. J. C. (2009). Interactions between synoptic, intraseasonal and interannual convective variability over Southern Africa. *Climate dynamics*, *33*(7-8), 1033-1050.

Power, S., Haylock, M., Colman, R., and Wang, X. (2006). The predictability of interdecadal changes in ENSO activity and ENSO teleconnections. *J. Climate.*, 19(19).

Puaud, Y., Pohl, B., Fauchereau, N., Macron, C., & Beltrando, G. (2016). Climate co-variability between South America and Southern Africa at interannual, intraseasonal and synoptic scales. *Climate Dynamics*, 1-22.

Ratna, S. B., Ratnam, J. V., Behera, S. K., Ndarana, T., Takahashi, K., & Yamagata, T. (2014). Performance assessment of three convective parameterization schemes in WRF for downscaling summer rainfall over South Africa. *Climate dynamics*, *42*(11-12), 2931-2953.

Ratnam, J. V., Behera, S. K., Masumoto, Y. and Yamagata, T. (2014). Remote Effects of El Niño and Modoki Events on the Austral Summer Precipitation of Southern Africa. *J. Climate*, 27, 3802–3815. doi: http://dx.doi.org/10.1175/JCLI-D-13-00431.1

Reason, C. J. C., & Mulenga, H. (1999). Relationships between South African rainfall and SST anomalies in the southwest Indian Ocean. *International Journal of Climatology*, *19*(15), 1651-1673.

Reason, C. J. C. (2001) Subtropical Indian Ocean SST dipole events and southern African rainfall. *Geophys. Res. Lett.*, 28(11), 2225-2227.

Renwick, J. A., and Michael, J. Revell. (1999). Blocking over the South Pacific and Rossby wave propagation. *Mon. Wea. Rev.*, 127.10, 2233-2247.

Reynolds, R. W., Smith, T. M., Liu, C., Chelton, D. B., Casey, K. S., & Schlax, M. G. (2007). Daily high-resolution-blended analyses for sea surface temperature. *Journal of Climate*, 20(22), 5473-5496.

Richard, Y., Trzaska, S., Roucou, P., & Rouault, M. (2000). Modification of the southern African rainfall variability/ENSO relationship since the late 1960s. *Climate Dynamics*, *16*(12), 883-895.

Rouault, M., & Richard, Y. (2005). Intensity and spatial extent of droughts in southern Africa. *Geophysical Research Letters*, *32*(15).

Rowell, D. (2012). Sources of uncertainty in future changes in local precipitation. Climate Dyn., 39, 1929–1950, doi:10.1007/ s00382-011-1210-2.

Rowell, D. P. (2013). Simulating SST Teleconnections to Africa: What is the State of the Art? *J. Climate*, 26, 5397–5418. doi: http://dx.doi.org/10.1175/JCLI-D-12-00761.1

Rowell, D. P., Booth, B. B., Nicholson, S. E., & Good, P. (2015). Reconciling past and future rainfall trends over east Africa. *Journal of Climate*, *28*(24), 9768-9788.

Rowell, D. P., Senior, C. A., Vellinga, M., & Graham, R. J. (2016). Can climate projection uncertainty be constrained over Africa using metrics of contemporary performance?. *Climatic Change*, *134*(4), 621-633.

Saji, N.H., Goswami, B.N., Vinayachandran, P.N. and Yamagata, T. (1999). A dipole mode in the tropical Indian Ocean, *Nature*, 401, 360-363

Schaller, N., Mahlstein, I., Cermak, J., and Knutti, R. (2011). Analyzing precipitation projections: A comparison of different approaches to climate model evaluation. *Journal of Geophysical Research: Atmospheres (1984–2012)*, 116(D10).

Scheff, J., & Frierson, D. (2012a). Twenty-first-century multimodel subtropical precipitation declines are mostly midlatitude shifts. *Journal of Climate*, *25*(12), 4330-4347.

Scheff, J., & Frierson, D. M. (2012b). Robust future precipitation declines in CMIP5 largely reflect the poleward expansion of model subtropical dry zones. *Geophysical Research Letters*, *39*(18).

Seager, R., Naik, N., & Vecchi, G. A. (2010). Thermodynamic and dynamic mechanisms for large-scale changes in the hydrological cycle in response to global warming*. *Journal of Climate*, *23*(17), 4651-4668.

Seidel, D. J., Fu, Q., Randel, W. J., & Reichler, T. J. (2008). Widening of the tropical belt in a changing climate. *Nature geoscience*, *1*(1), 21-24.

Shepherd, T. G. (2014). Atmospheric circulation as a source of uncertainty in climate change projections. *Nature Geoscience*, *7*(10), 703-708.

Shongwe, M. E., van Oldenborgh, G. J., van den Hurk, B., & van Aalst, M. (2011). Projected changes in mean and extreme precipitation in Africa under global warming. Part II: East Africa. *Journal of Climate*, 24(14), 3718-3733.

Soden, B. J., & Held, I. M. (2006). An assessment of climate feedbacks in coupled ocean-atmosphere models. *Journal of Climate*, *19*(14), 3354-3360.

Stevenson, S. L. (2012). Significant changes to ENSO strength and impacts in the twenty-first century: Results from CMIP5. *Geophys. Res. Lett.*, 39(17).

Streten, N. A. (1973). Some characteristics of satellite-observed bands of persistent cloudiness over the Southern Hemisphere. *Monthly Weather Review*, *101*(6), 486-495.

Sushama, L., Laprise, R., Caya, D., Frigon, A. and Slivitzky, M. (2006). Canadian RCM projected climate-change signal and its sensitivity to model errors. *Int. J. Climatol.*, 26, 2141–2159. doi: 10.1002/joc.1362

Swart, R., Bernstein, L., Ha-Duong, M., & Petersen, A. (2009). Agreeing to disagree: uncertainty management in assessing climate change, impacts and responses by the IPCC. *Climatic change*, *92*(1-2), 1-29.

Taljaard, J. J. (1953). The mean circulation in the lower troposphere over southern Africa. *South Afr. Geogr. J.*, 35, 33–45.

Taljaard, J. J., & Phil, D. (1996). *Atmospheric circulation systems, synoptic climatology and weather phenomena of South Africa*. Government Printer, South Africa.

Taylor, K. E. (2001). Summarizing multiple aspects of model performance in a single diagram. Journal of Geophysical Research: Atmospheres (1984–2012), 106(D7), 7183-7192.

Taylor, K. E., Stouffer, R. J., and Meehl, G. A. (2012). An Overview of CMIP5 and the Experiment Design. *Bull. Amer. Meteor. Soc.*, 93(4).

Tebaldi, C., & Knutti, R. (2007). The use of the multi-model ensemble in probabilistic climate projections. *Philosophical Transactions of the Royal Society A: Mathematical, Physical and Engineering Sciences*, *365*(1857), 2053-2075.

Tebaldi, Claudia, Julie M. Arblaster, and Reto Knutti. (2011). Mapping model agreement on future climate projections. *Geophysical Research Letters* 38.23.

Thibeault, J. M., & Seth, A. (2014). A Framework for Evaluating Model Credibility for Warm-Season Precipitation in Northeastern North America: A Case Study of CMIP5 Simulations and Projections. *Journal of Climate*, *27*(2), 493-510.

Todd, M., and R.Washington. (1998). Extreme daily rainfall in southern Africa and southwest Indian Ocean: Tropical–temperate links. *South Afr. J. Sci*., 94, 64–70.

Tyson, P. D., & Preston-Whyte, R. A. (2000). *weather and climate of southern Africa*. Oxford University Press.

Tyson, P. D. (1986). Climatic Change and Variability in Southern Africa. *Oxford University Press*, 220 pp.

Van der Wiel, K., Matthews, A. J., Stevens, D. P. and Joshi, M. M. (2015). A dynamical framework for the origin of the diagonal South Pacific and South Atlantic Convergence Zones. Q.J.R. Meteorol. Soc., 141: 1997–2010. doi:10.1002/qj.2508

van Vuuren, D. P., et al. (2011), The representative concentration pathways: An overview, *Clim. Chang.*, 109, 5–31, doi:10.1007/s10584-011-0148-z.

Vecchi, G. A., Soden, B. J., Wittenberg, A. T., Held, I. M., Leetmaa, A., & Harrison, M. J. (2006). Weakening of tropical Pacific atmospheric circulation due to anthropogenic forcing. *Nature*, *441*(7089), 73-76.

Vecchi, G. A., and Soden, B. J. (2007). Global warming and the weakening of the tropical circulation. *Journal of Climate*, *20*(17), 4316-4340.

Vigaud, N., Richard, Y., Rouault, M., & Fauchereau, N. (2009). Moisture transport between the South Atlantic Ocean and southern Africa: relationships with summer rainfall and associated dynamics. *Climate Dynamics*, *32*(1), 113-123.

Vincent, E. M., M. Lengaigne, C. E. Menkes, N. C. Jourdain, P. Marchesiello, and G. Madec. (2011). Interannual variability of the South Pacific convergence zone and implications for tropical cyclone genesis. *Climate Dyn*., doi:10.1007/s00382-009-0716-3.

Washington, R., & Todd, M. (1999). Tropical-temperate links in southern African and Southwest Indian Ocean satellite-derived daily rainfall. *International Journal of Climatology*, *19*(14), 1601-1616.

Washington, R., James, R., Pearce, H., Pokam, W. M., and Moufouma-Okia, W. (2013). Congo Basin rainfall climatology: can we believe the climate models? *Philosophical Transactions of the Royal Society B: Biological Sciences*, 368(1625), 20120296.

Webster, M. (2003). Communicating climate change uncertainty to policy-makers and the public. *Climatic Change*, *61*(1), 1-8.

Weller, E., Cai, W., Min, S. K., Wu, L., Ashok, K., & Yamagata, T. (2014). More-frequent extreme northward shifts of eastern Indian Ocean tropical convergence under greenhouse warming. *Scientific reports*, *4*.

Weigel, A. P., Knutti, R., Liniger, M. A., & Appenzeller, C. (2010). Risks of model weighting in multimodel climate projections. *Journal of Climate*, *23*(15), 4175-4191.

Widlansky, M. J., Webster, P. J., & Hoyos, C. D. (2011). On the location and orientation of the South Pacific Convergence Zone. *Climate dynamics*, *36*(3-4), 561-578.

Widlansky, M. J., Timmermann, A., Stein, K., McGregor, S., Schneider, N., England, M. H., ... & Cai, W. (2013). Changes in South Pacific rainfall bands in a warming climate. *Nature Climate Change*, *3*(4), 417-423.

Xie, P., and Arkin, P. A. (1997). Global precipitation: A 17-year monthly analysis based on gauge observations, satellite estimates, and numerical model outputs. *Bull. Amer. Meteor. Soc.*, 78(11), 2539-2558.

Xie, S. P., Deser, C., Vecchi, G. A., Ma, J., Teng, H., & Wittenberg, A. T. (2010). Global warming pattern formation: sea surface temperature and rainfall*. *Journal of Climate*, *23*(4), 966-986.

Yin, X., A. Gruber, and P. Arkin. (2004). Comparison of the GPCP and CMAP merged gauge-satellite monthly precipitation products for the period 1979 – 2001, *J. Hydrometeor*., 5, 1207-1222.

Zheng, X. T., Xie, S. P., Du, Y., Liu, L., Huang, G., & Liu, Q. (2013). Indian Ocean dipole response to global warming in the CMIP5 multimodel ensemble. *Journal of Climate*, *26*(16), 6067-6080.

Appendix

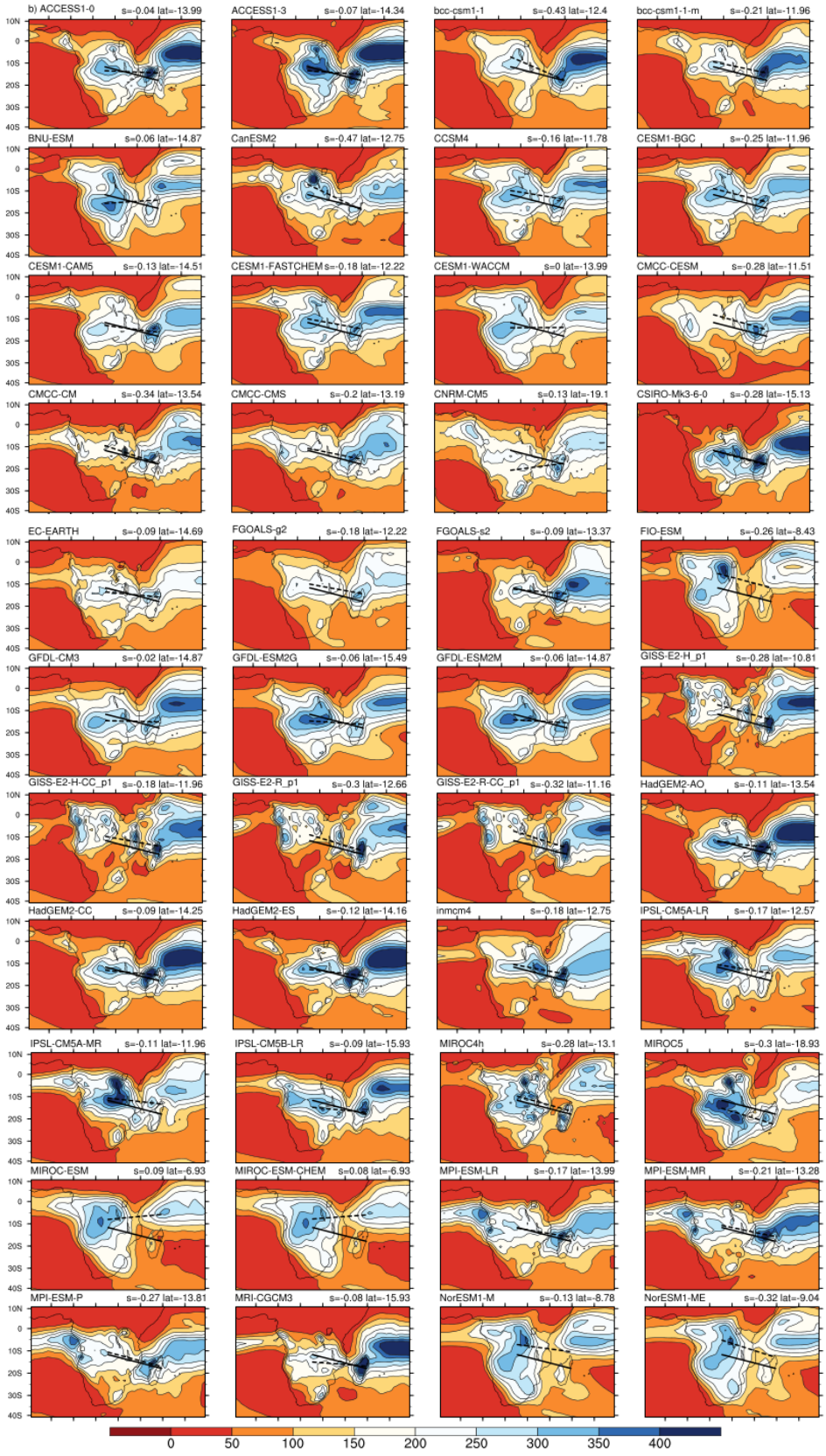
b) ACCESS1-0 s=-0.04 lat=-13.99
ACCESS1-3 s=-0.07 lat=-14.34
bcc-csm1-1 s=-0.43 lat=-12.4
bcc-csm1-1-m s=-0.21 lat=-11.96
BNU-ESM s=0.06 lat=-14.87
CanESM2 s=-0.47 lat=-12.75
CCSM4 s=-0.16 lat=-11.78
CESM1-BGC s=-0.25 lat=-11.96
CESM1-CAM5 s=-0.13 lat=-14.51
CESM1-FASTCHEM s=-0.18 lat=-12.22
CESM1-WACCM s=0 lat=-13.99
CMCC-CESM s=-0.28 lat=-11.51
CMCC-CM s=-0.34 lat=-13.54
CMCC-CMS s=-0.2 lat=-13.19
CNRM-CM5 s=0.13 lat=-19.1
CSIRO-Mk3-6-0 s=-0.28 lat=-15.13
EC-EARTH s=-0.09 lat=-14.69
FGOALS-g2 s=-0.18 lat=-12.22
FGOALS-s2 s=-0.09 lat=-13.37
FIO-ESM s=-0.26 lat=-8.43
GFDL-CM3 s=-0.02 lat=-14.87
GFDL-ESM2G s=-0.06 lat=-15.49
GFDL-ESM2M s=-0.06 lat=-14.87
GISS-E2-H_p1 s=-0.28 lat=-10.81
GISS-E2-H-CC_p1 s=-0.18 lat=-11.96
GISS-E2-R_p1 s=-0.3 lat=-12.66
GISS-E2-R-CC_p1 s=-0.32 lat=-11.16
HadGEM2-AO s=-0.11 lat=-13.54
HadGEM2-CC s=-0.09 lat=-14.25
HadGEM2-ES s=-0.12 lat=-14.16
inmcm4 s=-0.18 lat=-12.75
IPSL-CM5A-LR s=-0.17 lat=-12.57
IPSL-CM5A-MR s=-0.11 lat=-11.96
IPSL-CM5B-LR s=-0.09 lat=-15.93
MIROC4h s=-0.28 lat=-13.1
MIROC5 s=-0.3 lat=-18.93
MIROC-ESM s=0.09 lat=-6.93
MIROC-ESM-CHEM s=0.08 lat=-6.93
MPI-ESM-LR s=-0.17 lat=-13.99
MPI-ESM-MR s=-0.21 lat=-13.28
MPI-ESM-P s=-0.27 lat=-13.81
MRI-CGCM3 s=-0.08 lat=-15.93
NorESM1-M s=-0.13 lat=-8.78
NorESM1-ME s=-0.32 lat=-9.04
10N
0
10S
20S
30S
40S
0
50
100
150
200
250
300
350
400

Figure 1: Mean historical DJF precipitation climatology over southern Africa for the period 1971-2000 for the 44 CMIP5 models additionally overlaid with the model SIOCZ line (dashed) fitted to the maximum precipitation values along the longitudes 25˚E - 50˚E. CMAP SIOCZ line is the solid black line and the slope (s) and mean latitude (lat) are shown on the top right of each image. Units are in mm month^{-1}.

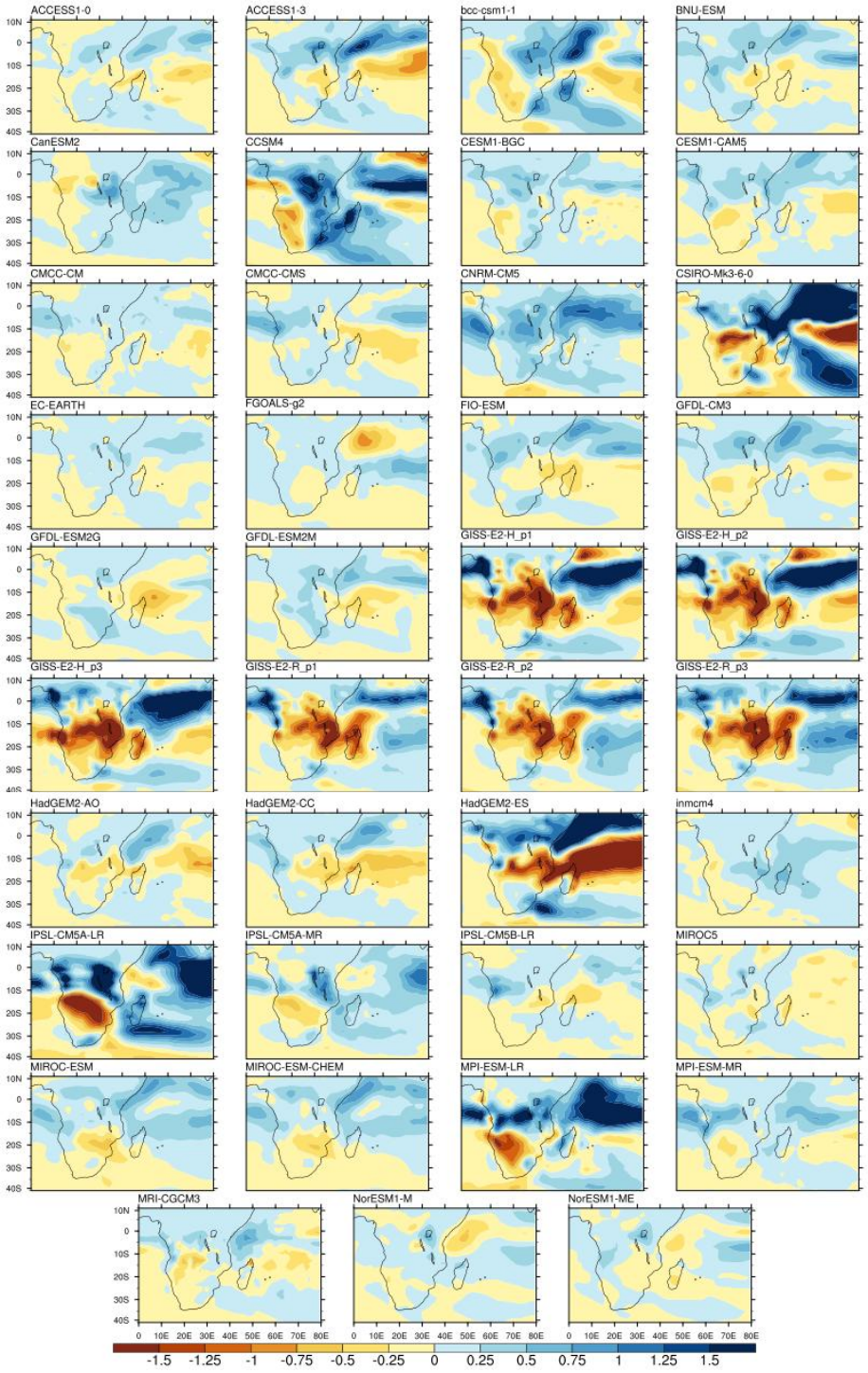

Figure 2: Absolute projected precipitation change for DJF over the southern African region and southwest Indian Ocean for 39 CMIP5 models for the period 2071-2100 minus 1971-2000. Units are in mm day^{-1}.

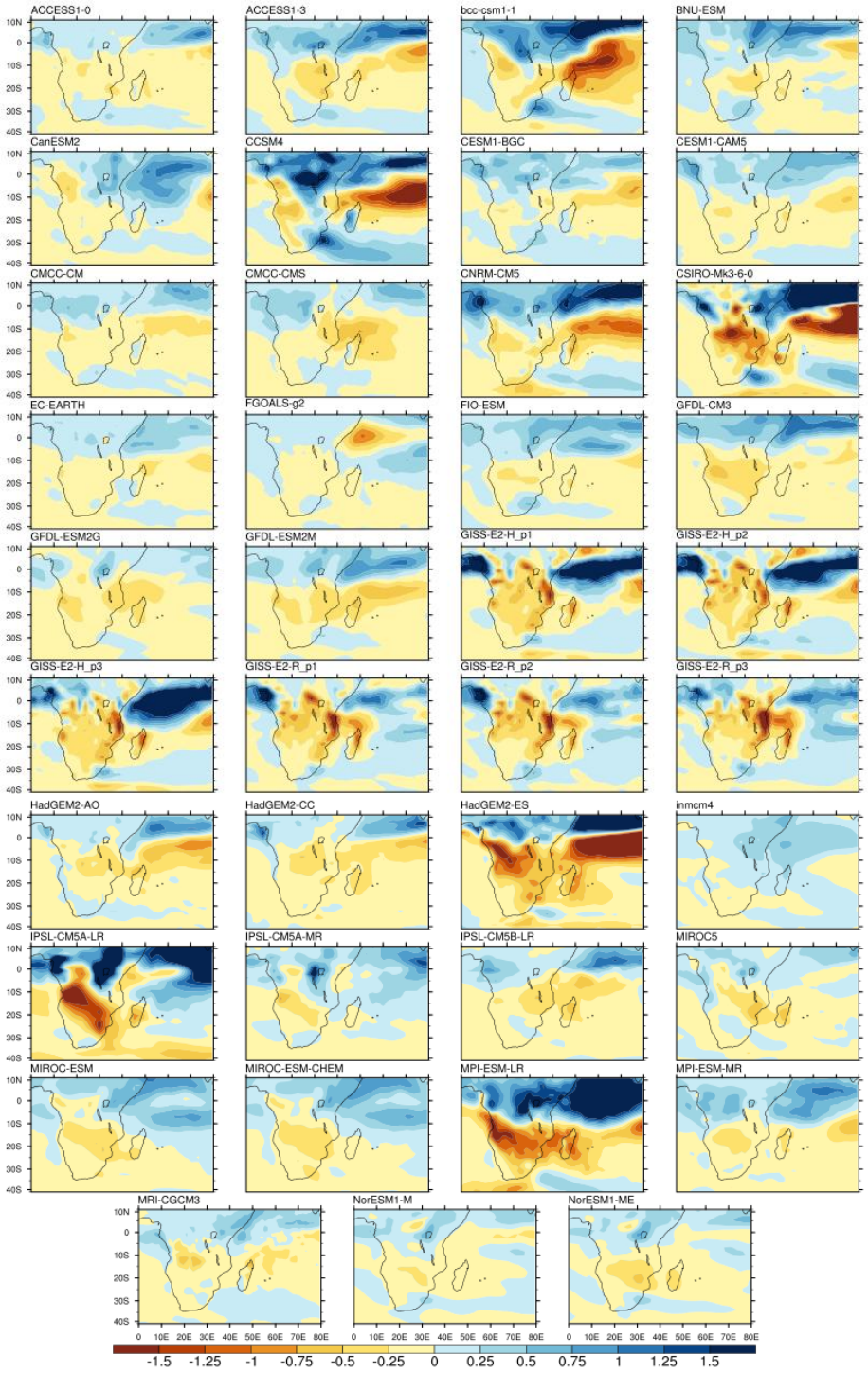

Figure 3: Same as Figure 2 but for OND.

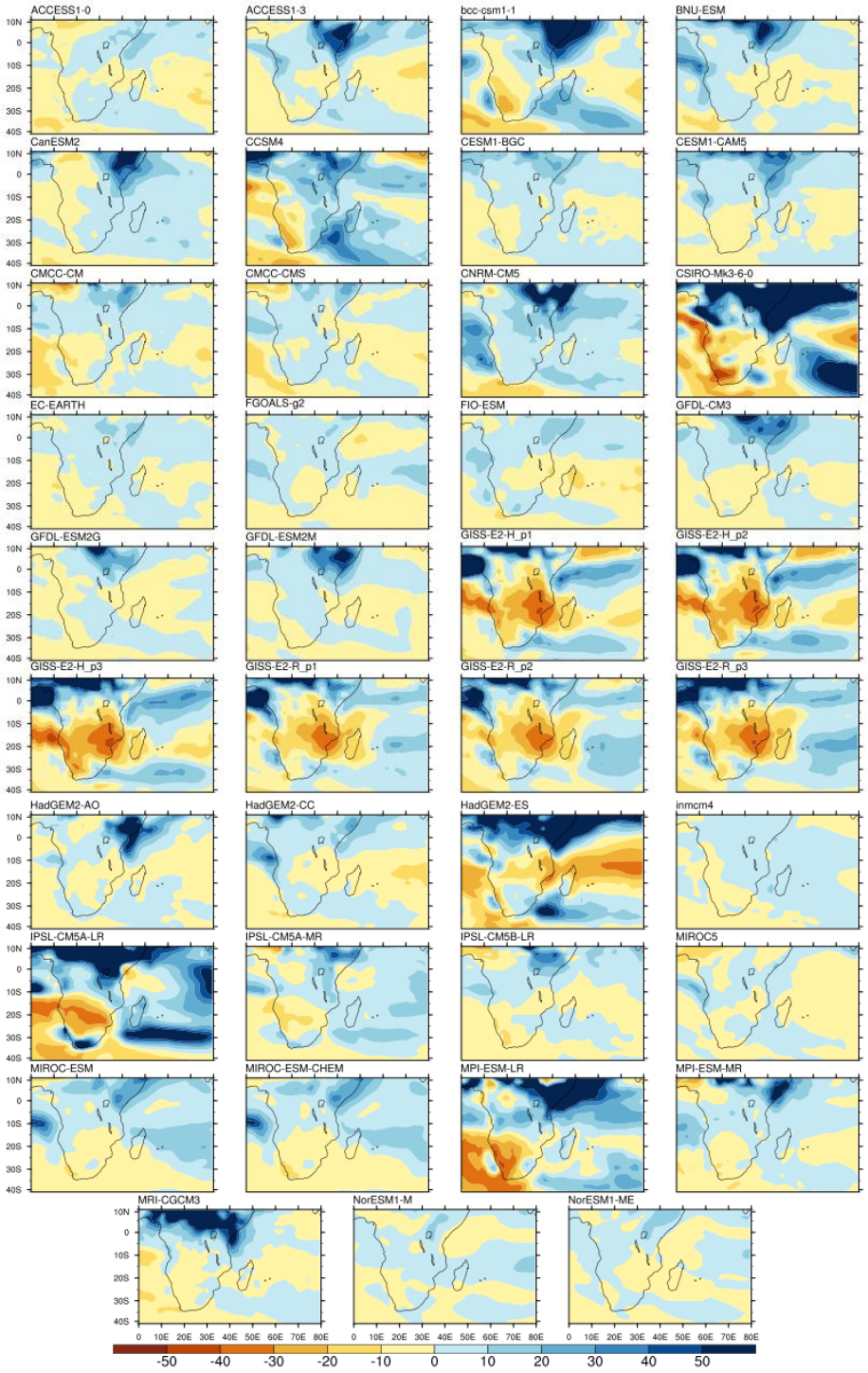

Figure 4: Percentage change of projected precipitation for DJF over the southern African region and southwest Indian Ocean for 39 CMIP5 models for the period 2071-2100 minus 1971-2000. Units are expressed as percentage change.

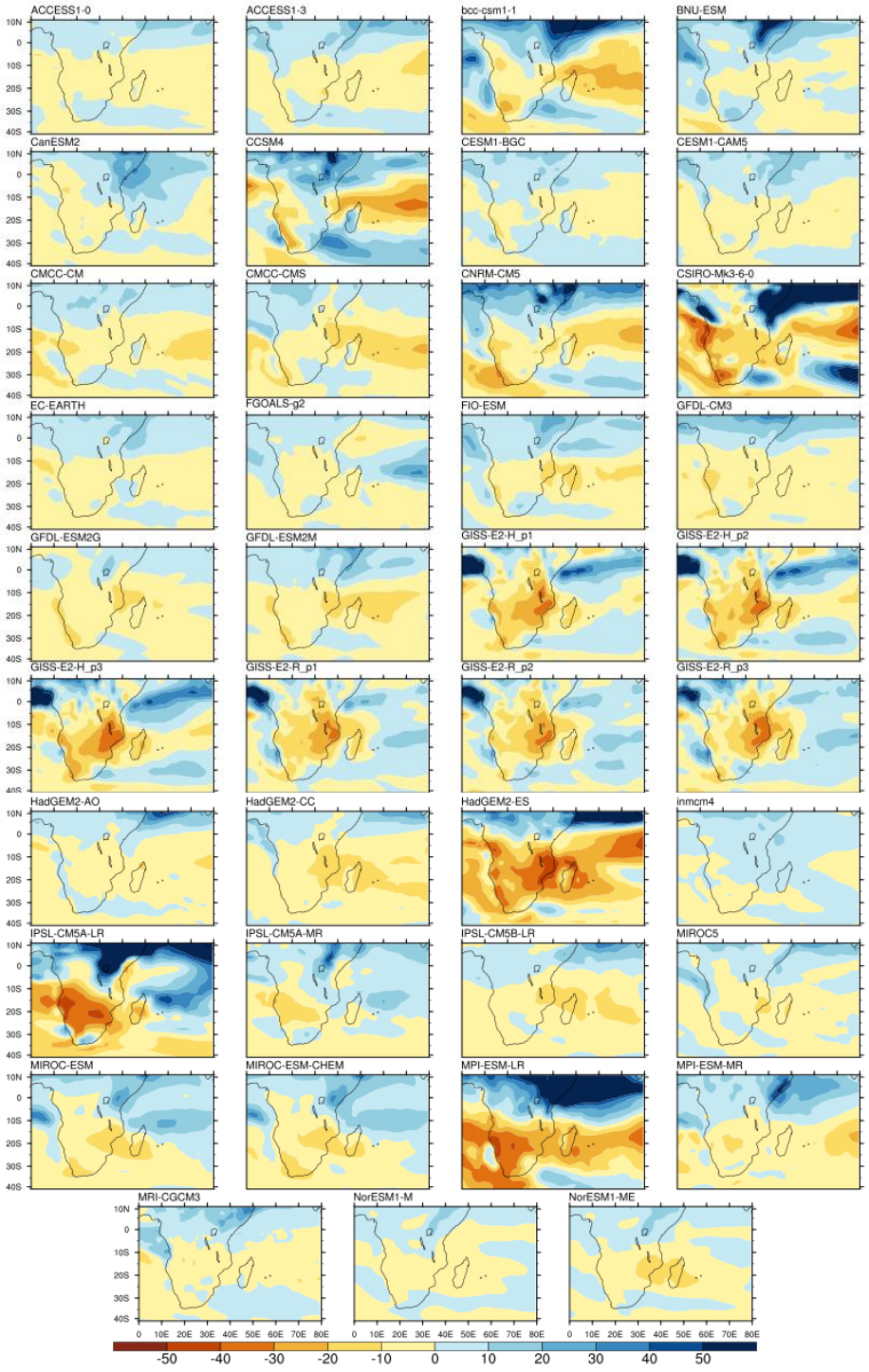

Figure 5: Same as Figure 4 but for OND.

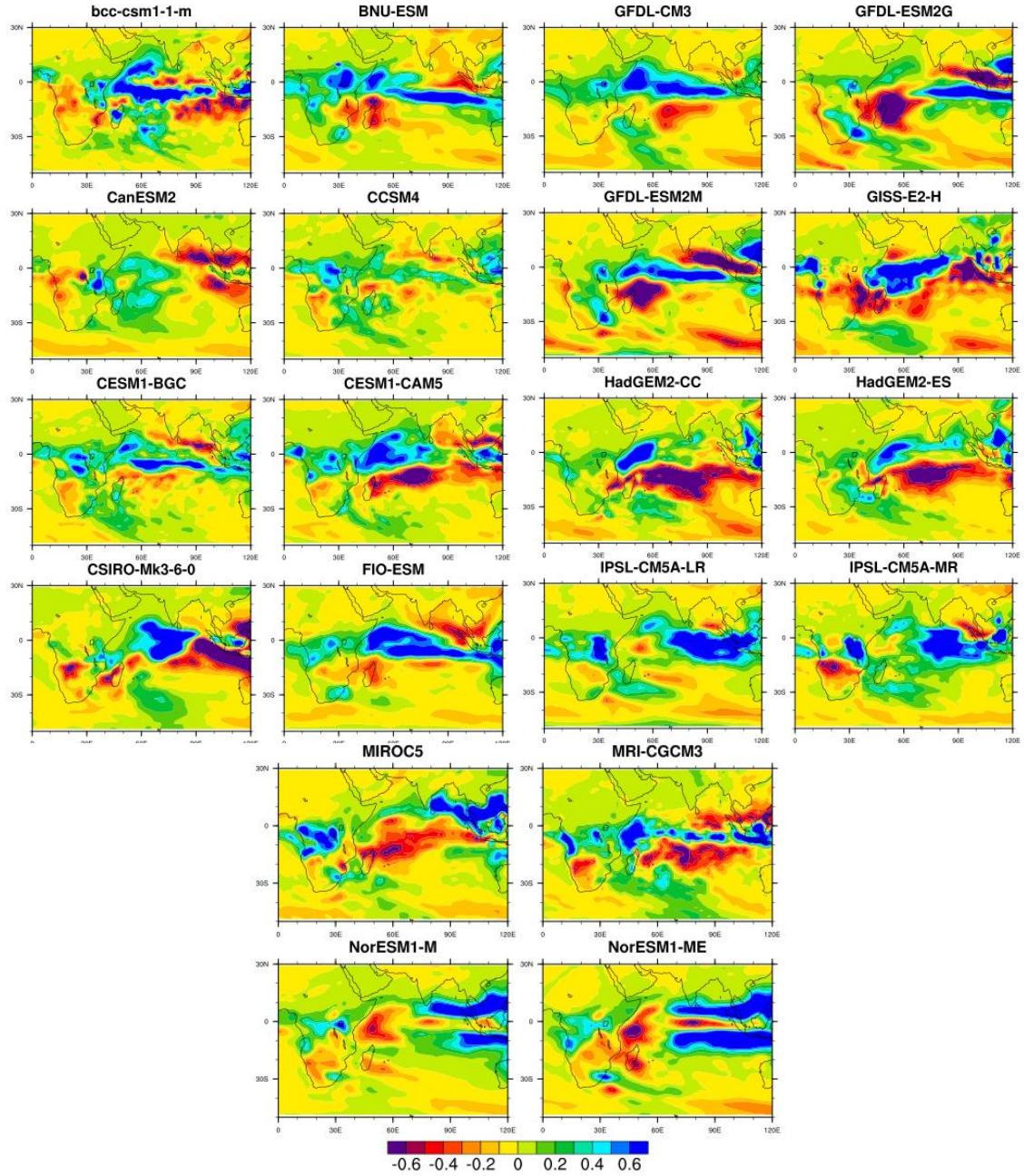

Figure 6: DJF ΔP for 20 CMIP5 models for the period 2071-2100 minus 1971-2000. Units are expressed as mm day^{-1} K^{-1}.

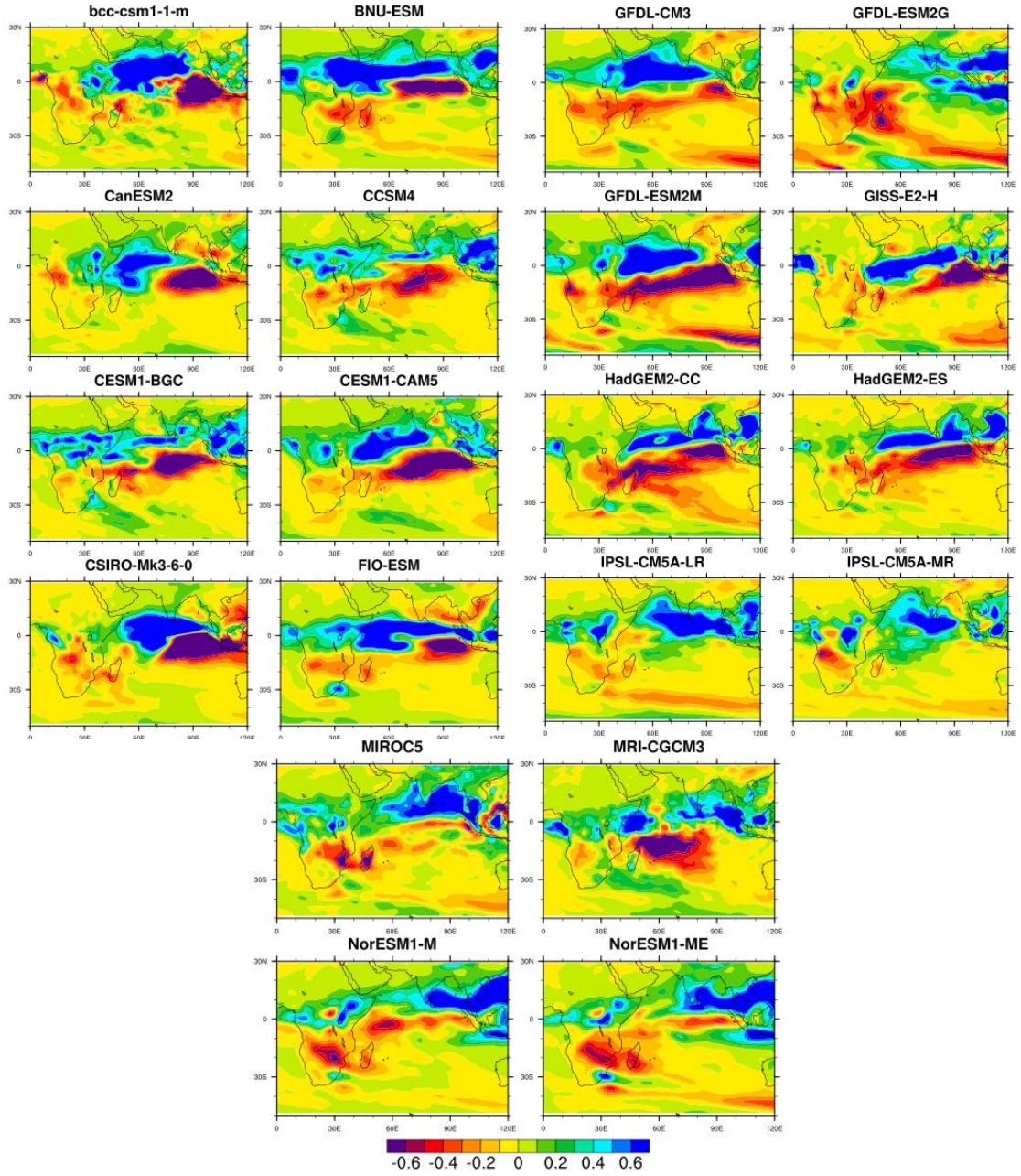

Figure 7: Same as Figure 6 but for OND

a.) MMM Mask

b.) Individual Masks

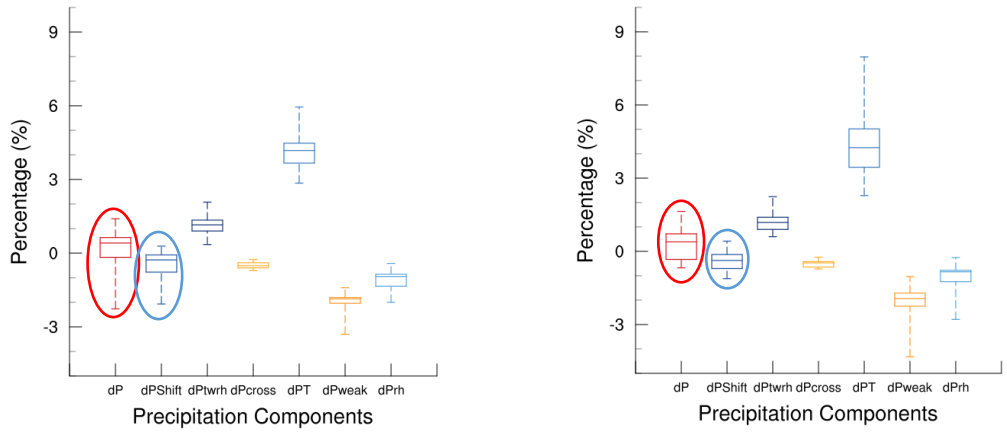

Figure 8: Box-whisker plots of DJF area averaged SIOCZ precipitation components with masks of greater than 5.5 mm day^{-1} applied to 20 CMIP5 (a) MMM (left) and (b) individual models (right). Area average is calculated over the domain (0˚ - 30˚S and 10˚ - 50˚E). Box represents the inclusion of the 25th and 75th percentile values, with the solid line representing the median and whiskers indicating the minimum and maximum values. Units are expressed as percentage change of each component.